Universitat Autònoma de Barcelona

**ESCOLA TÈCNICA SUPERIOR D'ENGINYERIA**

Departament d'Enginyeria Electrònica

# Resonant-type metamaterial transmission lines and their application to microwave device design

Doctoral Thesis written by
Marta Gil Barba

under the supervision of
Ferran Martín Antolín
and
Jordi Bonache Albacete

Bellaterra (Cerdanyola del Vallès), January 2009

# Acknowledgements

The work included in this Thesis would never have been possible without the help and support of many other people with whom I have shared these last four years.

I would like to specially thank my supervisors, Ferran Martín and Jordi Bonache for their invaluable help and for everything I have learnt with them. Thank you four your encouragement and patience. Thanks also to all members of GEMMA/CIMITEC and the Electronics Engineering Department for the support and help and for making it so nice to work with you. Thanks specially to M. Carmen and Javier for your not always visible but priceless work.

I also had the collaboration of the Electronics and Electromagnetism Department from the University of Seville, whose help has been very valuable. I would also thank the Microwave Engineering Group from the Technishe Universität Darmstadt for their hospitality and precious help and the opportunity that they gave me to further enrich this work. Special thanks are given to Prof. Dr.-Ing. Rolf Jakoby and Christian Damm.

Thanks to all those with whom I have shared so good moments at and outside the work. Thanks to all who, in the distance, have been for me an important support. To my family: thanks. To Fran: thanks.

Marta

# 1 Introduction

Recent advances have made possible the emergence of a new kind of materials: Metamaterials. In just some years, the development of this new scientific branch has given rise to numerous discoveries and technological advances based on the new properties shown by these novel materials. Optics and Electromagnetism are some of the fields in which Metamaterials have found interesting applications, among which is also the Microwave Engineering. The present Thesis gathers a part of the work developed during the last years in the Group GEMMA and CIMITEC (Centre d'Investigació en Metamaterials per la Innovació en Tecnologies Electrònica i de Comunicacions) in the application of resonant-type metamaterial transmission lines to the development of microwave devices.

The small size and the controllability of the electrical characteristics of metamaterial transmission lines based on sub-wavelength resonators are the main properties that make possible their use in the synthesis of microwave devices with compact dimensions and exceptional features. Microwave components based on metamaterial transmission lines are, therefore, of special interest in those applications in which compactness is a critical aspect. However, besides their small size, such devices can also offer a performance improvement or even new functionalities. These facts have awakened a big interest in metamaterial devices during the last years and this has become a research *hot topic* in which an important number of studies are regularly published.

This document has been written as a compendium of 13 articles, which are attached at the end of the document. The articles contain most of the results of the work developed during the realisation of this Thesis and the text frequently makes reference to them (the articles are marked in bold in the text when they must be looked up). The document has been divided in several sections devoted to different aspects:

- The second chapter presents a brief introduction about Metamaterials, and left-handed materials, including their properties and constituent elements. Special attention is paid to the application of such concepts to planar structures and the synthesis of metamaterial transmission lines.

- The third chapter delves into the implementation of metamaterial transmission lines by means of the resonant approach, which is applied in this work. Different kinds of resonant-type metamaterial transmission lines are presented and studied, with special emphasis on those structures which have been employed in the devices presented in chapter 4.

- The fourth chapter is devoted to the applications of the previously studied structures to the design of specific components, including different kinds of power dividers, narrow- and broad-band filters and reconfigurable structures based on ferroelectric materials.

- Finally, the fifth chapter includes some conclusions and possible next goals are exposed.

The work elaborated during the realisation of this Thesis has been carried out within the Group GEMMA/CIMITEC, which is part of the Electronics Engineering Department of the Universitat Autònoma de Barcelona. GEMMA/CIMITEC has been part of the European Network of Excellence NoE 500252-2 METAMORPHOSE (Metamaterials organized for radio, millimetre wave and photonic superlattice engineering), whose main objective was the research, the study and the promotion of artificial electromagnetic materials and metamaterials within the European Union and has recently given rise to the Virtual Institute for Artificial Electromagnetic Materials and Metamaterials (METAMORPHOSE VI AISBL). Furthermore, CIMITEC is one of the centres of the Technological Innovation Network of the CIDEM of the Catalan Government, created with the objective of promoting the transference of technology to the industry in the field of

Communication and Information Technology and has been recognized as Singular Research Group by the Catalan Government (AGAUR). This work has been, thus, supported by the European, Spanish and Catalan Governments by means of several projects and contracts and, specially, a Grant from the FPU (Formación de Profesorado Universitario) Grant Program of the Science and Innovation Ministry of the Spanish Government (Ref. AP2005-4523). The Universitat Autònoma de Barcelona contributes through the Vicerectorat de Projectes Estratègics-Parc de Recerca.

Among the projects and contracts with different institutions and companies which have given support to the developed research activities, we would like to stress:

- Project TEC2004-04249-C02-01 METASYSTEMS from the Spanish Government (Dirección General de Investigación). Project coordinated between the Universitat Autònoma de Barcelona (UAB) and the Universidad de Sevilla. Title: *Diseño, caracterización y aplicación de estructuras basadas en metamateriales al desarrollo de subsistemas de microondas y milimétricas*.

- Project TEC2007-68013-C02-02 METAINNOVA from the Spanish Government (Dirección General de Investigación). Project coordinated between the Universitat Autònoma de Barcelona and the Universidad de Sevilla. Title: *Tecnologías basadas en metamateriales y su aplicación a la innovación en componentes y subsistemas de RF microondas y milimétricas: circuitos de radiocomunicación.*

- International Project Eureka METATEC with title *METAmaterial-based TEchnology for broadband wireless Communications and RF identification.* Granted to a consortium formed by two companies and three research institutions from Serbia and Spain. This international Eureka Project has been funded in Spain by a PROFIT and an AVANZA I+D project.

- Project CSD2008-00066 CONSOLIDER INGENIO 2010 from the Spanish Government granted to a consortium formed by 8 research groups from different Spanish Universities. Title: *Ingeniería de Metamateriales (EMET)*

- Several contracts with SEIKO EPSON Corp. and EPSON Europe Electronics GmbH in the field of UWB bandpass filters.

# 2 Metamaterials

*The definition of metamaterials is not completely definite and can be done taking into account diverse aspects and considering different degrees of flexibility. Periodicity and exotic electromagnetic properties may be considered as essential issues for a structure to be regarded as a metamaterial. We will use, however, a wider definition of metamaterial, in which these two aspects are not essential. We will consider metamaterials as "*periodic or quasi-periodic structures which are artificially created to exhibit controllable electromagnetic properties*".*

*Regarding the size of the unit cell, these structures can be classified as electromagnetic crystals (or Electromagnetic Band-gaps –EBGs-) or effective media. Those structures whose period is on the order of the wavelength can be considered electromagnetic crystals. They exhibit interference effects which give rise to frequency band-gaps, what is known as Bragg dispersion. The period in effective media is, on the contrary, much smaller than the wavelength. This causes the medium to seem uniform for the electromagnetic fields and, therefore, to show effective electromagnetic properties. It is worth mentioning that the effective characteristics of the whole medium do not have to be the same as those of the unit cells of which it comprises. This fact is what makes possible that metamaterials show properties which can not be found in nature. Effective media are studied in section 2.1, whereas sub-wavelength resonators, which are used in the synthesis of $\mu$-negative effective media, are studied in 2.2.*

*Undoubtedly, the media which have specially stirred the interest within the scientific community are the effective media and, specifically, those known as left-handed media (LH media or LHM). In these metamaterials the dielectric permittivity ($\varepsilon$) and the magnetic permeability ($\mu$), which characterize the propagation of electromagnetic waves in a medium, are simultaneously negative. These new double negative (DNG) media behave like no other material found in nature does, what opens the door to new effects and application possibilities. Left-handed media are covered in section 2.3.*

*Section 2.4 deals with the application of the principles of LH media synthesis to the implementation of one-dimensional planar left-handed media. Metamaterial transmission lines are nowadays widely used in microwave device design and several approaches are devoted to this purpose. LC-loaded transmission lines are presented in 2.4.2, whereas resonant-type metamaterial transmission lines are studied in detail in chapter 3.*

## 2.1 Effective Media

As has been previously mentioned, effective media are those whose unit cells and period are much smaller than the wavelength. The incident radiation perceives the structure as a homogeneous medium with effective properties, which can be different from the constituent element ones. This is one of the most important characteristics of effective media, given that it allows the achievement of certain properties that natural materials do not exhibit.

Regarding the magnitudes $\varepsilon$ and $\mu$, which characterize the propagation of electromagnetic waves in media, we can classify the different materials into different types, depending on whether the dielectric permittivity and/or the magnetic permeability are negative or positive [1]. If only one of the two parameters is negative, the structure is considered as a single-negative medium (SNG), whereas those whose two parameters are negative are double-negative (DNG) media. The four different kinds of materials are depicted in Fig.2.1 and their properties can be deduced from the study of the equations describing the propagation of electromagnetic waves in media.

$$n^2 = \varepsilon\mu \tag{2.1}$$

$$k^2 = \frac{\omega^2}{c^2} n^2 \tag{2.2}$$

If we consider lossless isotropic materials with real values for the dielectric permittivity and the magnetic permeability, the inspection of the equations (2.1) and (2.2) shows that substances with $\varepsilon$ and $\mu$ having different sign exhibit imaginary values of the propagation constant $k$[1] and the refraction index $n$ and, as a result, they are not propagating media. However, if both parameters have the same sign, no matter if it is positive or negative, both $k$ and $n$ are real and the medium allows the propagation of electromagnetic (EM) waves. Taking this into account, we can conclude that SNG media are opaque media, whereas DNG and DPS (double positive) media are transparent.

We can try to sort the different kinds of media into the four different quadrants depicted in Fig.2.1 according to the signs of the parameters $\varepsilon$ and $\mu$. Conventional isotropic dielectric materials could be found in the quadrant I, since for such materials both $\varepsilon$ and $\mu$ are positive. On the contrary, materials located in the dark quadrants (SNG media) do not allow transmission. The fact that $\varepsilon$ and $\mu$ have opposite signs makes that both, $n$ and $k$, are imaginary and only evanescent modes are allowed. Some of these opaque materials can be found in nature, like ferrimagnetic materials, which have $\varepsilon$>0, but $\mu$<0 (mu negative MNG) and belong to the quadrant II. Another kind of SNG media would be metals at optic frequencies and plasmas under their plasma frequency, which have $\varepsilon$<0 and $\mu$>0 (epsilon negative ENG) and would be located in quadrant IV.

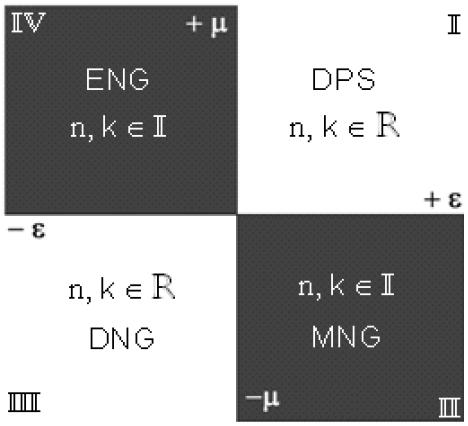


**Fig.2.1.** Representation of the different kinds of materials according to the signs of the parameters $\varepsilon$ and $\mu$. They can be transparent or opaque to electromagnetic waves, depending on whether the signs of $\varepsilon$ and $\mu$ are equal or opposite, respectively.

DNG media would be, thus, transparent. However, provided they do not exist as natural materials, their properties could only be theoretically studied up to recent years. The synthesis of the first DNG media in 2000 [2] opened the door to the study and application of such materials and their special properties. Some of the characteristics of double negative (also called left-handed (LH)) media are studied in section 2.3.

[1] Although the propagation constant is referred here as $k$, which is the conventional character to designate the propagation in continuous media analysis, in the following sections devoted to circuit analysis it will be denoted as $\beta$.

## 2.2 Sub-wavelength Resonators

The synthesis of effective media requires electrically small unit cells exhibiting specific properties. No DNG materials are available in nature. However, the artificial synthesis of such media by means of effective media was made possible by the appearance of the split-ring resonator (SRR) in 1999 [3].

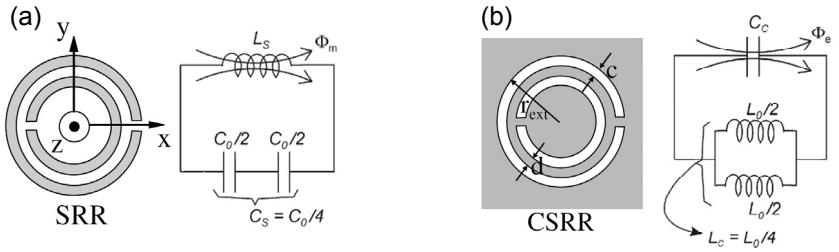


**Fig.2.2.** (a) Representation of a split-ring resonator (SRR) and its equivalent circuit model. The resonator is formed by two metallic split-rings (b) Representation of a complementary split-ring resonator (CSRR) and its equivalent circuit model. In this case the resonator is etched on a metallic surface. Metallic parts are represented in grey. Figures extracted from [4].

The SRR is formed by two concentric open metallic rings, as Fig.2.2(a) depicts. The resonator can be excited by an axial (z direction in the figure) time-varying external magnetic field, which induces currents in the rings. The splits present in the rings force the current to flow as displacement current between them. The current loop is thus closed through the distributed capacitance that appears between the inner and the outer ring (edge capacitance). The resonator can be modelled as is shown in Fig.2.2(a) [4,5]. $L_s$ is the resonator self-inductance, whereas $C_0/2$ is the capacitance related with each of the two SRR halves. $C_0$ can be obtained as $C_0=2\pi r C_{pul}$, where $C_{pul}$ represents the per unit length capacitance between de rings forming the resonator. As for $L_s$, it can be approximated to the inductance of a single ring with the average radius of the resonator and the width of the rings, $c$.

There are two characteristics of the SRR which make it especially interesting. One of them is its small electrical size. At the resonance frequency:

$$\omega_0 = \frac{1}{\sqrt{L_s C_s}} \tag{2.3}$$

the perimeter of the resonator is smaller than half the wavelength of the exciting wave. The electrical size of the resonator can be reduced decreasing the gap between the rings and the ring width (in order to increase $C_s$ and $L_s$, respectively). Thus, the minimal achievable resonance frequency will be determined by the limitations imposed by the considered technology. Their sub-wavelength characteristics make SRRs perfectly suitable to be applied as elemental units in the synthesis of effective media. The second and more important property of this resonator is the fact that an effective media formed by SRRs exhibits around their resonance frequency negative effective magnetic permeability, $\mu_{eff}$. The effective permeability of such a medium can be estimated (neglecting losses) as:

$$\mu_{eff} = 1 - \frac{F\omega^2}{\omega^2 - \omega_0^2} \tag{2.4}$$

where $F$ is the fractional area occupied by the interior of the resonator within the unit cell [2,3]. The typical behaviour of a MNG effective media is depicted in Fig.2.3. The variation of $\mu_{eff}$ around the resonance frequency is shown in Fig.2.3(a). Just above $\omega_0$ and up to $\omega_{mp}$ (the "magnetic plasma frequency"), the effective permeability is negative. The corresponding frequency gap, where no propagation is allowed, can be observed in the dispersion diagram

shown in Fig.2.3(b). The appearance of the split-ring resonator opened the door to the synthesis of the first effective MNG [3] and DNG [2] media, as will be exposed in section 2.3. Furthermore, it has been widely used in the implementation of different kinds of effective media, as well as metamaterial transmission lines with controllable characteristics (section 3.1). Due to the symmetry properties of the SRR, cross-polarization (electric excitation of magnetic dipoles and vice versa) is possible [6,7,8]. Although this fact can represent a drawback for the synthesis of isotropic media, it is in general not determining for its application in planar device implementation, as is our case.

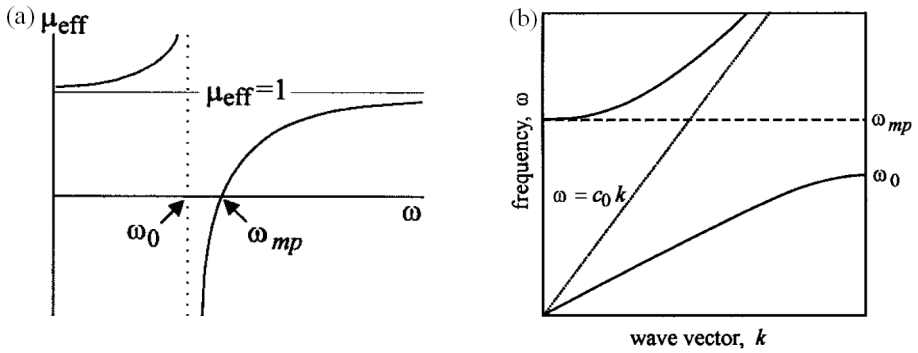


**Fig.2.3.** (a) Effective magnetic permeability of a MNG medium. (b) Dispersion diagram of a MNG medium. Transmission is inhibited in the frequency range $\omega_0$-$\omega_{mp}$, where $\mu_{eff}$ is negative. Figures extracted from [3].

On the basis of the SRR, numerous sub-wavelength resonators with similar topologies have been proposed. One of them is the complementary counterpart of de SRR, the complementary split-ring resonator (CSRR) (see Fig.2.2(b)). In this case, the rings forming the resonator are etched on a metallic surface. It appeared from the idea of applying the Babinet principle to the SRR [9,10]. According to this principle, in such complementary structures, electric and magnetic fields, currents, etc. interchange their roles. This occurs in such a way that, ideally, both structures have the same resonance frequency, but, contrary to the SRR, the CSRR exhibits negative values of the dielectric permittivity around its resonance, which can be excited by means of an axial electric field. Its circuit model can be seen in Fig.2.2(b), which is the dual of the SRR circuit model. Many other resonators admit a complementary counterpart, like, for example, the ones represented in Fig.2.4(a) to (e).

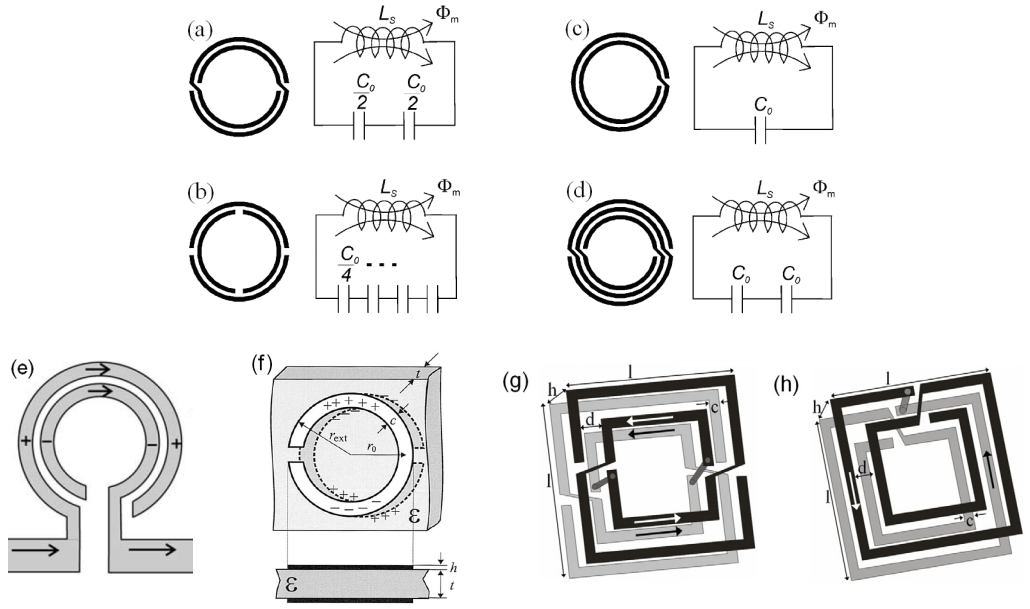


**Fig.2.4.** (a) Non-bianisotropic split-ring resonator (NB SRR) and its equivalent circuit model. (b) Double-slit SRR and circuit model (c) Spiral resonator (SR) and model (d) Double spiral resonator (DSR) and model. (e) Open split-ring resonator (OSRR) (f) Broad-side coupled split-ring resonator (BC SRR). (g) Broad-side coupled non-bianisotropic split-ring resonator (BC NB SRR) (h) Broad-side coupled spiral resonator with four turns (BC SR (4)). Figures extracted from [4,6, 12 and 15].

In order to find resonators with different symmetry properties and smaller size, many other structures, based on different spiral, multiple split, or multi-layer topologies, have been proposed and studied [4,6,11,12,15]. In Fig.2.4, some of these resonators can be seen. Fig.2.4(a) shows the non-bianisotropic split-ring resonator (NB SRR), which has the same resonance frequency as the SRR, but, due to its symmetry, neither the NB SRR nor its complementary counterpart exhibit cross-polarization effects [4]. The same happens with the double-slit split-ring resonator (DS SRR), which avoids cross-polarization, but its resonance frequency is twice the one of a SRR with the same dimensions (Fig.2.4(b)), given that the total capacitance $C_s$ is four times smaller than in the SRR. The resonance frequency, $f_0$, can be reduced, for example, using any of the rest of the particles shown in Fig.2.4. The spiral resonator (Fig.2.4 (c)), for example, reduces in a factor 2 the resonance frequency of the SRR.

The inclusion of additional rings or turns in the resonators contributes to further decrease the resonance frequency [4,13,14]. As an example, the double spiral resonator, which reduces $f_0$ in a factor $2^{1/2}$ with respect to the SRR, is shown in (Fig.2.4 (d)). The open split-ring resonator (OSRR) (Fig.2.4 (e)) also achieves a smaller electrical size (2 times smaller than for the SRR) since, contrary to the SRR, the two halves of the total capacitance are parallel connected [15]. Further size reduction can be achieved if the metallic strips forming the resonators are broad-side (instead of edge-side) coupled, like in figures (f) [6], (g) and (h) [12]. This is realized using two metal layers to implement the resonator. The broad-side coupling allows the achievement of higher capacitances, this reducing the resonance frequency of the resonator. Additionally, the inclusion of vias connecting the metallic strips (Figs. (g) and (h)) allows the elongation of the metallic strips and, thus, the enlargement of the resonator inductance, contributing to a further resonance frequency reduction. Most of the particles shown in Fig.2.4 have a complementary version. Along the development of this Thesis, the particles which have been mainly used are the SRR, the SR, their complementary counterparts, as well as the open complementary split-ring resonator (OCSRR).

## 2.3 Left-handed Media

We will now focus our attention on those materials belonging to quadrant III in Fig.2.1. Such materials are transparent like many conventional materials, since $\varepsilon$ and $\mu$ have the same sign. Nevertheless, they exhibit some special properties which had never been observed before the implementation of the first artificial medium with such properties in 2000 [2]. Although they cannot be found in nature, 40 years ago, in 1968, Viktor Veselago [1] already predicted many of the characteristics of such media in a merely theoretical work, in which he deduced the consequences of taking negative values for the magnetic permeability and the dielectric permittivity simultaneously. Studying Maxwell's and constitutive equations, we can infer some of these characteristics:

$$\nabla \times \vec{E} = - \frac{\partial \vec{B}}{\partial t} \tag{2. 5}$$

$$\nabla \times \vec{H} = \frac{\partial \vec{D}}{\partial t} \tag{2. 6}$$

$$\vec{B} = \mu \vec{H} \tag{2. 7}$$

$$\vec{D} = \varepsilon \vec{E} \tag{2. 8}$$

Considering a monochromatic plane wave, we can write:

$$\vec{k} \times \vec{E} = \omega\mu \vec{H} \tag{2.9}$$

$$\vec{k} \times \vec{H} = -\omega\varepsilon \vec{E} \tag{2.10}$$

where we can deduce that if $\varepsilon$ >0 and $\mu$ >0, the orthogonal vector system formed by the wave vector, **k**, and the electric and magnetic field vectors, **E** and **H**, is right-handed, whereas when they both are negative, the vector system is left-handed (see Fig.2.5). This is the reason why these media were called "left-handed media" by Veselago.

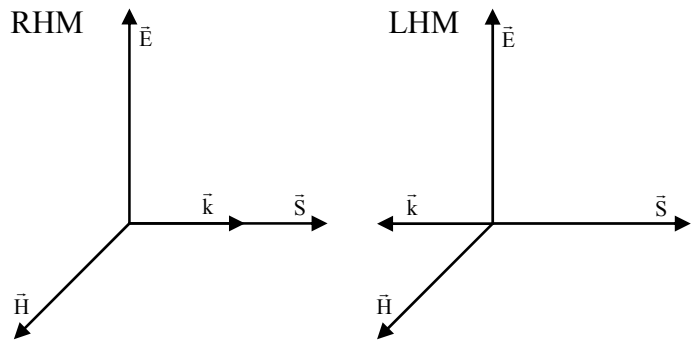


**Fig.2.5.** Representation of the field, wave and Poynting vectors for propagating waves in right-handed (RHM) and left-handed (LHM) media. In LHM the wave and Poynting vectors are antiparallel and the propagation is "backward".

Although the wave vector reverses its direction in LHM, the Poynting vector keeps it, given that the change in the signs of $\varepsilon$ and $\mu$ does not affect it.

$$\vec{S} = \vec{E} \times \vec{H} \tag{2.11}$$

As a consequence, the energy flux and the wave fronts travel in opposite directions or, in other words, the group and the phase velocities are antiparallel in LHM. This kind of propagation is called "backward propagation" and it gives rise to different phenomena which are

exclusive of left-handed media. The synthesis in 2000 of the first left-handed medium [2] allowed the corroboration of many of the predictions made by Veselago. The composite medium consisted in a periodic array of metallic posts, which was already known to exhibit "plasma behaviour" [16] ($\varepsilon$<0 below a certain frequency known as plasma frequency) and split-ring resonators (see inset in Fig.2.6(a)). The combination of both elements forming a periodic distribution resulted in an effective medium showing negative values of $\varepsilon$ and $\mu$ in a certain frequency range when it was illuminated with a properly polarised wave. In order to achieve the desired behaviour, the electric field of the incident wave should be parallel to the metallic posts, whereas the magnetic field has to be perpendicular to the planes containing the SRRs in order to ensure their excitation. By this means, it was experimentally corroborated that, whereas the composite medium (DNG) was transparent, a medium formed only by SRRs was able to inhibit the propagation around the resonance frequency of the resonators (where $\mu_{eff}$<0) (see Fig.2.6(a)). Backward propagation was later achieved in many different media based on different approaches like, for example, SRR-loaded waveguides [17] or transmission lines, and the LC-loaded transmission line (see following sections).

One of the consequences arising from this phase velocity reversal is negative refraction. Equation (2.1) is ambiguous regarding the sign of the refraction index. However, if a proper study is carried out, this ambiguity can be avoided [1,18]. One easy way to see if the sign of the refraction index in left-handed materials is negative or positive, is the next one [18,19]:

We can express the two negative magnitudes, $\varepsilon$ and $\mu$, in polar coordinates and give them the value -1. If do so, (2.1) can be rewritten as follows:

$$n = \sqrt{\varepsilon\mu} = \sqrt{\varepsilon}\sqrt{\mu} = e^{j\frac{\pi}{2}} e^{j\frac{\pi}{2}} = e^{j\pi} = -1 \qquad (2.12)$$

It must be taken into account that the imaginary parts of the square roots of $\varepsilon$ and $\mu$ must be positive, as it is in passive media. By these means, it can be deduced that the refraction index is negative in left-handed media. As a consequence, when a wave travels through a RHM and arrives to a LHM the refraction angle is also negative in such a way that the incident and the refracted beams lay at the same side of the normal (see Fig.2.6(b)). Negative refraction was experimentally verified for the first time in 2001 [20], in a medium similar to the one shown in Fig.2.6(a). Other phenomena, like Doppler effect or Cerenkov radiation [1,21] are also inversed in left-handed media.

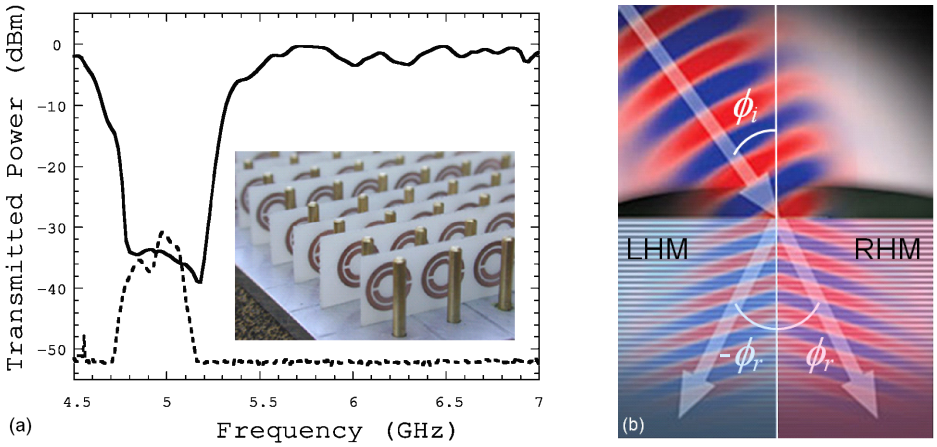


**Fig.2.6.** (a) Photograph of the first composite medium with left-handed characteristics (inset) and measured transmission of the composite medium containing SRRs and posts (dashed line) and a second medium with only SRRs (solid line). Figure extracted from [2]. (b) Comparison between the refraction of a radiation beam arriving to a LHM, when it is refracted with an angle $-\phi_r$, or to a RHM, when the refraction angle is $\phi_r$.

Metamaterials promptly stirred a big interest among the scientific community and many different applications were soon envisaged. The controllability over their characteristics and their exotic properties has made metamaterials become a "hot topic" during the last years. Although it is not based on a left handed medium (it is a DPS metamaterial), the most

innovative and spectacular application taking advantage of metamaterial properties is, undoubtedly, the use of cloaking structures to achieve invisibility. The first approach achieving it was based on the use of a cloak to direct the electromagnetic waves to surround an object [22,23] (see Fig.2.7(b)) in such a way that, behind the shield, the radiation contains no information (in terms of phase and direction) of the object. In this sense, it can be said that the object becomes invisible, since the radiation is not reflected by the object and behaves like if there was nothing in its way. The shells forming the cloak contain metallic resonators tuned to vary the permeability (and, thus, the refraction index) in the different layers (see Fig.2.7(a)). By this means, the light can be "bended" to surround an object located in the centre of the cloak. Up to now, however, cloaking has been only achieved for a specific frequency and at the microwave range. Many efforts are now devoted to achieve broadband cloak at visible frequencies, although it is a very complex technological challenge. A step forward in this subject was recently taken with the synthesis of a negative refractive index metamaterial at optical frequencies [24]. The structure presented in [24] consists of alternating layers of silver and magnesium fluoride ($MgF_2$) forming a fishnet prism, which was able to produce negative refraction at THz frequencies.

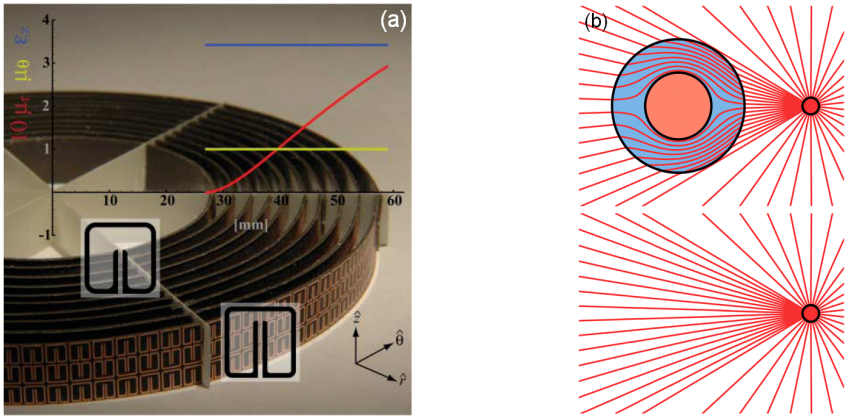


**Fig.2.7.** (a) Photograph of the first 2D cloaking structure. Figure extracted from [22] (b) Scheme of the effect of the cloak on the radiation beams. The cloak directs the radiation to surround the object avoiding reflexion and shadows from the object. The light penetrating the cloak is bended and forced to exit following the same trajectory as if there was no object in its way. Figure extracted from [23].

Super lenses have also been a very attractive application of metamaterials. Metamaterials allow the overcoming of the diffraction limit [25,26], giving rise to superresolution. Such subdiffraction imaging has been achieved using different types of slabs [27,28] and surfaces [29,30]. Some medical applications of magnetoinductive lenses in magnetic resonance imaging are already being studied [31].

## 2.4 Metamaterial Transmission Lines

Soon after the appearance of the first left-handed media, such interesting concepts were applied to the design of planar structures. Left-handed transmission lines were soon implemented in coplanar [32,33], strip line [34] and microstrip [35,10] technologies. In contrast to previous bulky structures, they were compatible with planar fabrication processes and, therefore, more suitable for microwave device design. The big advantages of these artificial transmission lines are their compact dimensions and design flexibility, given that phase and characteristic impedance can be tailored to some extent in order to obtain the suitable properties that each design requires. Two main approaches are devoted to the implementation of artificial transmission lines and their application in microwave device design: the CL-loaded transmission line and the resonant-type approach. The first of them is presented in section 2.4.2, whereas a wide study of the resonant-type approach and their applications is exposed in chapters 3 and 4. Both approaches are based on the dual transmission line concept, which is exposed next.

### 2.4.1 Dual Transmission Line

When it comes to study the propagation characteristics in a transmission line, it is possible to make an analogy between the propagation in a transmission line and the propagation of plane waves in a homogeneous and isotropic medium. By this means, if we make use of the equivalent T-circuit model of a transmission line unit cell (see Fig.2.8(a)), we can make an equivalence between the magnitudes $\varepsilon_{eff}$ and $\mu_{eff}$ characterising the propagation in media and the series impedance *Z'* and the shunt admitance *Y'* of the TL model [36] (the sign ' is here used to denote the per-unit-length magnitudes).

$$Z' = j\omega\mu_{eff} \tag{2.13}$$

$$Y' = j\omega\varepsilon_{eff} \tag{2.14}$$

This gives rise to four possible sorts of transmission lines, regarding the signs of *Z'* and *Y'* (actually the series reactance and the shunt susceptance). As indicated in Table I and in an equivalent way as it was illustrated in Fig.2.1 in section 2.1, the signs of the series impedance and shunt admittance determine the propagating or not propagating nature of the line.

| **Inmitances** | | **Medium** | **Propagating** |
|---|---|---|---|
| ***Z' (~$\mu_{eff}$)*** | ***Y'(~$\varepsilon_{eff}$)*** | | |
| >0 | >0 | Conventional TL. DPS | YES |
| >0 | <0 | SNG | NO |
| <0 | >0 | SNG | NO |
| <0 | <0 | Dual TL. DNG | YES |

Table I: Different kinds of transmission lines depending on the sign of the impedances of their circuit models.

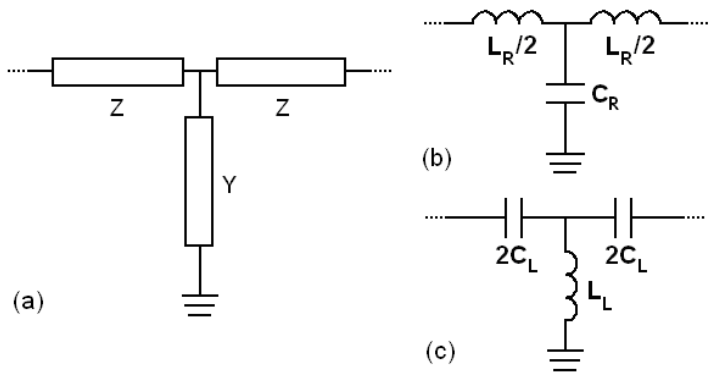


**Fig.2.8.** (a) Generic T-circuit model of a transmission line unit cell. (b) Unit cell for a conventional (right-handed) transmission line. $L_R$ and $C_R$ are the series inductance and shunt capacitance in the RH TL model. (c) Unit cell for a left-handed transmission line. $L_L$ and $C_L$ are the shunt inductance and series capacitance in the LH TL model.

Therefore, considering purely reactive inmitances (lossless TL), a conventional transmission line, modelled by series inductances and shunt capacitances (Fig.2.8 (b)), exhibits positive values of $\varepsilon_{eff}$ and $\mu_{eff}$.

$$\mu_{eff} = \frac{L_R}{2l} = \frac{L'_R}{2} \tag{2.15}$$

$$\varepsilon_{eff} = \frac{C_R}{l} = C'_R \tag{2.16}$$

where *l* is the length of the unit cell. On the contrary, if we intend to obtain negative values for $\varepsilon_{eff}$ and $\mu_{eff}$, *Z'* must be capacitive, and *Y'* must be inductive (Fig.2.8 (c)) giving rise to:

$$\mu_{eff} = \frac{-1}{\omega^2 2C_L l} \tag{2.17}$$

$$\varepsilon_{eff} = \frac{-1}{\omega^2 L_L l} \tag{2.18}$$

This results in what is known as “dual transmission line” (Fig.2.8 (c)), since it represents the dual circuit of a conventional transmission line. Regarding the propagation constant, $\beta$, and the phase, $v_p$, and group, $v_g$, velocities, they also show the differences between the conventional and the dual transmission lines [5,37]. The propagation constant can be obtained in terms of the series and shunt impedances of our lossless T-network as [38]:

$$\cos \beta l = 1 + ZY \tag{2.19}$$

where *l* is the unit-cell length. This expression can, in the long wavelength limit, be approximated to:

$$\beta = \pm\sqrt{-2Z'Y'} \tag{2.20}$$

Furthermore, for such a T-network, the characteristic impedance can be obtained as [38]:

$$Z_0 = \sqrt{Z\left(\frac{2}{Y} + Z\right)} \tag{2.21}$$

Phase and group velocities are given by the following expressions:

$$v_p = \frac{\omega}{\beta} \tag{2.22}$$

$$v_g = \frac{\partial \omega}{\partial \beta} \tag{2.23}$$

In the case of the conventional transmission line, if we take into account the expressions of *Z* and *Y* we can obtain the equations:

$$Z_R = j\omega \frac{L_R}{2} \tag{2.24}$$

$$Y_R = j\omega C_R \tag{2.25}$$

Therefore, we can obtain:

$$Z_0 = \sqrt{\frac{L_R}{C_R}\left(1 - \omega^2 \frac{L_R C_R}{4}\right)} \tag{2.26}$$

$$\cos \beta l = 1 - \frac{\omega^2 L_R C_R}{2} \tag{2.27}$$

Expression (2.27) can be approximated in the long-wave limit to [5]:

$$\beta = +\omega \frac{\sqrt{L_R C_R}}{l} = +\omega \sqrt{L'_R C'_R} \tag{2.28}$$

Regarding the phase and group velocities, we obtain:

$$v_p = \frac{\omega}{\beta} = +\sqrt{\frac{1}{L'_R C'_R}} \tag{2.29}$$

$$v_g = \frac{\partial \omega}{\partial \beta} = +\sqrt{\frac{1}{L'_R C'_R}} = v_p \tag{2.30}$$

The sign of the group velocity can, in principle, be arbitrarily chosen. Nevertheless, the group velocity can only be either positive or negative in order not to violate causality. We will assume that $v_g$>0 (2.30). As a consequence, the $\beta$ and $v_p$ are positive as well, what confirms forward propagation in conventional transmission lines.

On the other hand, for the dual transmission line we find:

$$Z_L = \frac{1}{j\omega 2C_L} \tag{2.31}$$

$$Y_L = \frac{1}{j\omega L_L} \tag{2.32}$$

$$Z_0 = \sqrt{\frac{L_L}{C_L}\left(1 - \frac{1}{\omega^2 4 C_L L_L}\right)} \tag{2.33}$$

Whereas in the long wavelength limit we obtain:

$$\beta = -\sqrt{-2Z'_L Y'_L} = -\frac{1}{\omega l \sqrt{C_L L_L}} \tag{2.34}$$

$$v_p = \frac{\omega}{\beta} = -\omega^2 l \sqrt{C_L L_L} \tag{2.35}$$

$$v_g = \frac{\partial \omega}{\partial \beta} = +\omega^2 l \sqrt{C_L L_L} \tag{2.36}$$

where, again, the sign of the propagation constant has been chosen in order to guarantee a positive value of the group velocity. The negative value of the phase velocity (2.35) evidences backward propagation in dual transmission lines. The dispersion diagrams and the characteristic impedance of the conventional and the dual transmission lines are depicted in Fig.2.9. It is worth mentioning that, although expression (2.28) predicts no dispersion, Fig.2.9(a) corresponds to a dispersive medium. It must be taken into account that (2.20) and, therefore, (2.28) and (2.34) are valid only under the long wavelength approximation.

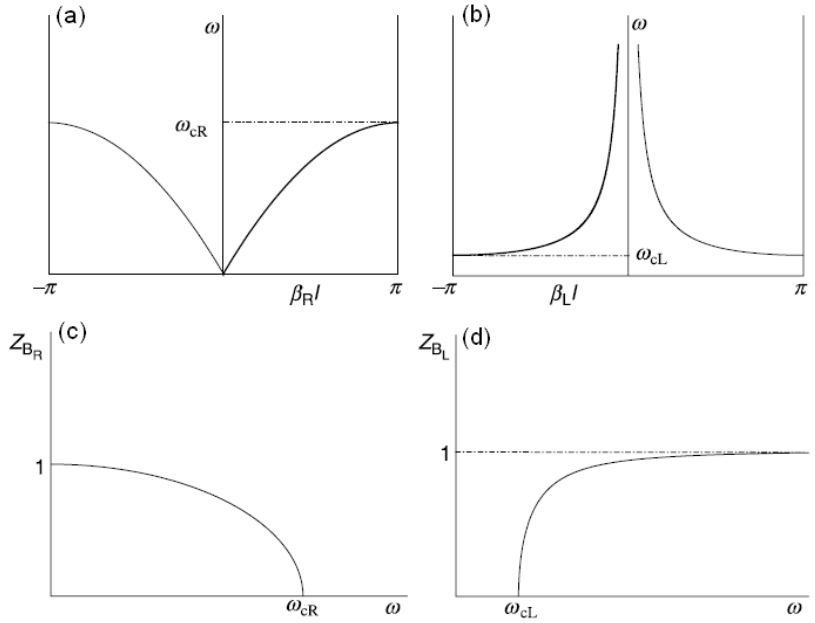


**Fig.2.9.** Dispersion diagrams for a conventional (a) and a dual (b) transmission line. Characteristic impedances of a conventional (c) and a dual transmission line. The impedance is normalized to the maximal value, which is reached at $\omega$=0 and $\omega$=∞ for the conventional and the dual transmission line, respectively. Figures obtained from [5]

From the theoretical point of view, the dual transmission line is a left-handed medium which supports backward waves. However, the practical realization of a pure dual transmission line is not possible. Its implementation requires a host conventional transmission line, which can be loaded with different elements in order to obtain the desired series and shunt impedances. Depending on the kind of loading elements, we can distinguish between two main approaches: the CL-loaded transmission line and the resonant-type approaches. Both approaches are described in section 2.4.2 and section 3.1, respectively.

### 2.4.2 CL-loaded Artificial Transmission Lines

A simply way to obtain a negative series reactance and shunt susceptance and, thus, left-handed propagation, is to load a host transmission line with series capacitances and shunt inductances. This strategy can be applied with different kinds of transmission lines, including microstrip [35] and coplanar waveguides [32] (see Fig.2.10). This strategy, however, does not allow to obtain a pure dual transmission line, since the host medium introduces parasitic elements ($L_R$ and $C_R$ in Fig.2.10 (b)). Nevertheless, at certain frequency ranges, the loading elements dominate the propagation characteristics, giving rise to a left-handed transmission band. On the other hand, the parasitics of the host line rule the propagation at higher frequencies. The behaviour of the so called CL-loaded transmission lines is, therefore, a composite behaviour and such lines are known as composite right-left handed (CRLH) transmission lines [39,40,41].

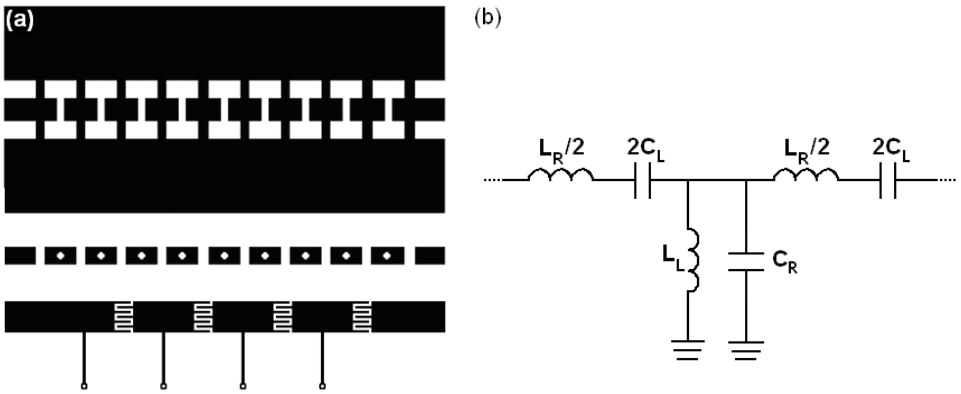


**Fig.2.10.** (a) Layouts of different kinds of CL-loaded transmission lines. From up to down: Coplanar waveguide (CPW) with capacitive gaps and shunt connections, microstrip line with capacitive gaps and vias to ground and, finally, microstrip line with interdigital capacitors and shunt-connected inductive stubs (b) T-circuit model of a composite right-left handed Transmission Line (CRLH TL). Figures obtained from [42]

The expressions of $\varepsilon_{eff}$ and $\mu_{eff}$ for such a CRLH TL can be obtained in a similar way as it has been done in the previous sections:

$$\mu_{eff} = \frac{L_R}{2l} - \frac{1}{\omega^2 2C_L l} \tag{2.37}$$

$$\varepsilon_{eff} = \frac{C_R}{l} - \frac{1}{\omega^2 L_L l} \tag{2.38}$$

As can be seen, both $\varepsilon_{eff}$ and $\mu_{eff}$ can be either positive or negative, depending on the frequency range. This results in two transmission bands, generally separated by a frequency gap where transmission is not allowed (see Fig.2.11 (a)). Observing expressions (2.37) and (2.38), it is easy to see that they both are negative at low frequencies and positive at high frequencies. Depending on the values of the capacitive and inductive elements forming the line, the frequency ranges at which $\varepsilon_{eff}$ and $\mu_{eff}$ have the same sign and, thus, propagation is possible, can be different, but the left-handed band appears always below the right-handed one (see Fig.2.11 (a)). The resonance frequencies of the series and shunt branches forming the line act as the limits of the frequency gap between both transmission bands. Any of them can be the lower ($\omega_{G1}$) or the upper ($\omega_{G2}$) limit, depending on which of the branches resonates at a lower frequency.

$$\omega_{G1} = \min(\omega_s, \omega_p) \tag{2.39}$$

$$\omega_{G2} = \max(\omega_s, \omega_p) \tag{2.40}$$

The composite behaviour allows the design of a specific and interesting kind of lines: the balanced line [37,39]. In such lines, the frequency gap that is normally present between the two transmission lines is forced to disappear. In order to do that, the resonance frequencies of the series and shunt branches must be equal. As a result, a single transmission band with left- and right-handed characteristics at different frequencies is obtained (Fig.2.11(b)). At the transition frequency, $\omega_0$, the phase velocity (as well as the wavelength) is infinity, whereas the group velocity is finite and different from zero. As a consequence, and contrary to the unbalanced case, in which at the resonance frequencies ($\omega_{G1}$, $\omega_{G2}$) the group velocity is zero, in balanced transmission lines there is energy transmission at the transition frequency. As will be shown in following sections, this kind of lines is especially interesting for broad band applications.

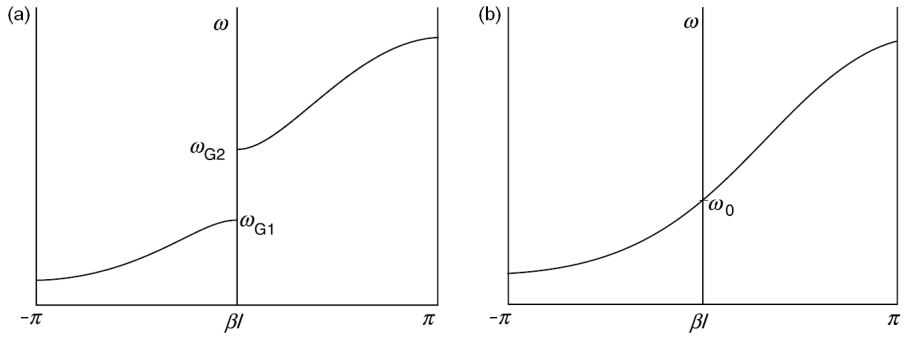


**Fig.2.11.** (a) Dispersion diagram of a non-balanced CRLH TL. The LH ($\beta l$<0) and the RH ($\beta l$>0) transmission bands can be observed separated by a frequency gap where transmission is forbidden. (b) Dispersion diagram of a balanced CRLH TL. The limits of the frequency gap have been forced to coincide and the gap disappears. Figures obtained from [5]

LC-loaded transmission lines exhibit controllable characteristics, which can be tailored in order to satisfy different requirements depending on the application. Taking advantage of this fact, they have been widely used in microwave device design, giving rise to a big number of different components based on the particular properties of metamaterial transmission lines. Coupled- [43,44] and branch- [45] line couplers, power dividers [46,47,48], filters [49] or antennas [50] are some examples of the application possibilities of LC-loaded transmission lines. This approach has also been applied to the design of three-dimensional metamaterials formed by LC-loaded transmission line networks exhibiting backward propagation [51,52,53].

# 3 Resonant-type Metamaterial Transmission Lines

*Soon after the appearance of the first artificial transmission lines with left-handed characteristics based on the CL-loaded TL approach, a new kind of metamaterial transmission lines based on sub-wavelength resonators came out. The design flexibility of artificial transmission lines makes them especially interesting and useful in microwave device design. Since the development of the first SRR-based transmission line, several kinds of resonant-type metamaterial transmission lines have been developed and applied in the implementation of a number of microwave components, such as filters, power dividers or hybrid couplers, among others. In this chapter, different kinds of resonant-type metamaterial transmission lines are described and studied, whereas their applications are exposed in chapter 4.*

## 3.1 Composite Right/left-handed Transmission Lines based on SRRs and CSRRs

As has been previously exposed, a necessary condition to have a propagating transmission line is that the signs of the series and shunt reactances in the circuit model of the unit cell are opposite. This is satisfied simply by conventional transmission lines, but it can also be achieved in an artificial way by means of loading elements. These elements can be capacitive gaps, strips and vias, surface mounted components or, as is the case in the resonant-type approach, resonators.

Two main types of resonators can be applied as loading elements: metallic (SRR-type) or complementary (CSRR-type) resonators. In both cases, the sub-wavelength dimensions of the resonators allow the synthesis of very compact structures with significant design flexibility. These resonant-type metamaterial transmission lines are, therefore, suitable for microwave device miniaturisation.

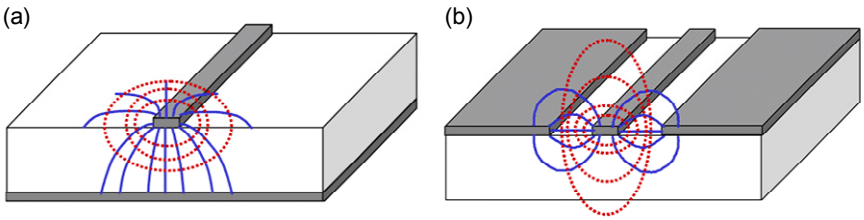


**Fig.3.1.** Scheme of a microstrip (a) and a coplanar (b) transmission line and the distribution of the electric (blue, solid) and the magnetic (red, dashed) fields.

The resonators can be coupled in different ways, giving rise to many different kinds of transmission lines. As has been previously explained, SRR-type resonators are excited by an axial magnetic field, whereas CSRR-type resonators are excited by an axial electric field. This allows different kinds of configurations for each kind of resonator. Split-ring resonators can be coupled to a coplanar waveguide by locating them on the bottom side of the substrate, just underneath the gaps separating the conducting strip and the ground planes, or even on the slot between the strip and the ground planes [54]. One more possibility is to place the SRRs close to a microstrip line (see Fig.3.1). These configurations allow the excitation of the SRRs by means of the magnetic field surrounding the conducting strips. Regarding the CSRRs, they can be etched on the ground plane under a microstrip line, as well as they can be etched on the metallic strip in both, microstrip and coplanar transmission lines.

Depending on the kind of resonator, how it is coupled to the line and the additional elements it is combined with, different kinds of transmission lines with diverse propagation properties can be obtained. Some examples of these metamaterial transmission lines are exposed in the following sections. Special emphasis will be done in the CSRR-type transmission lines, which have been mainly studied and applied throughout the realisation of this Thesis.

### 3.1.1 Purely Resonant Approach

The first resonant-type metamaterial transmission line consisted of a coplanar waveguide loaded with SRRs and shunt-connected metallic strips [33]. The SRRs were located on the bottom side of the substrate, as Fig.3.2(a) shows. By this means, the resonators were magnetically coupled to the coplanar waveguide. Their effect, together with the metallic strips acting as shunt inductances, gave rise to a LH transmission band around the resonance frequency of the resonators, where the series reactance is capacitive and the shunt reactance is inductive.

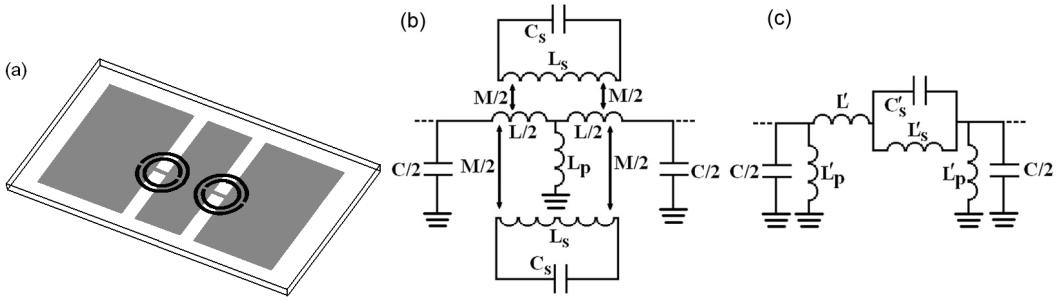


**Fig.3.2.** (a) Scheme of a unit cell of the first resonant-type metamaterial transmission line. SRRs (in black) and shunt-connected metallic strips were used as loading elements in a CPW to obtain LH propagation. Metallic parts are depicted in grey for the top layer (CPW and strips) and black for the bottom layer (SRRs) of the substrate (b) Recently-proposed improved circuit model for the structure shown in (a). (c) Modified circuit model for the structure shown in (a). Figures (b) and (c) obtained from [55].

The equivalent circuit model for a unit cell (Fig.3.2(a)) is depicted in Fig.3.2(b), which can be transformed into the $\pi$-circuit shown in Fig.3.2(c). In the circuit (b), the SRRs, modelled by the resonant tanks formed by $C_s$ and $L_s$, are magnetically coupled to the coplanar waveguide through the mutual inductive coupling represented by $M$. The line inductance and capacitance are taken into account by means of $L$ and $C$, respectively. On the other hand, the metallic strips are modelled by $L_p$. As can be seen, the coupled SRRs contribute to achieve a capacitive element in the series impedance, whereas the metallic strips are responsible for the shunt inductance $L_p$. This circuit has been recently proposed [42,55,56,57] as an improvement with respect to the previously existing one [33]. Although the former circuit could also be transformed into the circuit shown in Fig.3.2(c) and reproduced the response of the structure, it was not perfectly able to describe its physical behaviour. The transformation from (b) into (c) obeys the equations:

$$L_s' = 2M^2 C_s \omega_o^2 \frac{\left(1+\frac{L}{4L_p}\right)^2}{1+\frac{M^2}{2L_pL_s}} \tag{3.1}$$

$$C_s' = \frac{L_s}{2M^2\omega_o^2}\left(\frac{1+\frac{M^2}{2L_pL_s}}{1+\frac{L}{4L_p}}\right)^2 \tag{3.2}$$

$$L' = \left(2+\frac{L}{2L_p}\right)\frac{L}{2} - L_s' \tag{3.3}$$

$$L_p' = 2L_p + \frac{L}{2} \tag{3.4}$$

The series and shunt impedances ($Z_s$ and $Z_p$, respectively) of the resulting $\pi$-circuit are:

$$Z_s = j\omega\left(L' + \frac{L_s'}{(1-\omega^2 L_s' C_s')}\right) \tag{3.5}$$

$$Z_p = j\omega \frac{L_p'}{1-\omega^2 L_p' \frac{C}{2}} \tag{3.6}$$

whose sign varies depending on the frequency range. Therefore, at those frequencies where $\chi_s$<0 and $\chi_p$>0, left handed propagation arises. The opposite situation ($\chi_s$>0 and $\chi_p$<0) occurs at higher frequencies, giving rise to a right-handed transmission band. This composite behaviour is studied later in detail for CSRR based structures.

The dispersion relation of the line can be obtained as:

$$\cos\beta l = 1 + \frac{Z_s}{Z_p} \tag{3.7}$$

resulting:

$$\cos\beta l = 1 + \left(L' + \frac{L_s'}{(1-\omega^2 L_s' C_s')}\right)\frac{\left(1-\omega^2 L_p' \frac{C}{2}\right)}{L_p'} \tag{3.8}$$

Moreover, the characteristic (or Bloch) impedance can be calculated as [38]:

$$Z_0 = \sqrt{\frac{Z_s Z_p^2}{2Z_p + Z_s}} \tag{3.9}$$

The frequency response and the dispersion diagram of such a transmission line are depicted in Fig.3.3(c). As can be seen, the structure brings about a transmission band preceded by a transmission zero. In the dispersion diagram, the magnitude of the phase is represented. The negative derivative (entailing a negative group velocity) indicates that the sign of the phase is actually negative. The sign of the propagation constant is, in consequence, negative; in other words: the transmission band is left-handed.

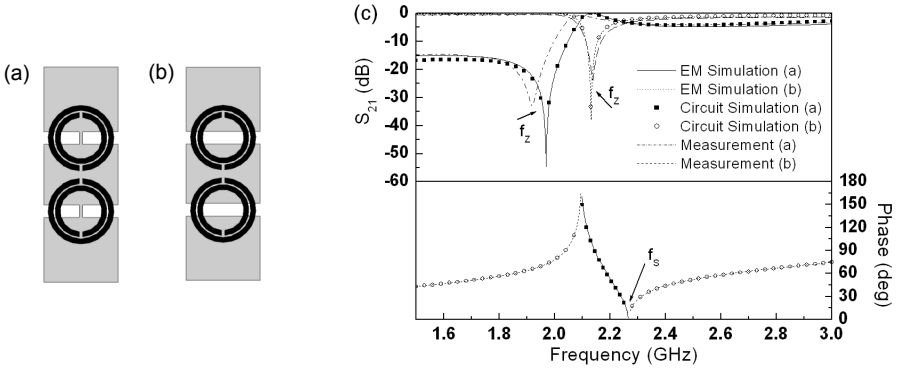


**Fig.3.3.** Layouts of a CPW loaded with SRRs and metallic strips (a) and only SRRs (b). Metallic parts are depicted in grey for the top layer (CPW and strips) and in black for the bottom layer (SRRs) of the substrate. (c) Simulated and measured insertion losses for the structures depicted in (a) and (b) and dispersion diagram for the structure (a). The right handed band of the structure shown in (a) is above 3GHz. Figures obtained from [55].

On the other hand, when a coplanar waveguide is loaded just with SRRs (Fig.3.3(b)), although the series reactance is capacitive around the resonance of the SRRs ($f_z$ for the (b) structure in Fig.3.3(c)), the shunt reactance is always capacitive. As a result, the transmission line is transparent, except about the resonance of the SRR, $f_z$ [58]. The high values of the characteristic impedance and the negative values of the effective permeability just above $f_z$ give rise to a frequency range where transmission is not allowed.

As mentioned above, resonant-type artificial transmission lines can also be implemented with complementary split-ring resonators (CSRRs). These resonators can be excited by an axial time-varying electric field. In order to ensure such excitation, CSRRs are generally etched on the ground plane of a microstrip line. The CSRRs themselves provide negative values of the effective permittivity, so if they are used alone as loading elements, the structure rejects the signal around the resonance frequency of the resonators [9]. Therefore, if backward propagation is intended, the addition of a second element providing negative $\mu$ (or negative $\chi_s$) is necessary [10]. This element can be a capacitive gap etched on the microstrip line just above the resonator, as Fig.3.4(a) shows. Since its origin, this CSRR-based metamaterial transmission line has been exhaustively studied and widely applied in microwave device design, what constitutes an important part of this Thesis. Other complementary resonators can also be applied in place of CSRRs. This allows further miniaturisation when electrically smaller resonators, like spiral resonators (SRs), for example, are used.

The equivalent circuit model is shown in Fig.3.4(b). In this circuit the rings are modelled by the resonant tank formed by $L_c$ and $C_c$, electrically coupled to the line through the capacitance $C$. $L$ represents the line inductance, whereas the gap capacitance is modelled by $C_g$ (and also $C$ as is explained below). Nevertheless, if $L$ is sufficiently small to ensure that the resonance frequency of the series branch is far enough from the CSRR resonance, the line inductance can be disregarded, since in the left-handed band its effects are negligible. This strategy was followed from Article A to Article D in order to simplify the circuit analysis and calculations.

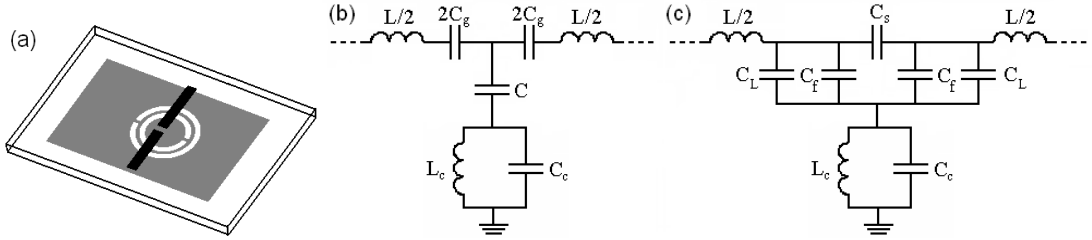


**Fig.3.4.** (a) Scheme of a unit cell of a CSRR-based resonant-type metamaterial transmission line. CSRRs are etched on the ground plane (in grey) of a microstrip line just below the capacitive gaps etched on the signal strip (black). (b) Equivalent T-circuit model of the structure shown in (a). (c) Recently-proposed improved circuit model for the structure shown in (a). Figures (b) and (c) obtained from [42].

This circuit model provides a good description of the structure, as has been widely reported [9,19]. However, a new model (Fig.3.4(c)), which provides a better description of the physical behaviour of the structure has been recently proposed. This new model is able to explain the important variation observed in the coupling capacitance $C$ when a capacitive gap is present or not. In fact, the addition of a capacitive gap does enhance the capacitance to ground, since a fringing capacitance appears, but it does not involve such an important increment as it is in practice observed. The improved model takes into account this fringing capacitance, modelling the gap as a $\pi$-circuit formed by the series capacitance $C_s$ and two shunt fringing capacitances, $C_f$. The line capacitance, $C_L$, and $C_f$ form the parallel capacitance $C_{par}$ (3.10). The new circuit model, can be transformed into the older one by means of the expressions (3.10) to (3.12), as reported in **Article J**.

$$C_{par} = C_f + C_L \tag{3.10}$$

$$2C_g = 2C_s + C_{par} \tag{3.11}$$

$$C = \frac{C_{par}(2C_s + C_{par})}{C_s} \tag{3.12}$$

The inspection of the preceding equations shows that both, $C_g$ and $C$, depend on $C_s$ and $C_{par}$. As a result, any change on the capacitive gap modifies $C$ and $C_g$ and their related parameters [42,56]. In conclusion, we can say that, although the original model is correct and able to accurately reproduce the response or the considered structure, in the improved circuit all parameters have a more realistic physical interpretation.

Nevertheless, the older T-circuit model is still preferred when it comes to analysing the transmission properties of the structure, since the analysis is much simpler. This model has the following series and shunt impedances:

$$Z_s = j\omega\frac{L}{2} + \frac{1}{j\omega 2C_g} = \frac{(1-\omega^2 C_g L)}{j\omega 2C_g} \tag{3.13}$$

$$Z_p = \frac{1}{j\omega C} + j\omega\frac{L_c}{(1-\omega^2 C_c L_c)} = \frac{1-\omega^2 L_c(C+C_c)}{j\omega C(1-\omega^2 C_c L_c)} \tag{3.14}$$

According to these expressions, the phase of the unit cell can be calculated using (3.7) or (2.19):

$$\cos\beta l = 1 + \frac{C}{C_g}\frac{(1-\omega^2 C_g L)(1-\omega^2 C_c L_c)}{1-\omega^2 L_c(C+C_c)} \tag{3.15}$$

The analysis of these equations allows the identification of several notable frequencies. Two of them are the lower and upper limits of the left-handed transmission band, at which the phase takes the values -180º and 0º, respectively. Observing (3.7), we can notice that $\cos(\beta l)$=-1 if $Z_s$=-2$Z_p$, whereas the zero-phase value can be reached in two different cases: $Z_s$=0 or $Z_p$=∞. These two last frequencies are the series ($\omega_s$) and shunt ($\omega_p$) resonance frequencies:

$$\omega_s = \frac{1}{\sqrt{LC_g}} \tag{3.16}$$

$$\omega_p = \frac{1}{\sqrt{C_c L_c}} \tag{3.17}$$

The minimum of these two frequencies is the upper limit of the left-handed band, while the maximum sets the lower limit for the right-handed band, present at higher frequencies due to the fact that resonant-type transmission lines do also exhibit a composite behaviour (see Fig.3.5). Examining expression (3.14), it is also possible to identify the transmission zero frequency, $\omega_z$, at which $Z_p$=0.

$$\omega_z = \frac{1}{\sqrt{L_c(C+C_c)}} \tag{3.18}$$

Furthermore, the characteristic impedance can be calculated following (2.21) as:

$$Z_0 = \sqrt{Z_s(2Z_p + Z_s)} \tag{3.19}$$

obtaining:

$$Z_0 = \sqrt{\frac{L}{C}\frac{(\omega^2-\omega_s^2)}{\omega^2} + \frac{L}{C_c}\frac{(\omega^2-\omega_s^2)}{(\omega^2-\omega_p^2)} - \frac{L^2}{4}\frac{(\omega^2-\omega_s^2)^2}{\omega^2}} \tag{3.20}$$

The series and shunt reactances, as well as the characteristic impedance, can be represented, allowing the easy identification of the resonance and transmission zero frequencies:

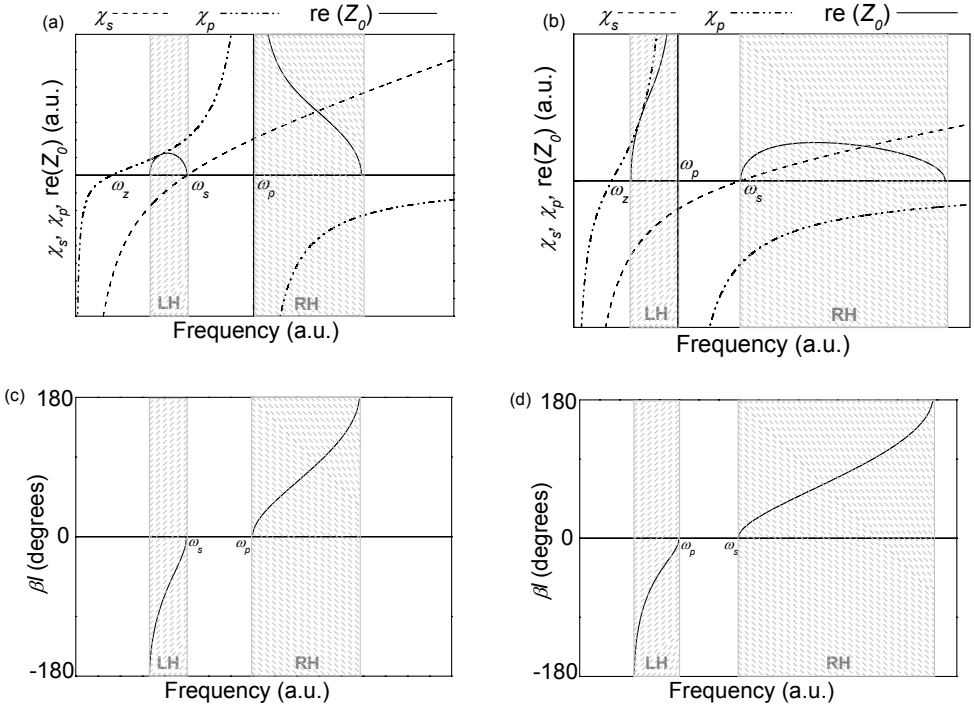


**Fig.3.5.** Representation of the series ($\chi_S$) and shunt ($\chi_p$) reactances, the characteristic impedance ($Z_0$), and the phase ($\beta l$) for a unit cell like the one represented in Fig.3.4. Two different cases have been considered: in (a) and (c) $\omega_s<\omega_p$, whereas in (b) and (d) $\omega_s>\omega_p$. The left- and right-handed bands have been marked, as well as the notable frequencies $\omega_s$, $\omega_p$ and $\omega_z$. In both cases the LH band appears below the RH band.

In addition to the reactances, Fig.3.5 shows the variation of the phase in the transmission bands (graphs (c) and (d)), where both, $\beta$ and $Z_0$, are real. The representation of the phase allows to clearly identify the LH and RH bands, where $\beta$ takes negative and positive values, respectively. Moreover, graphs (a) and (b) allow to verify that in the LH transmission bands, $\chi_s<0$ and $\chi_p>0$, whereas in the RH transmission bands $\chi_p<0$ and $\chi_s>0$. As can be seen, the characteristic impedance has a different behaviour depending on whether $\omega_s<\omega_p$ or vice versa. Given that the shunt impedance, $Z_p$, diverges at its resonance, it causes the divergence of the characteristic impedance as well. Consequently, in the LH band, $Z_0$ can either vary from zero to infinity (figure Fig.3.5(b)), or grow from zero to a maximum value to, next, diminish up to zero Fig.3.5(a). It depends on whether the upper limit of the band is $\omega_p$ or $\omega_s$, respectively. The most common case is the first one ($\omega_p<\omega_s$), since, normally, the required values for $L$ and $C_g$ to obtain very low resonance frequencies for the series branch result quite high for their practical implementation. The identification of different notable frequencies allows the use of a parameter extraction method to obtain the values of the circuit model elements describing the behaviour of the structure. The method will be described in section 3.2.3.

The graphs in Fig.3.5 evidence the composite behaviour of these resonant-type metamaterial transmission lines [59]. Above the left-handed band and after a frequency gap where propagation is forbidden, a second transmission band with right-handed characteristics appears. As occurred in the case of the CL-loaded transmission lines (section 2.4.2), the resonant-type artificial transmission lines can be designed to be balanced by forcing $\omega_p$ and $\omega_s$ to be equal. Balanced transmission lines exhibit, therefore, a continuous transition between both bands, giving rise to a wide transmission band with left- and right-handed characteristics depending on the frequency range. Resonant-type balanced transmission lines were presented

and studied for the first time in **Article E**, demonstrating that broadband characteristics were also possible for resonant-type artificial transmission lines and opening the door to broadband applications for this kind of lines. Resonant-type metamaterial balanced lines are applied in wide band filter design in Article F and Article G (these filters will be delved into in section 4.2.3), among others [60,61]. Article F studies balanced transmission lines based on the purely resonant and the hybrid approach, which is presented in section 3.1.2.

The propagation characteristics of CSRR-based balanced metamaterial transmission lines are studied in Article E on the basis of the equivalent circuit model, as well as electromagnetic simulations and experimental results. The analysis of the T-circuit modelling the structure provides the equations for the phase shift and the characteristic impedance particularised to the balanced case (equations (7) and (8) in Article E), which are expressed in terms of the transition frequency $\omega_0=\omega_p=\omega_s$. The series and shunt reactances are depicted, together with the characteristic impedance ($Z_B$ in the article), in the figure 2 in the article. The left- and the right-handed bands are marked and it can be verified that, as expected, in the LH zone the series impedance is capacitive whereas the shunt impedance is inductive. The inspection of the expression and the depiction of the characteristic impedance reveal a peculiarity of these structures regarding the position of the maximum of $Z_0$ ($Z_{0max}$). Although in LC-loaded balanced transmission lines $Z_{0max}$ is located at the transition frequency [37], in the case of the CSRR-based balanced lines the maximum value of the impedance is reached above $f_0$. If the circuit models of both transmission lines are compared, it can be seen that the only difference is the presence of the capacitance $C$ in the CSRR-based circuit model. Besides originating the transmission zero, this capacitance causes the displacement of the impedance maximum [5]. Otherwise, both circuits are essentially the same. Resonant-type balanced transmission lines do also exhibit at the transition frequency infinite phase velocity and finite and positive group velocity.

Taking into account the behaviour of $Z_0$ within the band (figure 2 in Article E), if the impedance of the structure is properly tailored, balanced lines offer the possibility of obtaining impedance values close to 50Ω over rather wide frequency ranges. If the maximum is set close over 50Ω, the structure will present three reflexion zeros: two of them at those frequencies where $Z_0$=50Ω and one more at the transition frequency, where the phase shift ($\phi$ in the article) is zero. Furthermore, if the impedance is flat enough between the two 50Ω-frequencies, the matching to the ports can be good enough to provide an excellent pass band where insertion losses are very close to 0dB (see Figure 5 in the article). Figures 4 and 5 in the article show simulation and measurement results for the dispersion relation and the frequency response of the structure shown in figure 3. The designed structure is quasi-balanced and exhibits a transition frequency around 1GHz. The frequency response shows a wide transmission band with a very low measured level of losses.

### 3.1.2 Hybrid Approach

In 2006, a new approach based on CSRRs was presented [62]. The new structure (Fig.3.6(a)), known as hybrid approach, consists in the addition of a shunt inductance to the previous structures combining CSRRs and capacitive gaps in order to obtain new propagation characteristics. The additional element contributes to obtain a negative value of $\varepsilon$ ($\chi_p$>0), increases design flexibility and provides a transmission zero above the left-handed transmission band Fig.3.6(c). This transmission zero can be especially useful in filter design, since it can be used to achieve a symmetric response improving the rejection above the transmission band. In fact, the hybrid approach has been applied in some of the works included in this Thesis (Article F , Article I and Article K), among others [62].

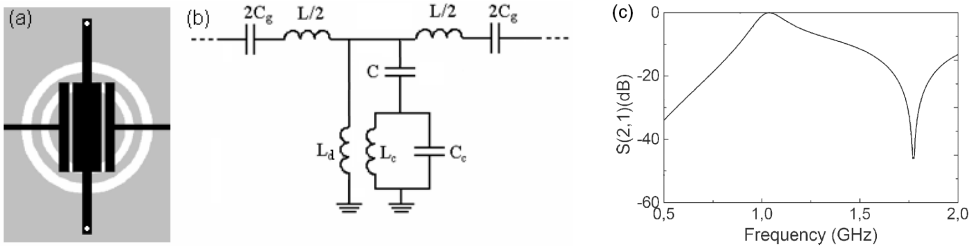


**Fig.3.6.** (a) Layout of a CSRR-based hybrid unit cell. Metallic parts are depicted in black for the top layer and in grey for the bottom layer of the substrate. Vias connecting the inductive stubs to ground are depicted in white. (b) Equivalent circuit model of the structure shown in (a). (c) Typical frequency response of a hybrid structure. A transmission zero is present above the main transmission band, with left-handed characteristics. Figures extracted from [62].

The equivalent circuit model proposed in [62] is shown in Fig.3.6(b). This model is, in general, able to describe the response of the considered structure at the frequency range of interest. It does not predict, however, a transmission zero, which is present below the main transmission band and, in most of the occasions, is neither visible nor exploited, given that it is normally at very low frequencies and hidden by the floor noise in measurements. This transmission zero is, however utilized in a recent work (Article K) to provide a high rejection level below the main transmission band in the design of narrow band pass filters. This makes necessary to find a new model able to provide a complete description of the structure. Although, in the moment, it has not been found yet, work is in progress in order to achieve it. Nevertheless, it should probably include additional elements taking into account different couplings, which would complicate the circuit too much to realize a simple and illustrative analysis. This analysis will be, therefore, carried out below on the basis of the firstly proposed circuit model.

We can, thus, carry out an analysis on the simplest model, which can give us an overall idea about the behaviour of the structure. This model is studied in Article F and Article I for the balanced and the unbalanced cases, respectively. In Article I the model is actually slightly modified in order to properly describe the structure, which differs from the one in Fig.3.6(a) (this new structure is described in section 3.1.3). As can be seen in Fig.3.6, the central stubs, shunt-connected by means of vias, are modelled in the circuit by means of the shunt inductance $L_d$. Whereas the shunt impedance is modified (3.22), the series impedance remains the same as in the purely resonant approach (3.21) and, thus, the series branch resonance is again given by (3.16). Besides the transmission zero, $\omega_z$,(3.23) the new element provides a second resonance frequency for the shunt branch. The two resonances are given by the expressions (3.24) and (3.25), where $\omega_r$ is the resonance frequency of the resonators ((3.26)).

$$Z_s = j\omega\frac{L}{2} + \frac{1}{j\omega 2C_g} = \frac{(1-\omega^2 C_g L)}{j\omega 2C_g} \tag{3.21}$$

$$Z_p = \left[\frac{1}{j\omega L_d} + \frac{1-\omega^2 L_c(C+C_c)}{j\omega C(1-\omega^2 C_c L_c)}\right]^{-1} \tag{3.22}$$

$$\omega_z = \frac{1}{\sqrt{L_c(C+C_c)}} \tag{3.23}$$

$$\omega_{pL} = \sqrt{\frac{\omega_r^2\left(1+L_d C\omega_z^2\right) - \sqrt{\omega_r^4\left(1+L_d C\omega_z^2\left(1+L_d C\omega_z^2\right)\right) - 4L_d C\omega_z^4\omega_r^2}}{2L_d C\omega_z^2}} \tag{3.24}$$

$$\omega_{pH} = \sqrt{\frac{\omega_r^2\left(1+L_dC\omega_z^2\right)+\sqrt{\omega_r^4\left(1+L_dC\omega_z^2\left(1+L_dC\omega_z^2\right)\right)-4L_dC\omega_z^4\omega_r^2}}{2L_dC\omega_z^2}} \qquad (3.25)$$

$$\omega_r = \frac{1}{\sqrt{C_cL_c}} \qquad (3.26)$$

This fact allows diverse combinations for the different notable frequencies and several responses. Some of the possible combinations are shown in Fig.3.7 and Fig.3.8, in which the position of the series resonance frequency changes with respect to the transmission zero and the shunt resonance frequencies.

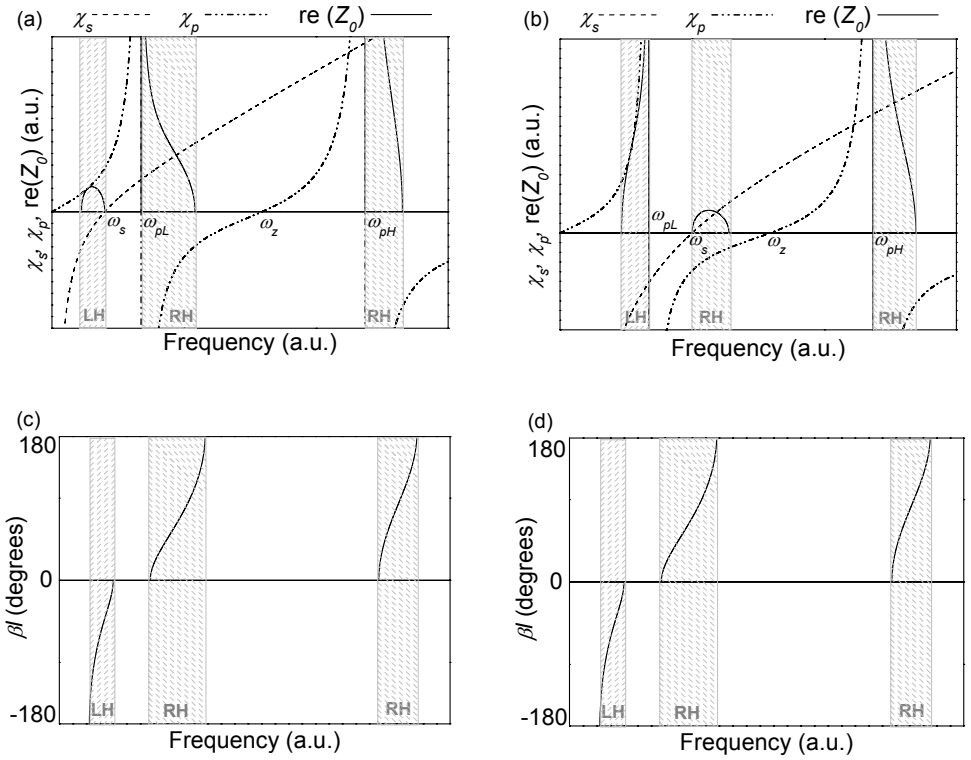


**Fig.3.7.** Representation of the series ($\chi_S$) and shunt ($\chi_p$) reactances, the characteristic impedance ($Z_0$), and the phase ($\beta l$) for a unit cell like the one represented in Fig.3.6. Two different cases have been considered: in (a) and (c) $\omega_s<\omega_{pL}<\omega_z<\omega_{pH}$, whereas in (b) and (d) $\omega_{pL}<\omega_s<\omega_z<\omega_{pH}$. The left- and right-handed bands have been marked, as well as the notable frequencies $\omega_s$, $\omega_{pL}$, $\omega_{pH}$ and $\omega_z$. In both cases the LH band appears below the RH bands.

Both figures show the characteristic impedance with the series and shunt reactances (figures (a) and (b)) as well as the dispersion diagrams ((c) and (d)). In Fig.3.7, the cases in which $\omega_s<\omega_{pL}<\omega_z<\omega_{pH}$ and $\omega_{pL}<\omega_s<\omega_z<\omega_{pH}$ are represented. The cases $\omega_{pL}<\omega_z<\omega_s<\omega_{pH}$ and $\omega_{pL}<\omega_z<\omega_{pH}<\omega_s$ are depicted in Fig.3.8. As occurred in the purely resonant approach, the series resonance frequency is usually above the first shunt resonance $\omega_{pL}$, since the contrary case requires quite high values of the series branch elements. As the graphs illustrate, the different combinations give rise to diverse distributions of the left- and right-handed transmission bands and different behaviours of the characteristic impedance.

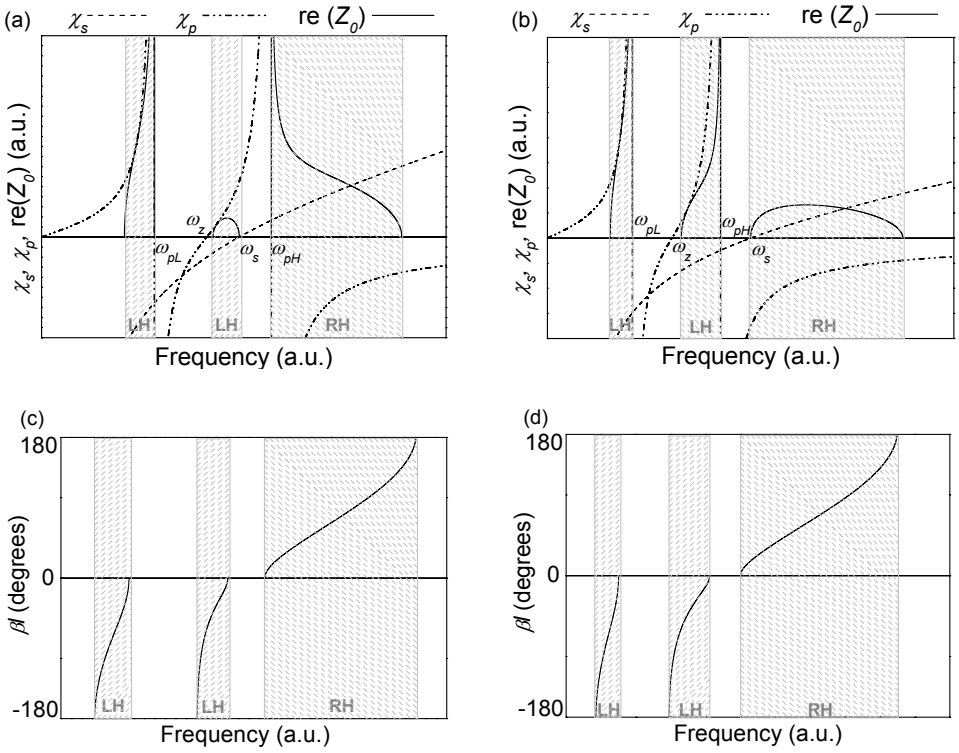


**Fig.3.8.** Representation of the series ($\chi_S$) and shunt ($\chi_P$) reactances, the characteristic impedance ($Z_0$), and the phase ($\beta l$) for a unit cell like the one represented in Fig.3.6. Two different cases have been considered: in (a) and (c) $\omega_{pL}<\omega_z<\omega_s<\omega_{pH}$, whereas in (b) and (d) $\omega_{pL}<\omega_z<\omega_{pH}<\omega_s$. The left- and right-handed bands have been marked, as well as the notable frequencies $\omega_s$, $\omega_{pL}$, $\omega_{pH}$ and $\omega_z$. In both cases the LH bands appear below the RH band.

Obviously, hybrid cells do also exhibit a composite behaviour and can, therefore, be balanced. This fact is explained in **Article F**, where balanced transmission lines based on the purely resonant and the hybrid approach are studied and applied in the design of ultra wide band (UWB) filters. In the section II of the article, the differences between purely resonant and hybrid balanced structures are pointed out. As is stated in the text, the two resonance frequencies of the shunt branch give rise to two possible ways to obtain a balanced structure. The resonance frequency of the series branch can be forced to be equal to either the first, or the second shunt branch resonance frequency (given by the expressions (3.24) and (3.25)). Both possibilities are illustrated in figure 2 in Article F, where the series and shunt reactances, together with the characteristic impedance, are depicted in the figures (a) and (b). The dispersion diagrams are represented as well (figures (c) and (d)), showing the left- ($\beta$<0) and right-handed ($\beta$>0) character of the different allowed bands. Figure 6(a) in the article shows an example of the frequency response of a balanced hybrid cell, which in this case corresponds to the unit cell depicted in the figure 1(b) of the article. Figure 6(b) should show the phase of the unit cell, although due to a mistake, it is figure 8, which has been repeated. The phase of the $S_{21}$ corresponding with the considered unit cell is, therefore, included here in Fig.3.9. As occurred in the purely resonant case, the balanced hybrid transmission line shows a wide and continuous transmission band in which left- and right-handed characteristics are possible. The backward and forward propagation frequency ranges can be identified as the regions where the phase has positive and negative sign, respectively.

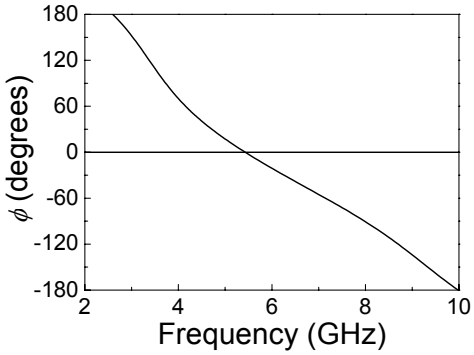


**Fig.3.9.** Phase of the $S_{21}$ for the hybrid unit cell considered in Article F. The frequency ranges where propagation is left- and right-handed can be identified.

### 3.1.3 CRLH TLs with CSRRs etched on the Signal Strip

Up to now, different types of CSRR-based structures have been presented and in all cases the resonators are etched on the ground plane. They offer very interesting propagation characteristics and have been shown to be practical for different applications. However, they may not be suitable for those applications in which the ground plane must lie on a metallic surface, since the CSRRs would be disabled. Nevertheless, this problem can be avoided if the resonators are not located on the ground plane. One possible solution is to etch them on the signal strip itself, as exposed in Article H and Article I.

This new kind of CSRR-based metamaterial transmission lines was firstly proposed in **Article H**. As Fig.2(a) in the article shows, the new structure is purely resonant and consists in a microstrip line where CSRR and capacitive gaps are etched. The new topology requires the location of two capacitive gaps at both sides of the resonator, since placing the gap in the central position above the CSRR is not possible anymore. Moreover, the circuit model must also be modified in order to take into account the presence of the lateral gaps. As Fig.2(b) in the article shows, the new circuit model includes two fringing capacitances, $C_f$, to properly model each of the capacitive gaps. The article shows the electrical and electromagnetic simulation of one of these structures in the figure 3. The frequency response is very similar to that of previous structures based on CSRR and gaps. It exhibits a transmission zero below the left-handed transmission band, which in this case is rather narrow, due to the fact that the coupling between the line and the rings is weaker than in previous structures. The left-handed behaviour of the structure is corroborated in two different ways in the article. The first and conventional one is the study of the phase, $\phi$, in the transmission band, which is shown in Fig.3 (b) and, as expected, is negative. The second one is related with the variation of the wavelength of the guided wave within the transmission band. Contrary to forward propagating structures, in left-handed media the wavelength increases with frequency, as a consequence of the phase velocity reversal. This fact is confirmed in Article H with the simulation of a 10-stage structure at different frequencies within the transmission band. The study of the current diagrams shown in Fig.6 verifies the increment of the guided wavelength with the frequency, what confirms backward propagation in the structure.

The new topology requires a specific parameter extraction method, as section III in the article expounds. The extraction is performed in two steps. On the one hand, the structure without gaps is simulated and the involved parameters $L$, $C$, $C_c$, $L_c$ are extracted following the procedure described in section 3.2.3. On the other hand, the gap is simulated separately and the capacitances $C_g$ and $C_f$ are obtained from the S-parameters by means of the expressions (1) indicated in the article (the negative sign is missing in the first of the two expressions in the article). Both structures can be treated independently thanks to the fact that, in contrast to previous structures, the gaps are not coupled to the CSRR. Table I in Article H shows the extracted parameter values, which provide the electrical simulation depicted in Fig.3. The figure evidences the good fitting between the electrical and the electromagnetic simulations, validating the proposed model. In order to improve frequency selectivity, a structure formed by three unit

cells was designed and fabricated. The simulated and measured responses are depicted in Fig.5, showing the good frequency selectivity of the structure.

A second structure based on CSRRs etched on the signal strip is proposed in **Article I**. In this case, the hybrid approach is applied to design a new structure adding a shunt inductive stub to the previously described structure. The layout of one example structure can be seen in figure 2(a) in the article, together with the proposed circuit model (figure (b)). With the addition of the new element, losses and bandwidth are improved with respect to the purely resonant structure and, moreover, design flexibility is increased. As occurred in the case of the hybrid structures in which the resonators were etched on the ground plane (described in section 3.1.2), this new hybrid structure presents a transmission zero above the main transmission band, which is left-handed. The comparison between the responses of two cells with CSRRs etched on the signal strip can be seen in figure 3 in the article. One of them is a purely resonant cell, whereas the second one is a hybrid cell. Both responses are centred around 2.25 GHz. The figure shows the improvement, regarding bandwidth and losses, achieved with the new structure with respect to the purely resonant one. Depending on whether the specific application requires a sharp cut-off above or below the main transmission band, either the resonant or the hybrid structure may be more suitable.

In the same way as in the purely resonant structures, new elements must be added to the previous hybrid circuit model in order to properly describe the behaviour of the new structure. Figure 2(b) in the article shows the proposed circuit model, in which four fringing capacitances have been included to take into account the effects of the lateral gaps. Consequently, the circuit models of the resonant and hybrid structure only differ on the presence of the shunt inductance $L_d$, which is responsible of the presence of the transmission zero above the main transmission band. A parameter extraction method can be applied to the structure in order to validate the circuit model. The method is explained in section 3.2.3.

As occurs with the rest of the structures which have been previously described, the characteristics of these transmission lines can be tailored to exhibit the desired values of phase and impedance at a certain operating frequency. This allows the synthesis of several kinds of devices. As an example, a power divider and a narrow band pass filter are shown in Article I. Sections 4.1.1 and 4.2.2.2, respectively will deal with these application examples.

## 3.2 Synthesis of Resonant-type Metamaterial Transmission Lines

The following sections delve into the dependence of the geometrical parameters of resonant-type metamaterial structures and how this influence can be exploited to synthesize transmission lines with controlled characteristics. A mathematical study on the feasibility of such structures on the basis of their circuit model is also exposed. Finally, a parameter extraction method which can be applied to different unit cells is included in the last section.

### 3.2.1 Geometrical Parameters

One interesting analysis related to this kind of transmission lines is the study of the influence of the geometrical parameters of such structures on their transmission characteristics. Devoted to this purpose, Article A considers the unit cell based on CSRRs and capacitive gaps and, besides performing a detailed analysis of the structure and its circuit model, it studies the effects of modifying some geometrical parameters of the structure, like the gap distance, $g$, the substrate thickness, $h$, and the line width, $W$. Furthermore, a parametric analysis of the CSRR dimensions (average radius, $r_0$, inter-ring distance, $d$, and ring width, $c$) and its influence on the circuit parameters of a CSRR-loaded transmission line is carried out in Article J.

In **Article A** several structures were designed varying the parameters under study in order to analyse how these modifications alter the frequency response in the left handed transmission band and to interpret these variations to the light of the circuit model. As has been previously mentioned, the considered circuit model was the simplified version of the T-circuit model, where the line inductance, $L$, is neglected (depicted in Fig.2(b) in Article A). The recent improvements

performed on the circuit model (exposed in section 3.1.1) allow now a more complete interpretation of the changes originated by the structure modifications, although all conclusions in Article A are in accordance with the new circuit model. The simplified model facilitates the calculation of the expressions of different magnitudes, like the characteristic impedance, the dispersion relation or the limit frequencies of the left-handed transmission band (equations (4) to (7) in Article A.). This study can help to identify the geometrical parameters which must be varied when the frequency response or the circuit elemnts must be modified in a certain way.

Figure 8 in the considered article shows the variation in the frequency response when the gap distance is modified. It can be observed that, as the gap distance increases, the lower limit of the band, $f_L$, is shifted towards higher frequencies, whereas the upper limit, $f_H$, remains almost fixed. The article claims the dependence of $f_L$ on the gap capacitance $C_g$ as the motive of the shift; the increment of the gap distance would cause a decrease in $C_g$, what involves the enlargement in $f_L$ (see equation (6) in the article). In this case, the left-handed band finishes at the resonance frequency of the CSRRs (equation (7) in the article), since the resonance of the series branch occurs at higher frequencies. Given that $f_H$ does not depend on $C_g$, no change is expected for this frequency. Taking into account the recently proposed circuit model and how it can be transformed into the old one (expressions (3.10) to (3.12)), it can be verified that a change in $g$ involves, not only a variation of $C_g$, but also (actually mostly) in $C$ [42,56]. When the gap is enlarged, $C_g$ slightly decreases, whereas $C$ experiences a considerable increase. These changes, effectively, involve the modification of $f_L$ in the expected way.

The effect of the variation of the substrate thickness, $h$, was studied in a similar way. Figure 9 in Article A illustrates the influence of $h$ on the bandwidth. In this case, $f_H$ moves towards higher frequencies when a thinner substrate is used. This variation of the resonance frequency of such resonators with the substrate thickness is a known fact [4]. Furthermore, the presence of the transmission line has also an influence on the resonators, which becomes more important as the substrate thickness decreases. On the other hand, the article claims the dependence of $C$ with $h$, what justifies the reduction in $f_L$ when $h$ is decreased. Considering the improved circuit model, it can be seen that the use of thinner substrates indeed involves an important increase in the capacitance $C$, as well as a slight rise in $C_g$, what causes the shift of $f_L$ toward lower frequencies. Consequently, this study confirms that thin substrates can be used for bandwidth enhancement.

The third considered parameter was the line width, $W$. Three different structures were simulated in order to study the effects of this parameter on the transmission. As stated in the article, when the line is widened, an increment in the capacitances $C$ and $C_g$ was expected. The upper limit of the band, however, was supposed to be faintly influenced by these modifications, since the resonance frequency is just slightly altered by the presence of the line and its widening. Taking into account the new model, it is easy to infer that, as in the previous cases, a change in $W$ will affect both, $C_s$ and $C_{par}$. This, effectively, entails the variation of the capacitances $C$ and $C_g$, which causes the diminution of $f_L$ when the line is widened (see figure 10 in Article A).

The structure considered in **Article J** is, as mentioned above, a microstrip transmission line loaded with a CSRR (see figure 1(a) in the article). The analysis of the structure dimensions includes the average radius, $r_0$, the inter-ring distance, $d$, and the ring width, $c$ (depicted in figure 1(a) in the article). No gaps are present in the structure and the series impedance in the considered circuit model is formed, therefore, just by the line inductance, $L$ (see figure 1(b)). The shunt impedance is formed by the resonator elements, $L_c$ and $C_c$, and the capacitance $C$ modelling the coupling between the line and the CSRR. Numerous structures varying the studied parameters were simulated and, by means of a parameter extraction method (section 3.2.3), the circuit model parameters of each structure were calculated.

The first varying parameter considered in the article is the average radius of the resonator, $r_0$. The two other parameters are constant and equal to 0.2mm, whereas $r_0$ is modified from 0.7mm to 8mm. The per-unit-length values of the four circuit elements are represented as a function of the resonator average radius in Fig.2. Despite not having a physical meaning, the magnitudes $L_{pul}$ and $C_{pul}$ are, above a certain value of $r_0$, constant (as expected). Regarding $C_{cpul}$ and $L_{cpul}$, although they saturate above a certain value of $r_0$, for small radius there is a dependence not accounted in the circuit model, which is probably related to the presence of the transmission line above the resonator.

In order to study the effects of varying $c$ and $d$, both parameters were modified in several structures maintaining $r_0$=8mm. With the purpose of reducing the variable number, $c$ was made

equal to *d*, although they varied from 0.05mm to 0.75mm. Figure 3 in the article shows that $C_c$ depends on *c* and *d* more strongly than $L_c$. It is also interesting to see the dependence of the ratio $L_c/C_c$ on the considered parameters (see Fig.4). As can be seen, this ratio varies with *c* and *d*, what can be used to obtain the required value for *c* and *d* once the desired ratio $L_c/C_c$ , determined by the specifications, has been deduced. Finally, once *c* and *d* are known, the resonator radius can be estimated from the absolute values of $C_c$ and $L_c$.

This parametric study can be used, when specific values of the resonator capacitance and inductance are required, for the estimation, in first approximation, of the CSRR dimensions, which can be finally determined through the optimization of the structure.

### 3.2.2 Synthesis

The key electrical characteristics in transmission lines are the phase shift and the characteristic impedance. Artificial transmission lines allow to control these two characteristics rather independently. Articles A and B are devoted to the study of the possibility of imposing desired values of these magnitudes at certain frequencies. Furthermore, Article B and Article D, among others, consider the application of such artificial transmission lines for microwave device design, which will be exposed in chapter 4.

**Article A**, besides studying the influence of different geometrical parameters on the frequency response of purely resonant CSRR-based transmission lines, includes a detailed analysis of the circuit model and the design possibilities offered by the structure. Section 3 studies the possibility of controlling line properties, like the phase or the characteristic impedance, in order to improve the transmission characteristics of the structure. These properties are of special interest due to the fact that they directly affect the impedance matching and ripple. The most desirable behaviour for the impedance would be that it was constant and equal to the reference impedance of the ports (usually 50Ω) along the whole transmission band. Given that, as has been previously exposed, the impedance varies from zero to infinity in the LH band, the most favourable situation is that in which $Z_0$ remains as close to 50Ω as possible within the transmission band. The followed strategy is the imposition of the 50Ω at a frequency as close to the central frequency as possible. By this means, the frequency range where the line impedance is maintained close to the reference impedance is optimized. Regarding the phase and taking into account that multi-cell structures present a number of transmission peaks equal to the number of cells, it is interesting to control the allocation of these peaks within the band. By these means, ripple can be improved if the peaks, where the phase condition is satisfied (equation (9) in the article), are homogeneously distributed along the band (see figure 5 in the article). Such considerations are taken into account in the study in order to find the most suitable configuration to obtain the desired response.

The analysis of the T-circuit is carried out neglecting the line inductance. Once the series inductance, *L*, is ignored, the circuit model is formed by four elements. This enables the imposition of four different conditions to perfectly determine the values of the circuit elements. Two of these conditions can be $f_L$ and $f_H$, so that the limits of the left-handed transmission band are determined. Furthermore, two more requirements, which can be used to improve the transmission in the pass band taking into account the previous considerations, can be imposed. With this intention, the values of the phase and the impedance are set at two different frequencies ($f_1$ and $f_2$) within the band, as is described in Article A. This allows to infer the values of the four circuit elements, which are perfectly determined (equations (11) to (16) in the article). There are, of course, restrictions which must be taken into account, like the fact that the resulting values for the circuit elements must be positive and not extreme values (equations (17) and (18)). Furthermore, equation (19) reveals the fact that the phase 90º cannot be imposed but at a frequency lower than the central frequency of the $f_L$-$f_H$ range. These facts restrain the freedom when it comes to choosing the frequencies and values to be imposed (equation (19)), although the imposition of the four parameters is possible.

Two prototypes were designed, fabricated and characterised for experimental verification. One of them consisted of ten unit cells, whereas the second one was formed by four cells. Figure 6 shows the good agreement between the measured and simulated responses. The 10-cell structure exhibits, as could be expected due to the high number or unit cells, a rather important loss level, which can be improved decreasing the unit cell number (see Fig.7). The

frequency selectivity, however, is better in the longer structure. The good agreement between the electrical and the electromagnetic simulations reveals the fact that the target parameters have been mostly achieved.

In the **Article B**, the possibility of designing transmission lines with the desired phase and impedance at a unique required frequency is studied. The considered structures are purely resonant CSRR-based left-handed transmission lines. In this study, the line inductance is again neglected in the considered circuit model. Given that the circuit under consideration contains four elements, the number of conditions which can be imposed to perfectly determine the values of the circuit elements is also four. The study of the derived equations reveals the possibility of, under certain limits, imposing the limits of the left-handed band ($f_L$ and $f_H$) together with the phase shift ($\phi_c$) and the characteristic impedance ($Z_c$) at the desired operating frequency ($f_c$). Equations (1) to (4) in Article B are the initial expressions, which can be inversed to obtain the values of the elements $C_g$, $L_c$, $C_c$ and $C$ (equations (5) to (8)) as a function of the input parameters. As in the previous case, two aspects must be taken into account in order to choose the input parameters: the circuit elements must take positive values and they must be reasonable in order to be layout implementable. To the light of the obtained expressions, only the capacitance $C$ can be negative, depending on the values of the input parameters. Therefore, in order to ensure that $C>0$, condition (9) must be satisfied. This reduces the possible values for the transmission band limits once the values of the operating frequency and the phase shift have been imposed (see Fig.3 in the article). Moreover, the resulting value for $C$ should not be extreme in order to be implementable. On the other hand, as **Article C** states, an additional aspect must be taken into account. Figure 2 in Article C depicts the variation of the phase shift and the characteristic impedance of a unit cell within the transmission band. As can be seen, in the limits of the band, the phase and the impedance take their extreme values (0º and 180º for the phase shift and 0Ω and infinity for the impedance). As a result, it is difficult to simultaneously obtain for a single unit cell very low phase shift and very low impedance, or vice versa. In spite of these limitations, it is possible to synthesize such artificial transmission lines based on CSRRs and gaps controlling, to a certain extent, phase shift, impedance and bandwidth.

The important variation of the characteristic impedance within the transmission band in such structures enables the design of extreme impedance value transmission lines. Article C includes some design examples of inmitance inverters with impedances varying from 300Ω to 10 Ω. Some of these impedance values are not achievable by means of conventional transmission lines, since they involve extreme dimensions which make them not implementable (the width of a 150Ω microstrip transmission line is 6μm and only few nanometres in the case of $Z_c$=300Ω in the considered substrate with $\varepsilon$=10.2 and $h$=1.27mm). All the designed structures have $\phi$=90º, including the 300Ω inverter. In this case, the required phase shift has been achieved by cascading two unit cells with $\phi$=45º. By this means, the difficulty of obtaining the desired phase shift when the impedance takes very high values is solved. These structures, besides showing smaller dimensions than conventional lines (the length of these artificial transmission lines is usually about half the length of a conventional one) offer the possibility of achieving impedance values which are unrealizable by ordinary means. Figures 4 to 8 in the article show layouts, photographs and characterisation of several structures designed to work as inmitance inverters with different impedances at 1.5GHz. The simulated and measured results show that the design parameters are achieved about the operating frequency, although a small frequency shift, attributable to fabrication tolerances, can be observed in the experimental results. The electromagnetic simulations depicted in figures 4 and 6 were performed using the target impedance value, $Z_c$, as reference port impedance. By these means, the frequency at which $Z_0$=$Z_c$, is satisfied can be easily found by identifying the reflexion zero. On the other hand, the dispersion diagrams allow the identification of the 90º frequency.

Besides these examples, other design options are also possible. Dual-band devices, for example, have been recently developed using different kinds of transmission lines based on complementary resonators. In such devices, phase and impedance are imposed at two different operating frequencies. Additionally, the dispersion diagram of metamaterial transmission lines can be modified in order to improve bandwidth. Baluns [63], power dividers [64] and hybrid couplers [65, 66] are some of the devices which can be designed following these strategies and will be considered in section 4.1.2.

### 3.2.3 Parameter Extraction Method

In the previous section, a technique to obtain the circuit element values providing the desired electrical characteristics is exposed. Once the electrical parameters are determined, they must be translated into the physical dimensions of the layout. This is not a simple challenge given that, up to now, no systematic method has been developed to univocally determine the topology of the structure. Nevertheless, the opposite process is possible and represents an important design tool, since it permits the extraction of the circuit element values from the electromagnetic simulation of a designed structure. Once the parameters are determined, the layout can be properly modified in order to achieve the desired response.

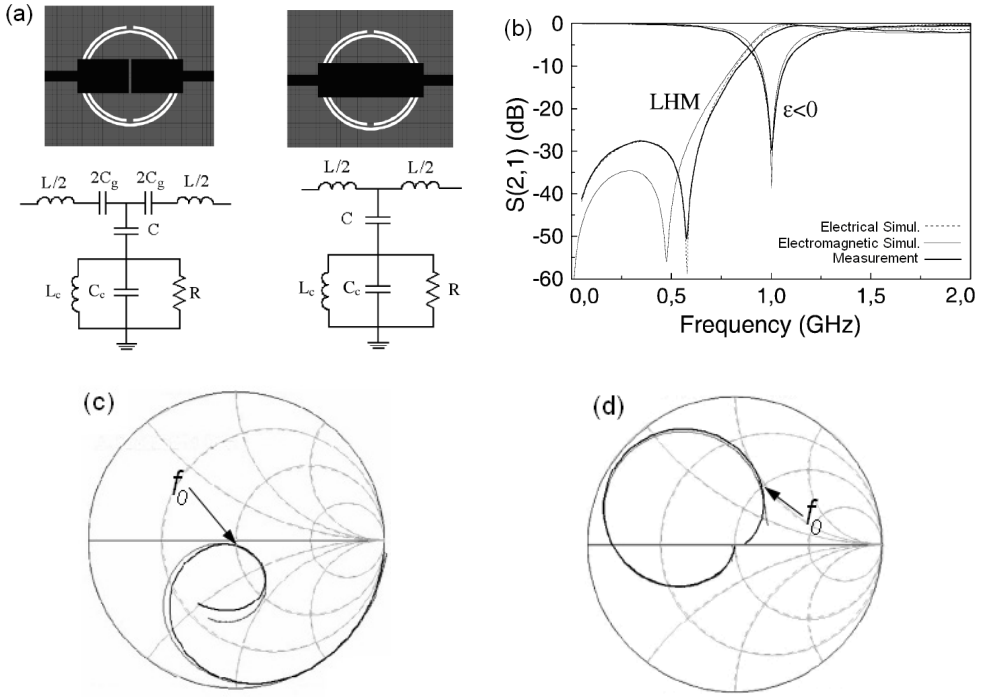


**Fig.10.** (a) Layouts and equivalent circuit models of a double- and single-negative CSRR-based structure (left and right figures, respectively). (b) Simulated and measured frequency responses of the DNG (LHM) and SNG ($\varepsilon$<0) structures. (c) Electrically simulated and measured reflection coefficient of the DNG structure. (d) Electrically simulated and measured reflection coefficient of the SNG structure. Figures extracted from [67].

The parameter extraction method allows the calculation of the circuit parameters describing the response of both, single- and double-negative CSRR-based purely resonant transmission lines [67]. Either their simulated or measured frequency responses permit the easy identification of some notable frequencies, like the transmission zero frequency, $f_z$, (expression (3.18) in section 3.1.1), the CSRR resonance frequency, $f_0$, ($f_p$ in expression (3.17)), at which the shunt branch opens, and the 90º phase shift frequency, at which:

$$Z_s(j\omega_{\pi/2}) = -Z_p(j\omega_{\pi/2}) \tag{3.27}$$

These three frequencies allow the imposition of three different conditions and the calculation of three circuit element values. Nevertheless, additional conditions must still be found to determine the rest of the parameters. At $f_0$, the shunt admittance is zero and the input impedance visible from the ports consists exclusively of the series impedance and the reference impedance of the opposite port (usually 50Ω).

$$Z_{in}(j\omega_0) = 50 + j\chi_s(\omega_0) \tag{3.28}$$

As a result, at this frequency the reflexion coefficient intercepts the unit resistance circle in the Smith Chart (see Fig.10) and the reactive part of the input impedance (formed by $L$, or $C_g$ and $L$, for the SNG and the DNG structure, respectively) can be easily obtained. By this means, the value of $L$ can be simply extracted from the SNG structure. Alternatively, $L$ can be obtained by means of a transmission line calculator. Once the value of $L$ has been determined, the reactance of the input impedance at $f_0$ can be used to obtain $C_g$ for the DNG structure. Regarding losses, which can also be taken into account by means of a resistive element, like $R$ in Fig.10(a), their value can be determined by sweeping $R$ to obtain a good matching between curves. As figures (b), (c) and (d) state, the matching between the curves provided by the fabricated structure and the electrical model is excellent.

Different variants of this parameter extraction method can be applied to similar structures, like those in which the CSRR is etched on the metallic strip described in section 3.1.3. In the case of the purely resonant structure (see **Article H**), the extraction is carried out in a very similar way as the previously described. The SNG structure (the structure with no gaps) is used to obtain all parameters except the capacitances related to the gaps, $C_g$ and $C_f$. In order to obtain these parameters, the isolated gap is simulated and, by means of the expressions (1) in Article H, both capacitance values are extracted (as has been previously indicated, a negative sign is missing in the first one). The rest of the parameters are obtained from the transmission zero frequency, the reactance at $f_0$ and the 90º frequency.

A different version can be applied to hybrid structures with CSRRs etched on the strip (see section 3 in **Article I**). In these structures, the gap capacitances are again obtained from the simulation of the isolated gap as in the previous structures. Regarding the rest of the parameters, which are obtained from the structure without gaps, given that the number of circuit elements is higher, new conditions must be imposed. In this case, provided the shunt impedance exhibits two resonance frequencies (expression (5)), both resonances ($f_{0+}$ and $f_{0-}$ in the article) can be used in the extraction method, together with the usual conditions ($f_z$, $f_{90}$ and the reactance at the resonance). The resulting parameters provide a good matching between the electromagnetic and the electrical simulation, as figure 4 in Article I shows. Among all the extracted parameters, only $C$ must be slightly swept in order to improve the matching due to the fact that this parameter is faintly affected by the presence of the capacitive gaps.

SRR-based transmission lines do also admit the application of a parameter extraction method, which must be adapted to the particular characteristics of these transmission lines. Its application provides excellent results [68] as in the case of the CSRR-based structures.

# 4 Applications

*Since the appearance of the first resonant-type metamaterial transmission lines their applications to microwave device design have been numerous. On the basis of their controllable characteristics, resonant-type metamaterial transmission lines have been applied in the design of many different devices showing compact dimensions, improved performance, multi-band operation, and tunability, among other interesting characteristics. In this chapter, many of these applications are gathered, showing the versatility of these novel structures.*

## 4.1 Device Miniaturisation

The controllability of phase shift and impedance in resonant-type metamaterial transmission lines allows, as has been previously stated, the design of transmission lines with the desired values of both magnitudes at a chosen frequency. These lines can, therefore, be applied in the design of microwave devices requiring specific values of both characteristics. Some of these devices can be power dividers, hybrid couplers, baluns and, of course, filters. The compact dimensions of these artificial lines allow to achieve an important level of miniaturisation with respect to conventional devices. Additionally, the controllability over their characteristics offers the possibility of tailoring the dispersion diagram in order to improve device performance.

### 4.1.1 Power Dividers

Article B, Article D and Article I are devoted to the synthesis of power dividers applying CSRR-based artificial transmission lines. Besides studying the synthesis of artificial transmission lines based on CSRRs, **Article B** applies such lines in the design of power dividers (section 3 in the article). Such devices can be implemented using two different topologies (see Fig.5 in the article). The first of them includes two inmitance inverters, whereas the second one includes only one. In both cases, the impedance of the inmitance inverters ($Z_B$ in the article) must be such that the input impedance seen from the input port, $Z_{in}$, is the reference impedance of the ports ($Z_0$ in the article), which is usually 50Ω. In the case of two-output dividers, $Z_{in}$=50Ω can be achieved either using two 70.71Ω output inverters or employing a 35.35Ω inverter as input line. Both kinds of dividers are implemented in the article, together with a four-output divider including a 25Ω input inverter.

The first of the dividers is shown in Fig.6, which includes the layout and the photographs of the device. In comparison with a conventional divider, the “metadivider” is about 50% smaller in area. The synthesis of the inverters was carried out following the procedure described in the section 3.2.2 (and in section 2 in Article B). In this case, the operating frequency was set to 1.5GHz, at which $\phi_c$=90º and $Z_B$=70.71Ω. After choosing the limits of the transmission band ($f_L$,$f_H$) providing reasonable values of the circuit parameters, the values of the circuit elements can be calculated. Once the circuit parameters are known, the layout of the structure can be obtained. The frequency response of the designed 70.71Ω inverters is shown in Fig.4 in the article. The simulation has been performed using 70.71Ω ports. By this means, the identification of the frequency at which $Z_B$=70.71Ω is as simple as finding the reflection zero frequency. From this response, the values of the circuit parameters can be extracted following the method exposed in section 3.2.3. The extracted parameters are in general close to the previously calculated ones, except for the series capacitance, $C_g$. This fact is not surprising due to the fact that, in the calculation of the parameters, the series inductance has been neglected and, to obtain an accurate value of $C_g$ it should be taken into account. The response provided by the extracted parameters depicted in figure 4 perfectly matches the electromagnetic simulation of the structure. Figure 7 in the article shows the simulated and measured scattering parameters of the whole device, which can be compared with the performance of a conventional device implemented in the same substrate. Measured insertion losses at the operating frequency are

very close to the ideal value (-3dB) in such devices. The designed component is compact and suitable for narrow band applications.

As was seen in Article A, bandwidth can be enhanced using thin substrates. This strategy was applied in **Article D**, to design a new power divider formed by two 70.71Ω inmitance inverters using a 0.127mm-thick substrate. Its frequency response is compared in Figure 6 with the response of the previously described divider, implemented in a thicker ($h$=1.27mm) substrate with the same permittivity ($\varepsilon_r$=10.2). A notable bandwidth enhancement can be appreciated, as well as a good agreement between the simulated and measured responses.

**Article B** also includes a power divider implemented by means of an only 35.35Ω inmitance inverter as input line (shown in figure 8 in the article). The inverter has approximately half the length of a conventional one, so the achieved size reduction is considerable. The simulated and measured scattering parameters are shown below in Fig.4.1 (figure 9 in Article B is mistaken)

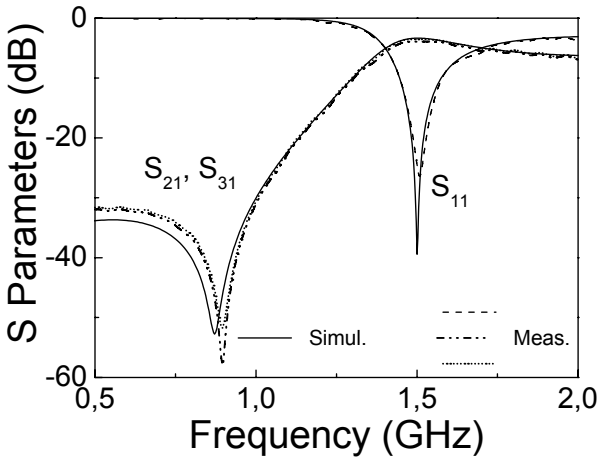


**Fig.4.1.** Simulated and measured S-parameters of the power divider implemented using a metamaterial 35.35Ω inmitance inverter.

The measured insertion losses, despite being slightly worse than in the previous examples, are still close to the -3 dB ideal value. As well as in the previous type, thin substrates could be employed to increase bandwidth in this kind of power dividers.

A third power divider, this time including four outputs, is also shown in Article B. This divider is designed following the topology shown in figure 5(b) and contains a 25Ω inverter. The designed inverter (shown in Fig.10) is more than two times shorter than a conventional one, involving a significant size reduction on the final device. As occurred in the previous cases, the experimental and simulated results (shown in Fig.11 in the article) reveal a very low insertion loss level at the operating frequency, which is in this case close to -6dB, as expected for such a four-output power divider.

A different unit cell is employed in **Article I** to design a two-output power divider including two 70.71Ω inverters (see figure 6(a) in Article I). In this case the inverters are formed by hybrid structures with CSRRs etched on the signal strip as the ones described in section 3.1.3. They are microstrip structures combining CSRRs etched on the metallic strip with lateral gaps and a shunt connected inductive stub. The frequency response and the dispersion diagram of the 90º transmission line are shown in figure 5(a) and (b), respectively, where the achievement of the target values of impedance and phase at the operating frequency ($f_0$=1.5GHz) can be confirmed. The performance of the power divider can be observed in Fig.6 (b). The measured and simulated transmission and reflection of the device are compared with the simulated response of a conventional power divider implemented in the same substrate. The "metadivider", despite having a narrower bandwidth, shows around the operating frequency a low insertion loss level, which is close to the ideal value. With respect to other CSRR-based dividers, the one presented in Article I presents the advantage of leaving unaltered the ground plane, besides having a smaller size. The bandwidth is, however, narrower than in the previously presented devices, what makes this later kind of power divider suitable for narrow band applications were the ground plane must be left intact. Article I presents, additionally, a narrow band pass filter using hybrid transmission lines with CSRRs etched on the strip. Such

components will be considered in following sections devoted to metamaterial filters (section 4.2).

These five examples of power dividers demonstrate the viability of CSRR-based metamaterial transmission lines for power divider design. In light of the results, these devices are suitable for narrow band applications where low losses and compactness are key issues. Furthermore, no lumped elements are needed in the implementation of these structures, what simplifies the implementation and reduces fabrication costs. Several other application examples of resonant-type metamaterial transmission lines are pointed out in following sections.

### 4.1.2 Dispersion Engineering

The large number of degrees of freedom of metamaterial transmission lines allows, not only the imposition of certain values of the phase shift and the impedance at certain frequencies, but also the controllability over the line dispersion characteristics.

Dispersion engineering strategies can be applied, for example, for bandwidth enhancement purposes. Microwave component bandwidth is given by the frequency range in which the required characteristics of the device are satisfied within certain limits. In metamaterial transmission lines, the group delay of single lines can be controlled to some extent. However, only in certain cases and above certain phase values, bandwidth can be improved with respect to conventional lines [69]. Nevertheless, dispersion engineering can be successfully applied to the design of devices based on the phase difference between two or more of the constituent transmission lines, like baluns [63,70] hybrid couplers [71] and phase shifters [72], among others [73, 74]. It is clear that, in such devices, bandwidth is related to the derivative of the phase difference between two or more transmission lines; the longer the phase difference remains close to the target value, the broader the bandwidth will be [5].

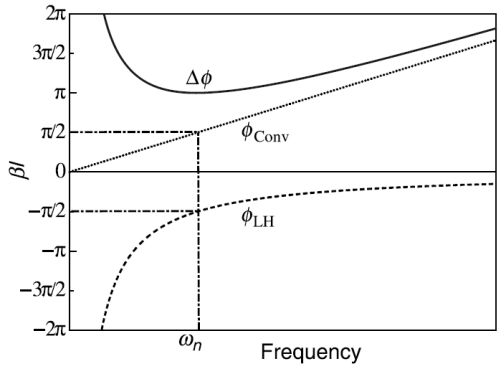


**Fig.4.2.** Phase difference between a conventional and a left-handed transmission line. Figure extracted from [5].

As long as the dispersion diagram of one (as is the case in Fig.4.2) or both transmission lines can be tailored and both curves are parallel around the desired point, the phase difference will be almost constant over a fairly wide range. The graph in Fig.4.2 shows the phase of a conventional and a left-handed transmission line and how the phase difference between them would behave. As can be seen, the phase difference is pretty flat around the design frequency, $\omega_n$. Due to the dispersion characteristics of metamaterial transmission lines, and their controllability, the phase difference between two transmission lines can be tailored to some extent in order to improve bandwidth.

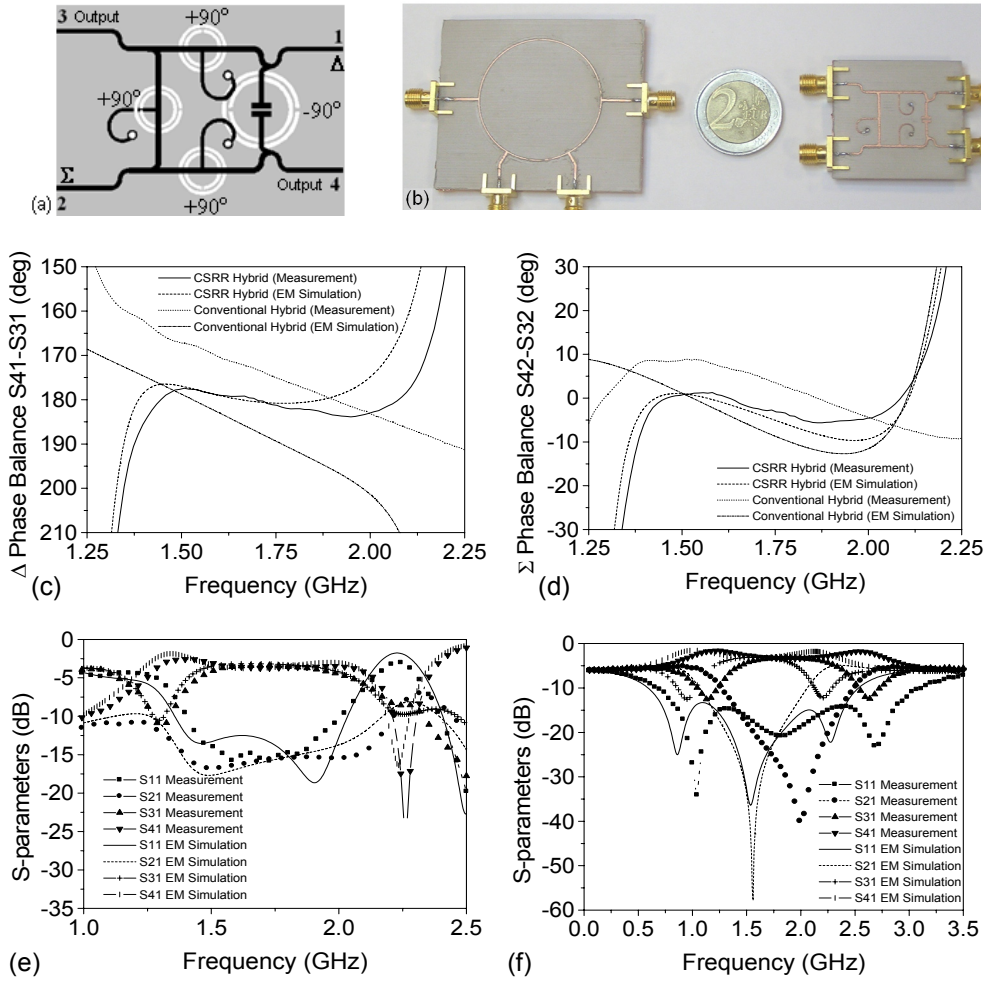


**Fig.4.3.** (a) Layout of a metamaterial rat-race hybrid coupler. (b) Photograph of the device compared with a conventional rat-race. Phase balance for the metamaterial and the conventional couplers for the Δ (c) and Σ (d) ports. S-parameters of the metamaterial (e) and the conventional (f) couplers. Figures extracted from [65].

The layout and the photograph of a rat-race hybrid coupler designed applying this idea are shown in Fig.4.3. It is formed by four resonant-type CSRR-based metamaterial transmission lines showing $Z_0$=70.71Ω at the design frequency ($f_0$=1.6GHz), as required in such components. The +90º conventional transmission lines are replaced by +90º right-handed transmission lines, whereas a -90º left-handed line substitutes for the +270º conventional line. The use of the metamaterial lines entails a considerable size reduction as can be observed from the comparison between both devices in Fig.4.3 (b). Moreover, graphs (c) and (d) show the comparison between the phase balance of the metamaterial and the conventional couplers for the Δ and Σ ports. It can be observed that the phase balance remains almost constant over a wider range in the coupler implemented by means of metamaterial transmission lines. Regarding isolation and matching, both devices exhibit comparable values at the design frequency.

One more possibility that these transmission lines with controllable characteristics present is the design of multi-band devices. Metamaterial lines offer a certain level of arbitrariness in their dispersion characteristics as an advantage over conventional transmission lines, in which the fixed linear dependence of the phase with frequency establishes the frequencies at which the lines exhibit certain phase values [75]. CL-loaded and resonant-type metamaterial transmission lines have been successfully applied in the design of dual-band components. The employment of more complicated artificial structures and models containing additional elements would allow

the achievement of multiband devices with not only two, but a higher number of arbitrary bands [76,77].

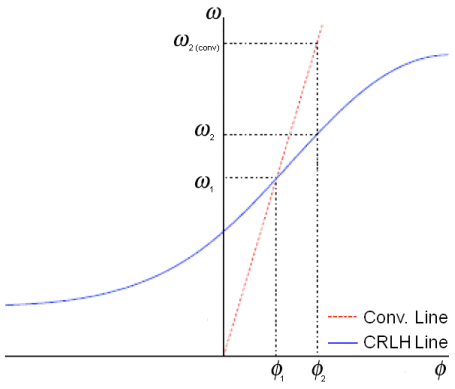


**Fig.4.4.** Dispersion diagrams of a conventional and a composite right/left-handed transmission line (balanced). Metamaterial lines can be designed to exhibit the desired frequency values at different frequencies, depending on the particular design requirements. Figure extracted from [78]

Dual-band operation for metamaterial transmission lines is illustrated in Fig.4.4. The figure shows the dispersion diagrams of a conventional and a composite right/left-handed transmission line. For given values of the phase shift ($\phi_1$, $\phi_2$) the frequencies in the case of the conventional line are fixed, whereas in the case of the artificial transmission line, they can be arbitrarily chosen. The controllable dispersion diagram of the metamaterial lines allows to choose the frequencies at which the required phases are satisfied and it can be done with both, balanced and not balanced lines. In Fig.4.4, the phase shift $\phi_2$ is achieved at a different frequency for the conventional ($\omega_{2conv}$) and the metamaterial ($\omega_2$) transmission lines lines.

On the other hand, the composite behaviour of metamaterial transmission lines allows the imposition of the same required characteristics at different frequencies lying on different transmission bands. This fact is illustrated in Fig.4.5. The figure shows the phase shift and characteristic impedance of a composite right/left-handed transmission line designed to exhibit $\phi_1$=-π/2 and $Z_{B1}$=50Ω at $f_1$=1GHz and $\phi_2$=+π/2 and $Z_{B2}$=50Ω at $f_2$=2GHz. In this case, the graphs illustrate the particular case of a CL-loaded balanced transmission line.

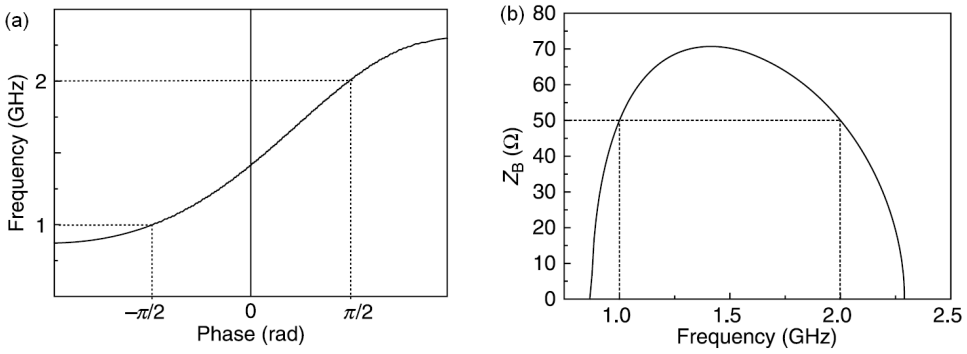


**Fig.4.5.** (a) Dispersion diagram for a balanced composite right/left-handed transmission line exhibiting -π/2 and +π/2 phase at $f_1$=1GHz and $f_2$=2GHz. Figures extracted from [5].

Dual band devices can also be designed applying resonant-type metamaterial transmission lines based on CSRRs. Balanced lines are, however, not always suitable in that case. As is explained in [66], the particularisation to the balanced case in the design of dual band components is not possible in the resonant approach if the target impedances, $Z_{B1}$ and $Z_{B2}$ have the same value, as usually happens. Therefore, in order to ensure finite, positive values for the equivalent circuit elements, unbalanced lines must be used. This does not actually imply any important limitation, since, as long as the target characteristics are satisfied at both design frequencies, a single, continuous band is, a priori, not required for dual-band operation. Considering two frequencies at which impedance and phase shift are imposed, the five circuit

elements are not univocally determined, leaving one degree of freedom that provides design flexibility. Different kinds of devices can be designed following this procedure, as has been recently demonstrated [63,64,66]. As an example, the application of resonant-type metamaterial transmission lines to the design of dual-band power dividers is shown in Fig.4.6. The layout of the device based on CSRRs is depicted in the figure Fig.4.6(a). The use of spirals, electrically smaller than the CSRRs, would contribute for a further miniaturisation [64]. The graph in Fig.4.6(c) shows the device frequency response. It can be easily seen that, at the operating frequencies, the insertion losses are very close to the ideal value (-3dB), proving the good performance of the power divider. The fulfilment of the required values for the phase (±90º) and the impedance (35.35Ω) at the design frequencies ($f_1$=0.9GHz, $f_2$=1.8GHz, the mobile GSM bands) can be corroborated in Fig.4.6(c).

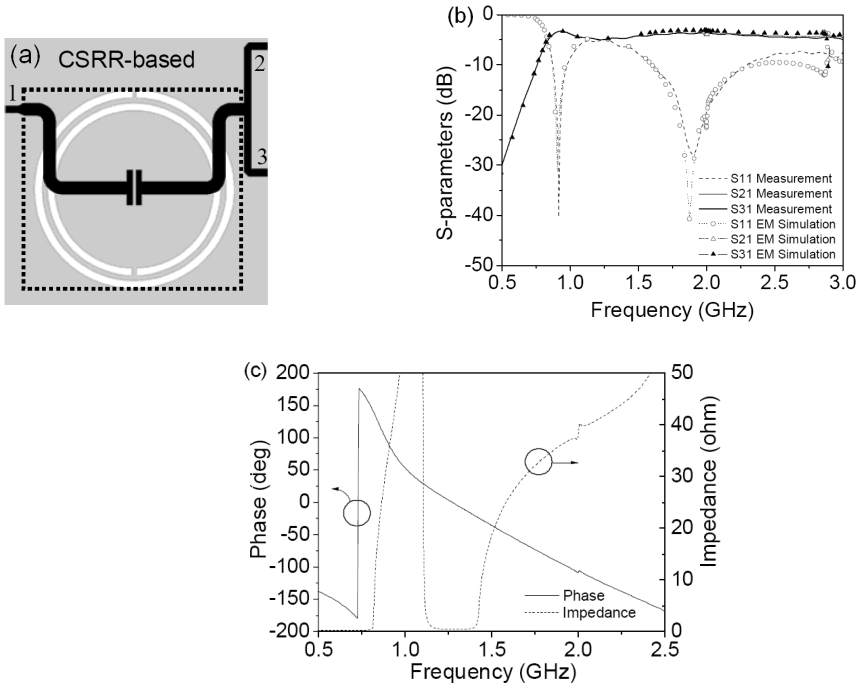


**Fig.4.6.** (a) Layouts of a two metamaterial dual-band power dividers based on CSRRs (b) Frequency response of the CSRR-based dual-band power divider. (c) Representation of the phase shift and impedance of the CSRR-based inmitance inverter forming the power divider. Figures extracted from [64].

## 4.2 Metamaterial Filters

The frequency selectivity that characterizes the response of resonant-type metamaterial transmission lines, lends itself well to their application in filtering devices. Since the implementation of the first resonant-type metamaterial transmission line, several kinds of lines have been applied in the implementation of filters with different performances. In the following sections, a general overview of the work developed during the recent years in filter design based on resonant-type metamaterial transmission lines is exposed.

### 4.2.1 State of the Art

One of the first applications of sub-wavelength resonators to the design of filtering microwave devices consisted in their use to load a host transmission line to create a stop band at those frequencies where, due to the presence of the resonators, the structure behaves as a SNG medium [9,58,79].

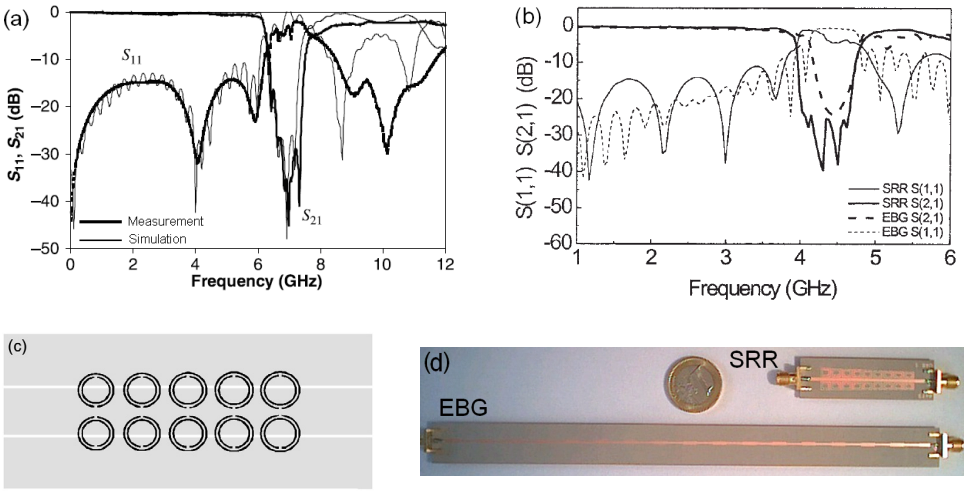


**Fig.4.7.** (a) Frequency response of a stop band filter formed by a coplanar waveguide loaded with SRRs. (b) Measured responses of an EBG and a SRR-based stop band filter. (c) Layout of the stop band filter with the response shown in (a). (d) Photograph of the filters whose responses are shown in (b). Figures obtained from [58,79].

The resonators can be tuned to reject the signal at slightly different frequencies and, thus, give rise to a rejection band with a certain bandwidth, which can be to some extent controlled with the number of resonators. The frequency response of a stop band filter consisting on a coplanar waveguide loaded with SRRs is shown in Fig.4.7(a), whereas the performance of a microstrip filter designed following a similar strategy can be seen in Fig.4.7(b). In this later figure, the measured responses of the SRR-loaded microstrip structure and an electromagnetic band gap (EBG) structure, which combines unit cells with different line widths and exhibits a similar performance, are compared. The important size reduction achieved with the use of SRRs to create the stop band can be observed in Fig.4.7(d). In that respect, the use of the SRR stop band filter is obviously very convenient. Other resonators, like CSRRs [9], SRs [80], etc., can also be applied with similar purposes.

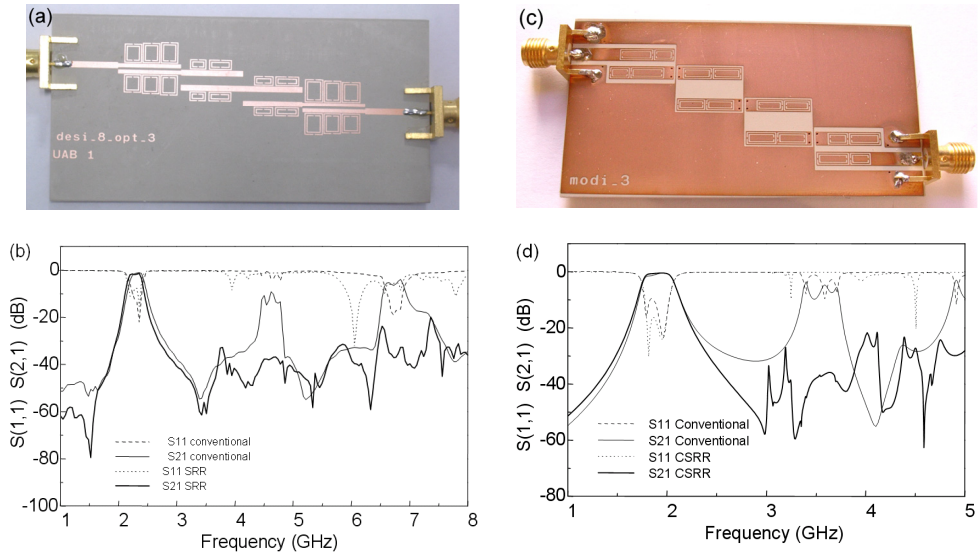


**Fig.4.8.** Photographs and frequency responses of coupled-line band pass filters loaded with sub-wavelength resonators to improve out-of-band performance. (a) Photograph of a microstrip filter loaded with SRRs. (b) Comparison between the measured responses of the filter shown in (a) and a conventional filter. (c) Photograph of a coplanar waveguide filter with CSRRs etched on the signal strip. (d) Comparison between the simulated responses of the filter shown in (c) and a conventional filter. Figures obtained from [79,83].

A different purpose for which sub-wavelength resonators have proved useful is the spurious pass band suppression. In a similar way as the resonators are used to create a stop band response, they can be included in the design of a conventional filter in order to eliminate undesired bands [81,82,83]. By this means, the out-of-band performance of the filter can be improved with one additional asset: the addition of the resonators does not entail any size increase. The photographs in Fig.4.8 show two examples of coupled line filters in microstrip (Fig.4.8(a)) and CPW (Fig.4.8(c)) technologies. In the first one, SRRs have been located close to the lines and, in the coplanar filter, CSRRs have been etched on the strips. In the graphs, the resonator-loaded filter performance can be compared with the response of the conventional filter to see the effect of the loading elements. As can be observed, thanks to the presence of the resonators, the first spurious bands are eliminated, achieving an important out-of-band performance improvement. Low-pass filters have also been implemented taking advantage of the rejection that CSRRs provide when they are employed to load a microstrip transmission line [84] giving rise to very compact devices.

In the previous filters, sub-wavelength resonators are employed as additional elements to improve a conventional distributed filter. However, in those filters the resonators are not basic elements contributing to create a controllable transmission band. Posteriorly developed works do in fact use metamaterial transmission lines based on sub-wavelength resonators to compose filters with controllable characteristics. **Article L** exposes an overview on such devices, reviewing different approaches based on the resonant-type metamaterial transmission lines and devoted to the synthesis of filters. Some of those approaches are exposed in the following sections with special attention (Sections 4.2.2 and 4.2.3), given that they represent an important part of this Thesis.

The alternation of right- and left-handed unit cells to create a band-pass response [19] was one of the first approaches applied to the design of filters based on resonant-type metamaterial transmission lines. These filters are taken up in section 3.1 in Article L. This strategy allows the generation of pass bands with very sharp edges, thanks to the presence of transmission zeros at both sides of the band. Figures 4(a) and (b) in the article show the responses and layouts of the left- and the right-handed unit cells. The first one consists in a CPW transmission line loaded with SRRs and shunt connections to create a backward-propagating transmission band preceded by a transmission zero. As for the RH unit cell, it combines SRRs and capacitive gaps giving rise to a transmission band followed by a transmission zero. When these two unit cells are designed to produce the transmission at the same frequency range and cascaded, they form a very compact structure providing a narrow band pass response (see figures 4(c) and (d) in Article L). The filter shown in Fig.4(d) in the article consists of two left- and one right-handed unit cell. If the transmission zeros are properly located, the structure can exhibit a sharp cut-off at both sides of the band. This strategy has shown useful in the design of compact-size filters [85,86,87] and diplexers [88]. A similar strategy was employed in [89], where a high- and a low-pass stages are cascaded to give rise to a band-pass filter based on CSRRs with very compact dimensions.

In section 3.4, Article L also mentions other approaches devoted to the synthesis of metamaterial filters. LC-loaded metamaterial transmission lines have been applied in filter design following different strategies. As Article L exposes, coupled-resonator-based CRLH transmission lines are useful in the design of broadband filters with improved selectivity above the pass band [90]. As has been previously mentioned, dual-band filters have also been implemented employing LC-loaded transmission line. This is the case of the filters presented in [49], where the non-linear behaviour of the phase of CRLH transmission lines is exploited to create two pass- or stop-bands at different arbitrary frequencies. Stepped-impedance resonator-based filters can also be implemented employing artificial transmission lines, as is shown in [91]. This work includes such a filter implemented by cascading RH and LH transmission line sections, which even allows the control of the first spurious resonance. Recently, narrow band-pass filters based on grounded spirals simultaneously showing very good performance and compact dimensions have been proposed [92].

The following sections include different techniques devoted to the implementation of narrow and broadband filters based on resonant-type transmission lines. Other approaches have also made use of sub-wavelength resonators, although they are not based on the synthesis of metamaterial transmission lines. This is the case of the coupled-resonator-based filters presented in [93], where SRRs and SRs are employed to miniaturize filter dimensions.

## 4.2.2 Narrow Band-pass Filters

In 2006, a methodology for the design of standard filters based on the hybrid approach was developed and successfully applied [19,62] in the design of narrow- and moderate-band bandpass filters. **Article L** addresses this method in section 3.3. During the development of this Thesis, this methodology has been applied to the synthesis of several devices, which were presented in Article I and Article K and also gathered in Article L. The following sections deal with this methodology and the results obtained from its application.

### *4.2.2.1 Methodology*

The considered filters follow the band-pass filter model based on impedance inverters and shunt resonators [94]. This model is illustrated in Fig.8(a) in Article L. Specifically, the structure is modelled by impedance inverters with normalized admittance $\overline{J}=1$ and parallel LC resonant tanks, as Fig.8(b) depicts. Given that the normalized admittance is equal to one, the presence of each inverter merely involves a phase shift of 90º.

The unit cell of the metamaterial filter will be a hybrid cell combining CSRRs, capacitive gaps and shunt-connected inductive stubs as loading elements of a host microstrip line (already described in section 3.1.2), which can be seen in Fig.2(b) in the article. The design method considers the model shown in Fig.2(e) in the article, but neglecting the series inductance in a similar way as it was previously done in some works applying the purely resonant approach. Provided the characteristics of the employed unit cell, the model shown in Fig.8(b) in Article L can be applied to this structure as a basis for standard narrow band-pass filter design [19].

Taking advantage of their design flexibility, each of the unit cells forming the filter is designed to, on the whole, exhibit characteristic impedance equal to the reference impedance of the ports ($Z_0$=50Ω) and phase $\phi$=90º at the considered central frequency of the pass band. By this means, one unique unit cell acts as a resonator and exhibits the required phase without needing the addition of different stages acting as inverters and resonators, what involves a considerable size reduction. The unit cells must satisfy several other conditions in order to obtain the desired standard response. Equations (8) to (16) in Article L represent the different imposed conditions and the derived expressions used to obtain the circuit element values, which can be univocally determined. The imposition of the phase and impedance at the central frequency forces the series and shunt impedances of the T-circuit model to be equal to $-jZ_0$ and $+jZ_0$, respectively. In the case of Chebyshev filters, the values of the $g_i$ elements of the low-pass filter prototype are determined by the required ripple and the rejection level. These element values, together with the fractional bandwidth of the filter, allow to determine the 3dB bandwidth of each of the unit cells (equations (8) and (12) in the article). The transmission zero and central frequencies are also imposed values. The position of the transmission zero can be chosen to eliminate spurious bands or increase the rejection just above the transmission band, improving the out-of-band performance of the filter.

### *4.2.2.2 Results*

The previously described methodology has been applied in different works to design periodic and Chebyshev filters. Besides the application examples using CSRRs included in [62] when the design method was introduced, other filters have been designed making use of electrically smaller resonators intending a further miniaturisation level. Article K and Article I include two different filters employing complementary spiral resonators (CSRs). **Article L** also gathers results from [62] and Article K. In [62], two design examples are shown. One of them is a periodic 3-stage filter, whereas the second one is a 3rd order Chebyshev filter. This last filter can be observed in Fig.9 in Article L. The device was designed to exhibit *FBW*=9% with central frequency $f_0$=2.5GHz and 0.3dB ripple. The layout of the structure can be seen in Fig.9(a), where the relevant dimensions are indicated. The whole device has a total length of 20mm, which is 0.4 times the guided wavelength, $\lambda$. Figure 9(b) shows the performance of the filter, with the simulated and measured S-parameters. The filter exhibits a very symmetric response, very low in-band insertion losses and an important rejection level, which has been improved making use of the transmission zero to eliminate the first spurious band. Figure 9 in Article L also shows the layout with dimensions (figure (c)) and the frequency response (d) of a CSR-based filter. Nevertheless, **Article K** provides a more detailed description of this filter in section

III. It has been designed following the previous strategy, which can be likewise applied with CSR-based structures. In this case, the central frequency of the filter is $f_0$=1.1GHz, *FBW*=10% and 0.3dB ripple. Each of the unit cells was designed to improve the out-of-band rejection controlling the position of the transmission zeros below and above the transmission band. Specifically, they have been located at different frequencies for each cell in order to widen the rejection band above the main transmission band. The required rejection level was -30dB at 1.3GHz. The frequency response of the filter can be seen in Fig.7 in Article K. Figure 7(a) shows the simulated response of the designed filter compared with that of a coupled-line filter with similar characteristics, but a higher ripple (0.5dB). As can be appreciated both responses are very similar within the transmission band. However, in the case of CSR-based metamaterial filter, the first spurious band appears at a rather higher frequency (close to $3f_0$). The simulated and measured responses of the designed filter are shown in Fig.7(b). The most remarkable characteristic of the filter is its small size, which can be appreciated in Fig.6 in the article. In the figure, the layout of the CSR-based filter is compared with those of the coupled-line filter and a similar filter based on CSRRs extracted from [62]. As can be appreciated, the CSR-based device (with an area $A$=0.22$\lambda$ x 0.08$\lambda$) is around 5 times shorter than the coupled-line filter and occupies a 5-times smaller area than the CSRR-based filter. As a drawback, the small electrical size of the resonators involves a smaller quality factor and, consequently, higher insertion losses in the pass band.

Section 4 in **Article I** includes, as an application example of transmission lines with complementary resonators etched on the signal strip (introduced in section 3.1.3), a periodic filter implemented following the same strategy. The employed resonators are, like in the previous example, complementary spiral resonators. The filter was designed with $f_0$=1GHz, like the periodic filter included in [62], with the aim of being able to compare them. The filter bandwidth is, however, different; whereas in [62] the fractional bandwidth was *FBW*=10%, in the case of the CSR-based filter, the considered bandwidth was smaller (*FBW*=4.5%). The three identical stages forming the filter have the same $g$ value. This is the case of a 3-order low-pass filter prototype with normalised cut-off angular frequency $\omega$=1rad/s, whose all elements are equal to $g$=1.521. The unit cell is, thus, designed to exhibit the required values of the phase shift, the impedance and the resonator bandwidth. The resulting device exhibits a symmetric pass band and an important out-of-band rejection level. As occurred in the previous example, the small bandwidth and the limited quality factor of the resonators gives rise to a significant increment in the in-band insertion loss level. This penalty must in general be paid when the electrical size of the resonators is decreased [12].

### 4.2.3 Broadband Filters

Within the resonant-type approach, two main strategies devoted to the synthesis of broad-band filters have been applied. One of them consists on the use of balanced transmission lines (described in section 3.1), which provide broad transmission bands, to design high- or band-pass filters. Such filters will be covered in detail in the following sections. A second method is the application of a modified version of the technique addressed in section 4.2.2.1, which is applied to a different unit cell providing wide transmission bands. By this means, wide and ultra-wide band-pass filters based on sub-wavelength resonators can be implemented following a complete design methodology. This strategy is delved into and exploited in several works [95,96,97] and is briefly exposed in **Article L.** It is based on a similar unit cell as the previous one; it also combines CSRRs and inductive shunt stubs, but they are coupled by means of $\lambda$/4 lines. As a consequence, although the methodology is basically the same and identical conditions are imposed, some of the design equations differ from the original ones. The employed unit cell is represented in Fig.10(a) in Article L. Next to it, the layout (b) and the frequency response (c) of a periodic ultra-wide band-pass filter based on this approach can be found. The use of this new unit cell allows the achievement of broad transmission bands (the given example shows *FBW*=90%) with a sharp cut-off at the upper edge, what involves a significant improvement of the out-of-band rejection with respect to other approaches [98].

### 4.2.3.1 Filters based on Balanced Transmission Lines

As has been previously mentioned, balanced transmission lines can be applied in the design of wide band filters. Some examples implemented using such lines are included in Article F and Article G. The main aspects of these devices are also reviewed in Article L. In section III in **Article F,** balanced structures based on the hybrid and the purely resonant approach are presented as band- and high-pass filters, respectively. By cascading several unit cells, purely-resonant balanced transmission lines provide a high-pass response whose frequency selectivity can be enhanced increasing the number of cells. Figure 5 in Article F shows the frequency response of several filters including different number of unit cells. The considered structures provide a wide transmission band with an important rejection level below the lower edge of the band. This limit can be controlled and, thus, be arbitrarily located in order to reject all undesired signals appearing below it. Given that the upper limit of the transmission band is not controlled, these structures must be considered as high-pass filters.

A step forward is taken in the work presented in **Article G**, where similar unit cells are employed to design ultra-wide band-pass filters (UWBPFs) covering the standard mask for UWB communications covering from 3.1GHz up to 10.6GHz. In these filters, additional resonators are included to control the upper limit of the band and, furthermore, create attenuation poles at arbitrary frequencies within the transmission band. These notches can be applied to reject undesired interfering signals which may appear within the transmission band. The basic unit cell forming the filter is depicted in Fig.3 in Article G, whereas the wide transmission band provided by this structure can be observed in Fig.4. As has been previously indicated, no control can be done over the upper limit of the band just cascading several of these unit cells. Nevertheless, this can be done by means of additional resonators which can be added to the basic structure of the filter formed by, in this case, three balanced unit cells. The new resonators can be either metallic or complementary. An example of such a structure including small CSRRs can be observed in Fig.5 in **Article L**, where the layout (a) and the response (b) of the structure are shown. The small resonators have in this case been located inside the bigger resonators forming the balanced structure. The additional CSRRs have been tuned to reject the signal around 10.6GHz and, thus, create the upper limit of the band. The big advantage of this strategy is that it does not involve any size increment. The attenuation poles can be created by including new properly tuned resonators to the structure. They can again be either metallic or complementary and be located either on the top or on the bottom layer of the substrate, respectively. Two examples of these different possibilities are shown in Fig.6 in Article L, which includes the layouts, photographs and responses of two different filters following this strategy. In the first of the filters all the additional resonators are complementary. In addition to the small CSRRs located inside the big ones, two CSRs have been located under the access lines to create a notch around 5GHz. The addition of these two new resonators involves a minor size increment. The marked rectangle occupies an area $A$=1.77cm x 0.41cm=0.73cm$^2$. In the case of the second filter (Fig.6(c)), all the additional resonators are metallic and they are located on the top layer of the substrate close to the signal strip. This filter is also dealt with in detail in Article G. Four square-shaped SRRs can be found close to both access lines and they are responsible for the control of the upper band limit. Two additional spiral resonators, tuned at 5.6GHz and located in the central part of the filter, create the attenuation pole without any effect on the rest of the transmission band nor on the device size. In this case, the area of the dashed rectangle is $A$=1.57cm x 0.42cm=0.66cm$^2$. The frequency of the attenuation pole can be arbitrarily chosen, depending on the frequency of the interfering signal which must be eliminated. Figure 6 in **Article G** shows the response of a second filter based on the same topology. In this case, the SRs responsible for the attenuation pole have been tuned at 4.5GHz. As in the previous case, the filter exhibits a wide frequency band covering the UWB mask a low in-band insertion loss level and the rejection of the notch exceeds the -20dB.

Article F shows an example of a filter based on balanced hybrid transmission lines. This filter was firstly presented in [60] and is also reviewed in **Article L**. The layout and the response of the filter can be seen in Fig.7 in Article L. The filter was designed to satisfy rather strong specifications, such as small size (area <1cm$^2$) and high rejection level below the transmission band (-80dB at 2GHz), among others. A four-stage structure implemented in a thin substrate ($h$=0.127mm) was necessary to satisfy the required rejection. The resulting filter exhibits a wide transmission band from 3.5GHz to 10GHz with a high frequency selectivity, this combined with a very small size ($A$<0.7cm$^2$), which is even smaller than the required.

The exposed examples demonstrate the utility of balanced resonant-type composite right/left-handed metamaterial transmission lines in the design of wide and ultra-wide band-pass filters with different application possibilities, small dimensions and good performance.

## 4.3 Reconfigurable Transmission Lines

Tunable or reconfigurable transmission lines and devices are of big interest on present communication systems which need to be adapted to varying conditions and requirements. Many efforts are devoted to the development of such reconfigurable devices applying different strategies. In the following sections, some examples of reconfigurable devices based on metamaterial concepts and structures making use of different technologies are shown. Special emphasis is put on tunable structures based on ferroelectric materials.

### 4.3.1 State of the Art

The design of reconfigurable devices has lead to the development and application of different strategies. Microelectromechanical systems (MEMS) and tunable capacitances are the main elements employed to achieve tunability. Both techniques have been applied in recent years to implement reconfigurable devices based on different kinds of metamaterial transmission lines, including the resonant-type [99]. Tunable LC-loaded metamaterial transmission lines based on varactor diodes or tunable ferroelectric capacitors have been applied in the design of many different devices, including antennas [100], phase shifters [101,102] or matching networks [103]. Such transmission lines have also been implemented making use of MEMS and employed in the design of microwave devices, like, for example, phase shifters [104].

Regarding the resonant-type approach, tunable SRRs [105] and CSRRs [106] have been implemented by means of varactor diodes and applied in the design of tunable transmission lines. The layout of both resonators can be seen in Fig.4.9. In both cases, the inclusion of a varactor allows the variation of the resonance frequency of the structure by means of a DC voltage.

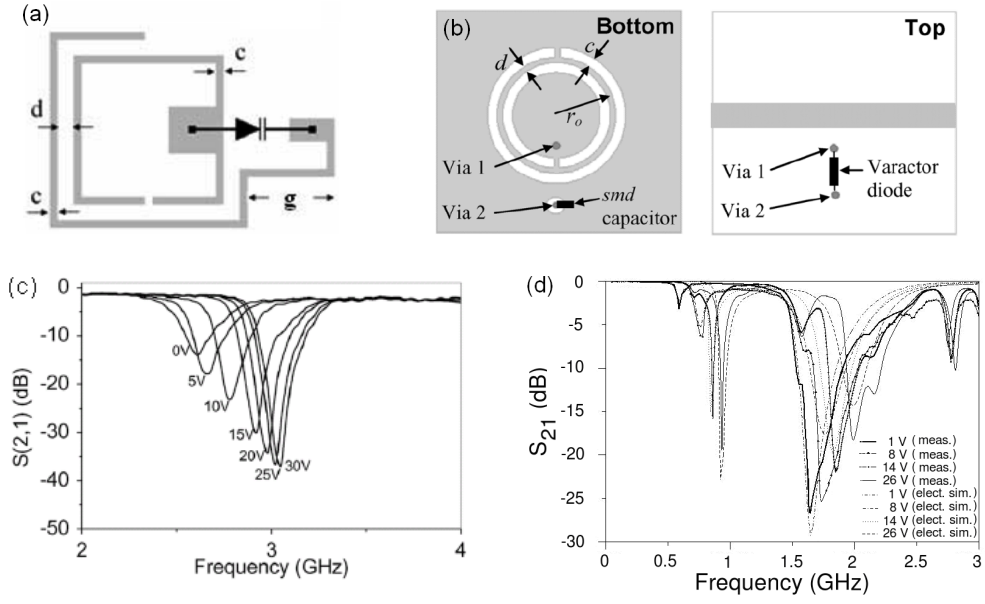


**Fig.4.9.** (a) Varactor-loaded split-ring resonator (VLSRR). (b) Varactor-loaded complementary split-ring resonator (VLCSRR). (c) Response of a VLSRR-loaded transmission line for different diode polarisations. (d) Response of a VLCSRR-loaded transmission line for different diode polarisations. Figures extracted from [105,106].

The addition of a varactor can be done in the case of the SRR by directly locating it between the two rings forming the resonator, what forces the inclusion of two patches to allow the varactor soldering (see Fig.4.9(a)). In the case of the CSRR, the varactor can be located on the top layer between the central and external parts of the resonator (see Fig.4.9(b)) and soldered with vias to the ground plane. In order to allow the varactor biasing, the port placed in the external part of the resonator (Via 2 in Fig.4.9(b)) is surrounded by a circular slot and connected to the ground plane by means of a SMD capacitor. These two tunable resonators have been mainly applied in the design of notch and stop band filters. The responses of two microstrip transmission lines loaded with VLSRRs and VLCSRRs for different diode polarisations can be observed in Fig.4.9(c) and (d), respectively. Other configurations of tunable transmission lines based on sub-wavelength resonators are also possible if the varactors are placed, not on the resonator, but, for example, on a capacitive gap or both [107,108].

As has been previously mentioned, MEMS have also been applied in the design of resonant-type metamaterial transmission lines. Coplanar waveguide structures loaded with complementary split-ring resonators can be tuned with the addition of MEMS switches which, when properly biased, allow the modification of the resonance frequency of the CSRRs [109].

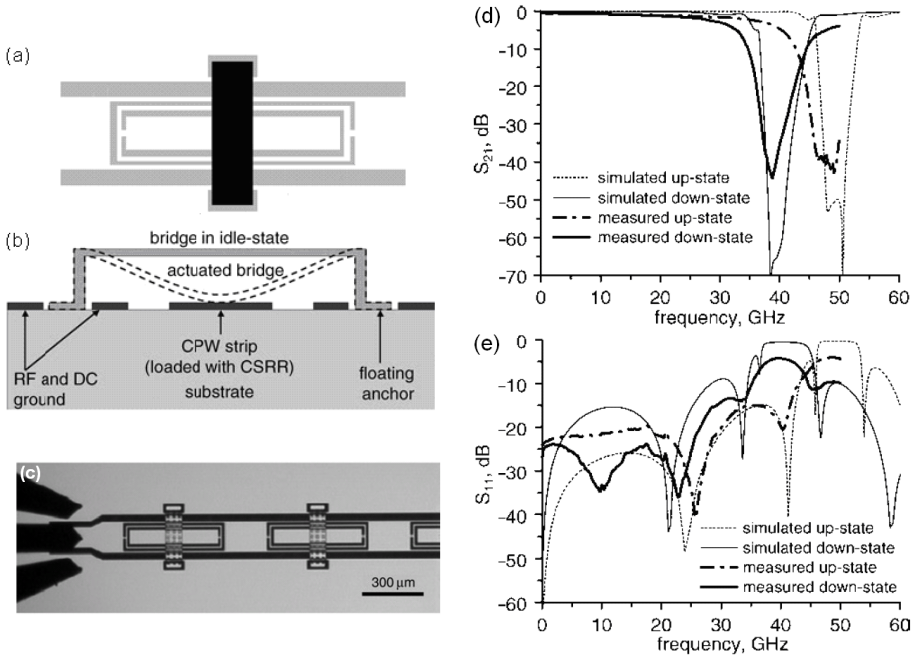


**Fig.4.10.** (a) Scheme of the unit cell formed by a coplanar waveguide loaded with a CSRR and a MEMS switch (in black). Metallic parts of the CPW are depicted in white and slots in grey (b) Cross-section representation of the MEMS switch loading the CPW line with CSRRs. (c) Photograph of the fabricated device. (d) Measured and simulated insertion losses of the 4-unit-cell fabricated device. (e) Measured and simulated return losses of the 4-unit-cell fabricated device. Figures extracted from [109].

The implemented structure exhibits a notch, which, thanks to the action of the bridges, can be tuned between 39GHz and 48GHz for the down- and up-states, respectively, as can be observed in Fig.4.10. The measurements show an achieved tuning range about 20% and very low insertion losses in the pass band.

These examples represent a proof-of-concept showing the possibility of applying these tuning strategies to the implementation of resonant-type reconfigurable metamaterial transmission lines. In the following sections, a different approach, based on the use of ferroelectric materials is presented as an alternative way to synthesize tunable resonant-type metamaterial structures.

### 4.3.2 Tunable Metamaterial Transmission Lines based on Ferroelectrics

One additional interesting approach devoted to the development of tunable microwave devices is based on the use of ferroelectric materials. The useful properties of ferroelectrics are numerous [110,111]. Thanks to their piezoelectric behaviour, they can be used in electromechanical sensors and transducers. They are massively used in memories, where the direction of their spontaneous polarizability is controlled to store information. They also exhibit pyroelectric behaviour, which can be exploited for infrared sensors. Moreover, the high values of their dielectric permittivity make these materials very useful as dielectrics in capacitors. When ferroelectrics are used in the design of reconfigurable devices, the tunability is mainly achieved in virtue of the dependence of the dielectric permittivity of such materials on the external electric field [110,112], although it can also be modified by the temperature [113]. In our case, we will take advantage of this dependence of the dielectric permittivity to create voltage-dependent reconfigurable frequency-selective structures based on metamaterial resonators.

#### *4.3.2.1 Ferroelectric Materials*

A dielectric crystal is considered a ferroelectric if it is able to exhibit spontaneous electric polarization and its direction can be reoriented between crystallographically defined states by means of an external electric field. Due to its similarities with the phenomenon of ferromagnetism, this effect received the name of ferroelectricity. Any dielectric experiences a polarization when it is subjected to an electric field. Its charges are reoriented forming dipoles, what can be described by means of the dipolar moment, ***p***.

$$\vec{p} = Q \cdot \vec{d} \tag{4.1}$$

where *Q* is the value of the charges forming the dipole, and ***d*** is the vector representing the distance between them. If the whole volume, *V*, of the dielectric is taken into account, one can obtain the total macroscopic dipole of the material, which is known as polarization, ***P***.

$$\vec{P} = \frac{\sum_i \vec{p}_i}{V} \tag{4.2}$$

Although polar dielectrics contain permanent dipoles in absence of an external electric field, they are randomly oriented, the total sum of dipolar moments is cero, and so is the polarization. However, the polarization in presence of an electric field is higher in polar dielectrics than it is in non-polar dielectrics, due to the contribution of the intrinsic and the induced dipoles.

The electrical displacement field, ***D***, in a dielectric can be described as:

$$\vec{D} = \varepsilon_0 \vec{E} + \vec{P} \tag{4.3}$$

On the other hand, the relation between polarization and electric field is:

$$\vec{P} = \varepsilon_0 \chi \vec{E} \tag{4.4}$$

where $\chi$ is the electrical susceptibility which is related to the relative dielectric permittivity:

$$\varepsilon_r = 1 + \chi \tag{4.5}$$

Therefore, the susceptibility can be obtained differentiating the polarization with respect to the electric field:

$$\chi = \frac{1}{\varepsilon_0} \frac{\partial \vec{P}}{\partial \vec{E}} \tag{4.6}$$

and the electric displacement can be rewritten as:

$$\vec{D} = \varepsilon_0 \vec{E} + \varepsilon_0 \chi \vec{E} = \varepsilon_0 \vec{E}(1 + \chi) = \varepsilon_0 \varepsilon_r \vec{E} \tag{4.7}$$

The ferroelectric properties of a material are related to the symmetry. Only those crystalline systems which do not contain any inversion centre are able to exhibit polar properties. Many ferroelectric materials are oxides showing a perovskite structure [110,114]. The most representative ferroelectric material is barium titanate ($BaTiO_3$), which is represented in Fig.4.11.

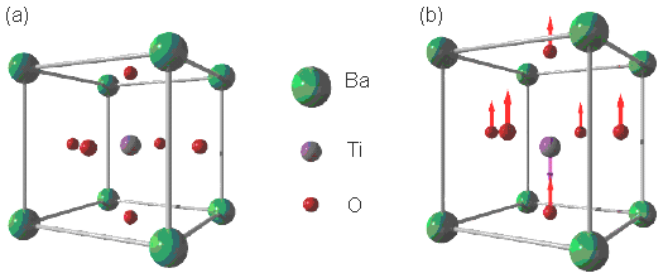


**Fig.4.11.** Representation of the unit cell of $BaTiO_3$ in the cubic phase. The atoms of the barium titanate are arranged just as a perovskite structure, adopted by many oxides having the chemical formula $ABO_3$. In the cubic phase (a), oxigen atoms sit at face centred positions, barium atoms are located at the corners of the cubic structure and the body centred position is occupied by the titanium atom. In the tetragonal phase (b) the relative positions of the positive and negative atoms changes and polarization arises.

In the cubic phase (Fig.4.11(a)), the body centred position occupied by the titanium atom is an inversion centre and, consequently, spontaneous polarization is not allowed. In this case, the material is paraelectric; there is no permanent dipole in absence of an external electric field. The temperature below which the material behaves as ferroelectric is the Curie temperature. Therefore, a temperature decrease causes a phase change, permitting the existence of a permanent dipole. If a tetragonal deformation occurs (Fig.4.11(b)), causing the displacement of the relative positions of positive and negative ions in the grid, spontaneous polarization arises. Consecutive transitions can lead the structure to new phases, like the orthorhombic and the rhomboedric with different orientations of the dipole [110]. The phase transitions can be induced by changes in the temperature, causing the appearance of the spontaneous polarisation and, thus, surface changes. This effect is known as pyroelectricity and is applied, for example, to detect temperature changes in passive infrared sensors. All ferroelectric materials can exhibit pyroelectricity and also piezoelectricity, since the electrical polarization can also be induced by a mechanical strain. Spontaneous polarization, however, is not enough to talk about ferroelectricity; it is the reorientability by means of an external field what defines a material as ferroelectric.

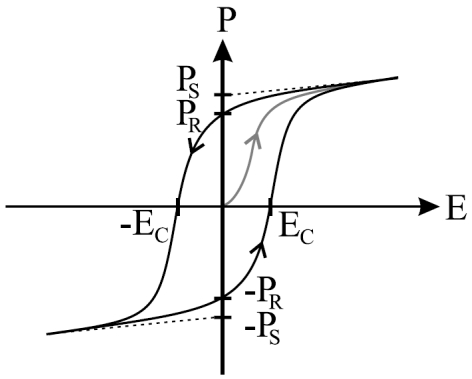


**Fig.4.12.** Typical hysteresis loop of a polycrystalline ferroelectric material. The polarisation ***P*** varies as a function of the ***E*** field. Figure obtained from [115].

The characteristic behaviour of a ferroelectric material is shown in Fig.4.12. The graph shows the typical hysteresis loop occurring during the reversal of the polarization in a

polycrystalline ferroelectric. Starting from $\boldsymbol{P}$=0, $\boldsymbol{E}$=0, when the material is subjected to an external rising electric field, the polarization describes a non-linear increment until it reaches saturation (grey curve). At this point, if the electric field is decreased to zero, a remaining polarization $\boldsymbol{P_R}$ is observed. The value $\boldsymbol{P_s}$ is obtained extrapolating the graph from the saturation zone to $\boldsymbol{E}$=0 and corresponds to the remaining polarization for single crystal ferroelectrics. A negative electric field is necessary to decrease polarization, which can be cancelled and reversed applying an electric field $\boldsymbol{E}$<-$\boldsymbol{Ec}$ until it saturates. $E_c$ is the coercive field necessary to null the polarisation. If the field is again increased, the hysteresis loop is closed. Typically, ferroelectric materials only show this behaviour under its Curie temperature, $T_c$, above which they behave as paraelectric materials. In paraelectric materials, $E_c$ vanishes and there is no hysteresis in the dependence of $\boldsymbol{P}$ with $\boldsymbol{E}$.

### *4.3.2.2 Reconfigurable Structures based on BST Thick-films*

For microwave applications, the most suitable behaviour is actually the paraelectric, since this prevents hysteresis, among other effects [111,115]. For this reason, materials whose Curie temperature is close to the operation temperatures are needed. On the other hand, given that the tunability decreases strongly as the temperature increases from the Curie temperature, the most favourable situation is when the operation temperature lies just above the Curie point, at which the dielectric permittivity reaches its maximum value [115]. There are no known single crystal perovskite-type ferroelectrics with Curie temperature close to 273 K. As a result, mixed crystal systems, whose Curie temperature depends on the ratio of components, must be artificially synthesized. In the case of the $BaTiO_3$ ($T_c$=120ºC), it can be mixed with $SrTiO_3$ ($T_c$=-235ºC) and form a mixed crystal system ($Ba_xSr_{1-x}TiO_3$) whose Curie temperature can vary between -80 ºC and 130ºC approximately, when the chiometric factor $x$, representing the ratio of Barium and Strontium contents varies from 1 to 0.4 [115] (see Fig.4.13). Such a mixed crystal is called Barium Strontium Titanate and is normally abbreviated as BST. Different studies point at the $Ba_{0.6}Sr_{0.4}TiO_3$ ($x$=0.6) as a good candidate to be used as tunable dielectric at room temperatures suitable for microwave applications [111,115]. The Curie point for a mixed crystal containing 60% barium is around $T_c$=-2ºC. $Ba_{0.6}Sr_{0.4}TiO_3$ exhibits, thus, paraelectric behaviour at room temperatures.

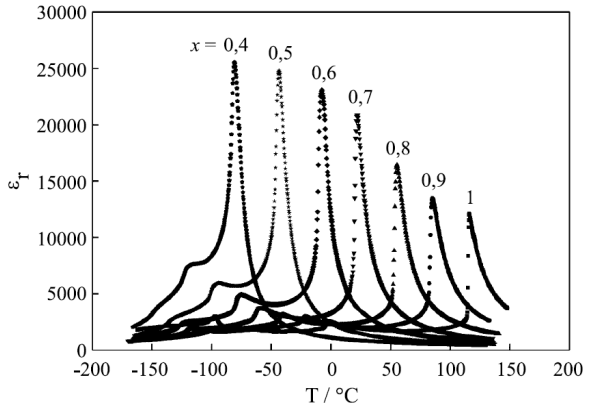


**Fig.4.13.** Variation of the dielectric permittivity of diverse samples of BST with different values of the stechiometric factor $x$. The relative content of Ba and Sr determines the Curie point, which is the temperature at which the highest value of $\varepsilon_r$ is reached. Figure obtained from [115].

Thick layers of BST can be screen printed on a carrier substrate and lay under the metallization layers of a planar circuit. By this means, capacitive gaps can be tuned applying a biasing voltage between the two sides of the gap [116]. The effective permittivity of the BST layer, taking into account the influence of the air due to its porous nature (the porosity is about 40%), can vary between $\varepsilon_{eff}$≃200…700. Due to the high values of the BST permittivity, film thicknesses of only 2-6μm are needed for planar microwave components. A thick-film of BST (few microns thickness) on a conventional aluminium oxide substrate ($Al_2O_3$) with dielectric permittivity $\varepsilon_r$≃10 is enough to achieve tunability maintaining reasonable values of the effective

permittivity of the whole substrate. Otherwise, too high values of the permittivity would force a decrease in the device dimensions up to critical values. The high breakdown field strength of the BST (around 400V/μm) allows high biasing voltages, what increases the achievable tunability.

In the work developed in this Thesis, two different kinds of sub-wavelength resonators have been implemented on BST in order to achieve tunability and they have been used to load microstrip transmission lines. The considered substrate for the design of the tunable resonators is shown in Fig.4.14, where the relevant parameters are indicated. It consists of an Alumina layer with thickness $t_{Alumina}$=650μm covered with a BST layer with thickness $t_{BST}$=3.5 μm. The gold metallization layer has a thickness $t_{Au}$= 2.5μm.

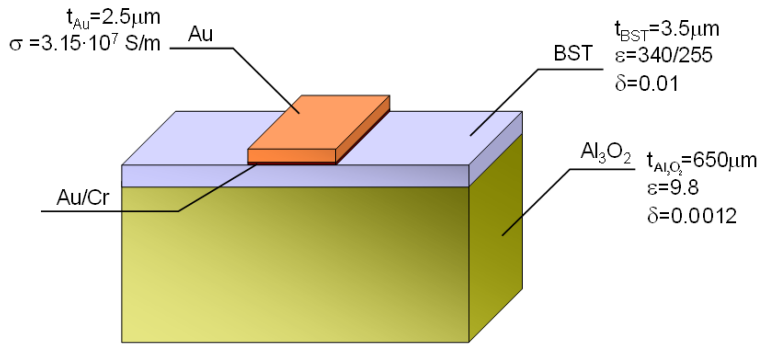


**Fig.4.14.** Scheme of the substrate employed in the implementation of the tunable sub-wavelength resonator structures.

The fabrication process comprises a considerable number of steps which includes the deposition of the BST layer, the metallization process and the biasing setup. The carrier substrate is a low-loss $Al_2O_3$ microwave ceramic with $\varepsilon_r$=9.8. The tunable BST thick-film is created by screen-printing a BST powder-based paste on the carrier substrate. The elaboration of the powder requires calcine and milling steps. By sintering the printed paste at 1250 ºC, a porous layer of BST with a thickness of a few microns is created [115].

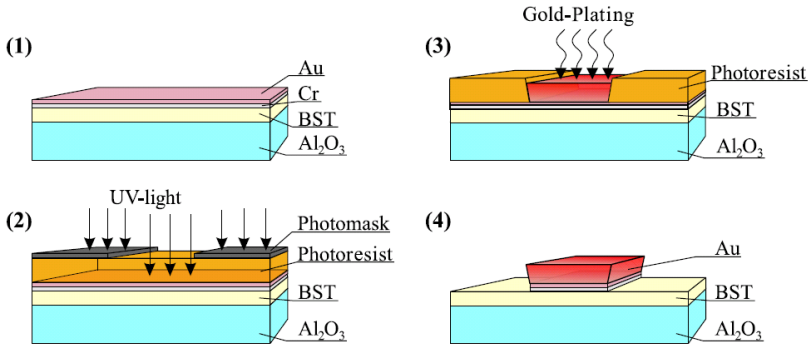


**Fig.4.15.** Scheme of the different steps for the implementation of the metallic structures on the BST substrate. (1) Evaporation of the starting-metallization layer. (2) Deposition of the photoresist, photomask positioning and UV-illumination. (3) Removal of the illuminated photoresist and gold plating. (4) Elimination of the remaining photoresist and starting layer. Figure extracted from [115].

The implementation of the planar metallic structures requires several additional steps (see 1-4 steps in Fig.4.15). First of all, a thin adhesion layer of chrome and a gold starting–metallization layer are thermally evaporated. Once the gold seed layer has been deposited, only a one-step lithography and gold galvanic plating process are necessary to obtain the

metallization. Finally, the starting gold/chrome layers are eliminated by wet etching. Once the structure has been implemented, it is cut and properly assembled for the biasing.

BST films have already been applied in the design of tunable SRRs in [113]. Nevertheless, in that work, tunability was achieved on the basis of the pyroelectric behaviour that BST exhibits. The variation in $\varepsilon_r$ was, thus, provoked by the modification of the temperature. In our case, however, tunability is achieved by means of a variable electric voltage that causes the change of $\varepsilon_r$ in the BST layer. The behaviour of the resonators is modified by tuning their associated capacitance. When the tuning voltage is applied between the two sides of a capacitive gap implemented on the considered substrate, the electrical field going through the BST layer is able to cause its polarisation. One important condition for tunability optimization is the homogeneity of the tuning field distribution in the BST thick film [116]. If the capacitive gaps are narrow enough, we can ensure that an important part of the electric field lines between the two parts of the gap appearing when the DC-voltage is applied, go through the BST layer. This electric field varies the polarisation of the material under the gap, changing its permittivity and, thus, the capacitance of the gap. However, too narrow gaps could give rise to inhomogeneities in the BST polarisation, decreasing tunabilitiy. The effects of the geometry on the tunability were studied in [116], where the influence of the thickness of the BST layer, the width of the gaps and the width of the central strip of a coplanar waveguide was evaluated. For a BST-layer thickness of approximately 3.5μm, as the one used in this work, a gap width around 10μm was found to be the optimal value. Tunability could be increased by decreasing the BST layer thickness, but it would require narrower gap widths, compromising the reliability of the fabrication process.

Although the breakdown voltage in bulky BST films is very high (around 400V/μm), breakdown occurs at lower field strengths in the case of planar structures, due to the presence of the air, what further limits the tuning. In our case, tuning voltages of 140V have been applied, what implies field strengths around 14V/μm. Some structures allow the addition of parylene coatings to cover the planar metallization and the BST film in order to increase tunability. In [117], field strengths up to 29V/μm could be applied thanks to the use of such coating, increasing the tunability in an important factor. In addition to this, the parylene coating protects the porous BST layer from humidity. In this work, however, no coating films have been used.

The objective of this work was to verify the feasibility of the application of this technology in the design of tunable sub-wavelength resonators. The selected structures for their implementation were two: the split-ring resonator (SRR) and the open complementary split-ring resonator (OCSRR) (Fig.4.16). OCSRRs have been recently proposed and they can be etched either on a CPW [118] or, like in our case, on a microstrip transmission line [119].

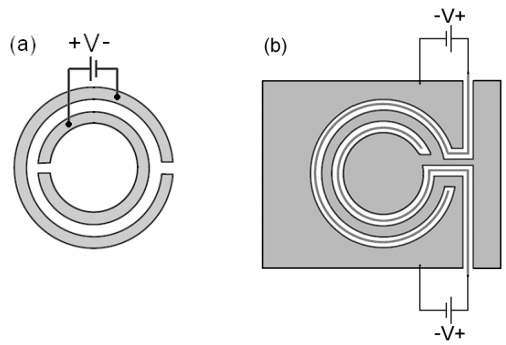


**Fig.4.16.** (a) Scheme representing a SRR and the application of the DC tuning voltage. The biasing is applied between the two rings forming the SRR. (b) Scheme representing an OCSRR etched on a microstrip line and the application of the DC tuning voltage. The polarization of the structure requires the inclusion of an electrode along the slots forming the OCSRR. The biasing is applied between the electrode and the microstrip line.

The topologies of these resonators allow their fabrication on the considered substrate and their polarization with the intention of obtaining the desired tunability. In our case, the resonance frequency of these structures is tuned by tuning their associated capacitances in a similar way as it is done in thick-film BST varactors [116]. Both resonators are modelled by a parallel LC

resonant tank. In the case of the SRR, the capacitance between the two open rings forming the resonator can be tuned applying a DC-voltage between both rings (see Fig.4.16(a)). On the other hand, in the case of the OCSRR, the tuned capacitance is that between the two sides of the paths etched on the transmission line forming the structure. In this particle, there is a direct connection between the two edges of the transmission line and this forces the use of an electrode in the middle of the paths in order to apply the required polarisation voltage to obtain the tunability. By this means, the tuning voltage is applied between the electrode and the transmission line (Fig.4.16(b)).

The design and implementation of a SRR-based reconfigurable stop-band structure is described in **Article M**. Figure 1 in the article shows the cross section of the substrate and the layout of the fabricated structure with the relevant dimensions. The device consists in a microstrip line loaded with two rectangular SRRs. One electrode is joined to each of the rings forming the resonator by means of a high impedance section in order to apply the biasing voltage between them. This structure is fabricated on the BST substrate and then placed on a carrier substrate. A photograph of the whole device, including the biasing network can be seen in Fig. 2 of the article. The 100KΩ SMD resistors used to block the RF signal can be observed in the photograph. The DC signal needs no blocking, since the rings are isolated from the transmission line and, thus, from the ports. The applied tuning voltage was varied from $V$=0V (untuned state) up to $V$=140V (tuned state), what causes an important variation in $\varepsilon_r$. The values of $\varepsilon_r$ considered in the simulations are $\varepsilon_{r,untuned}$=255 and $\varepsilon_{r,tuned}$=340, which have been chosen taking into account the kind of substrate, the applied voltage and the distance between the electrode and the line. The simulated and measured frequency response of the device in these two states is shown in Fig.3 in Article M. Very low insertion losses are observed in the pass band, whereas the rejection in the notch is around -5dB. This rejection level can be increased by cascading several unit cells as can be observed below in Fig.4.17(a), which shows some recent results from a 3-stage structure. The achieved tuning range is around 13% in both cases, which is in agreement with previous results in similar substrates. The photograph in Fig.4.17(b) shows the whole fabricated device including the biasing network, in which 100KΩ resistors are employed to block the RF signal and 0Ω resistors are simply used as connecting elements.

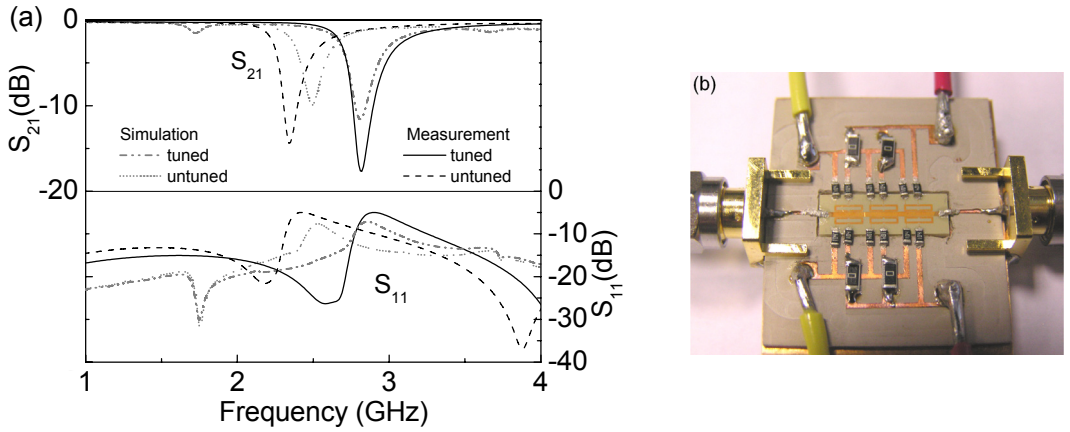


**Fig.4.17.** (a) Simulated and measured frequency response of a tunable SRR-loaded microstrip transmission line formed by 3 unit cells. The measured tuning range is 12.7%. (b) Photograph of the complete fabricated device.

Regarding the OCSRR, it was also designed to be polarised and used to load a microstrip transmission line. Two structures formed by 1 and 3 unit cells were implemented and characterised. The OCSRRs have a rectangular form, as can be seen in Fig.4.18 (b), where the main dimensions are indicated. The picture shows the electrodes used to apply the DC voltage to tune the capacitance and, therefore, the resonance frequency of the resonator. The simulated and measured frequency responses of the 1- and 3-unit-cell structures are shown in Fig.4.18(a) and (c), respectively. The designed structures exhibit a low-pass response with a very low insertion loss level in the pass band. The measurements reveal the achieved tunability, which arrives at 12.5% in the case of the 3-unit-cell structure. In this case a difference of up to 30dB is achieved around 3.2GHz between the tuned and untuned states around 1.8GHz. In the 1-unit-cell structure, the measured tuning range is about 7%, which is considerably lower than the expected. This low tunability is probably related to fabrication tolerances, since other structures evidence higher achievable values. Fig.4.18(d) shows the photograph of the fabricated device formed by 3 unit cells.

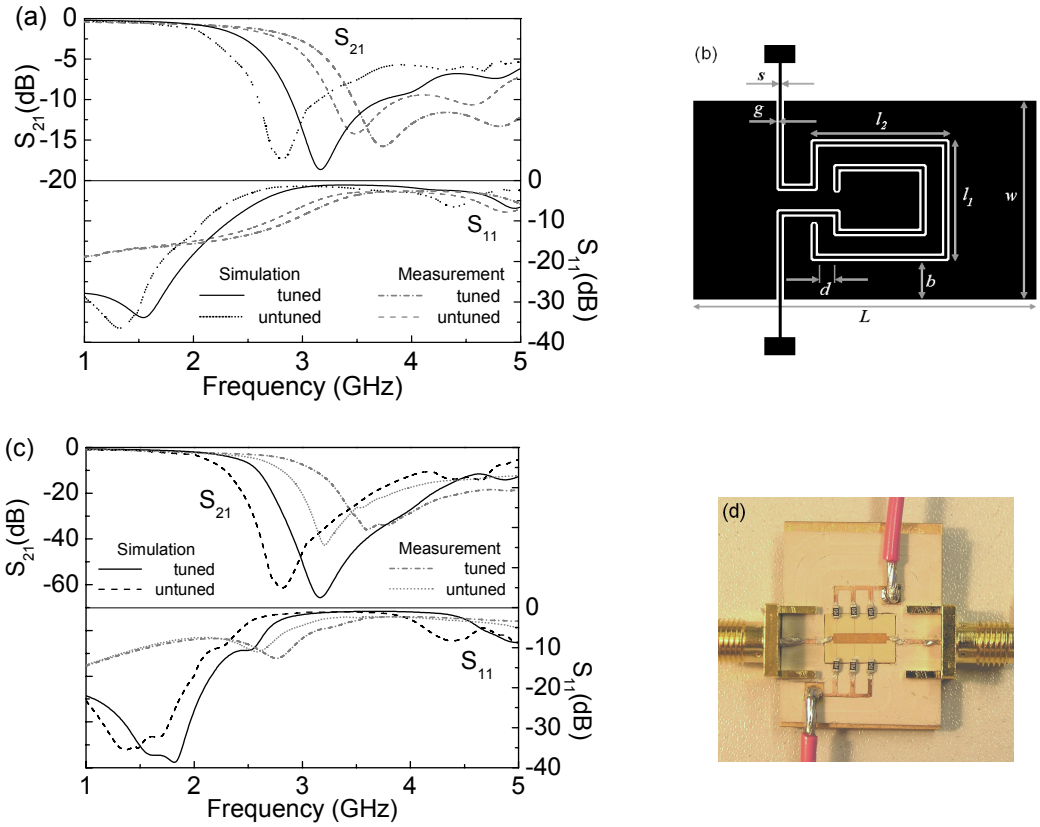


**Fig.4.18.** (a) Simulated and measured frequency response of a tunable OCSRR-loaded microstrip transmission line formed by 1 unit cell. The measured tuning range is 7%. (b) Scheme of the fabricated unit cell (not to scale). The real dimensions are $s$=30μm, $g$=10μm, $d$=70μm, $b$=0.33mm, $l_1$=0.69mm, $l_2$=1.47mm, $w$=1.35mm, $L$=2.33mm. (c) Simulated and measured frequency response of a tunable OCSRR-loaded microstrip transmission line formed by 3 unit cells. The measured tuning range is 12.5%. (b) Photograph of the fabricated device with 3 unit cells.

The developed work represents a first step in the implementation of tunable devices based on ferroelectric materials and metamaterial structures. The presented results evidence the possibility offered by this strategy to implement tunable resonators. On the basis of these results, possible next stages could be the implementation of transmission lines with controllable and tunable phase and impedance, or tunable devices, like, for example, filters.

# 5 Conclusions and Future Research Lines

*This document gathers the results of the work developed during the elaboration of this Thesis, focussed on the study and implementation of resonant-type metamaterial transmission lines and their application in microwave device design. The resonant-type approach employs different kinds of sub-wavelength resonators in the synthesis of metamaterial transmission lines exhibiting compact dimensions and controllable characteristics. Different kinds of microwave devices can be implemented by means of these metamaterial transmission lines and this Thesis includes some of them as application examples.*

The document has been divided in several chapters and sections devoted to different aspects of the work carried out during the last years. After a first chapter, in which the work is introduced, three chapters are devoted to the study of the employed concepts and the presentation of the obtained results:

- Chapter 2 consists in a general and short introduction about metamaterials. It includes brief considerations about effective media, whose period is much smaller than the wavelength, this allowing those media to exhibit exotic properties, different from those of their constituent elements. Within media with effective characteristics, left-handed media and their exceptional properties are considered with special attention. As basic elements in resonant-type metamaterial transmission lines, sub-wavelength resonators are also studied in this chapter. Special attention is also paid to metamaterial planar structures based on the dual line concept.

- Chapter 3 studies different kinds of metamaterial transmission lines based on the resonant approach. Structures based on split-ring resonators (SRRs) and complementary split-ring resonators (CSRRs) are presented and studied, although special attention is paid to those lines based on complementary split-ring resonators, which have been mainly applied along this Thesis. These structures are basically microstrip transmission lines loaded with CSRRs and capacitive gaps. A second approach called hybrid approach includes also shunt connected inductive stubs, which additionally contribute to obtain backward propagation. The transmission properties of purely resonant and hybrid transmission lines are studied in detail on the basis of their equivalent circuit model. The presented microstrip structures include complementary resonators, which can be etched either on the ground plane or on the signal strip; both kinds of structures are presented in this chapter. Balanced transmission lines are also studied in this chapter. On the basis of the composite behaviour of resonant-type metamaterial transmission lines, balanced transmission lines showing a continuous transition between the right- and left-handed transmission bands can be designed. Wide band responses can, thus, be obtained by the elimination of the frequency gap that usually separates the RH and the LH transmission bands in composite structures, opening the door to the application of resonant-type metamaterial transmission lines for wide band applications. The second part of the chapter is devoted to the synthesis of this kind of transmission lines controlling their transmission properties. The first part studies the influence of the modification of the geometrical dimensions of different elements of the purely resonant structure on its frequency response. Additionally, a parametric analysis shows the effect of the modification of the resonator dimensions on the values of the related elements of the circuit model. These studies provide a guide when it comes to design a transmission line with specific values of the phase and impedance at certain frequencies. Additionally, the equivalent circuit model is theoretically analysed. In a first study it is shown that it is possible to modify the phase and the impedance of the structure in order to control the frequency response and improve it in terms of matching and ripple within the band. Several restrictions apply, since the elements of the circuit model must be positive and not extreme, but it is perfectly possible. A second study shows that it is also possible to impose both, phase and impedance, at the same frequency. As in the previous case, certain considerations

must be taken into account in order not to obtain extreme or negative values of the circuit elements, but it can, in general, be achieved without important restrictions. The chapter finishes with a brief description of a parameter extraction method which can be applied to obtain the circuit parameters of some of the considered structures from its simulated or measured frequency response.

- Chapter 4 is devoted to applications of the studied structures to specific devices. Once the transmission properties of the resonant-type metamaterial transmission lines have been studied, they can be properly designed to form part of specific devices. The first devices presented in this chapter are power dividers. The implementation of such devices requires the design of impedance inverters with specific values of the characteristic impedance. Several components implemented by means of metamaterial inverters and based on different topologies are shown. The fabricated devices include two types of two-output dividers comprising one and two “meta-inverters”, as well as a four-output divider. The measured frequency responses of the fabricated devices evidence the achievement of the required phase and impedance at the design frequency, which is 1.5GHz. The inclusion of metamaterial transmission lines involves a size reduction which is around a 50% in the case of the components based on purely resonant structures and significantly higher in the case of hybrid structures with the resonators etched on the signal strip. Insertion losses are very low (very close to the ideal values) in all cases, what makes these devices suitable for narrow band applications. As the experimental results confirm, bandwidth can be to some extent enlarged in this devices employing thin substrates.

Other strategies for bandwidth enlargement are exposed in the section devoted to dispersion engineering. This fragment deals with the handling of the dispersion diagram of the metamaterial transmission lines. The controllability over the electric characteristics of these structures allows the achievement of certain conditions which are not possible when only conventional transmission lines are employed. This fact can be exploited with bandwidth enhancement purposes or even to create devices operative at multiple and arbitrary frequencies (multi-band devices). Bandwidth can be enhanced, for example, in devices based on phase differences by manipulating the dispersion diagrams of the different transmission lines forming the device to be parallel along a wider frequency range. By imposing phase and impedance at different frequencies, a device can be designed to be dual- or multi-band.

Metamaterial filter design is one more of the application possibilities of resonant-type metamaterial transmission lines. The section devoted to such devices starts with a review of the state of the art in metamaterial filters based on the resonant approach. The inclusion of SRRs to create a stop band or improve the out-of-band performance of conventional filters by suppressing spurious bands and the alternation of right- and left-handed transmission line sections are some of the strategies employed. Some examples of metamaterial filters based on different approaches are also included. The section continues with the presentation of new results based on different strategies suitable for the implementation of narrow- and broad-band filters. A methodology for the design of standard filters with narrow and moderate bandwidths is briefly exposed and some results obtained from its application are shown. The results apply two different kinds of hybrid structures. The first one is an order-3 Chebyshev filter based on CSRs etched on the ground plane of a microstrip transmission line. The complementary resonators are combined with capacitive gaps and shunt-connected inductive stubs. The use of CSRs involves an additional size reduction with respect to previous results employing CSRRs, which are electrically larger. The position of the transmission zeros of the different unit cells is controlled to improve the out-of-band rejection. The result is a very compact filter with central frequency $f_0$=1.1GHz and $FBW$=10% exhibiting a total area $A$=0.22$\lambda$ x 0.08$\lambda$ and the first spurious band around 3$f_0$. A second example is a periodic filter based on CSRs like in the previous case, but this time the resonators are etched on the signal strip. The advantage of this structure is the fact that it leaves the ground plane unaltered. This fact can be of interest in those applications in which the components must rest on a metallic surface, since this would disable the resonators if they were etched on the ground plane. Additionally, size reduction is achieved thanks to the use of CSRs, although their inclusion also involves a light increment of the loss level. Regarding broadband filters, two strategies are exposed. One of them is based on

a methodology similar to the one developed for narrow-band bandpass filters, but employing a different topology providing broad transmission bands. The second one employs balanced transmission lines. The union of the left- and the right-handed transmission bands that resonant-type metamaterial transmission lines exhibit thanks to their composite behaviour allows to obtain broad transmission bands. Cascaded purely resonant balanced transmission lines can be used to implement high-pass filters, whereas if additional resonators are included to reject the signal at certain frequencies a band-pass response can be obtained. Several device examples are shown, in which metallic or complementary resonators are included to control the upper edge of the band or even to include attenuation poles. The designed devices cover the standard mask for ultra wideband (UWB) applications and the attenuation poles are included to eliminate undesired interfering signals that may appear within the transmission band. Different topologies can be used to implement such filters and all of them give rise to very compact devices, smaller than $1cm^2$. UWBPF filters based on balanced transmission lines can also be implemented by means of the hybrid approach. A four-stage filter based on such structures is shown as an application example. The filter exhibits a good frequency selectivity and very compact dimensions.

The chapter devoted to applications finishes with the section dedicated to reconfigurable transmission lines, paying special attention to those based on ferroelectric materials. A short introduction is devoted to tunable components based on the application of varactor diodes and MEMS, which have been applied in the design of resonant-type metamaterial structures. Ferroelectric-based tunable structures are studied in more detail. Some basic concepts related to ferroelectric materials are exposed before the presentation of the obtained results. Barium Strontium Titanate (BST) thick layers are used under the metallisation layer to implement tunable structures. Reconfigurable structures based on SRR and open complementary split-ring resonators (OCSRR) are synthesized taking advantage of the dependence of the dielectric permittivity of the BST layer with the external electric field to tune the associated capacitance of the resonators by means of a DC-voltage. The achieved tunability is around 13% for both kinds of structures. The results are a proof-of-concept showing the feasibility of this technique to implement reconfigurable structures based on metamaterial resonators. It could represent a first step in the future application of such structures in the design of tunable microwave devices.

The exposed results represent a part of the work developed during the last years in this research group in the analysis of resonant-type metamaterial transmission lines and their application in microwave device design. Different structures based on sub-wavelength resonators have been studied and employed in the implementation of specific components, like power dividers or filters, showing the suitability of this kind of transmission lines for such purposes. The small dimensions of these structures allow the design of compact devices, which may be of special interest in those applications in which size or weight are critical aspects, like, for instance, aerospace or portable communication systems.

The possibilities that resonant-type metamaterial transmission lines can offer are still not exhausted. New structures and applications are being found and studied in order to improve the existing results or to find new ones. Efforts are being devoted, for example, to the study and implementation of coplanar structures based on SRRs or other resonators with the intention of applying them in a similar way as structures based on microstrip lines and complementary resonators are employed. The possibility of synthesizing, for example, balanced structures based on such topologies for their application in broadband devices is being studied. Resonators which have recently been proposed by the Group, like the OCSRR, and their application in low-pass and band-pass filter design are also being analysed in detail. Further steps in the application of MEMS technology in the synthesis of reconfigurable components are also in progress in collaboration with IMEC (Leuven, Belgium) and the MINACOM Department from the XLIM Research Institute of the Université de Limoges/CNRS (France). The improvement of the equivalent circuit models of different structures is one additional objective which is under study. One more interesting scope is the development of a synthesis method based on space mapping which allows the determination of the topology of a structure from the electrical parameters of the circuit model. This methodology is planned to be carried out in collaboration with the GAM Group of the iTEAM Reseach Centre of the Universidad Politécnica

de Valencia. Multi- (more than two) band device design is one more interesting scope which is also being studied.

Regarding concrete applications, radio frequency identification (RFID) is a very promising field in which resonant-type metamaterial devices could contribute good solutions. Work is in progress in this direction developing dual-band matching networks and antennas with small dimensions for UHF-RFID systems suitable for the operation at the European and American bands. The implementation of such components on paper substrates, what would involve important reductions in costs and weight, is one more possibility which is being explored. Regarding device miniaturisation, geo-radar systems represent one example of a specific application in which metamaterial based components can involve important improvements.

In conclusion, the results presented in this Thesis show the particular properties of resonant-type metamaterial transmission lines and how they can be exploited in the design of innovative microwave devices with compact dimensions and improved performances.

# References


[1] V. G. Veselago. "The electrodynamics of substances with simultaneously negative values of $\varepsilon$ and $\mu$", *Soviet Physics Uspekhi*, pp. 509-514, 1968.

[2] D. R. Smith, W. J. Padilla, D. C. Vier, S. C. Nemat-Nasser and S. Schultz. "Composite medium with simultaneously negative permeability and permittivity", *Physical Review Letters*, vol. 84, pp. 4184-4187, 2000.

[3] J. B. Pendry, A. J. Holden, D. J. Robbins and W. J. Stewart. "Magnetism from conductors and enhanced nonlinear phenomena", *IEEE Transactions on Microwave Theory and Techniques,* vol. 47, pp. 2075-2084, 1999.

[4] J. D. Baena, J. Bonache, F. Martín, R. Marqués Sillero, F. Falcone, T. Lopetegi, M. A. G. Laso, J. Garcia-Garcia, I. Gil, M. F. Portillo and M. Sorolla. "Equivalent-circuit models for split-ring resonators and complementary split-ring resonators coupled to planar transmission lines", *IEEE Transactions on Microwave Theory and Techniques*, vol. 53, pp. 1451-1461, 2005.

[5] R. Marqués, F. Martín and M. Sorolla. *Metamaterials with Negative Parameters: Theory, Design and Microwave Applications*. John Wiley & Sons, Inc., New Jersey, 2007.

[6] R. Marqués, F. Mesa, J. Martel and F. Medina. "Comparative analysis of edge- and broadside-coupled split ring resonators for metamaterial design - Theory and experiments," *IEEE Transactions on Antennas and Propagation*, vol. 51, pp. 2572-2581, 2003.

[7] J. D. Baena, "Diseño, Análisis y Aplicaciones de Metamateriales Electromagnéticos", *Doctoral Thesis,* Universidad de Sevilla, December 2005.

[8] J. García-García, F. Martín, J. D. Baena, R. Marqués, and L. Jelinek, "On the resonances and polarizabilities of split ring resonators", *Journal of Applied Physics*, vol. 98, pp. 033103-9, 2005.

[9] F. Falcone, T. Lopetegi, J. D. Baena, R. Marqués, F. Martín and M. Sorolla, "Effective negative-epsilon stopband microstrip lines based on complementary split ring resonators", *IEEE Microwave and Wireless Components Letters*, vol. 14, pp. 280-282, 2004.

[10] F. Falcone, T. Lopetegi, M. A. G. Laso, J. D. Baena, J. Bonache, M. Beruete, R. Marqués, F. Martín and M. Sorolla, "Babinet Principle Applied to the Design of Metasurfaces and Metamaterials", *Physical Review Letters*, vol. 93, pp. 197401-4, 2004.

[11] F. Aznar, M. Gil, J. Bonache, J. Garcia-Garcia and F. Martin, "Metamaterial transmission lines based on broad-side coupled spiral resonators", *Electronics Letters*, vol. 43, pp. 530-532, 2007.

[12] F. Aznar, J. García-García, M. Gil, J. Bonache and F. Martín, "Strategies for the miniaturization of metamaterial resonators", *Microwave and Optical Technology Letters*, vol. 50, pp. 1263-1270, 2008.

[13] F. Bilotti, A. Toscano, L. Vegni, K. Aydin, K. B. Alici and E. Ozbay, "Equivalent-Circuit Models for the Design of Metamaterials Based on Artificial Magnetic Inclusions", *IEEE Transactions on Microwave Theory and Techniques*, vol. 55, pp. 2865-2873, 2007.

[14] K. B. Alici, F. Bilotti, L. Vegni and E. Ozbay, "Miniaturized negative permeability materials", *Applied Physics Letters*, vol. 91, pp. 071121-3, 2007.

[15] J. Martel, R. Marqués, F. Falcone, J. D. Baena, F. Medina, F. Martín and M. Sorolla, "A new LC series element for compact bandpass filter design", *IEEE Microwave and Wireless Components Letters*, vol.14, pp.210-212, 2004.

[16] J. B. Pendry, A. J. Holden, D. J. Robbins and W. J. Stewart, "Low frequency plasmons in thin-wire structures", *Journal of Physics Condensed Matter*, vol. 10, pp. 4785-4809, 1998.

[17] R. Marqués, J. Martel, F. Mesa and F. Medina, "Left-handed-media Simulation and Transmission of EM Waves in Subwavelength Split-ring-resonator-Loaded Metallic Waveguides", *Physical Review Letters*, vol. 89, pp. 183901-4, 2002.

[18] J. B. Pendry and D. R. Smith. "Reversing light with negative refraction", *Physics Today*, vol. 57, pp. 37-43, 2004.

[19] J. Bonache. "Filtros de microondas basados en metamateriales y en resonadores concentrados". *Doctoral Thesis*, Universitat Autònoma de Barcelona, December 2006.

[20] R. A. Shelby, D. R. Smith and S. Schultz, "Experimental verification of a negative index of refraction", *Science*, vol. 292, pp. 77-79, 2001.

[21] J. Lu, T. Grzegorczyk, Y. Zhang, J. Pacheco Jr, B.-I. Wu, J. Kong and M. Chen, "Cerenkov radiation in materials with negative permittivity and permeability", *Opt. Express*, vol.11, pp. 723-734, 2003.

[22] D. Schurig, J. J. Mock, B. J. Justice, S. A. Cummer, J. B. Pendry, A. F. Starr and D. R. Smith, "Metamaterial Electromagnetic Cloak at Microwave Frequencies", *Science*, vol. 314, pp. 977-980, 2006.

[23] J. B. Pendry, D. Schurig and D. R. Smith, "Controlling Electromagnetic Fields", *Science*, vol. 312, pp. 1780-1782, 2006.

[24] J. Valentine, S. Zhang, T. Zentgraf, E. Ulin-Avila, D. A. Genov, G. Bartal and X. Zhang, "Three-dimensional optical metamaterial with a negative refractive index", *Nature*, vol. 455, pp. 376-379, 2008.

[25] J. B. Pendry, "Negative Refraction Makes a Perfect Lens", *Physical Review Letters*, vol. 85, pp. 3966-4, 2000.

[26] A. Grbic and G. V. Eleftheriades, "Overcoming the Diffraction Limit with a Planar Left-Handed Transmission-Line Lens", *Physical Review Letters*, vol. 92, pp. 117403-4, 2004.

[27] N. Fang, H. Lee, C. Sun and X. Zhang, "Sub-Diffraction-Limited Optical Imaging with a Silver Superlens", *Science*, vol. 308, pp. 534-537, 2005.

[28] R. Marqués, F. Mesa and F. Medina, "Near-field enhanced imaging by a magnetized ferrite slab", *Applied Physics Letters*, vol. 86, pp. 023505-3, 2005.

[29] M. J. Freire and R. Marqués, "Planar magnetoinductive lens for three-dimensional subwavelength imaging", *Applied Physics Letters*, vol. 86, pp. 182505-3, 2005.

[30] M. J. Freire and R. Marqués, "Optimizing the magnetoinductive lens: Improvement, limits, and possible applications", *Journal of Applied Physics*, vol. 103, pp. 013115-7, 2008.

[31] M. J. Freire and R. Marqués, "Superlentes basadas en resonadores tipo split-ring para aplicaciones en imagen por resonancia magnética," *XXIII Simposium Nacional de la Unión Científica Internacional de Radio (URSI)*, Madrid, 2008.

[32] A. K. Iyer and G. V. Eleftheriades, "Negative refractive index metamaterials supporting 2D waves", *IEEE MTT-S International Microwave Symposium Digest*, Seattle (WA), USA, pp. 1067-1070, 2002.

[33] F. Martín, J. Bonache, F. Falcone, M. Sorolla and R. Marqués, "Split ring resonator-based left-handed coplanar waveguide", *Applied Physics Letters*, vol. 83, pp. 4652-4654, 2003.

[34] A. A. Oliner, "A planar negative-refractive-index medium without resonant elements", *IEEE MTT-S International Microwave Symposium Digest*, Philadelphia (CA), (USA), 2003.

[35] C. Caloz and T. Itoh, "Application of the transmission line theory of left-handed (LH) materials to the realization of a microstrip "LH line"", *IEEE Antennas and Propagation Society International Symposium*, pp. 412-415, vol.2*,* 2002.

[36] G. V. Eleftheriades, A. K. Iyer, and P. C. Kremer, "Planar negative refractive index media using periodically L-C loaded transmission lines," *Microwave Theory and Techniques, IEEE Transactions on*, vol. 50, pp. 2702-2712, 2002.

[37] C. Caloz and T. Itoh, *Electromagnetic Metamaterials: Transmission Line Theory and Microwave Applications*. Wiley Interscience, 2005.

[38] D. M. Pozar, *Microwave Engeneering*, John Wiley & Sons, 1998.

[39] C. Caloz and T. Itoh, "Novel microwave devices and structures based on the transmission line approach of meta-materials," *IEEE MTT-S International Microwave Symposium Digest,* Philadelphia (PA), USA, vol.1, pp. 195-198, 2003.

[40] A. Sanada, C. Caloz and T. Itoh, "Characteristics of the composite right/left-handed transmission lines", *IEEE Microwave and Wireless Components Letters,* vol. 14, pp. 68-70, 2004.

[41] A. Lai, T. Itoh, and C. Caloz, "Composite right/left-handed transmission line metamaterials", *IEEE Microwave Magazine,* vol. 5, pp. 34-50, 2004.

[42] F. Aznar, M. Gil, J. Bonache and F. Martin, "Modelling metamaterial transmission lines: a review and recent developments", *Opto-Electronics Review*, vol. 16, pp. 226-236, 2008.

[43] C. Caloz, A. Sanada and T. Itoh, "A novel composite right-/left-handed coupled-line directional coupler with arbitrary coupling level and broad bandwidth", *IEEE Transactions on Microwave Theory and Techniques*, vol. 52, pp. 980-992, 2004.

[44] R. Islam and G. V. Eleftheriades, "Printed high-directivity metamaterial MS/NRI coupled-line coupler for signal monitoring applications", *IEEE Microwave and Wireless Components Letters*, vol. 16, pp. 164-166, 2006.

[45] R. Islam and G. V. Eleftheriades, "Phase-agile branch-line couplers using metamaterial lines", *IEEE Microwave and Wireless Components Letters*, vol. 14, pp. 340-342, 2004.

[46] M. A. Antoniades and G. V. Eleftheriades, "A broadband series power divider using zero-degree metamaterial phase-shifting lines", *IEEE Antennas and Wireless Propagation Letters*, vol. 15, pp. 808-810, 2005.

[47] C. H. Tseng and C. L. Chang, "A broadband quadrature power splitter using metamaterial transmission line", *IEEE Microwave and Wireless Components Letters*, vol. 18, pp. 25-27, 2008.

[48] E. Sáenz, A. Cantora, I. Ederra, R. Gonzalo and P. de Maagt, "A metamaterial T-junction power divider", *IEEE Microwave and Wireless Components Letters*, vol. 17, pp. 172-174, 2007.

[49] C.H. Tseng and T. Itoh, "Dual-Band Bandpass and Bandstop Filters Using Composite Right/Left-Handed Metamaterial Transmission Lines", *IEEE MTT-S International Microwave Symposium Digest*, pp. 931-934, 2006.

[50] S. Lim, C. Caloz and T. Itoh, "Metamaterial-based electronically controlled transmission-line structure as a novel leaky-wave antenna with tunable radiation angle and beamwidth", *IEEE Transactions on Microwave Theory and Techniques,* vol. 53, pp. 161-173, 2005.

[51] W. J. R. Hoefer, P. P. M. So, D. Thompson and M. M. Tentzeris, "Topology and design of wide-band 3D metamaterials made of periodically loaded transmission line arrays", *IEEE MTT-S International Microwave Symposium Digest,* pp. 313-316, 2005.

[52] M. Zedler, C. Caloz and P. Russer, "A 3-D Isotropic Left-Handed Metamaterial Based on the Rotated Transmission-Line Matrix (TLM) Scheme", *IEEE Transactions on Microwave Theory and Techniques*, vol. 55, pp. 2930-2941, 2007.

[53] A. Grbic and G. V. Eleftheriades, "An isotropic three-dimensional negative-refractive-index transmission-line metamaterial", *Journal of Applied Physics*, vol. 98, pp. 043106-5, 2005.

[54] F. Falcone, F. Martín, J. Bonache, R. Marqués and M. Sorolla, "Coplanar waveguide structures loaded with split-ring resonators", *Microwave and Optical Technology Letters*, vol. 40, pp. 3-6, 2004.

[55] F. Aznar, J. Bonache and F. Martín, "Improved circuit model for left-handed lines loaded with split ring resonators", *Applied Physics Letters*, vol. 92, pp. 043512-3, 2008.

[56] F. Aznar, M. Gil, J. Bonache and F. Martín, "Revising the equivalent circuit models of resonant-type metamaterial transmission lines", *IEEE MTT-S International Microwave Symposium Digest*, Atlanta (GA), pp. 323-326, 2008.

[57] L. J. Roglá, J. Carbonell and V. E. Boria, "Study of equivalent circuits for open-ring and split-ring resonators in coplanar waveguide technology", *IET Microwaves, Antennas & Propagation*, vol. 1, pp. 170-176, 2007.

[58] F. Martín, F. Falcone, J. Bonache, R. Marqués, and M. Sorolla, "Miniaturized coplanar waveguide stop band filters based on multiple tuned split ring resonators", *IEEE Microwave and Wireless Components Letters*, vol. 13, pp. 511-513, 2003.

[59] I. Gil, J. Bonache, M. Gil, J. García-García and F. Martín, "Left-handed and right-handed transmission properties of microstrip lines loaded with complementary split rings resonators", *Microwave and Optical Technology Letters*, vol. 48, pp. 2508-2511, 2006.

[60] J. Bonache, J. Martel, I. Gil, M. Gil, J. García-García, F. Martín, I. Cairo and M. Ikeda, "Super compact (<1cm2) band pass filters with wide bandwidth and high selectivity at c-band", *European Microwave Conference,* Manchester, United Kingdom, pp. 599-602, 2006.

[61] M. Gil, J. Bonache, J. Selga, J. García-García and F. Martín., "High-pass filters implemented by composite right/left handed (CRLH) transmission lines based on complementary split rings resonators (CSRRs)", *Progress in Electromagnetic Research Symposium (PIERS)*, vol.3, pp. 251-253, Beijing, China, 2007.

[62] J. Bonache, I. Gil, J. Garcia-Garcia and F. Martin, "Novel microstrip bandpass filters based on complementary split-ring resonators", *IEEE Transactions on Microwave Theory and Techniques*, vol. 54, pp. 265-271, 2006.

[63] G. Sisó, J. Bonache, M. Gil and F. Martín, "Enhanced bandwidth and dual-band microwave components based on resonant-type metamaterial transmission lines," *International Journal of Microwave and Optical Technology*, vol. 3, pp. 345-352, 2008.

[64] G. Sisó, J. Bonache and F. Martín, "Dual-band Y-junction power dividers implemented through artificial lines based on complementary resonators," *IEEE MTT-S International Microwave Symposium Digest*, Atlanta (GA), USA, pp. 663-666, 2008.

[65] G. Sisó, J. Bonache, M. Gil, J. García-García and F. Martín, "Compact Rat-Race Hybrid Coupler Implemented Through Artificial Left Handed and Right Handed Lines," *IEEE MTT-S International Microwave Symposium Digest*, Honolulu (HA), USA, pp. 25-28, 2007.

[66] J. Bonache, G. Sisó, M. Gil, A. Iniesta, J. Garcia-Rincón and F. Martín, "Application of composite right/left handed (CRLH) transmission lines based on complementary split ring resonators (CSRRs) to the design of dual-band microwave components," *IEEE Microwave and Wireless Components Letters*, vol. 18, pp. 524-526, 2008.

[67] J. Bonache, M. Gil, I. Gil, J. García-García and F. Martín, "On the electrical characteristics of metamaterial resonators", *IEEE Microwave and Wireless Components Letters*, vol. 16, pp. 543-545, 2006.

[68] F. Aznar, M. Gil, J. Bonache, L. Jelinek, J. D. Baena, R. Marqués and F. Martín, "Characterization of miniaturized metamaterial resonators coupled to planar transmission lines through parameter extraction", *Journal of Applied Physics*, vol. 104, pp. 114501-8, 2008.

[69] G. Sisó, M. Gil, J. Bonache and F. Martín, "On the dispersion characteristics of metamaterial transmission lines", *Journal of Applied Physics*, vol.102, 074911-7, 2007.

[70] M. A. Antoniades and G. V. Eleftheriades, "A broadband Wilkinson balun using microstrip metamaterial lines", *IEEE Antennas and Wireless Propagation Letters*, vol. 4, pp. 209-212, 2005.

[71] G. Sisó, M. Gil, J. Bonache and F. Martín, "Applications of resonant-type metamaterial transmission lines to the design of enhanced bandwidth components with compact dimensions", *Microwave and Optical Technology Letters*, vol. 50, pp. 127-134, 2008.

[72] G. Sisó, M. Gil, J. Bonache and F. Martín, "Application of metamaterial transmission lines to design of quadrature phase shifters", *IEEE Electronics Letters*, vol. 43, pp. 1098-1100, 2007.

[73] D. Kholodnyak, P. Kapitanova, S. Humbla, R. Perrone, J. Mueller, M. A. Hein and I. Vendik, "180° Power Dividers Using Metamaterial Transmission Lines", *14th Conference on Microwave Techniques ( COMITE),* pp. 1-4, 2008.

[74] Y.-H. Chun, J.-S. Hong, J.-Y. Moon and S.-W. Yun, "High Directivity Directional Coupler using Metamaterial", *European Microwave Conference,* pp. 329-331, 2006.

[75] I. H. Lin, M. DeVincentis, C. Caloz and T. Itoh, "Arbitrary dual-band components using composite right/left-handed transmission lines", *IEEE Transactions on Microwave Theory and Techniques*, vol. 52, pp. 1142-1149, 2004.

[76] G. V. Eleftheriades, "A Generalized Negative-Refractive-Index Transmission-Line (NRI-TL) Metamaterial for Dual-Band and Quad-Band Applications", *IEEE Microwave and Wireless Components Letters*, vol. 17, pp. 415-417, 2007.

[77] G. Sisó, M. Gil, J. Bonache and F. Martín, "Generalized Model for Multiband Metamaterial Transmission Lines", *IEEE Microwave and Wireless Components Letters*, vol. 18, pp. 728-730, 2008.

[78] G. Sisó, M. Gil, F. Aznar, J. Bonache and F. Martín, "Dispersion engineering with resonant-type metamaterial transmission lines", *Laser & Photonics Review*, DOI:10.1002/lpor.200810026, 2008.

[79] J. García-García, J. Bonache, I. Gil, F. Martín, R. Marqués, F. Falcone, T. Lopetegi, M. A. G. Laso and M. Sorolla, "Comparison of electromagnetic band gap and split-ring resonator microstrip lines as stop band structures", *Microwave and Optical Technology Letters*, vol. 44, pp. 376-379, 2005.

[80] F. Falcone, F. Martín, J. Bonache, M. A. G. Laso, J. García-García, J. D. Baena, R. Marqués and M. Sorolla, "Stop-band and band-pass characteristics in coplanar waveguides coupled to spiral resonators", *Microwave and Optical Technology Letters*, vol. 42, pp. 386-388, 2004.

[81] J. García-García, F. Martín, F. Falcone, J. Bonache, I. Gil, T. Lopetegi, M. A. G. Laso, M. Sorolla and R. Marqués, "Spurious passband suppression in microstrip coupled line band pass filters by means of split ring resonators", *IEEE Microwave and Wireless Components Letters*, vol. 14, pp. 416-418, 2004.

[82] J. García-García, J. Bonache, F. Falcone, J. D. Baena, F. Martín, I. Gil, T. Lopetegi, M. A. G. Laso, A. Marcotegui, R. Marqués and M. Sorolla, "Stepped-impedance lowpass filters with spurious passband suppression", *Electronics Letters*, vol. 40, pp. 881-883, 2004.

[83] J. García-García, F. Martín, F. Falcone, J. Bonache, J. D. Baena, I. Gil, E. Amat, T. Lopetegi, M. A. G. Laso, J. A. M. Iturmendi, M. Sorolla and R. Marqués, "Microwave filters with improved stopband based on sub-wavelength resonators", *IEEE Transactions on Microwave Theory and Techniques*, vol. 53, pp. 1997-2006, 2005.

[84] M. K. Mandal, P. Mondal, S. Sanyal and A. Chakrabarty, "Low Insertion-Loss, Sharp-Rejection and Compact Microstrip Low-Pass Filters", *IEEE Microwave and Wireless Components Letters*, vol. 16, pp. 600-602, 2006.

[85] J. Bonache, F. Martín, F. Falcone, J. García-García, I. Gil, T. Lopetegi, M. A. G. Laso, R. Marqués, F. Medina and M. Sorolla, "Super compact split ring resonators CPW band pass filters", *IEEE MTT-S International Microwave Symposium Digest*, Fort Worth (TX), USA, vol. 3, pp. 1483-1486, 2004.

[86] J. Bonache, F. Martín, F. Falcone, J. D. Baena, T. Lopetegi, J. G.-G. Miguel, A. G. Laso, I. Gil, A. Marcotegui, R. Marqués and M. Sorolla, "Application of complementary split-ring resonators to the design of compact narrow band-pass structures in microstrip technology", *Microwave and Optical Technology Letters*, vol.46, pp.508-512, 2005.

[87] J. Bonache, F. Martín, F. Falcone, J. García-García, I. Gil, T. Lopetegi, M. A. G. Laso, R. Marqués, F. Medina and M. Sorolla, "Compact coplanar waveguide band-pass filter at the S-band", *Microwave and Optical Technology Letters*, vol.46, pp.33-35, 2005.

[88] J. Bonache, I. Gil, J. García-García and F. Martín, "Complementary split ring resonators for microstrip diplexer design", *Electronics Letters*, vol.41, pp.810-811, 2005.

[89] P. Mondal, M. K. Mandal, A. Chaktabarty and S. Sanyal, "Compact bandpass filters with wide controllable fractional bandwidth", *IEEE Microwave and Wireless Components Letters*, vol. 16, pp. 540-542, 2006.

[90] H. V. Nguyen and C. Caloz, "Broadband highly selective bandpass filter based on a Tapered Coupled-resonator (TCR) CRLH structure", *Proceedings of the European Microwave Association*, vol. 2, pp. 44-51, 2006.

[91] I. B. Vendik, D. V. Kholodnyak, I. V. Kolmakova, E. V. Serbryakova, P. V. Kapitanova, F. Martín, J. Bonache, J. García-García, I. Gil and M. Gil, "Applications of Right/Left Handed and Resonant Left Handed Transmission Lines for Microwave Circuit Design", *36th European Microwave Conference*, Manchester, United Kingdom, pp. 955-958, 2006.

[92] B. Jokanovic and V. Crnojevic-Bengin, "Super-compact left-handed resonator for filter applications", *37th European Microwave Conference*, Munich, Germany, pp. 716-719, 2007.

[93] J. García-García, J. Bonache, I. Gil, F. Martín, M. C. Velazquez-Ahumada and J. Martel, "Miniaturized microstrip and CPW filters using coupled metamaterial resonators", *IEEE Transactions on Microwave Theory and Techniques*, vol. 54, pp. 2628-2635, 2006.

[94] J.-S. Hong and M. J. Lancaster, *Microstrip Filters for RF/Microwave Applications*, John Wiley & Sons, Inc., 2001.

[95] J. Bonache, F. Martín, I. Gil, J. García-García, R. Marqués and M. Sorolla, "Microstrip bandpass filters with wide bandwidth and compact dimensions", *Microwave and Optical Technology Letters*, vol.46, pp.343-346, 2005.

[96] J. Bonache, F. Martín, J. García-García, I. Gil, R. Marqués and M. Sorolla, "Ultra wide band pass filters (UWBPF) based on complementary split rings resonators", *Microwave and Optical Technology Letters*, vol.46, pp.283-286, 2005.

[97] J. Bonache, I. Gil, J. García-García and F. Martín, "Complementary split rings resonators (CSRRs): Towards the miniaturization of microwave device design", *Journal of Computational Electronics*, vol.5, pp.193-197, 2006.

[98] J. Bonache, I. Gil, J. García-García and F. Martín, "Complementary split rings resonators (CSRRs): Towards the miniaturization of microwave device design", *Journal of Computational Electronics*, vol.5, pp.193-197, 2006.

[99] I.Gil, "Diseño, Modelado y Caracterización de Estructuras Reconfigurables basadas en Metamateriales". *Doctoral Thesis*, Universitat Autònoma de Barcelona, March 2007.

[100] S. Lim, C. Caloz and T. Itoh, "Metamaterial-based electronically controlled transmission-line structure as a novel leaky-wave antenna with tunable radiation angle and beamwidth", *IEEE Transactions on Microwave Theory and Techniques*, vol. 53, pp. 161-173, 2005.

[101] A. Giere, C. Damm, P. Scheele and R. Jakoby, "LH phase shifter using ferroelectric varactors", *IEEE Radio and Wireless Symposium*, San Diego (CA), USA, pp. 403-406, 2006.

[102] D. Kuylenstierna, A. Vorobiev, P. Linner and S. Gevorgian, "Composite right/left handed transmission line phase shifter using ferroelectric varactors", *IEEE Microwave and Wireless Components Letters*, vol. 16, pp. 167-169, 2006.

[103] C. Damm, J. Freese, M. Schüssler and R. Jakoby, "Electrically controllable artificial transmission line transformer for matching purposes", *IEEE Transactions on Microwave Theory and Techniques*, vol. 55, pp. 1348-1354, 2007.

[104] J. Perruisseau-Carrier, T. Lisec and A. K. Skrivervik, "Circuit model and design of silicon-integrated CRLH-TLS analogically controlled by MEMS", *Microwave and Optical Technology Letters*, vol. 48, pp. 2496-2499, 2006.

[105] I. Gil, J. Bonache, J. García-García and F. Martín, "Tunable metamaterial transmission lines based on varactor-loaded split-ring resonators", *IEEE Transactions on Microwave Theory and Techniques*, vol.54, pp.2665-2674, 2006.

[106] A. Vélez, J. Bonache and F. Martín, "Varactor-Loaded Complementary Split Ring Resonators (VLCSRR) and Their Application to Tunable Metamaterial Transmission Lines", *IEEE Microwave and Wireless Components Letters*, vol.18, pp.28-30, 2008.

[107] A. Vélez, J. Bonache and F. Martín, "Effects of varying the series capacitance in CSRR-loaded metamaterial transmission lines", *Microwave and Optical Technology Letters*, vol. 49, pp. 2245-2248, 2007.

[108] A. Vélez, J. Bonache and F. Martín, "Doubly tuned metamaterial transmission lines based on complementary split-ring resonators", *Electromagnetics*, vol. 28, pp. 523-530, 2008.

[109] I. Gil, F. Martín, X. Rottenberg and W. De Raedt, "Tunable stop-band filter at Q-band based on RF-MEMS metamaterials", *Electronics Letters*, vol. 43, pp. 1153-1154, 2007.

[110] R. Waser (Editor), *Nanoelectronics and Information Technology: Advanced Electronic Materials and Novel Devices*, 2nd edition, Wiley-VCH, 2005.

[111] R. Jakoby, P. Scheele, S. Muller and C. Weil, "Nonlinear dielectrics for tunable microwave components", *15th International Conference on Microwaves, Radar and Wireless Communications. MIKON*, vol. 2, pp. 369-378, 2004.

[112] D. K. Ferry and J. P. Bird, *Electronic Materials and Devices*, Academic Press, 2001.

[113] E. Ozbay, K. Aydin, S. Butun, K. Kolodziejak and D. Pawlak, "Ferroelectric based tuneable SRR based metamaterial for microwave applications", *Microwave Conference, 2007. European*, pp. 497-499, 2007.

[114] W. D. Callister(Jr.), *Material Science and Engineering. An Introduction*. Salt Lake City, Utah, John Wiley & Sons, Inc., 1985.

[115] P. Scheele, "Steuerbare passive Mikrowellenkomponenten auf Basis hochpermittiver ferroelektrischer Schichten", *Doctoral Thesis*, Technische Universität Darmstadt, 2007.

[116] A. Giere, P. Scheele, C. Damm and R. Jakoby, "Optimization of uniplanar multilayer structures using nonlinear tunable dielectrics", *European Microwave Conference,* Paris (France), vol.1, pp. 4, 2005.

[117] A. Giere, Y. Zheng, H. Gieser, K. Marquardt, H. Wolf, P. Scheele and R. Jakoby, "Coating of planar Barium-Strontium-Titanate thick-film varactors to increase tunability", *European Microwave Conference*, Munich (Germany), pp.114-117, 2007.

[118] A. Vélez, J. Bonache, M. C. Velázquez-Ahumada, J. Martel and F. Martín, "Open Complementary Split Ring Resonators (OCSRRs) and Their Application to Wideband CPW Band Pass Filters ", *IEEE Microwave and Wireless Components Letters*, (accepted), 2009.

[119] F. Aznar, A. Vélez, J. Bonache, J. Menés and F. Martín, "Compact low pass filters with very sharp transition bands based on open complementary split ring resonators (OCSRRs)", *IEEE International Workshop on Antenna Technology*, Santa Monica (CA), USA, 2009.

# Appendix: Articles

The articles composing this work are fruit of the collaboration with the different members of GEMMA/Cimitec, as well as the Microwave Group of the Universidad de Sevilla and the Group of Microwaves and Optics from the Technische Universität Darmstadt, to whom I express my gratitude.

**Article A:** M. Gil, J. Bonache, I. Gil, J. García-García and F. Martín, "On the transmission properties of left handed microstrip lines implemented by complementary split rings resonators", Int. *Journal Numerical Modelling: Electronic Networks, Devices and Fields*, vol. 19, pp 87-103, 2006.

**Article B:** M. Gil, J. Bonache, I. Gil, J. García-García and F. Martín, "Miniaturization of planar microwave circuits by using resonant-type left handed transmission lines", *IET Microwave Antennas and Propagation*, Vol.1, pp. 73-79, 2007.

**Article C:** M. Gil, I. Gil, J. Bonache, J. García-García and F. Martín, "Metamaterial transmission lines with extreme impedance values", *Microwave and Optical Technology Letters*, vol. 48, pp. 2499-2505, 2006.

**Article D**[1]**:** M. Gil, J. Bonache, I. Gil, J. García-García and F. Martín, "Artificial Left-handed Transmission Lines for Small Size Microwave Components: Application to Power Dividers", presented at *36th European Microwave Conference (EuMC)*, Manchester (UK), pp. 1135-1138, 2006.

**Article E:** M. Gil, J. Bonache, J. Selga, J. García-García, F. Martín, "Broadband resonant type metamaterial transmission lines ", *IEEE Microwave and Wireless Components Letters*, vol. 17, pp. 97-99, 2007.

**Article F:** M. Gil, J. Bonache, J. García-García, J. Martel and F. Martín, "Composite Right/Left-Handed Metamaterial Transmission Lines Based on Complementary Split-Rings Resonators and Their Applications to Very Wideband and Compact Filter Design", *IEEE Transactions on Microwave Theory and Techniques*, Vol. 55, No. 6, pp. 1296-1304, 2007.

**Article G:** M. Gil, J. Bonache, F. Martín, "Metamaterial Filters with Attenuation Poles in the Pass Band for Ultra Wide Band Applications", *Microwave and Optical Technology Letters*, Vol. 49, Issue 12, pp 2909-2913, 2007.

**Article H**[1]**:** M. Gil, J. Bonache, J. García-García and F. Martín, "New Left Handed Microstrip Lines With Complementary Split Rings Resonators (CSRRs) Etched in the Signal Strip", *IEEE MTT-S Int'l Microwave Symposium Digest*, Honolulu (HA), USA, pp. 1419-1422, 2007.

**Article I:** M. Gil, J. Bonache and F. Martín, "Synthesis and applications of new left handed microstrip lines with complementary split-ring resonators etched on the signal strip", *IET Microwaves, Antennas & Propagation*, Vol. 2, Issue 4, pp. 324 – 330, 2008.

**Article J:** J. Bonache, M. Gil, O. García-Abad and F. Martín, "Parametric analysis of microstrip lines loaded with complementary split ring resonators", *Microwave and Optical Technology Letters*, Vol. 50 , Issue 8, pp. 2093-2096, 2008.

**Article K**[1]**:** M. Gil, J. Bonache, F. Martín. "Ultra Compact Band Pass Filters Implemented Through Complementary Spiral Resonators (CSRs)", *IEEE MTT-S Int'l Microwave Symposium Digest*, Atlanta, USA, pp.323-326, 2008.

[1] NOTE: Due to regulation reasons, these articles cannot be considered as a basic part of this Thesis, since they are Conference, but not Journal Articles. Nevertheless, they have been included given that some of the results included in them are referenced in the text.

**Article L:** M. Gil, J. Bonache, and F. Martín, "Metamaterial filters: A review", *Metamaterials*, vol. 2, pp. 186-197, 2008.

**Article M**[2]**:** M. Gil, C. Damm, A. Giere, M. Sazegar, J. Bonache, R. Jakoby, F. Martín. "Electrically Tunable SRRs at Microwave frequencies based on BST thick films". *Electronic Letters* (submitted).

[2] NOTE: Due to regulation reasons, Article M cannot be considered as a basic part of this Thesis, since, in the moment of the submission of this document, it is pending acceptance. Nevertheless, it has been included given that some of the results included in it are referenced in the text.

INTERNATIONAL JOURNAL OF NUMERICAL MODELLING: ELECTRONIC NETWORKS, DEVICES AND FIELDS
*Int. J. Numer. Model.* 2006; **19**:87–103
Published online in Wiley InterScience (www.interscience.wiley.com). DOI: 10.1002/jnm.601

# On the transmission properties of left-handed microstrip lines implemented by complementary split rings resonators

M. Gil, J. Bonache, I. Gil, J. García-García and F. Martín*,†

*Departament d'Enginyeria Electrònica, Universitat Autònoma de Barcelona 08193, Bellaterra, Barcelona, Spain*

SUMMARY

In this paper, the transmission properties of left-handed microstrip lines implemented by etching complementary split rings resonators (CSRRs) and capacitive gaps in the ground plane and conductor strip, respectively, are investigated. To this end, we make use of the lumped element equivalent circuit model of the structure, from which an accurate analysis is carried out, and the influence of the main electrical parameters on the transmission properties is pointed out through electrical simulations. Aspects such as bandwidth and in-band ripple control are discussed in detail. The influence of the geometrical parameters is also discussed and interpreted to the light of the equivalent circuit model. From the results obtained, there are inferred design guidelines that are suitable for the design of metamaterial transmission lines subjected to specifications. Copyright © 2006 John Wiley & Sons, Ltd.

KEY WORDS: metamaterials; left-handed; Complementary Split Ring Resonators (CSRRs)

## 1. INTRODUCTION

Metamaterials are artificially fabricated materials, based on periodic or quasi-periodic structures, with electromagnetic properties beyond those that can be readily found in nature [1]. These unique characteristics are possible because the relevant dimensions (period) of these structures are typically much smaller than signal wavelength at the frequencies of interest. Therefore, these materials can be considered as effective (continuous) media able to exhibit electromagnetic properties different from those of their constitutive elements. Among them, there are the so-called left-handed metamaterials (LHMs), which simultaneously exhibit negative values of the effective dielectric permittivity and magnetic permeability. These negative

*Correspondence to: Ferran Martín, Departament d'Enginyeria Electrònica, Universitat Autònoma de Barcelona, 08193 Bellaterra, Barcelona, Spain.
†E-mail: ferran.martin@uab.es

Contract/grant sponsor: MEC (Spain); contract/grant number: TEC2004-04249-C02-01 METASYSTEMS
Contract/grant sponsor: UAB-CIRIT; contract/grant number: PNL2004-22
Contract/grant sponsor: European Commission; contract/grant number: E 500252-2 METAMORPHOSE

 *Accepted 16 December 2005*

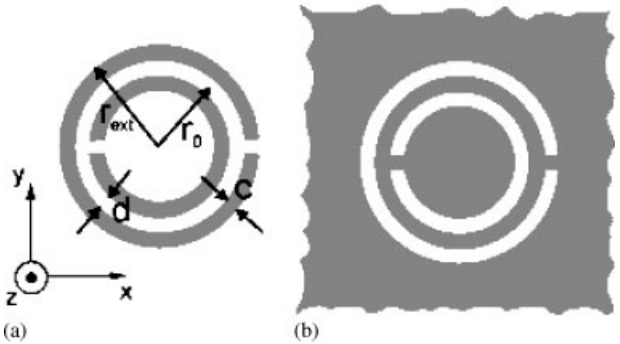


Figure 1. Topology of the SRR (a) and CSRR (b) and relevant dimensions. In case that ring widths are different, we call them $c_{in}$ and $c_{out}$ for the inner and outer ring, respectively.

parameters lead to the propagation of backward waves in such materials, and also to a negative value of their index of refraction, a reason that justifies the alternative nomenclature given to these media, i.e. negative refractive index (NRI) materials. Although the electrodynamics of LHMs were already studied by Veselago in the late 1960s [2], and their main electromagnetic and optical properties (such as the inversion of the Snell law and Cherenkov radiation, among others) predicted in 1968, it was not until 2000 that a left-handed material was synthesized [3]. The structure was due to Smith and co-workers and consisted on the combination of an array of metallic posts, which behaves as an electric plasma (with negative valued permittivity below a cut-off, or plasma frequency) scaled down to microwave frequencies, and an array of split rings resonators (SRRs), namely high-$Q$ resonant particles, electrically small, previously proposed by Pendry *et al.* [4] (see Figure 1). In the experiment, the required negative value of the magnetic permeability was due to the SRRs, which behave as a magnetic plasma in a narrow band above their resonant frequency, provided the magnetic field of incident radiation has a non-negligible component in the axial direction. After this seminal and imaginative structure, the works aimed to the synthesis of LHMs [5–8], to the experimental demonstration of their exotic electromagnetic properties [9–12] and to the design of novel functional microwave devices based on them has dramatically increased, and is still growing up. In particular, in planar technology numerous applications of metamaterials have been already pointed by the team of Itoh at the University of California at Los Angeles (UCLA) [13–15], and by the group of Eleftheriades at the University of Toronto [16, 17], and many others are expected. Essentially, these teams have designed and fabricated planar one- and two-dimensional LHM structures and microwave devices based on the dual transmission line concept, where shunt inductors and series capacitors are used as loading elements in planar transmission lines to achieve left-handedness.

Based on SRRs, the first planar one-dimensional LHM was reported by Martín *et al.* [18]. It was a coplanar waveguide (CPW) transmission line with SRRs etched in the back substrate side, and wire shorts between the central strip and ground planes placed at periodic positions. However, the first functional microwave device based on SRRs, a narrow band pass filter implemented in CPW technology, was obtained by combining SRRs with wires and series capacitive gaps to form a structure with left-handed and right-handed cells alternating [19]. In microstrip technology it has been demonstrated that LHMs can be obtained by combining

 

square-shaped SRRs and metallic vias connected between the ground plane and conductor strip [20]. However, in microstrip technology, there is an alternative to SRRs for obtaining a LHM structure. It consists on using a resonant particle, recently reported by some of the authors, which provides a negative value of the effective permittivity (rather than permeability) in the vicinity of resonance: the complementary split rings resonators (CSRRs) [21]. This particle, also depicted in Figure 1, is the negative image of SRRs, exhibits roughly the same resonant frequency as that of a SRR with identical dimensions, and can be excited by an axial electric field. Therefore, by etching CSRRs in the ground plane of a microstrip line, underneath the conductor strip, a one-dimensional effective medium with negative value of the effective permittivity in a narrow band (below the intrinsic resonant frequency) is thus obtained [21]. In order to manufacture LHMs based on CSRRs, additional elements, able to provide the required negative permeability, are necessary. It has been demonstrated that capacitive gaps etched in the conductor strip at periodic positions are appropriate for this purpose, and the first LHM microstrip line based on CSRRs was recently designed by combining CSRRs with series gaps [22]. It has been also demonstrated that by adding inductive stubs to the structure, an additional degree of flexibility is obtained that allows us for the design of band pass filters with controllable characteristics and small dimensions [23–25].

Typically, in LHM microstrip lines loaded with CSRR and gaps (i.e. without the presence of the inductive stubs), measured frequency responses exhibit narrow bands with sharp cut-off in the lower band edge and a soft transition above the upper edge of the band [22]. Actually, the CSRR/gap-based structures reported so far have not been subjected to any given specifications. They have been simply designed to guarantee a gap-related cut-off frequency above the resonant frequency of the CSRRs (a necessary condition to obtain a backward propagation band). Moreover, the influence of the main parameters of the structure on propagation characteristics has not been yet analysed. However, in order to obtain design guidelines for these structures that may allow for the synthesis of LHM microstrip lines with controllable characteristics, it is necessary to know the effects of the geometry of the structure. Since the geometry is intimately related to the electrical characteristics of the structure and a lumped element circuit model of the basic cell has been reported [26], it follows that from the accurate analysis of this model it is possible to infer the above-cited design guidelines. The main purpose of this work is thus to carry-out an exhaustive analysis of the transmission properties of LHM microstrip lines loaded with CSRRs and series gap, on the basis of the lumped element equivalent circuit model of the structure. From the results obtained concerning the effects of the electrical parameters, several structures will be designed and simulated (by means of an electromagnetic solver), in order to corroborate the main conclusions inferred from the previous analysis. It will be also discussed the possibility of using these metamaterial transmission lines in practical applications.

## 2. EQUIVALENT CIRCUIT MODEL OF CSRR LEFT-HANDED MICROSTRIP LINES AND DISPERSION RELATION

The basic cell of the structure under study and its lumped element equivalent T-circuit model are depicted in Figure 2 (losses and inter-resonators coupling have been excluded in this model). This equivalent circuit has been already reported [26], but it is reproduced here for coherence and completeness. The model is valid under the assumption that the size and distance between adjacent CSRRs are both electrically small, and it only applies in the frequency region of

 

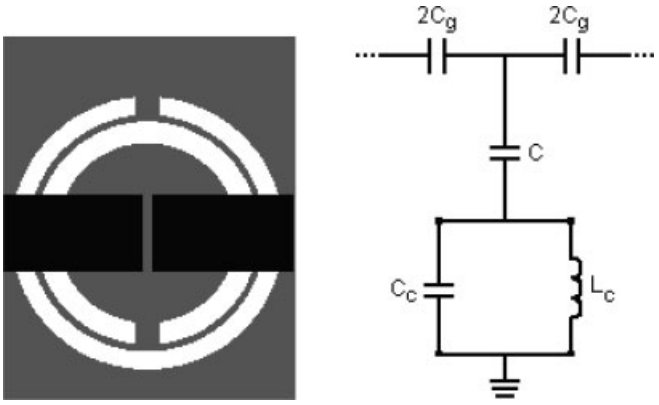


Figure 2. Topology of the basic cell of the structure under study (a) and its lumped element equivalent circuit model (b). The upper metallization is depicted in black, whereas the bottom metal regions are depicted in grey.

interest, namely the backward allowed band. The series gaps are modelled by the capacitance $C_g$, while CSRRs are described by parallel resonant tanks (with inductance $L_c$ and capacitance $C_c$), which are electrically coupled to the host line through the line capacitance $C$. The line inductance, $L$, which is series connected to the gap capacitance in this model, can be actually neglected provided in the region of interest (i.e. the transmission band) the series impedance is clearly dominated by $C_g$. Namely, the cut-off frequency, $f_c$, of the high-pass structure solely formed by the series gaps should be set clearly beyond the intrinsic resonant frequency of CSRRs, $f_0$. This frequency is given by

$$f_c = \frac{1}{2\pi\sqrt{LC_g}} \tag{1}$$

and the series impedance is capacitive below it, the reactance being more significant as lower the frequency is.

The periodic structure formed by cascading several cells is highly disperse, as can be inferred from the Bloch impedance, $Z_B$, and phase shift, $\phi$, of the elemental cell (dispersion relation). The general expressions for these magnitudes can be obtained following [27]:

$$Z_B = \sqrt{Z_s(j\omega)[Z_s(j\omega) + 2Z_p(j\omega)]} \tag{2}$$

$$\cos\phi = 1 + \frac{Z_s(j\omega)}{Z_p(j\omega)} \tag{3}$$

where $Z_s(j\omega)$ and $Z_p(j\omega)$ are the series and shunt impedances of the T-circuit model. In our particular case, the previous expressions lead to

$$Z_B = \sqrt{\frac{L_c/C_c}{\dfrac{1}{C_c\omega} - L_c\omega}\frac{1}{C_g\omega} - \frac{1}{4C_g^2\omega^2} - \frac{1}{CC_g\omega^2}} \tag{4}$$

 

$$\cos\phi = 1 + \frac{1/2C_g\omega}{\dfrac{1}{C\omega} + \dfrac{L_c/C_c}{L_c\omega - \dfrac{1}{C_c\omega}}} \tag{5}$$

The structure supports propagating waves in that frequency interval where $\phi$ is a real number. Analysis of expression (5) indicates that this occurs in the region delimited by the following frequencies:

$$f_L = \frac{1}{2\pi}\frac{1}{\sqrt{L_c\left(C_c + \dfrac{4}{\dfrac{1}{C_g} + \dfrac{4}{C}}\right)}} \tag{6}$$

$$f_H = \frac{1}{2\pi\sqrt{L_cC_c}} \tag{7}$$

where the sub-indexes simply make reference to the lower and higher frequencies of the interval. At these frequencies, both the phase and Bloch impedance take extreme values, i.e. $Z_B \to \infty$ and $\phi = 0$ at $f_H$, whereas $Z_B = 0\,\Omega$ and $\phi = \pi$ at $f_L$. Obviously, these results are valid under the assumption of negligible losses. To gain more insight on the dispersion characteristics of the structure, expression (5) has been depicted in a reduced Brillouin diagram, as shown in Figure 3 (the considered electrical parameters are indicated in the caption). As can be seen from the diagram, there is a region delimited by $f_L$ and $f_H$ where the phase and group velocities are anti-parallel. This is the region of interest, where the structure exhibits left-handedness. Above this region, there is another interval starting at $f_c$ (not represented) where signal propagation is also possible. In this frequency range the structure exhibits a positive series impedance (inductive) and shunt admittance (capacitive). Therefore, forward signal propagation, rather than backward, is expected.

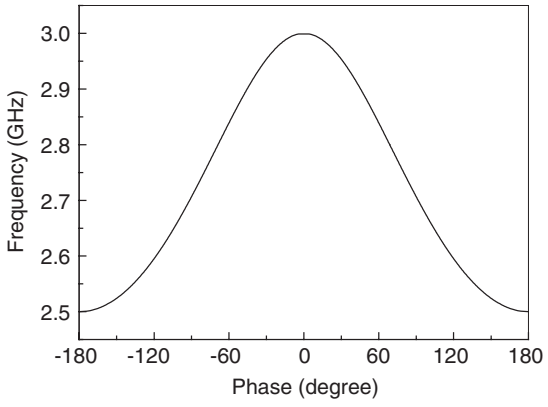


Figure 3. Dispersion relation represented in a Brillouin diagram corresponding to the equivalent circuit model of the basic cell. Element values are: $C_g = 0.69$ pF, $C = 34.38$ pF, $L_c = 0.036$ nH and $C_c = 78.15$ pF. The delimiting frequencies of the left-handed propagation interval are $f_L = 2.5$ GHz and $f_H = 3$ GHz.

 

Inspection of the circuit of Figure 2(b) also reveals that there is a transmission zero frequency given by

$$f_z = \frac{1}{2\pi\sqrt{L_c(C + C_c)}} \tag{8}$$

As long as $C \ll C_g$, $f_z$ and $f_L$ are very close, and the structure exhibits a very sharp cut-off in the lower edge of the left-handed allowed band regardless of the number of stages. However, to properly understand the transmission characteristics of these structures, and to obtain design guidelines that permit us to control these transmission characteristics, it is necessary to further analyse the structure and the previous expressions, which is the main aim of the next section.

## 3. ANALYSIS OF THE TRANSMISSION CHARACTERISTICS OF CSSR-LOADED MICROSTRIP LINES

Let us now focus on the detailed analysis of the transmission characteristics of the structures under study. Essentially, they behave as band pass elements where, due to the presence of the transmission zero, they typically exhibit an abrupt transition at the lower band edge. It has been previously indicated that there are two frequencies, $f_L$ and $f_H$, where both the phase and the Bloch impedance take extreme values. These frequencies delimit that region where the structure is transparent and supports backward waves. However, the effective bandwidth of the structure is not actually given by these frequencies, since there is an increasing mismatch at the boundaries of the interval. Namely, there is only one frequency where the Bloch impedance coincides with the reference impedance of the ports (usually set to 50 Ω). At this frequency, total transmission is expected provided losses are neglected. However, for any other frequency, impedance mismatch will lead to only partial transmission, as can be appreciated in the electrical simulation (obtained by means of the *Agilent ADS* commercial software) of a single-cell structure (Figure 4). In this figure the simulated transmission coefficients, $S_{21}$ that have been obtained in three- and

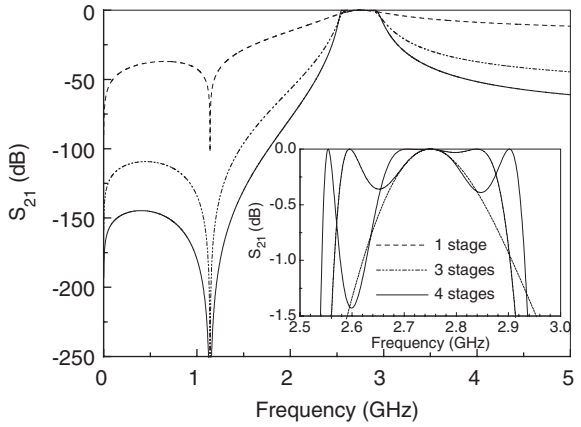


Figure 4. Frequency responses obtained through electrical simulation of the equivalent circuit model of the structure under study, for different number of stages. Element values are: $C_g = 0.69$ pF, $C = 34.38$ pF, $L_c = 0.036$ nH and $C_c = 78.15$ pF.

 

four-stage devices are also depicted. Contrarily to the single-cell structure, multiple transmission peaks arise and the number of them coincides with the number of stages. One of these peaks corresponds to the matching condition (as in the single cell), whilst the others can be identified with those frequencies where the total phase shift is an integer multiple of $\pi$, and hence complete transmission also occurs (phase condition). Since the whole phase variation through the left-handed band for a single cell is $\pi$ (see Figure 3), it immediately follows that the number of transmission peaks associated to the phase condition is given by the number of cells minus one, and the exact location of these frequencies within the left-handed band is given by the following rule:

$$\phi_i = \frac{\pi}{N} i \tag{9}$$

where $N$ is the number of cells and $i$ labels the transmission peak frequency ($i$ is an integer number which should satisfy $N - 1 \geqslant i \geqslant 1$). Actually, Equation (9) provides the phase condition, from which the frequencies can be inferred following the dispersion relation.

Once the analysis of the transmission characteristics in the left-handed allowed band has been carried out, the main objective now is to infer, from the model equations, design guidelines that allow us to control these transmission characteristics; namely, the width of the propagation band, the level of ripple, etc. The presence of ripple is unavoidable in periodic structures near the band edges. However, as will be later shown, it can be controlled to some extent. Indeed, if conduction and dielectric losses are neglected, in-band losses are limited by an envelope function, $f_{\text{env}}(\omega)$ that depends on the Bloch impedance variation along the allowed band, following:

$$f_{\text{env}}(\omega) = 10 \log \left\{ 1 - \left| \frac{Z_{\text{B}}^2(\omega) - 50^2}{Z_{\text{B}}^2(\omega) + 50^2} \right|^2 \right\} \tag{10}$$

Since the Bloch impedance experiences a continuous variation between $0\,\Omega$ and $\infty$ within the interval delimited by $f_{\text{L}}$ and $f_{\text{H}}$, there is a region, in the vicinity of that frequency where the Bloch impedance is $Z_{\text{B}} = 50\,\Omega$, where in-band losses and ripple are small. Ideally, a Bloch impedance independent of frequency and matched to the ports would be desirable to minimized ripple. Obviously, this is not possible, but we can impose certain conditions in order to control the frequency response in the region of interest. Another relevant aspect to handle is the phase variation with frequency. This has influence on the positions of the transmission peaks. If the aim is to uniformly distribute such transmission peaks within the band as much as possible, then it is convenient that the phase variation of a single cell is as close as possible to $90^\circ$ in the central frequency of the band. It is the purpose of this section to determine to what extent it is possible to independently control these aspects. We must have in mind that the basic cell of the equivalent circuit model is dependent on four reactive elements. Hence, to univocally determine the element values, 4 conditions are required. However, it is not *a priori* evident that any combination of conditions is valid for a solution to exist. For instance, it would be of interest to set $f_{\text{L}}$ and $f_{\text{H}}$ at certain locations (and thus delimit the allowed band), and simultaneously chose two frequencies within this band (as close as possible to the limits) where the envelope function, $f_{\text{env}}(\omega)$, is smaller than a given reference value (and hence in-band losses). This gives two different values for the Bloch impedance for such frequencies (one above and the other below $50\,\Omega$), and, in general, there is no solution for the element values of the basic circuit cell.

 

To demonstrate this, we can rewrite Equation (4) as

$$\frac{1}{4C_g^2}+\frac{1}{CC_g}=-\frac{\omega^2 Z_B^2}{\omega^2\tau(\omega)^2+1} \tag{11}$$

where

$$\tau(\omega)=\sqrt{\frac{\omega_H^2}{\omega^2-\omega_H^2}\left[\frac{1}{\omega_L^2-\omega_H^2}\right]} \tag{12}$$

and $\omega_H = 2\pi f_H$ and $\omega_L = 2\pi f_L$. Inspection of Equations (11) and (12) reveals that, in general, Equation (11) cannot be simultaneously satisfied for two (or more) combinations of $Z_B$ and $\omega$, unless $\tau(\omega)$ (that depends on $f_L$ and $f_H$) takes the appropriate value. Therefore, if we choose to set the limits of the allowed left-handed band, then it is not possible to limit in-band ripple below a certain value within any desired interval in the band.

Depending on the specific application, it may be convenient to set $f_L$ and $f_H$, or to set two frequencies with limited values of the envelope function. If the structure has to be used as a filtering element with strong rejection outside a given interval, then the former procedure is preferred. Contrarily, if we want to exploit the small dimensions of the device and its left-handed nature over a relative wide band, then the latter approach is more convenient. In this work, we have followed the former approach, namely we have set $f_L$ and $f_H$. The other conditions for the determination of circuit parameters are discussed as follows. We have considered the criteria of having minimum losses at the central region of the band. Therefore, we have forced the Bloch impedance to be $Z_B = 50\,\Omega$ at the central frequency, or close to this frequency, which means that the right-hand side of Equation (11) is fixed, and hence the relationship between $C$ and $C_g$ (to avoid extreme values of the element parameters, it can be convenient to slightly shift the matching condition from the central frequency). The other condition we need comes from the phase shift per cell, namely, we can set a value of this shift between $\phi = 0$ and $\phi = \pi$ for a given frequency. As has been previously commented a phase shift of $\phi = \pi/2$ at the central frequency leads to the same amount of transmission peaks at both sides of that frequency. This may produce a quasi-symmetric frequency response within the band. However, we have to investigate if this is possible and, if not, how to obtain an optimum criterion, or solution. To this end, we start by isolating $C_g$ in Equation (5). After some tedious calculation, we obtain

$$C_g=\sqrt{\frac{1+\cos\phi}{1-\cos\phi}\frac{1}{4\mathbf{D}_1(\mathbf{E}(\omega)\mathbf{A}+1)}} \tag{13}$$

where $\mathbf{D}_1$ is the right-hand side of Equation (11) (excluding the negative sign) with $Z_B = 50\,\Omega$ and $\omega$ set to the central frequency or to another frequency close to it, $\mathbf{A}$ is a constant dependent on the band limits:

$$\mathbf{A}=\frac{1}{\omega_L^2}-\frac{1}{\omega_H^2} \tag{14}$$

and $\mathbf{E}(\omega)$ is a frequency-dependent function given by

$$\mathbf{E}(\omega)=\frac{\omega^2\omega_H^2}{\omega^2-\omega_H^2} \tag{15}$$

 

From (13) by forcing the phase to have a certain value, at a given frequency, we can infer $C_g$. From it, by using (11) and $\mathbf{D}_1$, the value of $C$ is perfectly determined. Finally, $L_c$ and $C_c$ can be obtained from (6) and (7). Now, a question arises: do we have some restriction to choose the value of the phase for a given frequency within the interval $f_L$–$f_H$? From a mathematical point of view, we have freedom to do that. However, we must guarantee positive values for the elements of the equivalent circuit model. Namely, from expression (11), we can isolate $C$ to obtain

$$C = \frac{-4C_g}{4C_g^2\mathbf{D}_1 + 1} \tag{16}$$

Since $C$ must be positive, this means that the denominator in the above expression must be negative, which means that

$$\frac{1+\cos\phi}{1-\cos\phi}\frac{1}{(\mathbf{E}(\omega)\mathbf{A}+1)} < -1 \tag{17}$$

By substituting (14) and (15) into (17) we obtain

$$\frac{1+\cos\phi}{1-\cos\phi} > \frac{\omega_H^2}{\omega_L^2}\frac{\omega^2-\omega_L^2}{\omega_H^2-\omega^2} \tag{18}$$

Therefore, any combination $[\omega, \phi]$ is possible if the previous inequality is satisfied. Inspection of (18) reveals that for a given left-handed propagation interval delimited by the frequencies $f_L$ and $f_H$, there is an upper limit for the phase $\phi$ that can be assigned to a given frequency $\omega$ within this interval. This limit is given by

$$\phi_L = \arccos\left(\frac{\mathbf{F}-1}{\mathbf{F}+1}\right) \tag{19}$$

$\mathbf{F}$ being the right-hand side of (18). In particular, since the right-hand side of (18) is always higher than one, it follows that it is not possible to obtain a 90° phase shift per cell at the central frequency of the interval, but a smaller value. Therefore, we are forced to set a 90° phase shift at a lower frequency within the above-cited limit. In summary, the four conditions for the determination of the element parameters of the equivalent circuit model are given by the position of the two limiting frequencies, $f_L$ and $f_H$, and by the frequencies where the Bloch impedance, $f_1$, and phase variation per unit cell, $f_2$, are 50 Ω and 90°, respectively. As long as the element parameters inferred from the model equations do not take extreme values, these latter frequencies shall be chosen as close as possible to the central frequency of the interval (taking into account the previously cited restriction) in order to generate a quasi-symmetric response with small ripple in the central region of the allowed band. In practice, $C$ and $C_g$ cannot take very high values since this would imply very small gap separation and/or substrate thickness, and this is limited by the resolution of the fabrication process and by the availability of the substrate. We have analysed the effects of varying $f_1$ and $f_2$ on the frequency response that has been obtained by electrical simulation of a 10-stage structure (Figure 5). Since the number of stages is relatively high, we obtain similar responses regardless of the specific values of $f_1$ and $f_2$. Therefore, we should choose these frequencies according to the resulting element values, which should allow us to physically implement the structure. Nevertheless, $f_1$ has some more influence on the symmetry of the frequency response. In fabricated devices, since losses obscure in-band ripple, symmetry is preferred to obtain insertion losses as flat as possible in the vicinity of the central frequency.

 

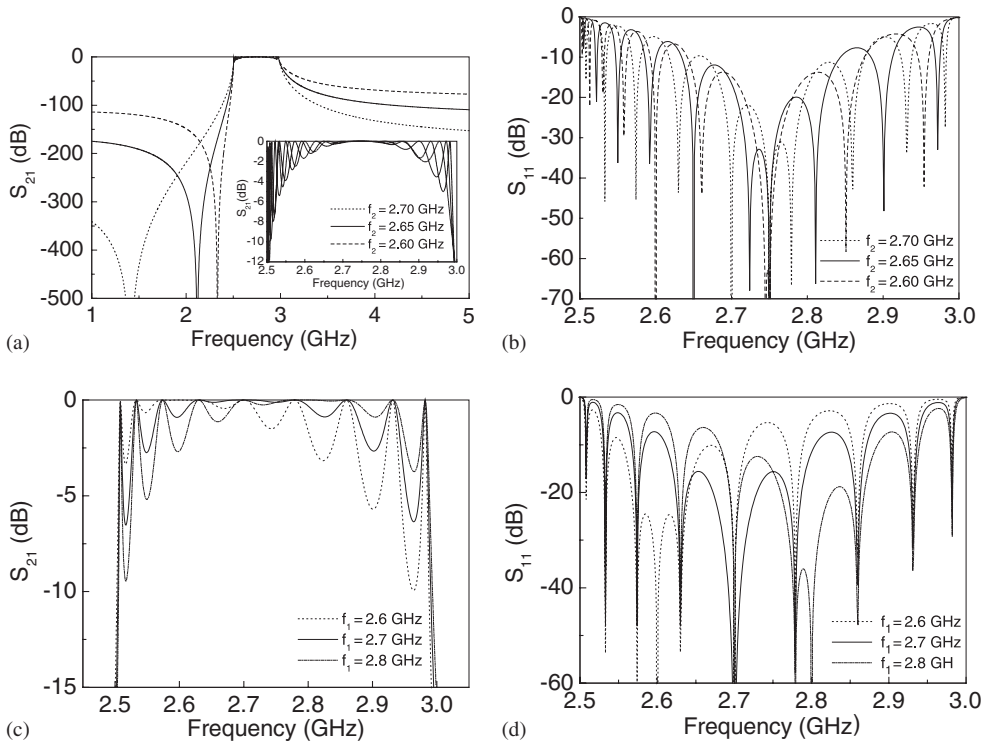


Figure 5. Effects of varying $f_1$ and $f_2$ in the electrical response of a 10-stage structure with $f_L = 2.5\,\text{GHz}$ and $f_H = 3\,\text{GHz}$: (a) insertion losses obtained by varying $f_2$ for $f_1$ set to the central frequency of the propagation interval; (b) return losses obtained by varying $f_2$ for $f_1$ set to the central frequency of the propagation interval; (c) insertion losses obtained by varying $f_1$ for $f_2 = 2.7\,\text{GHz}$; and (d) return losses obtained by varying $f_1$ for $f_2 = 2.7\,\text{GHz}$.

## 4. A PROTOTYPE DEVICE EXAMPLE

In order to validate the equivalent circuit model of the basic cell and the previous synthesis method, a prototype device example has been designed from the model equations. The specifications are: $f_L = 2.6\,\text{GHz}$, $f_H = 3.1\,\text{GHz}$, $f_1 = 2.73\,\text{GHz}$ and $f_2 = 2.76\,\text{GHz}$. Application of the model equations has led us to $C_g = 0.50\,\text{pF}$, $C = 3.12\,\text{pF}$, $L_c = 0.93\,\text{nH}$ and $C_c = 2.81\,\text{pF}$. From these values, the geometry of the structure has been obtained according to the following procedure: gap separation has been obtained by comparing the frequency response of the device without CSRRs, obtained by electromagnetic simulation (using *Agilent Momentum*), to that obtained by electrical simulation (through *Agilent ADS*) of the same structures with the gaps replaced by ideal capacitances of value $C_g$. The coupling capacitance, $C$, is a parameter difficult to handle because series gaps are placed underneath the CSRRs and this enhances capacitive coupling between the line and the CSRRs. Nevertheless, this parameter should be dependent on the width of the host line, which has been considered as a fitting parameter; finally, the geometry of the CSRRs has been inferred from $L_c$ and $C_c$ following the model reported in Reference [26]. Obviously, since there exists some non-negligible interaction between

 

the CSRRs and the series gaps (which has not been taken into account in the model) and the resonant frequency of the CSRRs is influenced by the presence of the metallic line on the other side of the substrate, adjustment of the geometry has been required to fit the electromagnetic response of the structure to that obtained from electrical simulation of the equivalent circuit model. The final prototype device has been fabricated on the *Rogers RO3010* substrate (dielectric constant $\varepsilon_r = 10.2$, thickness $h = 1.27$ mm, $\tan\delta = 0.0023$). The photograph as well as the simulated (both electrical and electromagnetic) and measured frequency responses (obtained by means of the *Agilent 8720ET* vector network analyser) are depicted in Figure 6 (the relevant dimensions are indicated in the caption). Good agreement between the electrical simulation (losses excluded) and the electromagnetic simulation has been obtained, which is indicative of the validity of the lumped element equivalent circuit model. Measured in-band losses are higher than those obtained through electromagnetic simulation because *Agilent Momentum* does not properly model ground plane (where CSRRs are etched) losses. It is also remarkable that the number of stages is considerable, this contributing to substantial in-band losses. We have also fabricated a four-stage device with identical dimensions and measured in-band losses have been reduced to 3 dB (see Figure 7), although at the expense of lower level of frequency selectivity. We would like also to mention that no significant leakage radiation occurs, as has been verified

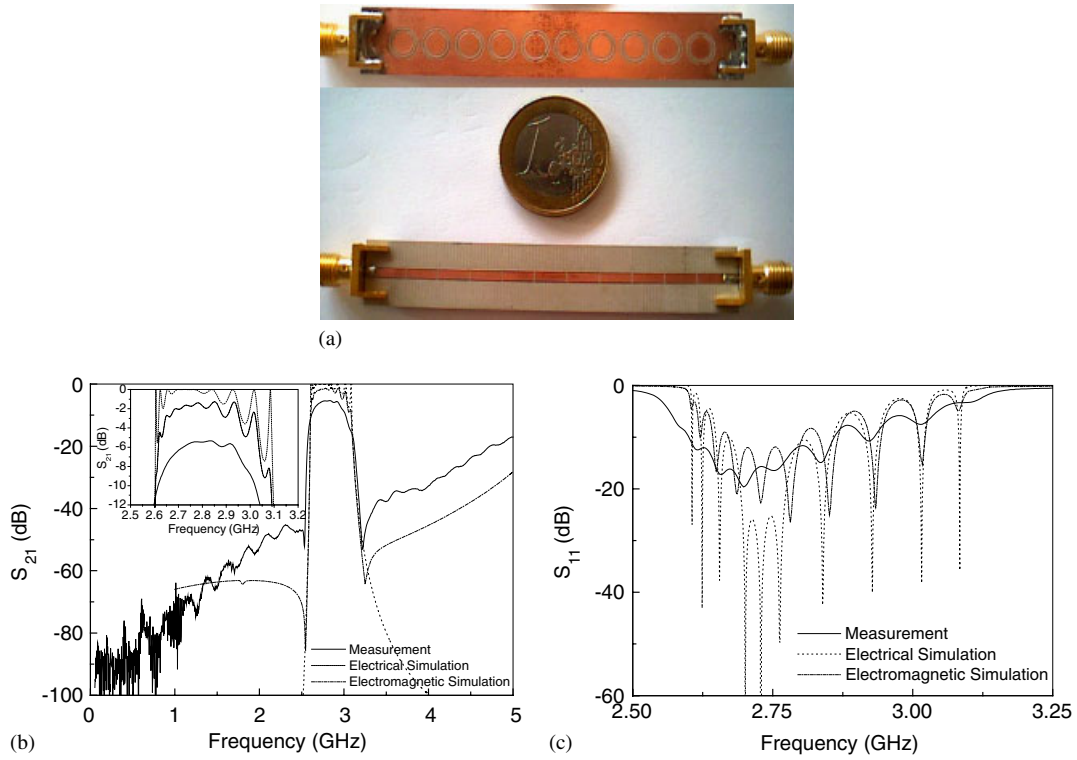


Figure 6. Fabricated 10-stage prototype device (a), insertion losses (b) and return losses (c). The period is $l = 6.4$ mm, gap spacing $g = 0.2$ mm and strip width $W = 1.69$ mm. The dimensions of the CSRRs are $c_{in} = 0.472$ mm, $c_{out} = 0.391$ mm, $d = 0.149$ mm and $r_{ext} = 2.972$ mm. In (a) top and bottom views are shown.

 

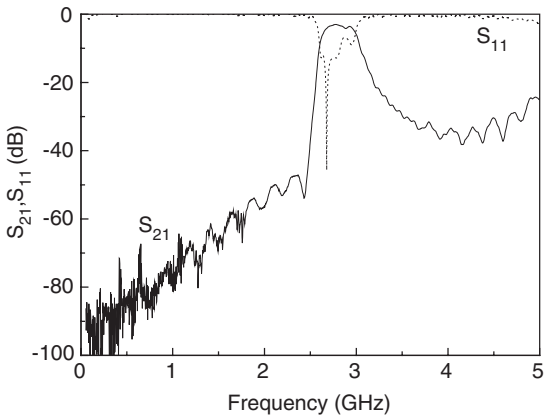


Figure 7. Measured insertion and return losses for the fabricated four-stage device.

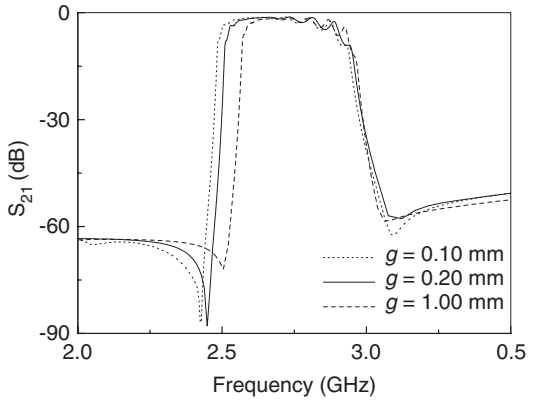


Figure 8. Simulated insertion losses for a 10-stage device with different values of gap distance, $g$, obtained by means of *Agilent Momentum*. The dimensions are $l = 6.4$ mm, strip width $W = 1.69$ mm. The dimensions of the CSRRs are $c_{in} = 0.472$ mm, $c_{out} = 0.391$ mm, $d = 0.149$ mm and $r_{ext} = 2.972$ mm. The minimum value of insertion losses in the band is IL $= -1.26$ dB.

through full wave electromagnetic simulation by excluding Ohmic and dielectric losses (not shown).

## 5. EFFECTS OF CELL GEOMETRY ON FREQUENCY RESPONSE

In this section the effects of varying gap separation, substrate thickness and the width of the host transmission line will be analysed and interpreted in the framework of the proposed circuit model. To this end, the *Agilent Momentum* commercial software, which provides a reasonable fit to measured frequency responses (as has been shown in Figure 6) will be used. In Figure 8, are represented three frequency responses corresponding to different gap separations. As gap

 

decreases, the upper band edge is not substantially altered. However, the lower band edge is clearly displaced towards lower values, with the result of a wider allowed band. This effect can be explained from expressions (6) and (7). Namely, the upper edge of the band only depends on the parameters of the resonant tank that models the CSRRs. Therefore, we do not expect a modification of the upper fall-off since gap width reduction does not affect the intrinsic resonant frequency of the CSRRs. However, the lower edge depends on $C_g$ and this capacitance increases as gap separation decreases. This explains the shift of the band onset towards lower frequencies when gap separation is decreased. In view of these results, the left-handed band of these structures can be widened by tailoring gap separation. Another possibility to control bandwidth is to tailor the height of the substrate. The results are depicted in Figure 9. The thinner the substrate is, the wider the bandwidth results. However, in this case, both band edges are shifted to expand the left-handed band. The upper band edge is moved towards higher frequencies because, the thinner the dielectric is, the higher the resonant frequency of the CSRRs becomes [26], and hence $f_H$. On the other hand, as substrate height is reduced the coupling capacitance $C$ is augmented, this having the effect of reducing $f_L$ (in spite that $C_g$ is slightly reduced). Obviously, by modifying these geometrical parameters, bandwidth has been tailored, but the frequency response in the region of interest has not been optimized. For this reason, in-band losses, essentially due to mismatch-related ripple are significant in some of the responses. Finally, we have studied the effects of varying line width. This modifies both $C_g$ and $C$ and it may slightly affect the resonant frequency of the CSRRs through the influence of the upper metallic strip on $L_c$ and $C_c$. According to this, we expect a variation of the lower band edge towards lower frequencies when line width is widened (since both $C$ and $C_g$ are expected to increase), and a small (although probably non-negligible) shift in the upper transition band. This behaviour has been verified by electromagnetic simulation (Figure 10).

According to the results shown in this section, it is clear that one-dimensional left-handed structures with moderate bandwidths based on CSRRs can be designed. To enhance bandwidth, thin substrates are preferred since this favours the possibility to move away $f_L$ and $f_H$. As long as

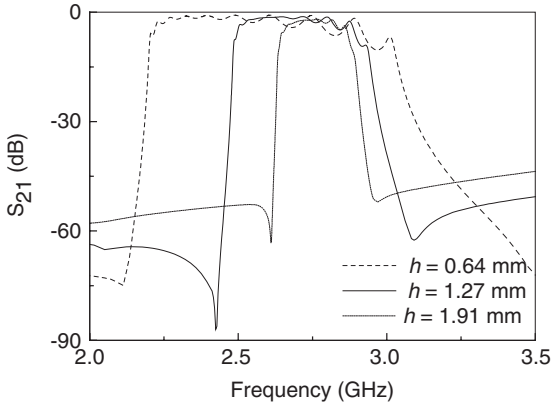


Figure 9. Simulated insertion losses for a 10-stage device with different values of substrate height, $h$, obtained by means of *Agilent Momentum*. The dimensions are $l = 6.4$ mm, gap spacing $g = 0.2$ mm, strip width $W = 1.69$ mm. The dimensions of the CSRRs are $c_{in} = 0.472$ mm, $c_{out} = 0.391$ mm, $d = 0.149$ mm and $r_{ext} = 2.972$ mm. The parameters of the *Rogers RO3010* substrate, except thickness, which is the varying parameter, have been considered. The minimum value of insertion losses in the band is IL $= -0.91$ dB.

 

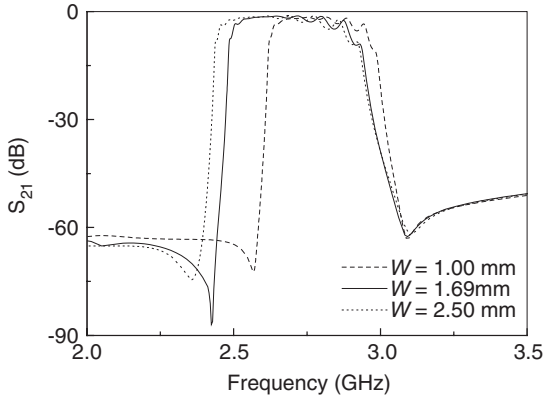


Figure 10. Simulated insertion losses for a 10-stage device with different values of strip width, $W$, obtained by means of *Agilent Momentum*. The dimensions are $l = 6.4$ mm, gap spacing $g = 0.2$ mm. The dimensions of the CSRRs are $c_{in} = 0.472$ mm, $c_{out} = 0.391$ mm, $d = 0.149$ mm and $r_{ext} = 2.972$ mm. The minimum value of insertion losses in the band is IL $= -1.26$ dB.

bandwidth, out-of-band rejection (mainly dependent on the number of stages although not discussed in this paper) and in-band losses can be controlled, these structures can be applied to the synthesis of frequency selective structures with compact dimensions. Also these structures can be of interest for the design of transmission line sections where impedance and phase shift can be independently and easily controlled over wide margins without the need to manipulate line width and length (as occurs in conventional transmission lines), with potential application in impedance matching networks, and many other microwave devices where control of these parameters and miniaturization are key issues. Work is in progress towards this direction.

## 6. CONCLUSIONS

In summary, we have presented an accurate analysis of the transmission properties of left-handed microstrip lines loaded with CSRRs. From the lumped element equivalent circuit model, we have derived the band-delimiting frequencies where left-handed wave propagation, as well as the dependence of the Bloch impedance and phase on frequency are allowed. From these expressions, we have proposed a procedure to determine the element parameters of the equivalent circuit model from given specifications, namely, the band-delimiting frequencies and two additional frequencies within the band: one corresponding to the matching condition (Bloch impedance $Z_B = 50\,\Omega$), $f_1$, the other providing a phase variation of $\phi = 90^\circ$, $f_2$. We have also studied the possible restrictions to freely set these specifications as desired, and we have demonstrated that in order to obtain real positive values of the electrical parameters, $f_2$ is limited to a certain frequency range. Although, ideally, to obtain symmetric in-band responses, $f_1$ and $f_2$ should be set as close as possible to the central frequency of the band, it has been found that in practice this is not possible in general. However, we have analysed the influence of varying these frequencies, and no substantial differences have been obtained, unless they are set to values close to the extremes of the band. A prototype device example has been designed from

 

the model equations, following the proposed procedure. This device has been fabricated and good agreement has been obtained between the measured and the simulated frequency responses obtained by electrical simulation of the equivalent circuit model and electromagnetic simulation of the device structure. Finally, we have studied the effects of varying the main physical parameters of the devices, namely gap separation, substrate thickness and line width. We have found that the effects mainly concern bandwidth control, and they can be explained to the light of the equivalent circuit model. It has been demonstrated that to enhance bandwidth thin substrates are preferred. The presented results show that it is possible to design left-handed structures with moderate bandwidths by using CSRRs. However, bandwidth is limited by the value of the gap capacitance and coupling capacitance and, in general, it is not possible to achieve left-handedness in such wide band as those achieved by means of the dual transmission line approach.

## ACKNOWLEDGEMENTS

This work has been supported by MEC (Spain) by project contract TEC2004-04249-C02-01 METASYSTEMS, by UAB-CIRIT through the project PNL2004-22 and by the European Commission (VI Framework Programme) through the contract NoE 500252-2 METAMORPHOSE.

## REFERENCES

1. Oliner AA, Itoh T (eds). *IEEE Transactions on Microwave Theory and Techniques*: *Special Issue on Metamaterial Structures. Phenomena and Applications* 2005; **53**(4).
2. Veselago VG. The electrodynamics of substances with simultaneously negative values of $\varepsilon$ and $\mu$. *Soviet Physics Uspekhi USSR* 1968; **10**:509–514.
3. Smith DR, Padilla WJ, Vier DC, Nemat-Nasser SC, Schultz S. Composite medium with simultaneously negative permeability and permittivity. *Physics Review Letters* 2000; **84**:4184–4187.
4. Pendry JB, Holden AJ, Robbins DJ, Stewart WJ. Magnetism from conductors and enhanced nonlinear phenomena. *IEEE Transactions on Microwave Theory and Techniques* 1999; **47**:2075–2084.
5. Shelby RA, Smith DR, Nemat-Nasser SC, Schultz S. Microwave transmission through a two-dimensional isotropic left handed metamaterial. *Applied Physics Letters* 2001; **78**:489–491.
6. Marqués R, Martel J, Mesa F, Medina F. Left handed media simulation and transmission of EM waves in sub-wavelength SRR-loaded metallic waveguides. *Physics Review Letters* 2002; **89**:183901 (1–4).
7. Marqués R, Martel J, Mesa F, Medina F. A new 2D isotropic left handed metamaterial design: theory and experiment. *Microwave and Optical Technology Letters* 2002; **35**:405–408.
8. Eleftheriades GV, Iyer AK, Kremer PC. Planar negative refractive index media using periodically L-C loaded transmission lines. *IEEE Transactions on Microwave Theory and Techniques* 2002; **50**:2702–2712.
9. Shelby RA, Smith DR, Schultz S. Experimental verification of a negative index of refraction. *Science* 2001; **292**:77–79.
10. Parazzoli CG, Greegor RB, Li K, Koltenbah BEC, Tanielian M. Experimental verification and simulation of negative index of refraction using Snell's law. *Physics Review Letters* 2003; **90**:107401 (1–4).
11. Houck AA, Brock JB, Chuang IL. Experimental observations of a left handed material that obeys Snell law. *Physics Review Letters* 2003; **90**:137401 (1–4).
12. Grbic A, Eleftheriades GV. Experimental verification of backward wave radiation from a negative refractive index metamaterial. *Journal of Applied Physics* 2002; **92**:5930–5935.
13. Caloz C, Itoh T. Novel microwave devices and structures based on the transmission line approach of metamaterials. *IEEE MTT-S International Microwave Symposium Digest*, Philadelphia, PA, June 2003; 195–198.
14. Okabe H, Caloz C, Itoh T. A compact enhanced bandwidth hybrid ring using an artificial lumped-element left handed transmission line section. *IEEE Transactions on Microwave Theory and Techniques* 2004; **52**:798–804.
15. Horii Y, Caloz C, Itoh T. Super compact multilayered left handed transmission line and diplexer application. *IEEE Transactions on Microwave Theory and Techniques* 2005; **53**:1527–1534.
16. Antoniades M, Eleftheriades GV. Compact linear lead/lag metamaterial phase shifters for broad band applications. *IEEE Antennas and Wireless Propagation Letters* 2003; **2**:103–106.

 

17. Islam R, Eleftheriades GV. Phase agile branch line couplers using metamaterial lines. *IEEE Microwave and Wireless Components Letters* 2004; **14**:340–342.
18. Martín F, Falcone F, Bonache J, Marqués R, Sorolla M. A new split ring resonator based left handed coplanar waveguide. *Applied Physics Letters* 2003; **83**:4652–4654.
19. Bonache J, Martín F, Falcone F, García J, Gil I, Lopetegi T, Laso MAG, Marqués R, Medina F, Sorolla M. Super compact split ring resonators CPW band pass filtres. *IEEE-MTT International Microwave Symposium Digest*, Fort Worth (TX), USA, June 2004; 1483–1486.
20. Gil I, Bonache J, García-García J, Falcone F, Martín F. Metamaterials in microstrip technology for filter applications. *Proceedings of the APS-URSI*, Washington (USA), July 2005.
21. Falcone F, Lopetegi T, Baena JD, Marqués R, Martín F, Sorolla M. Effective negative-$\varepsilon$ stop-band microstrip lines based on complementary split ring resonators. *IEEE Microwave and Wireless Components Letters* 2004; **14**:280–282.
22. Falcone F, Lopetegi T, Laso MAG, Baena JD, Bonache J, Marqués R, Martín F, Sorolla M. Babinet principle applied to the design of metasurfaces and metamaterials. *Physics Review Letters* 2004; **93**:197401.
23. Bonache J, Martín F, García-García J, Gil I, Marqués R, Sorolla M. Ultra wide band pass filters (UWBPF) based on complementary split rings resonators. *Microwave and Optical Technology Letters*, August 2005, **46**:283–286.
24. Bonache J, Martín F, Gil I, García-García J, Marqués R, Sorolla M. Microstrip bandpass filters with wide bandwidth and compact dimensions. *Microwave and Optical Technology Letters* 2005; **46**:343–346.
25. Bonache J, Martín F, Gil I, García-García J. Novel microstrip filters based on complementary split rings resonators. *IEEE Transactions on Microwave Theory and Techniques*, January 2006; **54**:265–271.
26. Baena JD, Bonache J, Martín F, Marqués R, Falcone F, Lopetegi T, Laso MAG, García J, Gil I, Sorolla M. Equivalent circuit models for split ring resonators and complementary split rings resonators coupled to planar transmission lines. *IEEE Transactions on Microwave Theory and Techniques* 2005; **53**:1451–1461.
27. Pozar DM. *Microwave Engineering*. Addison-Wesley: New York, 1993.

## AUTHORS' BIOGRAPHIES

**Marta Gil Barba** was born in Valdepeñas (Ciudad Real), Spain, in 1981. She received the degree in Physics from the Universidad de Granada in 2005. She studied 1 year in the Friedrich Schiller Universität Jena, in Jena, Germany. She has collaborated during her studies in different projects on popularization of Physics with Miguel Cabrerizo Vílchez, professor in the Universidad de Granada. She is currently working toward her PhD degree in subjects related to metamaterials and microwave circuits within the framework of METAMORPHOSE.

**Jordi Bonache** was born in 1976 in Barcelona, Spain. He received the Physics and Electronics Engineering Degrees from the Universitat Autònoma de Barcelona in 1999 and 2001, respectively, and is currently working toward his PhD degree. In 2000, he joined the 'High Energy Physics Institute' of Barcelona (IFAE), where he was involved in the design and implementation of the control and monitoring system of the MAGIC telescope. In 2001, he joined the Department of Electronics Engineering of the Universitat Autònoma de Barcelona and he is currently Assistant Professor at this university. His research interests include active and passive microwave devices and metamaterials.

 

**Ignacio Gil** was born in 1978 in Barcelona, Spain. He received the Physics and Electronics Engineering Degrees from the Universitat Autònoma de Barcelona in 2000 and 2003, respectively, and is currently working toward his PhD degree. He is also Assistant Professor at the Universitat Autònoma de Barcelona. His research interests include active and passive microwave devices and metamaterials.

**Joan García-García** was born in Barcelona, Spain, in 1971. He received the degree in physics from the Universitat Autònoma de Barcelona in 1994, and the PhD degree in Electrical Engineering from the Universitat Autònoma de Barcelona in 2001. After PhD degree, he became a post-doctoral research fellow at the Institute of Microwaves and Photonics at the Leeds University, U.K., into the INTERACT European project. In 2002, he was working at the Universitat Autònoma de Barcelona as a post-doctoral research fellow joining the Ramon y Cajal project from the Spanish Government. In November 2003, he became Associate Professor in Electronics in the Department d'Enginyeria Electònica Universitat Autònoma de Barcelona.

**Ferran Martín** was born in Barakaldo (Vizcaya), Spain, in 1965. He received the BS Degree in Physics from the Universitat Autònoma de Barcelona (UAB) in 1988 and the PhD degree in 1992. From 1994 he is Associate Professor in Electronics in the Departament d'Enginyeria Electrònica, Universitat Autònoma de Barcelona. In recent years, he has been involved in different research activities including modelling and simulation of electron devices for high-frequency applications, millimeter wave and THz generation systems, and the application of electromagnetic bandgaps to microwave and millimeter wave circuits. He is now also very active in the field of metamaterials and their application to the miniaturization and optimization of microwave circuits and antennas. He is the head of the Microwave and Millimeter Wave Engineering Group at UAB and a partner of the Network of Excellence of the European Union METAMORPHOSE. He has organized several international events related to metamaterials, including a Workshop in the *2005 IEEE International Microwave Symposium*. He is currently acting as Guest Editor for two Special Issues on Metamaterials in two International Journals. He has authored and coauthored over 185 technical conference, letter and journal papers and he is currently coauthoring the monograph on Metamaterials entitled 'Metamaterials with Negative Parameters: Theory, Design and Microwave Applications'. Ferran Martín has filed several patents on metamaterials and has headed several Development Contracts.

*Special Issue on Metamaterials LHM*

# Miniaturisation of planar microwave circuits by using resonant-type left-handed transmission lines

M. Gil, J. Bonache, I. Gil, J. García-García and F. Martín

**Abstract:** It is demonstrated that planar microwave circuits and components such as impedance inverters or power dividers, among others, can be compacted by using artificial left-handed transmission lines in their designs. Key to this size reduction is the possibility to control the electrical characteristics of these lines (namely electrical length and image impedance) over wide margins by means of a single cell structure. It consists of a microstrip line section with a series capacitive gap etched in the conductor strip and loaded with a complementary split rings resonator etched in the ground plane. A recently reported model of the artificial line is used as a first step in the design of the desired devices. To demonstrate the viability of the approach, several prototype device examples are provided, that is a 90° impedance inverter and several power dividers with different topologies. A 50% size reduction (as compared to conventional devices) has been achieved by implementing the devices in conventional low loss microwave substrates, but further levels of miniaturisation can be obtained if the devices are fabricated on advanced technologies such as low temperature co-fired ceramic or multi chip module-deposited, among others.

## 1 Introduction

Several techniques to reduce the size of planar microwave components have been proposed so far. For instance the semi-lumped element approach, where capacitors, inductors and resonators are implemented by means of electrically small topologies, compatible with printed circuit board or thin film technology, has been successfully applied to the design of filters and diplexers [1, 2]. Typically, capacitors have been implemented by the well-known interdigitated concept or by means of signal-to-ground metal patches, and inductors have been designed by means of wire loops and narrow strips (a good description of semi-lumped element filters and related references is given in the work of Hong and Lancaster [3]). Concerning resonators, these elements have been implemented by combining narrow metallic strip, which behave inductively, and capacitive patches to ground. Semi-lumped resonators have been successfully applied, for instance, to the design of miniature low pass filters with attenuation poles properly located in order to obtain a sharp cut-off [4].

Another well-known miniaturisation technique consists of periodically loading transmission lines and stubs with shunt connected capacitors (semi-lumped, chip capacitors or surface mount device components), with the result of a slow wave effect [5–8]. It has been also demonstrated that the slow wave effect can be achieved by properly microstructuring the ground plane [9], in microstrip configurations, or the conductor strip, in Coplanar waveguide (CPW) technology [10]. In these capacitively loaded and microstructured transmission lines, the slow wave effect is due to the modification of the effective parameters (dielectric constant) of the transmission line medium.

Within effective media there are also the negative index media, namely artificial structures with effective dielectric permittivity and magnetic permeability both being negative [double negative or left-handed media (LHM)], or with only one of these electromagnetic parameters taking a negative value (single negative materials) [11]. The electromagnetic properties of LHM (negative refraction and reversal of the Doppler Effect, Cerenkov radiation and Goos–Hänchen effect), which are consequence of the anti-parallelism between the phase and group velocities, go beyond the behaviour that conventional materials exhibit [12]. For this reason these substances have been termed as metamaterials. Nevertheless, since the properties and parameter values of SNG media can also be artificially controlled, these structures are also considered to belong to the category of metamaterials. A key aspect for the fabrication of metamaterials, or to achieve effective (or continuous) index media, is to use constitutive elements, or particles, with dimensions much smaller than signal wavelength at the frequencies of interest. This is not very distinct than the semi-lumped element approach for the design of planar microwave circuits, which is in turn contrary to the distributed approach, where transmission lines and stubs scale with frequency. However, owing to left-handedness and to the possibility to control their electrical characteristics, artificial metamaterial transmission lines are of interest not only for device miniaturisation but also for the design of microwave devices and circuits based on new functionalities. Two main approaches have been used for the synthesis of such lines: (i) the dual transmission lines concept, in which series capacitances and shunt inductances loading the line are the key elements to achieve left-handedness [13–15]; (ii) the resonant-type approach, where split rings resonators (SRRs) or complementary SRRs (CSRRs), shown in Fig. 1, have been combined with shunt connected wire (or via) inductances and series capacitances, respectively, to implement one-dimensional



doi:10.1049/iet-map:20050302

Paper first received 29th November 2005 and in revised form 7th April 2006

The authors are with the Departament d'Enginyeria Electrònica (GEMMA Group), Universitat Autònoma de Barcelona, 08193 Bellaterra, (Barcelona), Spain

E-mail: marta.gil.barba@uab.es

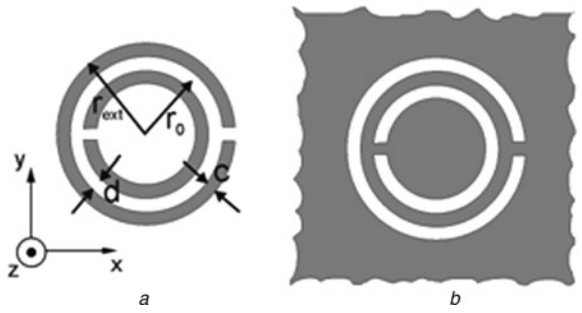


**Fig. 1** *Topology and relevant dimensions of SRR*
*a* SRR
*b* CSRR

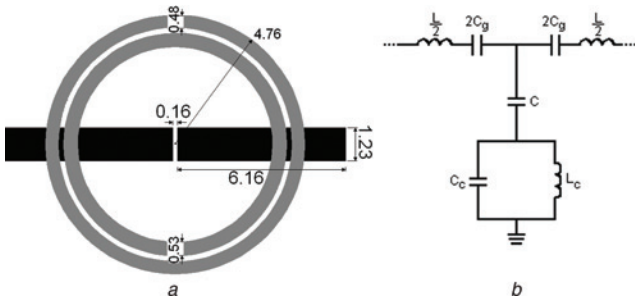


**Fig. 2** *Left-handed artificial lines*
*a* Topology of the artificial transmission line section
*b* Lumped element equivalent circuit model
The upper metallisation is depicted in black, whereas the bottom slot regions are depicted in grey
Dimensions correspond to a 90° impedance inverter designed with an image impedance of 70.7 Ω to be operative at 1.5 GHz
Dimensions are expressed in millimetres

left-handed structures [16, 17]. The second approach was introduced by some of the authors of this work, and it was inspired in the first synthesised left-handed effective media, which was implemented by Smith *et al*. [18] at the University of California, San Diego, USA. By combining SRRs with shunt connected wires, a one-dimensional artificial medium with negative effective permeability (due to the presence of the SRRs) and permittivity (thanks to the inductance of the wires) was implemented in the CPW technology [16]. In microstrip technology, the required negative values of permeability and permittivity to achieve a backward wave structure were obtained by etching series gaps in the conductor strip, and CSRRs in the ground plane, the latter providing the negative effective permittivity [19].

In this work, compact microwave components are designed in microstrip technology by using artificial left-handed lines implemented by means of CSRRs. As will be shown later, these artificial lines are highly dispersive, and both the phase shift per cell (or the electrical length) as well as the characteristic impedance (image impedance) can be independently tailored to some extent. This allows us for the design of microwave devices based on the control of the electrical length and impedance of transmission lines and stubs, but by using single CSRR-based cell structures. The results are small size, and the possibility to fabricate microwave circuits with extreme values for the characteristic impedance of transmission lines and/or stubs. Several prototype device examples are provided to illustrate the potentiality of the approach, including impedance inverters, which can be used as impedance matching networks and power dividers.

## 2 CSRR-based left-handed lines: topology, equivalent circuit model and synthesis

CSRR-loaded transmission lines can be implemented in both CPW [20] and microstrip [17, 19] technologies. In the former case, since lateral dimensions are not univocally determined, the conductor strip can be designed to be wide enough to accommodate the CSRRs. In microstrip technology, these particles are preferably etched in the ground plane, underneath the conductor strip. This guarantees that CSRRs can be excited by the time varying electric field of the quasi-TEM signal propagating in the line, since it exhibits a significant component in the axial direction (actually, CSRRs can be alternatively excited by a time varying magnetic field applied parallel to the plane of the particle [21], although this excitation mode is weaker). In the present work, the left-handed artificial lines are implemented by following the second approach. The topology of the basic cell and its lumped element equivalent T-circuit model are depicted in Fig. 2 (losses and inter-resonators coupling have been excluded in this model). This equivalent circuit has been already reported [21], but it is reproduced here for coherence and completeness. The model is valid under the assumption that the size and distance between adjacent CSRRs are both electrically small. The series gaps are modelled by the capacitance $C_g$, while CSRRs are described by parallel resonant tanks (with inductance $L_c$ and capacitance $C_c$), which are electrically coupled to the host line through the capacitance $C$. The line inductance, $L$, which is series connected to the gap capacitance in this model, has been previously neglected. The reason is that in the region of interest (i.e. the transmission band), the series impedance must be dominated by $C_g$. This is a necessary condition to achieve left-handedness. Moreover, for filter applications, negligible inductive impedance is required in order to obtain a reasonable selectivity in the upper band edge [21]. In general, $L$ may not be negligible, and it may be necessary to account for it in order to accurately describe the structure, regardless of the specific conditions. However, if we take $L$ into account, the obtained equations are too complicated to be intuitively useful for the design. Therefore in the analysis carried out in the present section, $L$ has been omitted. We will use the model equations to obtain the parameters of the simplified (i.e. by excluding $L$) model from given specifications, and these parameters will be used to generate the layout of the structures. By optimising these layouts (to achieve the target specifications), the final topology is obtained, and the electrical parameters (including $L$) are extracted, so that the validity of the simplified model can be checked.

The structure under study (Fig. 2) is highly dispersive, as can be inferred from the phase shift of the elemental cell, which is given by

$$\cos\,\phi = 1 + \frac{Z_s(j\omega)}{Z_p(j\omega)} \tag{1}$$

$Z_p$ and $Z_s$ being the shunt and series impedance, respectively, of the T-circuit model. The image impedance of the structure is given by

$$Z_B = \sqrt{Z_s(j\omega)[Z_s(j\omega) + 2Z_p(j\omega)]} \tag{2}$$

$Z_B$ and $\phi$ are the key electrical characteristics of the artificial left-handed lines implemented by means of CSRRs. They must be set to the desired values (according to the designs required) at the operating frequency. In view of the equivalent circuit model given in Fig. 2, we have

some flexibility for the synthesis of such artificial lines because expressions (1) and (2) are dependent on four parameters (the reactive elements of the model, except $L$). However, in practice it may be convenient to broaden the operative bandwidth of the devices as much as possible. Hence, an analysis of the circuit model is necessary in order to appropriately choose the circuit parameters. Obviously, it must also be taken into account the limitations of the structure to physically implement a layout from the inferred circuit parameters. This analysis is carried out in the following paragraphs.

First of all, we must have in mind that the structure of Fig. 2 exhibits a backward allowed band in an interval delimited by the frequencies

$$f_L = \frac{1}{2\pi}\frac{1}{\sqrt{L_c(C_c + (4/(1/C_g + 4/C)))}} \tag{3}$$

$$f_H = \frac{1}{2\pi\sqrt{L_c C_c}} \tag{4}$$

as results by forcing $\phi$, or $Z_B$, to be real numbers. Within this interval, $\phi$ varies between 0 (at $f_H$) and $-\pi$ (at $f_L$), whereas $Z_B = 0\ \Omega$ at $f_L$ and $Z_B \to \infty$ at $f_H$. This strong variation of the electrical parameters of the artificial line through the allowed band is very important for our purposes. Namely, as long as these parameters can be independently controlled, which is valid to some extent, it is potentially possible to achieve the required values for $Z_B$ and $\phi$ by using a single cell structure. This will be later verified. Now, let us focus on the synthesis of the artificial left-handed lines from the previous equations. The input parameters for design are the operating frequency $f_c$, the required phase variation at that frequency $\phi_c = \phi(f_c)$ and the image impedance $Z_c = Z_B(f_c)$. The frequencies $f_L$ and $f_H$, which must be set below and above $f_c$, respectively, are also design parameters. In order to obtain devices with reasonable bandwidth, it is convenient to move these frequencies apart from $f_c$ as much as possible. However, in practice, this is limited by the element values resulting from the previous equations, which not only must be positive, but they should also have reasonable values for physical implementation of the device to be possible. One of the aims of this section is to analyse the intrinsic limits of the operative bandwidth of the device.

From (1) and (2), the capacitance value of the series gap can be easily inferred, namely

$$C_g = \frac{1}{2\omega_c Z_c}\sqrt{\frac{1+\cos\phi_c}{1-\cos\phi_c}} \tag{5}$$

where $\omega_c = 2\pi f_c$. To obtain other electrical parameters of the equivalent circuit model, inversion of (1)–(4) is necessary. This involves a tedious calculation. The final results are given by

$$L_c = \frac{Z_c}{2}\sqrt{\frac{1+\cos\phi_c}{1-\cos\phi_c}}\frac{\omega_C}{\omega_H^4}\frac{(\omega_H^2-\omega_L^2)(\omega_H^2-\omega_C^2)}{(\omega_C^2-\omega_L^2)} \tag{6}$$

$$C_c = \frac{1}{L_c\omega_H^2} \tag{7}$$

$$C = \frac{2\omega_H^2(\omega_C^2-\omega_L^2)\sqrt{1-\cos^2(\phi_c)}}{Z_c\omega_C\left[\omega_C^2(1+\cos\phi_c)(\omega_H^2-\omega_L^2) - 2\omega_H^2(\omega_C^2-\omega_L^2)\right]} \tag{8}$$

where $\omega_L = 2\pi f_L$ and $\omega_H = 2\pi f_H$. Inspection of (5)–(8) reveals that $C_g$, $L_c$ and $C_c$ are always positive provided $\omega_L < \omega_C < \omega_H$. However, depending on the relative values of these angular frequencies, $C$ may be negative. Therefore the operative bandwidth of the device is limited by the value of $C$, which must be a real positive number. The analysis of (8) indicates that the numerator is positive. Therefore to obtain a positive value of $C$, the following condition must be satisfied

$$1 + \cos\phi_c > 2\frac{\omega_H^2(\omega_C^2-\omega_L^2)}{\omega_c^2(\omega_H^2-\omega_L^2)} \tag{9}$$

According to (9), for a given value of the operating angular frequency, $\omega_c$, and phase, $\phi_c$, only a limited range of $\omega_L$ and $\omega_H$ combinations is possible. As an illustrative example, the region in the $\omega_H - \omega_L$ space where solution to (9) is obtained, for a value of phase given by $\phi_c = \pi/2$ is depicted in Fig. 3. This value will be considered in the prototype devices designed in the following section. It is interesting to mention that, as long as $L$ can be neglected in the model, the intrinsic limits for $\omega_L$ and $\omega_H$ are $1/\sqrt{2}\omega_C < \omega_L < \omega_C$ and $\omega_H > \omega_C$, respectively. Namely, if $\omega_L$ and $\omega_H$ are chosen according to this rule, positive values of the reactive elements result. However, in practice, positively defined values of the model elements may not suffice to be physically possible to implement the layout and hence, we need to be more restrictive, as will be later discussed.

## 3 Application to microwave circuit design and miniaturisation

We have applied the CSRR-loaded lines to the design of planar circuits with small dimensions. Key to this are the small electrical size of the resonators and the possibility to control phase and line impedance over wide margins with a single cell structure. We have designed 90° impedance inverters, and we have applied them to the synthesis of narrow band power dividers, which have been implemented, tested and compared to conventional devices.

In the design of 90° impedance inverters, the line impedance is usually set to the required value to match the input port. As a first step to the design of power dividers, we have designed a $\phi_c = 90°$ impedance inverter with a characteristic impedance set at $Z_c = 70.7\ \Omega$ (these electrical parameter values will be justified later). The operating frequency is set to $f_c = 1.5$ GHz. From this impedance and phase, we have determined the parameters of the equivalent

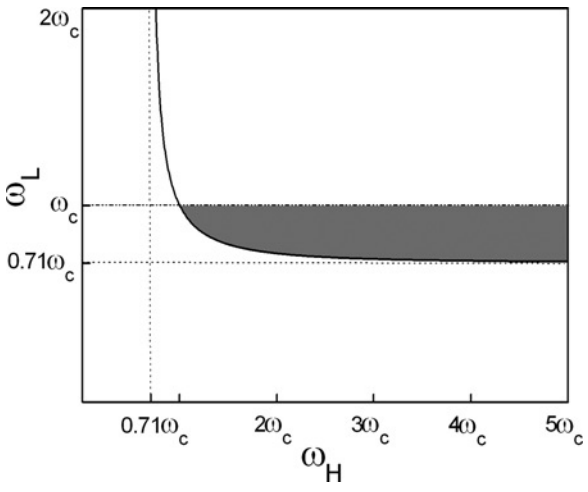


**Fig. 3** *Plot of the possible values of $\omega_L$ and $\omega_H$ for an artificial line with $\phi_c = 90°$*

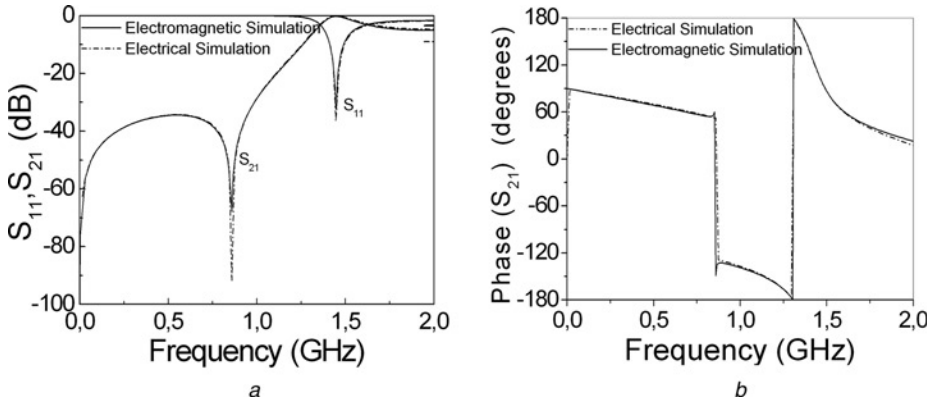


**Fig. 4** *Comparison between the frequency responses of the impedance inverter of Fig. 2 obtained by full wave electromagnetic simulation and electrical simulation of the equivalent circuit model*

*a* Magnitude
*b* Phase of $S_{21}$

circuit model following the procedure described in the previous section. To this end, the frequencies delimiting the allowed band have been set to $f_L = 1.39$ GHz and $f_H = 1.68$ GHz. These values lie within the above cited limits and provide reasonable results for the element parameters. The results are $C_g = 0.75$ pF, $C = 14.9$ pF, $L_c = 1.76$ nH and $C_c = 5.08$ pF. From these reactive elements, we have obtained the layout of the inverter [22]. The parameters of the Rogers RO3010 substrate (dielectric constant $\varepsilon_r = 10.2$, thickness $h = 1.27$ mm) have been considered. Optimisation has been actually required to obtain the desired impedance and phase at the operating frequency. Dimensions of the final structure are indicated in Fig. 2. The length of the inverter is 12.9 mm, which represents a significant miniaturisation as compared to a conventional 90° line implemented in microstrip technology by using the same substrate (the length in this case is 21.0 mm). The simulated frequency response of this impedance inverter, obtained by using an electromagnetic solver (Agilent Momentum), is depicted in Fig. 4. From this simulation, we have extracted the parameters of the complete (i.e. by including $L$) model. To infer the elements of the series branch, the reflection coefficient is depicted on a Smith Chart. At the intrinsic resonant frequency of the CSRRs (4), the shunt admittance is null and the impedance seen from the input port is given by the impedance of the output port (50 Ω) plus the reactive impedance of the $L$ and $C_g$ combination. Therefore from the reflection coefficient at that frequency (which can be identified from the intersection with the unit resistance circle), we can obtain the series reactance, and from the value of $L$, which can be estimated from a transmission line calculator, we can infer the value of $C_g$. To determine the elements of the shunt admittance, we use (4) and two additional equations. One of them is the expression that gives the transmission zero frequency

$$f_z = \frac{1}{2\pi\sqrt{L_c(C + C_c)}} \tag{10}$$

which can be easily identified from simulation or experiment. Equation (3) can be inferred from the dispersion of the structure (1). For that frequency where $\phi = \pi/2$, namely $f_{\pi/2} = \omega_{\pi/2}/2\pi$, we have

$$Z_s(j\omega_{\pi/2}) = -Z_p(j\omega_{\pi/2}) \tag{11}$$

and hence (3). The three characteristic frequencies, $f_o$, $f_z$ and $f_{\pi/2}$ can be easily determined from simulation or experiment. Therefore by isolating (4), (10) and (11), the three elements of the shunt reactance can be inferred. Following this procedure, the line inductance has been found to be $L = 5.2$ nH. The other element values coincide with the parameters inferred from the simplified model (see results above) to a good approximation, with only one exception, that is the gap capacitance, which has been now found to be $C_g = 0.59$ pF. This discrepancy is explained by the fact that the line inductance, $L$, cannot be actually neglected. Hence, the result obtained from the model equations for $C_g$ must be considered as an effective capacitance. The electrical simulation of the equivalent circuit model (obtained by means of Agilent ADS), with the extracted parameters, including $L$, is also depicted in Fig. 4. Excellent agreement between both the electrical and electromagnetic simulations has been obtained, which is indicative of the validity of the model. This impedance inverter has not been fabricated since it has been used as an intermediate step for the design and fabrication of a CSRR-based power divider.

Power dividers can be implemented by means of 90° impedance inverters as it is depicted in Fig. 5. The device that has been implemented as a first prototype device to demonstrate the potentiality of CSRR left-handed lines on miniaturisation has been designed according to the topology shown in Fig. 5*a*. Hence the previous impedance inverter is useful for our purposes provided the same substrate is considered in the design of the power divider. The layout, compared to that of a conventional device, and the photograph of the fabricated prototype are shown in Fig. 6. The prototype has been characterised by using the Agilent 8720ET Vector Network Analyzer. The relevant scattering parameters (measured and simulated) are depicted in Fig. 7. Good agreement between full wave electromagnetic simulation and measurement has been obtained (the small shift

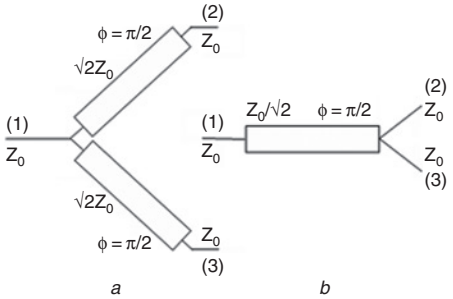


**Fig. 5** *Basic topologies for power dividers*
*a* and *b* 90° impedance inverters

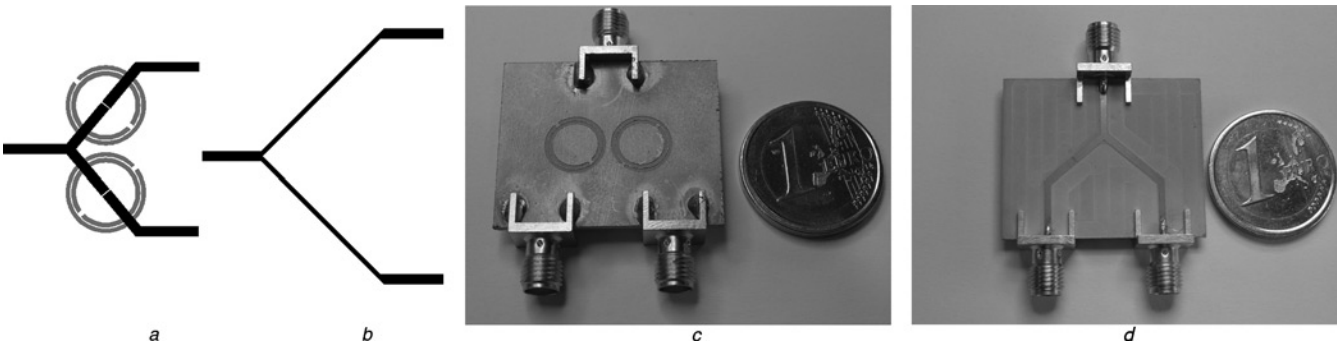


**Fig. 6** *CSRR-based power divider implemented by following the topology of Fig. 5a*

*a* Layout of the CSRR-based power divider
*b* Layout of a conventional power divider
*c* Bottom face of the power divider
*d* Top face of the power divider
The dimensions of the two impedance inverters forming the device are those indicated in Fig. 2

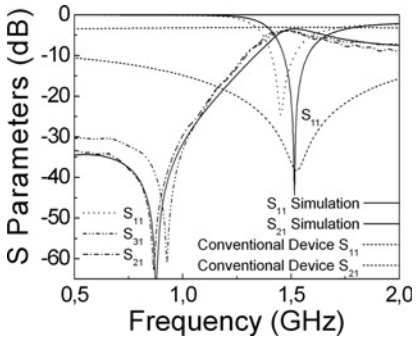


**Fig. 7** *Simulated and measured frequency responses for the power divider shown in Fig. 6*

The simulated frequency response of a conventional device is also depicted for comparison

is due to fabrication related tolerances). Measured transmission between the input and the output ports is $dB(S_{21}) = dB(S_{31}) = -3.2$ dB, which is close to the value corresponding to an ideal lossless device. Concerning dimensions, these are approximately 50% smaller than those of a conventional implementation. Therefore it is clear that the approach proposed in this work can be used to reduce the size of microwave devices. Actually size reduction is limited by CSRR dimensions, which in turn are limited by the critical dimensions of the technology in use. Namely, the size of CSRRs (for a given resonant frequency) can be reduced by decreasing the slot and interslot widths (*c* and *d* in Fig. 1). Hence, by implementing these structures in advanced technologies such as LTCC or MCM-D, among others, where lateral resolution is small, further miniaturisation is expected. We would also like to mention that the width of the host lines for the 90° impedance inverters is roughly the same as that of the 50 Ω access lines. This width (host lines) does not depend on the characteristic impedance of the inverter (as occurs in conventional lines). Therefore by means of this technique, it is potentially possible to achieve extreme values of line impedance without the need to implement very narrow (or wide) transmission line sections.

We have also designed a power divider according to the topology shown in Fig. 5*b*. In this case, a single 90° impedance inverter with 35.3 Ω characteristic impedance is required. The synthesis of this device has been done by following the steps discussed previously. The layout is depicted in Fig. 8 together with the photograph of the fabricated prototype. The simulated, using Agilent Momentum, and measured frequency responses of this power divider are depicted in Fig. 9. Again, good agreement between simulation and experiment has been obtained. Device dimensions are small ($l = 12.3$ mm, excluding access lines), whereas measured performance is good [i.e. $dB(S_{21}) = dB(S_{31}) = -3.9$ dB]. This slightly higher loss value (as compared to Fig. 7) is attributed to inaccuracies in fabrication since from simulation no distinguishable results arise. By increasing the number of output ports, *N*,

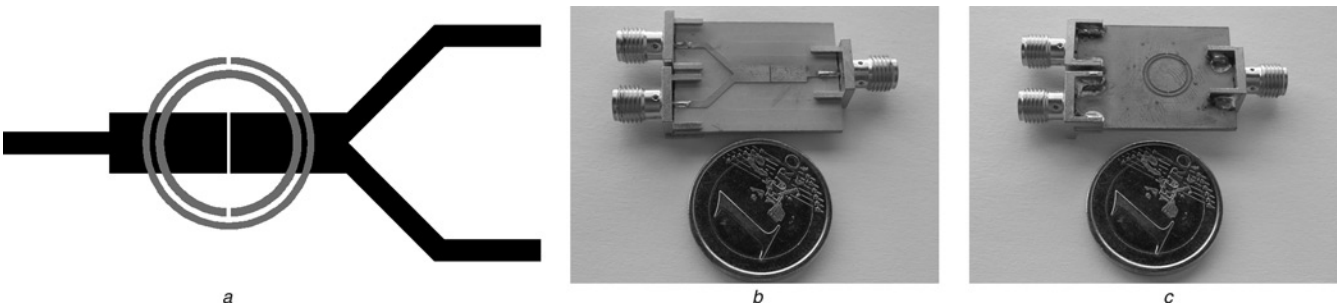


**Fig. 8** *CSRR-based power divider implemented by following the topology of Fig. 5b*

*a* Layout
*b* Top face of the power divider
*c* Bottom face of the power divider
Gap separation and width are 0.16 mm and 3.10 mm, respectively; CSRR dimensions are: inner slot width 0.42 mm, outer slot width 0.35 mm, interslot distance 0.26 mm; external radius 4.40 mm

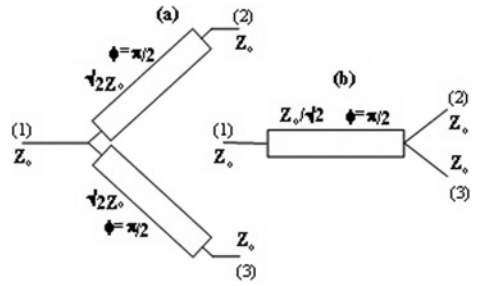


**Fig. 9** *Simulated and measured frequency responses for the power divider shown in Fig. 8*

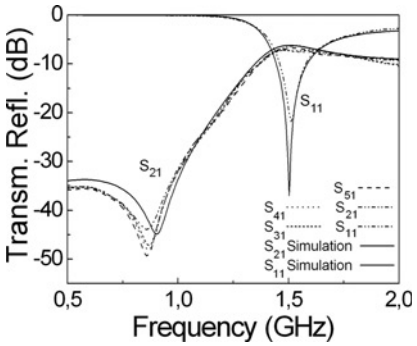


**Fig. 11** *Simulated and measured frequency responses for the device of Fig. 10*

of the divider, the characteristic impedance of the inverter must be decreased according to

$$Z_B = \frac{Z_o}{\sqrt{N}} \tag{12}$$

where $Z_o$ is the reference impedance of the ports (normally $Z_o = 50\ \Omega$). Hence, the characteristic impedance of the impedance inverter may take very low values for practical implementation if $N$ is high. The idea of implementing these devices by means of CSRR-based artificial lines has also been carried out. Specifically, we have designed a power divider with four output ports. The characteristic impedance of the 90° impedance inverter is in this case 25 Ω. We have designed such a transmission line and we have implemented the power divider by cascading 50 Ω lines to the input and output ports, as shown in Fig. 10. The simulated and measured frequency responses for this device are depicted in Fig. 11. The measured transmission between the input and any of the output ports (at the design frequency) is −6.2 dB, which is very close to the ideal transmission for such a four-port power divider. The width of the host line for the 90° artificial transmission line of Fig. 10 is $W = 6.0$ mm. This is actually wider than a conventional 25 Ω line implemented in the same substrate ($W = 3.9$ mm). The reason for implementing such relatively wide (but realisable) host line is the required value of the gap capacitance (5), which is relatively high on account of the low value of $Z_B = Z_c$. By using the interdigitated concept, line and gap widths can be substantially reduced, but this has not been applied to the design of Fig. 10 since the width of the resulting host line is still implementable. Also, gap separation could have been made smaller in order to achieve the required capacitance with a narrower line, but we have set this geometrical parameter to 0.16 mm (far above the resolution limit) to minimise tolerance effects. However, in applications requiring much lower (or higher) line impedances, conventional lines may not be implementable. Therefore the artificial transmission lines based on the combination of CSRRs and series capacitive gaps are useful not only to decrease device dimensions, but also to make possible the synthesis of planar transmission media requiring extreme values of the characteristic impedance. This may be the case of impedance matching networks with high (or low) impedance loads, or multi-output power dividers, among other devices.

The application of left-handed lines to the design of multi-output power dividers has also been reported by Antoniades and Eleftheriades [23]. In that work, they pursue broadband in-phase power division at all ports, and they successfully achieve this by using zero-degree artificial lines in order to inject in-phase signal at the output channels. Equal phase shift in the 1:4 power divider presented in this work has not been considered, but it would be possible to substitute the output access lines with zero-degree (or equal phase) lines implemented by means of CSRRs, in order to achieve in-phase output signals. Conversely, the miniaturisation technique presented in this paper could also be applied to reduce the size of the output channels in the power dividers presented in the work of Antoniades and Eleftheriades [23].

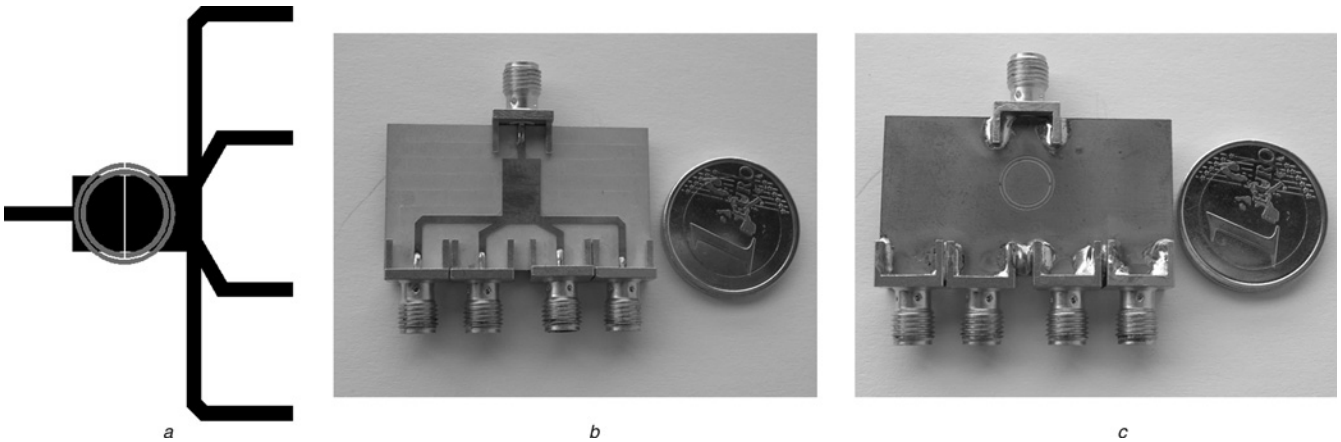


**Fig. 10** *Fabricated power divider with four output ports*

*a* Layout
*b* Top face of the fabricated power divider
*c* Bottom face of the fabricated power divider
Gap separation and width are 0.16 mm and 6.00 mm, respectively; CSRR dimensions are: inner slot width 0.39 mm, outer slot width 0.32 mm, inter-slot distance 0.18 mm; external radius 4.01 mm

Actually, the artificial lines presented in this work can be applied in many scenarios to reduce device dimensions, and this has been the main aim of this work. The bandwidth of the reported devices is limited and hence they are of interest in narrow band applications. Nevertheless, by combining CSRR/gap cells with shunt connected (grounded) stubs, an additional degree of flexibility is introduced and it is expected that bandwidth can be improved (this aspect is under investigation).

## 4 Conclusions

In conclusion, it has been demonstrated that artificial left-handed lines, implemented by etching CSRRs and series gaps in a host microstrip medium, can be useful for the design of compact microwave devices, such as impedance inverters and power dividers, among others. A method for the synthesis of these lines, in which the phase shift per cell and the characteristic impedance are the target specifications, has been proposed. Several prototype devices have been designed, fabricated and characterised to validate the approach presented in this work, and to point out the achievable levels of miniaturisation. The compactness factor has been found to be of the order of 50% in fabricated power dividers, as compared to conventional implementations. Measured transmission coefficients between the input and any of the output ports in such devices have revealed very good performance for narrow band applications. Moreover, it has been highlighted that by means of the artificial CSRR-based left-handed lines, it is possible to tailor line impedance over wide ranges. A multi-output power divider, that uses a 25 $\Omega$ impedance inverter, has been designed and fabricated to further demonstrate the potentiality of these artificial lines. Thus, CSRR left-handed lines are of interest to reduce the size of planar microwave circuits and to implement circuits requiring transmission lines or stubs with extreme values of line impedance.

## 5 Acknowledgments

This work has been supported by MEC (Spain) by project contract TEC2004-04249-C02-01 METASYSTEMS, by UAB-CIRIT through the project PNL2004-22 and by the European Commission (VI Framework Program) through the contract NoE. 500252-2 METAMORPHOSE.

## 6 References

1 Swanson, D.G., Forse, R., and Nilsson, B.J.L.: 'A 10GHz thin film lumped element high temperature superconductor filter'. IEEE MTT-S Int. Microwave Symp. Digest, Piscataway, NJ, June 1992, pp. 1191–1193
2 Menzel, W.: 'A novel miniature suspended stripline filter'. 33rd European Microwave Conf. Digest, Munich, Germany, October 2003, pp. 1047–1050
3 Hong, J.-S., and Lancaster, M.J.: 'Microstrip filters for RF/microwave applications' (John Wiley & Sons, New York, USA, 2001)
4 Mathaei, G.L., Young, L., and Jones, E.M.T.: 'Microwave filters impedance-matching networks, and coupling structures' (Artech House, Norwood, MA, 1980)
5 Görür, A., Karpuz, C., and Alkan, M.: 'Characteristics of periodically loaded CPW structures', *IEEE Microw. Guid. Wave Lett.*, 1998, **8**, pp. 278–280
6 Martín, F., Falcone, F., Bonache, J., Laso, M.A.G., Lopetegi, T., and Sorolla, M.: 'New CPW low pass filter based on a slow wave structure', *Microw. Opt. Technol. Lett.*, 2003, **38**, pp. 190–193
7 Martín, F., Falcone, F., Bonache, J., Laso, M.A.G., Lopetegi, T., and Sorolla, M.: 'Dual electromagnetic bandgap CPW structures for filter applications', *IEEE Microw. Wirel. Compon. Lett.*, 2003, **13**, pp. 393–395
8 Görür, A., Karpuz, C., and Akpinar, M.: 'A reduced size dual mode bandpass filter with capacitively loaded open-loop arms', *IEEE Microw. Wirel. Compon. Lett.*, 2003, **13**, pp. 385–387
9 Yang, F.R., Ma, K.P., Qian, Y., and Itoh, T.: 'A uniplanar compact photonic-bandgap structure and its applications for microwave circuits', *IEEE Trans. Microw. Theory Tech.*, 1999, **47**, p. 1509
10 Sor, J., Qian, Y., and Itoh, T.: 'Miniature low loss CPW periodic structures for filter applications', *IEEE Trans. Microw. Theory Tech.*, 2001, **49**, pp. 2336–2341
11 'Metamaterial Structures, phenomena and applications', *IEEE Trans. Microwave theory Techniques*, 2005, **53**, (4)
12 Veselago, V.G.: 'The electrodynamics of substances with simultaneously negative values of $\varepsilon$ and $\mu$', *Sov. Phys. Usp.*, 1968, **10**, pp. 509–514
13 Iyer, A.K., and Eleftheriades, G.V.: 'Negative refractive index metamaterials supporting 2-D waves'. IEEE-MTT Int'l. Symp., Seattle, WA, June 2002, vol. 2, pp. 412–415
14 Oliner, A.A.: 'A periodic-structure negative-refractive-index medium without resonant elements'. URSI Digest, IEEE-AP-S USNC/URSI National Radio Science Meeting, San Antonio, TX, June 2002, pp. 41
15 Caloz, C., and Itoh, T.: 'Application of the transmission line theory of left-hande (LH) materials to the realisation of a microstrip LH transmission line'. Proc. IEEE-AP-S USNC/URSI National Radio Science Meeting, San Antonio, TX, June 2002, vol. 2, pp. 412–415
16 Martín, F., Falcone, F., Bonache, J., Marqués, R., and Sorolla, M.: 'A new split ring resonator based left-handed coplanar waveguide', *Appl. Phys. Lett.*, 2003, **83**, pp. 4652–4654
17 Falcone, F., Lopetegi, T., Laso, M.A.G., Baena, J.D., Bonache, J., Marqués, R., Martín, F., and Sorolla, M.: 'Babinet principle applied to the design of metasurfaces and metamaterials', *Phys. Rev. Lett.*, 2004, **93**, p. 197401
18 Smith, D.R., Padilla, W.J., Vier, D.C., Nemat-Nasser, S.C., and Schultz, S.: 'Composite medium with simultaneously negative permeability and permittivity', *Phys. Rev. Lett.*, 2000, **84**, pp. 4184–4187
19 Falcone, F., Lopetegi, T., Baena, J.D., Marqués, R., Martín, F., and Sorolla, M.: 'Effective negative-$\varepsilon$ stop-band microstrip lines based on complementary split ring resonators', *IEEE Microw. Wirel. Compon. Lett.*, 2004, **14**, pp. 280–282
20 García-García, J., Martín, F., Amat, E., Falcone, F., Bonache, J., Gil, I., Lopetegi, T., Laso, M.A.G., Marcotegui, A., Sorolla, M., and Marqués, R.: 'Microwave filters with improved stop band based on sub-wavelength resonators', *IEEE Trans. Microw. Theory Tech.*, 2005, **53**, pp. 1997–2006
21 Baena, J.D., Bonache, J., Martín, F., Marqués, R., Falcone, F., Lopetegi, T., Laso, M.A.G., García, J., Gil, I., and Sorolla, M.: 'Equivalent circuit models for split ring resonators and complementary split rings resonators coupled to planar transmission lines', *IEEE Trans. Microw. Theory Tech.*, 2005, **53**, pp. 1451–1461
22 Gil, M., Bonache, J., Gil, I., García-García, J., and Martín, F.: 'On the transmission properties of left-handed microstrip lines implemented by complementary split rings resonators', *Int. J. Num. Model,*, 2006, **19**, pp. 87–103
23 Antoniades, M.A., and Eleftheriades, G.V.: 'A broadband series power divider using zero-degree metamaterial phase shifting lines', *IEEE Microw. Wirel. Compon. Lett.*, 2005, **15**, pp. 808–810

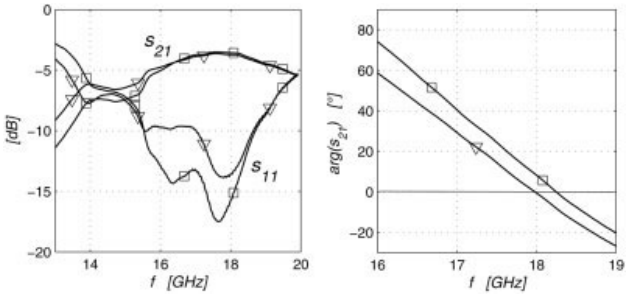


**Figure 7** Measured *S*-parameters with actuation voltage of 0 V (plain lines) and 42 V (dashed lines)

43 V and the phase shift can consequently be varied continuously between the two states shown in Figure 7 by applying a DC voltage between 0 and 42 V, which correspond to bridge heights of about 3 and 2 $\mu$m, respectively.

## 6. CONCLUSION

We have successfully designed and fabricated a CRLH-TL phase shifter that can be analogically controlled by means of a MEMS device. In addition, an accurate circuit model and a design strategy specific to the design of MEMS CRLH-TL have been presented and validated.

This work has shown that MEMS technology allows simultaneously adding variability, compactness, and monolithic integration to previously demonstrated capabilities of CRLH-TLs. It is therefore believed that MEMS technology, associated with appropriate modeling methods, should help widen the field of application of CRLH-TL metamaterials in the future.

## ACKNOWLEDGMENT

This work was supported by the AMICOM European Network of Excellence.

## REFERENCES

1. M.A. Antoniades and G.V. Eleftheriades, Compact linear lead/lag metamaterial phase shifters for broadband applications, IEEE Antennas Wireless Propag Lett 2 (2003), 103–106.
2. I.-H. Lin, M. DeVincentis, C. Caloz, and T. Itoh, Arbitrary dual-band components using composite right/left-handed transmission lines, IEEE Trans Microwave Theory Tech 52 (2004), 1142–1149.
3. A. Grbic and G.V. Eleftheriades, Experimental verification of backward-wave radiation from a negative refractive index metamaterial. J Appl Phys 92 (2002), 5930–5935.
4. Z. Qi, Z. Zhongxiang, X. Shanjia, and D. Wenwu, Millimeter wave microstrip array design with CRLH-TL as feeding line, IEEE Antennas Propag Soc Int Symp 2004, 3413–3416.
5. J. Perruisseau-Carrier, R. Fritschi, P. Crespo-Valero, and A.K. Skrivervik, Modeling of periodic distributed MEMS, application to the design of variable true-time delay lines, IEEE Trans Microwave Theory Tech 54 (2006), 383–392.
6. S. Lee and et al., Low-loss analog and digital reflection-type MEMS phase shifters with 1:3 bandwidth, IEEE Trans Microwave Theory Tech 52 (2004), 211–219.
7. J. Perruisseau-Carrier and A.K. Skrivervik, Composite right/left handed transmission line metamaterial phase shifters (MPS) in MMIC technology, IEEE Trans Microwave Theory Tech 54 (2006), Part I, 1582–1589.
8. T. Lisec, C. Huth, M. Shakhhray, B. Wagner, and C. Combi, Surface-micromachined capacitive RF switches with high thermal stability and low drift using Ni as structural material, In: MEMSWAVE 2004, 2004, pp. C33–C36.
9. R.E. Collin, Foundations for microwave engineering, 2nd ed., McGraw-Hill, New York, 1992.

# METAMATERIAL TRANSMISSION LINES WITH EXTREME IMPEDANCE VALUES

**Marta Gil, Ignacio Gil, Jordi Bonache, Joan García-García, and Ferran Martín**
Departament d'Enginyeria Electrónica,
Universitat Autónoma de Barcelona,
08193 Bellatera (Barcelona), Spain

*Received 25 May 2006*

**ABSTRACT:** *In this work, it is demonstrated that it is possible to synthesize the metamaterial transmission lines with extreme characteristic impedances. The structures consist on left-handed microstrip lines based on the combination of complementary split rings resonators (CSRRs), which are etched in the ground plane, and series capacitive gaps. By means of an adequate design, it is possible to tailor the characteristic impedance of the lines over a wide margin. The realizable impedance values are not easily achievable through conventional transmission lines implemented in commercial microwave substrates. Several illustrative examples are provided and the limitations of the technique (relative to the maximum and minimum achievable impedances) are discussed. The compact dimensions of these artificial lines, related to the small electrical size of CSRRs, are also pointed out. These structures can be applied to the design of microwave components with severe requirements concerning characteristic impedance.* © 2006 Wiley Periodicals, Inc.
Microwave Opt Technol Lett 48: 2499–2505, 2006; Published online in Wiley InterScience (www.interscience.wiley.com). DOI 10.1002/mop.22013

**Key words:** *metamaterials; left-handed lines; complementary split rings resonators (CSRRs)*

## 1. INTRODUCTION

Metamaterial transmission lines are microstructured propagating media with controllable electrical parameters and high dispersion. Among them, the so called left-handed (LH) lines, composed of electrically small unit cells, exhibit backward wave propagation. Two different approaches have been used so far for the synthesis of LH lines: (i) the composite right/left handed (CRLH) approach, where a host line is loaded with series capacitors and shunt inductors [1–4], and (ii) the resonant type approach, where electrically small resonant elements such as split rings resonators (SRRs) [5, 6], or their dual counterparts (complementary split rings resonators, CSRRs) [7, 8], are coupled to a host line. In both cases, there is a frequency band where wave propagation is backward. This behavior can be interpreted as due to the coexistence of negative effective permeability and permittivity in that band. For resonant type LH lines implemented by means of CSRRs, these resonant elements provide the negative effective permittivity [6], whereas the required negative permeability is achieved by etching series capacitive gaps in the conductor strip. These CSRR-based LH lines have been successfully applied to the design of compact microwave filters [9]. In this work, the main aim is to take benefit of the wide variation of the phase constant and characteristic impedance over the allowed band, to design artificial transmission

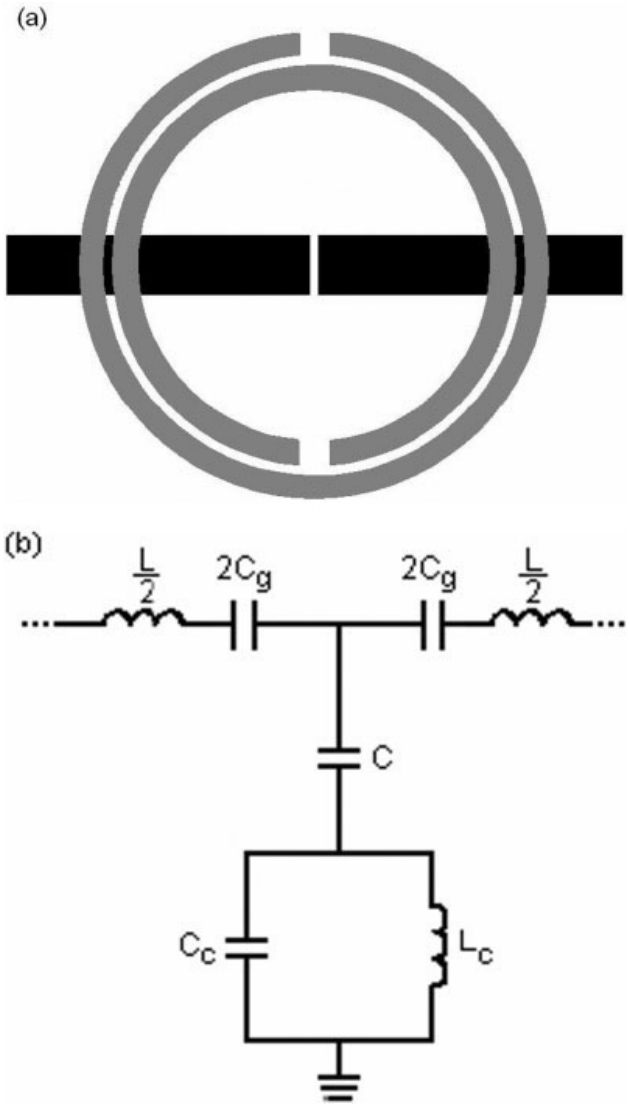


**Figure 1** Basic cell of the CSRR/gap loaded microstrip line (a) and equivalent circuit model (b). In this and the following layouts, the conductor strip is depicted in black, whereas the CSRRs, which are etched in the ground plane, are depicted in grey

lines where the characteristic impedance can be set to values beyond those that can be achieved through conventional implementations.

## 2. THE BASIC CELL AND EQUIVALENT CIRCUIT

The basic cell for such lines is depicted in Figure 1 together with the lumped element equivalent circuit model. CSRRs are etched in the ground plane, underneath the positions of the series gaps. The gaps are modeled by the capacitance $C_g$, whereas $L$ models the inductance of the line. CSRRs are described by the resonators formed by the parallel combination of $L_c$ and $C_c$, and their coupling to the host line is modeled by the capacitance $C$. To minimize dimensions as much as possible, these artificial transmission lines are preferably implemented by using a single cell. However, as will be later shown, this is not always possible. Nevertheless, coupling between adjacent CSRRs (in case of multiple stage devices) is ignored since it has been found that interaction between neighbor CSRRs is negligible for circular geometries [10]. Actually, in this circuit model, the line inductance $L$ is ignored since we are only interested in the backward wave transmission band of the structure. However, to properly describe the transmission characteristics of the CSRR structure by ignoring $L$, it is necessary that the resonator formed by $L$ and the gap capacitance $C_g$ exhibits a resonance frequency well above the intrinsic resonant frequency of the CSRRs, i.e.

$$f_0 = \frac{1}{2\pi\sqrt{L_c C_c}}. \tag{1}$$

The analysis of the circuit model of Figure 1(b) can be done with the help of the dispersion relation and Bloch impedance, which are given by [11]

$$\cos\phi = 1 + \frac{Z_s(j\omega)}{Z_p(j\omega)}, \tag{2}$$

and

$$Z_B = \sqrt{Z_s(j\omega)[Z_s(j\omega) + 2Z_p(j\omega)]}, \tag{3}$$

respectively, where $\phi = \beta l$ is the phase of the basic cell, and $Z_s$ and $Z_p$ are the series and shunt impedances, respectively, of the basic circuit cell. In Figure 2 the variation of $\phi$ and $Z_B$ with frequency are depicted, within the LH allowed band, for a basic cell with the electrical parameters indicated in the caption. The structure is transparent (i.e. it supports propagating modes) within the interval delimited by the frequencies given by

$$f_L = \frac{1}{2\pi}\frac{1}{\sqrt{L_c\left(C_c + \dfrac{4}{\dfrac{1}{C_g} + \dfrac{4}{C}}\right)}}, \tag{4}$$

$$f_H = \frac{1}{2\pi\sqrt{L_c C_c}}. \tag{5}$$

Within this interval, $\phi$ varies between 0 (at $f_H$) and $-\pi$ (at $f_L$), whereas $Z_B = 0\ \Omega$ at $f_L$ and $Z_B \to \infty$ at $f_H$. This analysis and Figure

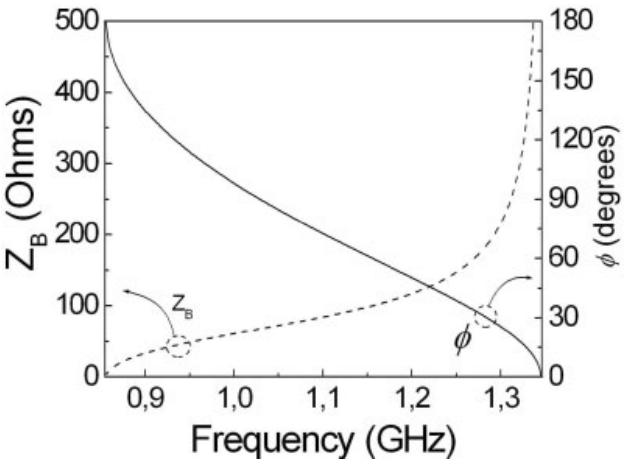


**Figure 2** Dependence of $\phi$ and $Z_B$ with frequency for the structure of Figure 1(b), with the following parameters: $L = 3$ nH, $C_g = 1$ pF, $C = 30$ pF, $C_c = 3.5$ pF, and $L_c = 4$ nH

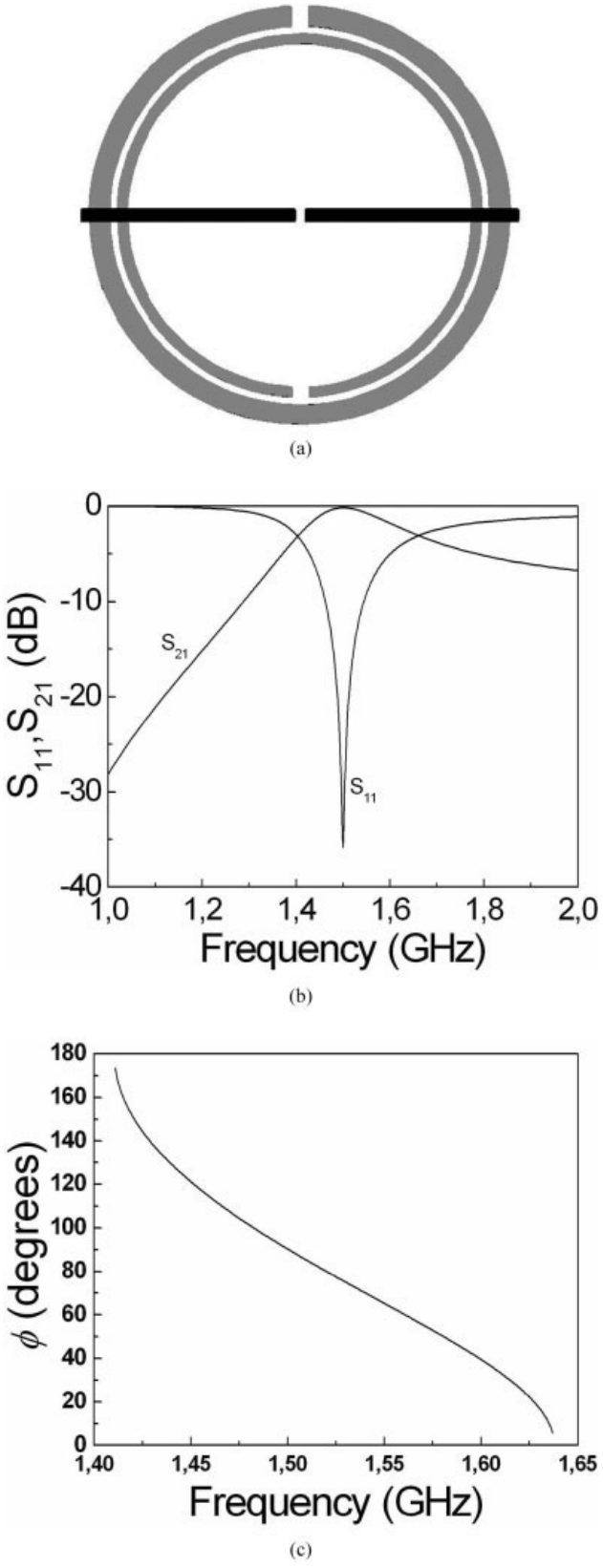


**Figure 3** Layout (a), insertion and return losses (b), and phase shift (c) for the artificial transmission line with characteristic impedance of 150 Ω and 90° phase shift at 1.5 GHz. Gap separation is 0.2 mm; CSRR dimensions are as follows: external radius $r_{ext} = 4.85$ mm, slot widths $c_{in} = 0.26$ mm, $c_{out} = 0.50$ mm, and slot separation $d = 0.14$ mm

2 suggest that it is possible (by using these CSRR-based cells) to synthesize artificial transmission lines with impedances not easily achievable through conventional implementations. The main aim of this work is to demonstrate this, and to establish the limitations of this approach, which are mainly caused by the fact that $\phi$ and $Z_B$ are not fully independent parameters. In Figure 2 and the following figures, the phase $\phi$ is depicted in absolute value, but it is actually negative due to the LH nature of the structures.

## 3. THE SYNTHESIS METHOD

Let us call $\phi_c = \phi(f_c)$ and $Z_c = Z_B(f_c)$ the phase shift per cell and the desired line impedance, respectively, at the operating frequency $f_c$. From these input parameters, the parameters of the equivalent circuit model of the elemental cell can be inferred from the following equations [12]:

$$C_g = \frac{1}{2\omega_c Z_c}\sqrt{\frac{1+\cos\phi_c}{1-\cos\phi_c}}, \tag{6}$$

$$L_c = \frac{Z_c}{2}\sqrt{\frac{1+\cos\phi_c}{1-\cos\phi_c}}\frac{\omega_C}{\omega_H^4}\frac{(\omega_H^2-\omega_L^2)(\omega_H^2-\omega_C^2)}{(\omega_C^2-\omega_L^2)}, \tag{7}$$

$$C_c = \frac{1}{L_c\omega_H^2}, \tag{8}$$

$$C = \frac{2\omega_H^2(\omega_C^2-\omega_L^2)\sqrt{1-\cos^2(\phi_c)}}{Z_c\omega_C[\omega_C^2(1+\cos\phi_c)(\omega_H^2-\omega_L^2)-2\omega_H^2(\omega_C^2-\omega_L^2)]}, \tag{9}$$

where $\omega_C = 2\pi f_c$, $\omega_L = 2\pi f_L$, and $\omega_H = 2\pi f_H$. These parameters must be positive and they should take reasonable values to lay out the basic cell with reasonable dimensions (i.e. within the tolerance limits dictated by the fabrication process). In Ref. 12, this aspect is considered, and it is concluded that there is a limited range of values of $f_L$ and $f_H$ that make the parameters given by expressions (6)–(9) to take positive values. Thus, there is an intrinsic limitation concerning the achievable bandwidth for such artificial lines. However, in practice, this is further limited by the dimensions of the resulting layout, which must be realizable. Since there is a link between impedance and phase (namely, as impedance varies between $Z_B = 0\ \Omega$ at $f_L$ and $Z_B \to \infty$ at $f_H$, the phase goes from $\phi = -\pi$ to $\phi = 0$), it is not possible to simultaneously obtain low line impedance and phase by means of a single cell, or, alternatively, a high impedance line with a phase shift close to $\phi = -\pi$. In the next section, these limitations will be discussed on the basis of artificial line design and implementation.

## 4. ILLUSTRATIVE EXAMPLES

Since many microwave circuits (admittance inverters, power dividers, filters, directional couplers, etc.) are based on 90° transmission lines or stubs, this has been the considered target value of $\phi$, whereas the operating frequency has been set to $f_c = 1.5$ GHz. The aim of this section is to study the maximum range of achievable line impedances with the previous phase constraint. We have used Eqs. (6)–(9), by giving tentative values to $\omega_L$ and $\omega_H$, to obtain the electrical parameters of the basic cell, and by following an optimization procedure, the layout of the structure has been generated. We have considered both the synthesis of high impedance (in reference to 50 Ω) and low impedance artificial lines. Concerning high impedance lines, it has been found that it is possible to synthesize 150 Ω lines with 90° phase shift by means of a single cell. The layout and the simulated (using the *Agilent Momentum* commercial software) frequency response are shown in

Figure 3. The impedance of the ports has been set to 150 Ω since, by doing this, total transmission at the target frequency must be obtained. The phase shift $\phi$ has been obtained from the simulated phase of the transmission coefficient, $\phi_{21}$, (with 50 Ω ports) following:

$$\cos\phi = \frac{\cos\phi_{21}}{T}, \tag{10}$$

where $T$ is the modulus of $S_{21}$. Inspection of Figure 3 indicates that $Z_B = 150\ \Omega$ and $\phi = 90°$ at 1.5 GHz. As compared to a conventional transmission line implemented on identical substrate (*Rogers RO3010*, dielectric constant $\varepsilon_r = 10.2$, thickness $h = 1.27$ mm) the length of the CSRR line is smaller (10.1 mm). The 90° conventional line is 22 mm long, and it is not implementable since it is only 6 $\mu$m wide, and this is not achievable with any known fabrication process in this type of substrates.

If the line impedance is set to 300 Ω, which gives a width for the conventional line in the nanometre scale, it is not possible to implement a 90° line with a single cell. The reason is that as impedance increases, the phase decreases (as has been explained in earlier section). Therefore, to achieve the required phase shift, a solution in this case is to cascade two CSRR cells each contributing with 45° to the phase shift. The layout and simulated frequency response for this structure are depicted in Figure 4. Obviously, in this case, since two sections are needed, we do not take benefit of the small length of a single cell and the length of the artificial line (20.8 mm) is comparable to that of the conventional, but not realizable, structure (21.7 mm). This structure has been fabricated by cascading 50 Ω access lines. The photograph of the structure is shown in Figure 5. Also in this figure is depicted the frequency dependence of $Z_B$ and $\phi$ that has been inferred from measurement (by using the *Agilent 8720ET* VNA). The frequencies where $Z_B = 300\ \Omega$ and $\phi = 90°$ do not exactly coincide with the nominal values. This is due to fabrication related tolerances and to the fact that the impedance is very sensitive on frequency at these high values. Nevertheless, we are able to synthesize artificial lines with very high impedance values. Because of the presence of the access lines, the procedure to experimentally obtain the characteristic impedance and the phase shift corresponding to the CSRR structure (i.e. by excluding the access lines) is not as simple as just using Eq. (10) or representing the frequency response. We have obtained the characteristic impedance from the measured $S_{11}$ coefficient. This gives the impedance seen from the input port, and from the electrical length of the access lines, we can obtain the impedance seen from the interface between the access line and the CSRR cell. Once this impedance has been obtained, the characteristic impedance of the CSRR structure can be inferred from the well-known formula giving the input impedance of a loaded transmission line. To obtain the phase shift corresponding to the region of interest, we have experimentally obtained the phase of the transmission coefficient $\phi_{21}$ for the whole structure (including access lines). From it, we have inferred the phase shift according to Eq. (10), and by subtracting the experimentally measured phase shift of the access lines, we have finally obtained the phase shift $\phi$ of the CSRR structure.

With regard to the synthesis of low impedance lines, we have designed a single cell 25 Ω line with 90° phase shift. The layout and simulated frequency response are depicted in Figure 6. In this case, the conventional line is realizable, but the length of the artificial lines (8.1 mm) is substantially shorter (as compared with the length, 17.98 mm, of the conventional line).

We have also designed a single cell 90° and 10 Ω line at 1.5 GHz. The corresponding layout, frequency response, and phase shift are depicted in Figure 7. The conventional line is in this case 12.5 mm wide (i.e., implementable), whereas its length is 16.7 mm, i.e. longer than the artificial line (13.84 mm). This structure

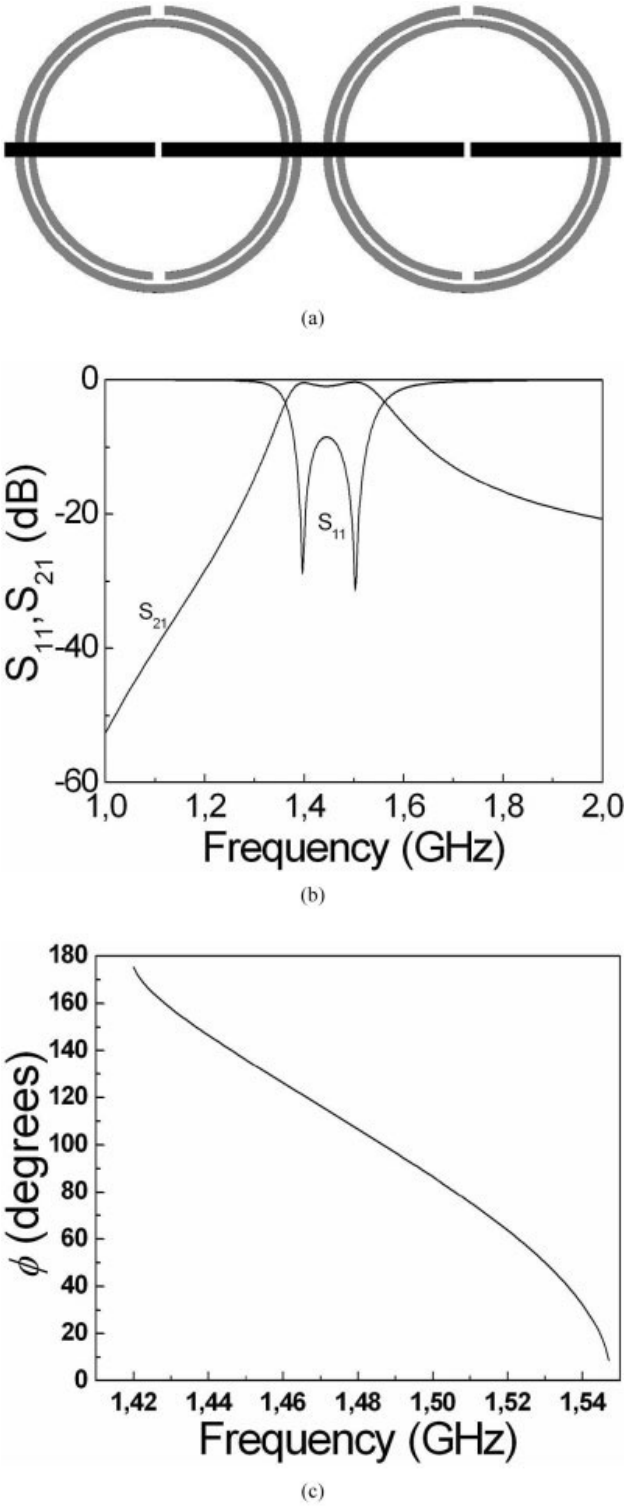


**Figure 4** Layout (a), insertion and return losses (b), and phase shift (c) for the two-stage artificial transmission line with characteristic impedance of 300 Ω and 90° phase shift at 1.5 GHz. Gap separation is 0.2 mm; CSRR dimensions are as follows: external radius $r_{ext} = 4.85$ mm, slot widths $c_{in} = 0.27$ mm, $c_{out} = 0.30$ mm, and slot separation $d = 0.14$ mm

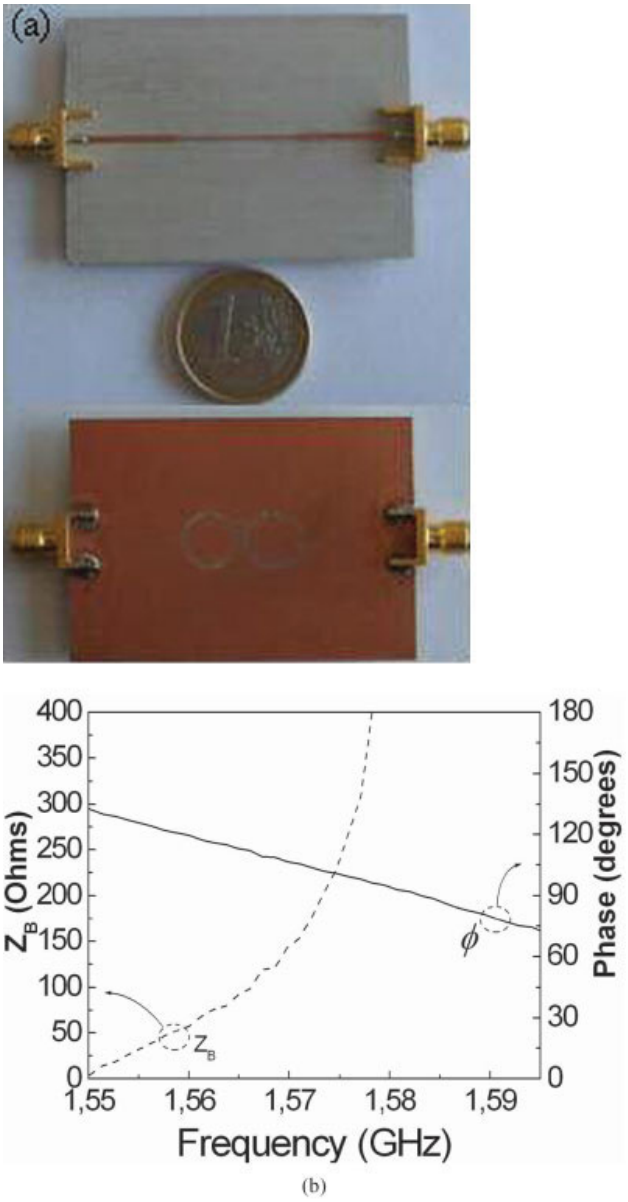


**Figure 5** Photograph of the structure of Figure 4 with access lines (a), and dependence of the characteristic impedance and phase shift (b) with frequency [Color figure can be viewed in the online issue, which is available at www.interscience.wiley.com]

has been also fabricated (see photograph in Fig. 8), and by following the procedure described before, we have experimentally obtained the dependence of $Z_B$ and $\phi$ on frequency (Fig. 8). Again there is some discrepancy between the frequencies where the measured electrical parameters of the line take the target values and the nominal frequency (1.5 GHz), which can be also attributed to certain inaccuracies in fabrication.

Essentially, in this work, the possibility of implementing artificial metamaterial transmission lines with impedance values in the range 10–300 Ω (with 90° electrical length) has been demonstrated. Theoretically, it is possible to achieve impedances beyond these limits, but in practice either the resulting topologies are not easily realizable or the sensitivity of impedance with frequency (high impedances) is too high (as is indeed the case for the 300 Ω line). This type of artificial transmission lines can find application

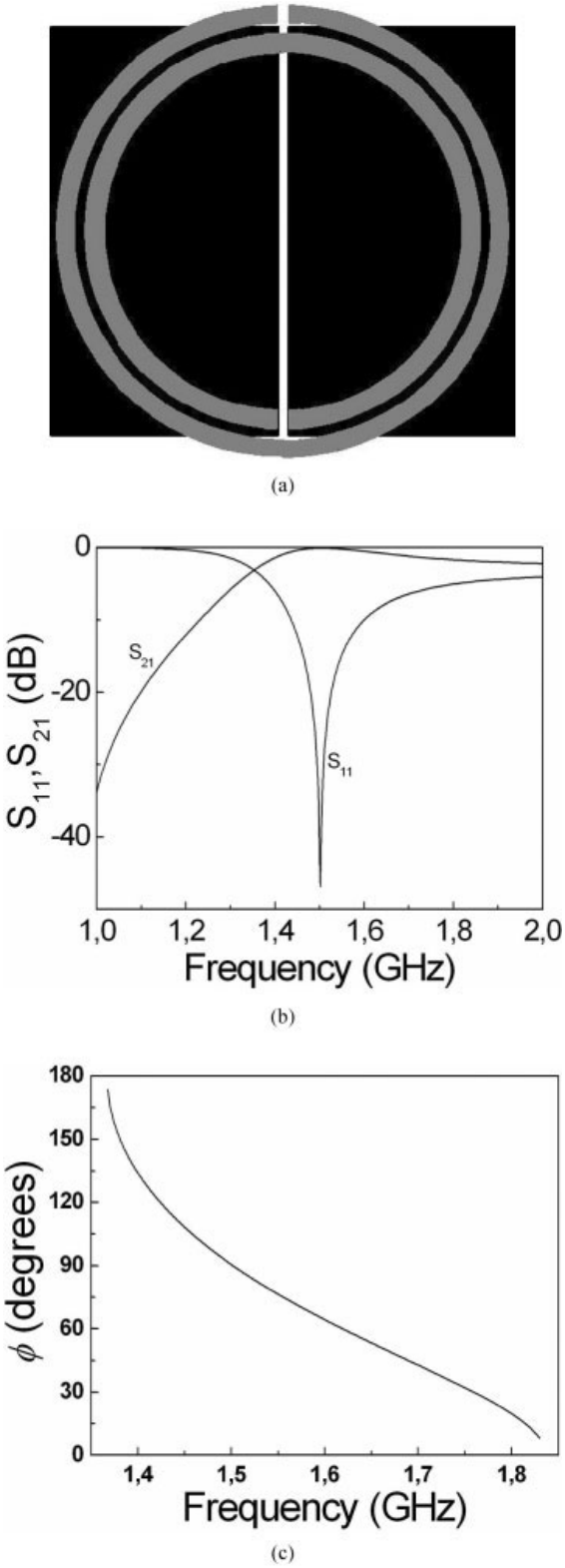


**Figure 6** Layout (a), insertion and return losses (b), and phase shift (c) for the artificial transmission line with characteristic impedance of 25 Ω and 90° phase shift at 1.5 GHz. Gap separation is 0.16 mm; CSRR dimensions are as follows: external radius $r_{ext}$ = 4.05 mm, slot widths $c_{in}$ = 0.36 mm, $c_{out}$ = 0.32 mm, and slot separation $d$ = 0.18 mm

in narrow band microwave circuits that require transmission lines and stubs with extreme impedance values. They are also interesting to reduce device size, as has been demonstrated from the

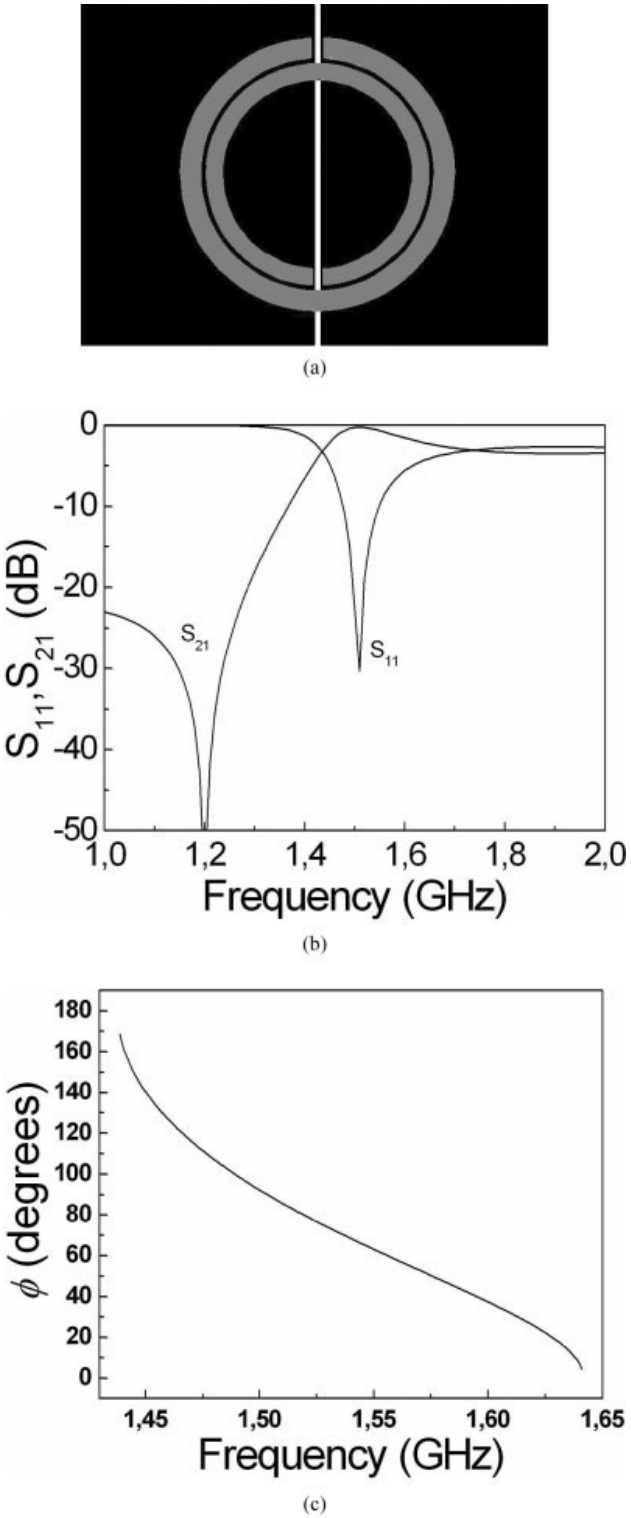


**Figure 7** Layout (a), insertion and return losses (b), and phase shift (c) for the artificial transmission line with characteristic impedance of 10 Ω and 90° phase shift at 1.5 GHz. Gap separation is 0.18 mm; CSRR dimensions are as follows: external radius $r_{ext}$ = 4.06 mm, slot widths $c_{in}$ = 0.51 mm, $c_{out}$ = 0.62 mm, and slot separation $d$ = 0.14 mm

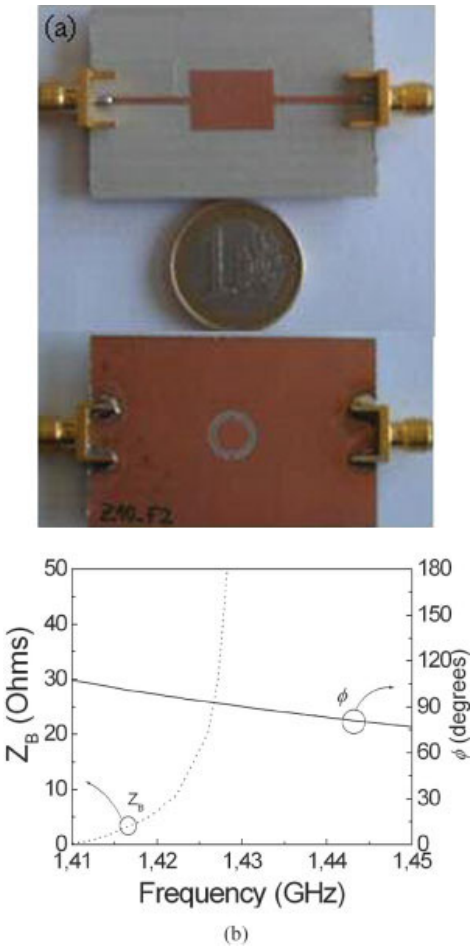


**Figure 8** Photograph of the structure of Figure 7 with access lines (a), and dependence of the characteristic impedance and phase shift (b) with frequency [Color figure can be viewed in the online issue, which is available at www.interscience.wiley.com]

comparison to conventional transmission lines. As has been seen in the preceding examples bandwidth is limited. It has been found that bandwidth is somehow wider for the small impedance structures. The reason is that in these structures, $C_g$ and $C$ are larger, and this enhances bandwidth [Eqs. (4)–(9)]. However, caution must be taken with Eqs. (4)–(9) since they are valid under the assumption that line inductance $L$ gives a negligible impedance as compared with the impedance associated to $C_g$. Moreover, strictly speaking, bandwidth in these structures is related to that frequency band where impedance lies within a certain range, and a more rigorous analysis, which is out of the scope of this paper, is required to study the effects of electrical parameters on bandwidth. Work is in progress to introduce additional elements to the topology of the basic cell to increase bandwidth.

## 5. CONCLUSIONS

In conclusion, it has been demonstrated that by loading microstrip lines with CSRRs and series gaps, it is possible to perform the synthesis of LH artificial transmission lines with extreme impedance values. Both high and low characteristic impedance lines have been designed and fabricated. While impedance and phase shift for such lines are not fully independent variables, the design of CSRR based lines with 90° phase shift (useful in many applications) and different impedance values (as high as 300 Ω and as

low as 10 Ω) has been carried out. This method is useful to reduce the physical length of the transmission lines and to obtain impedance values not easily achievable through conventional printed lines.


## ACKNOWLEDGMENTS

This work has been supported by Spain-MEC (project contract TEC2004–04249-C02–01), by UAB-CIRIT (project contract. PNL2004–22), and by the EU through the *NoE METAMORPHOSE*. The authors are also in debt to AGAUR (Generalitat de Catalunya) for funding this activity through the contract 2005SGR00624.


## REFERENCES


1. A.K. Iyer and G.V. Eleftheriades, Negative refractive index metamaterials supporting 2-D waves, In: IEEE-MTT International Symposium, Seattle, WA, June 2002, Vol. 2, pp. 412–415.
2. A.A. Oliner, A periodic-structure negative-refractive-index medium without resonant elements, In: URSI Digest IEEE-AP-S USNC/URSI National Radio Science Meeting, San Antonio, TX, June 2002, p. 41.
3. C. Caloz and T. Itoh, Application of the transmission line theory of left-handed (LH) materials to the realization of a microstrip LH transmission line, In: Proceedings of IEEE-AP-S USNC/URSI National Radio Science Meeting, San Antonio, TX, June 2002, Vol. 2, pp. 412–415.
4. A. Sanada, C. Caloz, and T. Itoh, Characteristics of the composite rigth/left handed transmisión lines, IEEE Microwave Wireless Compon Lett 14 (2004), 68–70.
5. F. Martín, F. Falcone, J. Bonache, R. Marqués, and M. Sorolla, A new split ring resonator based left handed coplana waveguide, Appl Phys Lett 83 (2003), 4652–4654.
6. F. Falcone, F. Martín, J. Bonache, R. Marqués, T. Lopetegi, and M. Sorolla, Left handed coplanar waveguide band pass filters based on bi-layer split ring resonators, IEEE Microwave Wireless Compon Lett 14 (2004), 10–12.
7. F. Falcone, T. Lopetegi, J.D. Baena, R. Marqués, F. Martín, and M. Sorolla, Effective negative-ε stop-band microstrip lines based on complementary split ring resonators, IEEE Microwave Wireless Compon Lett 14, (2004), 280–282.
8. F. Falcone, T. Lopetegi, M.A.G. Laso, J.D. Baena, J. Bonache, R. Marqués, F. Martín, and M. Sorolla, Babinet principle applied to the design of metasurfaces and metamaterials, Phys Rev Lett 93 (2004), 197401.
9. J. Bonache, F. Martín, I. Gil, J. García-García, R. Marqués, and M. Sorolla, Novel microstrip band pass filters based on complementary split rings resonators, IEEE Trans Microwave Theory Tech 54 (2006), 265–271.
10. I. Gil, J. Bonache, M. Gil, J. García, F. Martín, and R. Marqués, Modelling complementary-split-rings-resonator (CSRR) left-handed lines with inter-resonator's coupling, Presented at the 13th IEEE Mediterranean Electrochemical Conference (MELECON 2006), Torremolinos (Málaga), Spain, May 16–19, 2006.
11. D.M. Pozar, Microwave engineering, Addison Wesley, New York, 1993.
12. M. Gil, J. Bonache, I. Gil, J. García-García, and F. Martín, Miniaturization of planar microwave circuits by using resonant-type left handed transmission lines, IEE Proc Microwave Antennas Propag, in press.




# TRANSPARENT-FERROMAGNETIC THERMOPLASTIC POLYMERS FOR OPTICAL COMPONENTS


**G. Carotenuto,[1] G. Pepe,[2] D. Davino,[3] B. Martorana,[4] P. Perlo,[4] D. Acierno,[5] L. Nicolais[1]**

[1]Istituto per i Materiali Compositi e Biomedici
CNR. P.le Tecchio
80 - 80125 Napoli
[2]Dip. Scienze Fisiche
Università "Federico II" di Napoli. P.le Tecchio
80 - 80125 Napoli
[3]Dipartimento di Ingegneria
Università del Sannio
Piazza Roma 21 - 82100, Benevento
[4]Centro Ricerche FIAT
Strada Torino
50 - 10043 Orbassano (TO)
[5]Dip. di Ingegneria dei Materiali e Produzione
Università "Federico II" di Napoli
P.le Tecchio, 80 - 80125 Napoli


*Received 25 May 2006*


**ABSTRACT:** *Optical plastics filled by nanosized magnetic particles may have important applications in the optical field (e.g. magneto–optics, etc.). Amorphous polystyrene filled by acicular magnetite particles of nanosized dimension (ca. 10 nm × 50 nm) has been obtained by thermal decomposition (at 200°C) of iron(II) mercaptide dissolved in the polymer. This nanocomposite material is quite transparent to visible light and shows ferromagnetic characteristics at room temperature. In particular, magnetic properties behaves anisotropically in the material and are related to the magnetite content.* © 2006 Wiley Periodicals, Inc. Microwave Opt Technol Lett 48: 2505–2508, 2006; Published online in Wiley InterScience (www.interscience.wiley.com). DOI 10.1002/mop.22012


**Key words:** *magnetite; polystyrene; nanocomposites; ferromagnetism; mercaptides*

## 1. INTRODUCTION

Optical plastics (e.g., polystyrene, polycarbonate, poly(methyl methacrylate), etc.) embedding nanosized ferromagnetic phases have unique physical properties. Owing to the small filler size (less than 50 nm), these materials do not scatter visible light and therefore they are quite transparent in the visible spectral region. In addition, depending on the particle size (i.e., multi-domain or single-domain magnetic particles), these nanocomposite materials show ferromagnetic or super-paramagnetic behaviors. Optically transparent magnetic plastics may have important technological applications especially in the magneto–optical field [1–3]. In particular, the Verdet's constant of a polymeric material is quite low and it can be significantly increased by filling the polymer with ferromagnetic nanoparticles. Consequently, when subject to a magnetic field, such special nanocomposites can rotate the vibration plane of a plane-polarized light and therefore they can be used to fabricate optical modulators, optical insulators, optical shutters, etc. In addition, these nonmetallic magnets efficiently absorb microwaves and therefore they can be used as transparent electromagnetic interference and radiofrequency shields (EMI/RFI) and microwave-processable plastics [4].

Recently, a very simple chemical method for the synthesis of polymer-embedded noble metal and sulfide clusters have been developed [5–7]. This method is based on the thermal decomposition of homoleptic mercaptide molecules dissolved in polymers. The thermolysis of mercaptide molecules takes place at temperatures compatible with polymer thermal stability; in addition nor-

# Artificial Left-handed Transmission Lines for Small Size Microwave Components: Application to Power Dividers

Marta Gil, Jordi Bonache, Ignacio Gil, Joan García-García and Ferran Martín

Departament d'Enginyeria Electrònica (GEMMA/CIMITEC). Universitat Autònoma de Barcelona. 08193 BELLATERRA (Barcelona), Spain. E-mail: Ferran.Martin@uab.es

***Abstract*** **— In this work, we demonstrate that artificial transmission lines based on complementary split rings resonators (CSRRs) are useful for the design of microwave circuits with reduced size as compared to conventional implementations. The structures consist on microstrip line sections with CSRRs etched in the ground plane, underneath the conductor strip, and series capacitive gaps. By these means, a dispersive transmission medium supporting backward (or left handed) wave propagation within a certain frequency band around the CSRRs' resonance, is obtained. Key factors to achieve size reduction in functional devices are the small electrical size of the CSRRs and the possibility to control the electrical length and the image impedance of the lines over wide margins with a single cell. To illustrate the potentiality of the approach two CSRR-based power dividers were designed and fabricated. Reduced size by a factor of two is demonstrated, whilst performance is good for narrow band applications.**

***Index Terms*** **— Metamaterials, complementary split rings resonators (CSRRs), left handed lines, power dividers.**

## I. INTRODUCTION

The miniaturization of planar microwave devices has been a subject of interest for many years. For instance, in the field of filters, the semi-lumped element approach has been proposed as an alternative to the distributed (i.e. transmission line based) approach, and high levels of compactness have been demonstrated (see [1] and references therein). Other well known techniques to make microwave devices smaller are based on the reduction of the phase velocity of the propagating signals. This can be achieved by using microwave substrates with high dielectric constant, or by structuring the devices to exhibit the so called slow wave effect, among other possibilities. Indeed, through the last approach, the dispersion diagrams of the guiding media are tailored in order to decrease the phase velocities as much as possible (within certain limits). This can be realized, for example, by periodically loading transmission lines and/or stubs with shunt connected planar capacitances (patch or edge capacitors) [2],[3], or by etching periodic patterns in the ground plane [4]. These artificial periodic structures inhibit signal propagation at certain frequencies (Bragg condition) and, for this reason, they have been termed as electromagnetic bandgaps (EBGs) [5].

However, there is still another possibility to further reduce (as compared to EBGs) the dimensions of planar microwave circuits. The idea is to enhance dispersion in order to make signal wavelengths small at the desired frequencies, and this can be achieved by means of left handed (or backward) transmission lines. Two main approaches have been used for the synthesis of such lines: (i) the dual transmission line concept, where series capacitances and shunt inductances loading the line are the key elements to achieve left-handedness [6]-[8]; and (ii) the resonant-type approach, where split rings resonators (SRRs) or complementary SRRs (CSRRs) have been combined with shunt connected wire (or via) inductances and series capacitances, respectively, to implement one-dimensional left-handed structures [9],[10]. The second approach was introduced by some of the authors of this work, and it was inspired in the first synthesized left handed effective medium, which was implemented by Smith and co-workers at the University of California San Diego (UCSD) [11]. By combining SRRs with shunt connected wires, a one-dimensional artificial medium with negative effective permeability (due to the presence of the SRRs) and permittivity (thanks to the inductance of the wires) was implemented in coplanar waveguide (CPW) technology [9]. In microstrip technology, the required negative values of permeability and permittivity to achieve a backward wave structure were obtained by etching series gaps in the conductor strip, and CSRRs in the ground plane, the latter providing the negative effective permittivity [10].

These artificial transmission lines support backward waves within a limited frequency band, they are highly dispersive and their constitutive *particles* (SRRs or CSRRs) are electrically small. Therefore, they are promising candidates for the design of compact microwave devices in planar technology [12]. In addition, as will be later shown, the image (or Bloch) impedance of these artificial lines strongly varies with frequency within the left handed allowed band, and it can be controlled to some extent through the geometrical parameters. This aspect, combined with the dispersion characteristics, makes the SRR- or CSRR-based transmission lines to be very interesting for the design of compact microwave devices where both the phase and impedance of transmission lines and stubs are target parameters.

In this contribution, artificial microstrip lines loaded with CSRRs and series gaps are used for the design of small size power dividers. Two illustrative examples with different bandwidths will be provided and they will be compared to conventional implementations. The application of these

artificial lines to the design of other microwave devices is under study.

## II. The CSRR transmission line: equivalent circuit model and analysis

The basic cell of the CSRR-based artificial microstrip line and its lumped element equivalent T-circuit model are depicted in Fig. 1 (losses and inter-resonators coupling have been excluded in this model). This equivalent circuit has been already reported [13], but it is reproduced here for coherence and completeness. The model is valid under the assumption that the electrical size of CSRRs is small. CSRRs (etched in the ground plane) are described by parallel resonant tanks (with inductance $L_c$ and capacitance $C_c$), while their coupling to the host line is modelled by the capacitance $C$. The series gaps, which are etched above the CSRRs to enhance line-to-CSRRs coupling, are modelled by the capacitance $C_g$. In [13], the line inductance, $L$, was neglected, since the series impedance was clearly dominated by $C_g$ in the region of interest (i.e. the backward allowed band). This assumption is also considered here in order to simplify the analysis of the equivalent circuit and the synthesis of the devices.

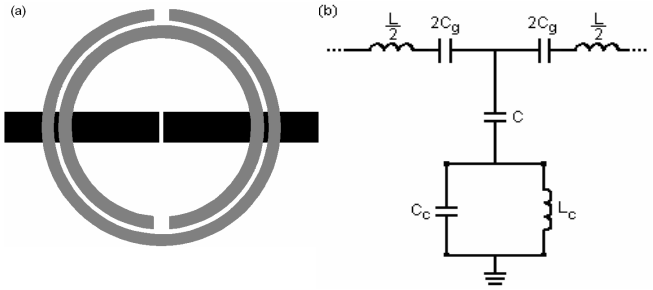


Fig. 1. Basic cell of the CSRR-based transmission line (a) and equivalent circuit model (b). The upper metallization is depicted in black, whereas the slot regions of the ground plane are depicted in grey.

To infer the transmission characteristics of the structure, it is useful to obtain the Bloch (or image) impedance, $Z_B$, and the phase shift, $\phi$, of the elemental cell (dispersion relation). These quantities are given by [14]:

$$Z_B = \sqrt{Z_s(j\omega)[Z_s(j\omega) + 2Z_p(j\omega)]} \quad (1)$$

$$\cos\phi = 1 + \frac{Z_s(j\omega)}{Z_p(j\omega)} \quad (2)$$

respectively. By substituting the series, $Z_s$, and shunt, $Z_p$, impedances of the T-circuit model in (1) and (2), we obtain:

$$Z_B = \sqrt{\frac{L_c/C_c}{\frac{1}{C_c\omega} - L_c\omega}\frac{1}{C_g\omega} - \frac{1}{4C_g^2\omega^2} - \frac{1}{CC_g\omega^2}} \quad (3)$$

$$\cos\phi = 1 + \frac{1/2C_g\omega}{\frac{1}{C\omega} + \frac{L_c/C_c}{L_c\omega - \frac{1}{C_c\omega}}} \quad (4)$$

From the analysis of equations (3) and (4), the limits of the left handed transmission band can be obtained (i.e., signal propagation is allowed in that region where $Z_B$ and $\phi$ are real numbers). Therefore, these limits are given by the frequencies:

$$f_L = \frac{1}{2\pi}\frac{1}{\sqrt{L_c(C_c + \frac{4}{\frac{1}{C_g} + \frac{4}{C}})}} \quad (5)$$

$$f_H = \frac{1}{2\pi\sqrt{L_cC_c}} \quad (6)$$

where the sub-indexes simply make reference to the lower and higher frequency of the interval. At these frequencies, both the phase and Bloch impedance take extreme values, i.e., $Z_B \to \infty$ and $\phi$=0 at $f_H$, whereas $Z_B$=0Ω and $\phi$=π at $f_L$. Thus, we can implement artificial transmission lines based on CSRRs with controllable (positive) phase shift and impedance. As long as these parameters are not too close to the limits, it is potentially possible to synthesize artificial lines with the required electrical characteristics by simply using a single CSRR cell. This is relevant in terms of miniaturization and prospective applications of this idea are pointed out in this work. Specifically, it will be shown that we can design compact (as compared to conventional implementations) power dividers where the typical 90° transmission line sections (impedance inverters) can be substituted by smaller left handed transmission lines (composed of a single CSRR) with identical (although positive) phase shift and characteristic impedance (i.e. related to the port impedance by a factor of √2) .

## III. Synthesis of power dividers by means of CSRR-based transmission lines

As has been indicated, the main aim of this work is to apply the CSRR artificial transmission line concept to the design of compact power dividers in planar technology. These devices are usually implemented by means of transmission lines sections with an electrical length $\beta l$=π/2 [14]. The fundamental topologies are depicted in Fig. 2. In order to match the input port (1), the characteristic impedance of the π/2 lines must be set to $Z_o$=50√2Ω=70.7Ω for the layout shown in Fig. 2(a), and to $Z_o$=50/√2Ω=35.3Ω for the topology depicted in Fig. 2(b) [14]. We have implemented a smaller power divider based on the structure shown in Fig. 2(a), where we have replaced the pair of impedance inverters by single cell CSSR-based left handed lines. The artificial lines must be tailored in order to achieve the required electrical

length (+90°) and impedance (70.7Ω) at the operating frequency. To this end equations (3) and (4) are used. Obviously, this does not univocally determine the element values of the equivalent circuit model (except $C_g$). Nevertheless, in order to enhance bandwidth, $C$ should be as high as possible. This widens the left handed band since $f_L$ is driven towards lower values as $C$ increases (see equations 5). From expression (6), it is obvious that bandwidth is also determined by the elements modeling the CSRRs. In practice, $C$, $C_c$ and $L_c$ cannot take extreme values and this limits the operative bandwidth of the device. However, as will be latter shown acceptable results in terms of bandwidth will be obtained by using narrow substrates.

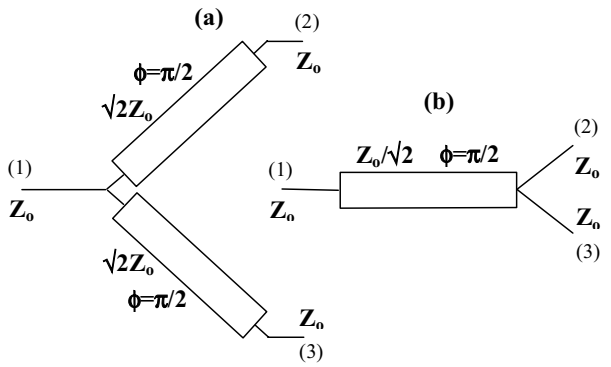


Fig. 2. Fundamental topologies of distributed power dividers implemented in microstrip technology.

We have designed a power divider operative at $f_o$=1.5GHz on a *Rogers RO3010* substrate (dielectric constant $\varepsilon_r$=10.2, thickness $h$=1.27mm). We have set the Bloch impedance and the phase to $Z_B$=70.7Ω and $\phi$=+90° at this frequency, and we have given tentative values to $f_L$ and $f_H$ until the parameters of the equivalent circuit model (obtained through inversion of equations (3)-(6)) have resulted in a realizable layout. This has been obtained after an optimization procedure carried out by means of the *Agilent Momentum* Commercial software, where the target parameters have been the impedance and phase shift at the operating frequency of the device. The final device layout is depicted in Fig. 3 and it is compared to the layout of a conventional implementation on the same substrate with identical operating frequency. The CSRR-based divider is much smaller (approximately a 50% reduction in area has been obtained).

The simulated (through *Agilent Momentum*) and measured (by means of a *Agilent 8720ET* VNA) frequency response of this device is depicted in Fig. 4 (for comparison, the simulated frequency response of the conventional power divider is also shown). As can be appreciated, both devices exhibit comparable transmission between the input and the output ports (i.e. in the vicinity of -3dB) and $S_{11}$ indicates that the input port is well matched. The slight deviation between simulation and measurement is due to the presence of the connectors and to some discrepancy between the actual device dimensions and the nominal values (which is in turn due to fabrication related tolerances). Nevertheless, the electrical characteristics of the fabricated CSRR-based device are good and dimensions are small.

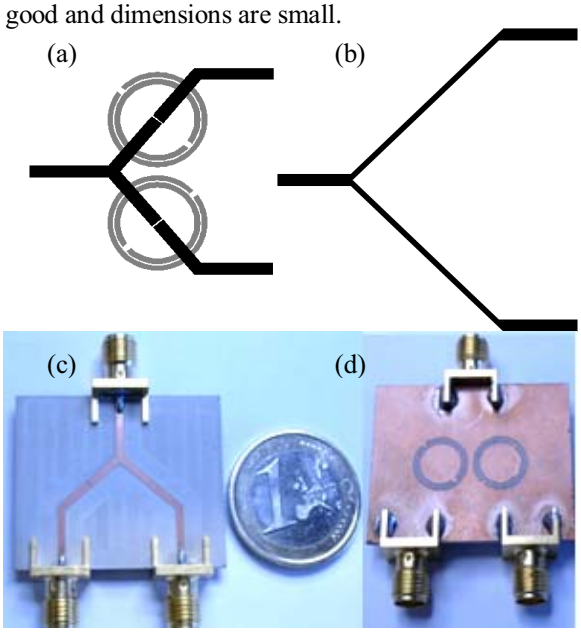


Fig. 3. Topology of the fabricated CSRR-based power divider implemented on the *Rogers RO3010* substrate with thickness $h$=1.27mm (a) and conventional implementation (b). The photographs of the prototype (top and bottom faces) are depicted in (c) and (d). For the CSRR-base device dimensions are as follows: gap separation, $l_g$=0.16mm; width of the host and access lines $w_H$=1.23mm, $w_A$=1.15mm, respectively; internal radius of the CSRRs $r$=3.57mm, distance between concentric rings $d$=0.16mm; and width of the inner and outer rings $c_I$=0.53mm and $c_O$=0.48mm, respectively.

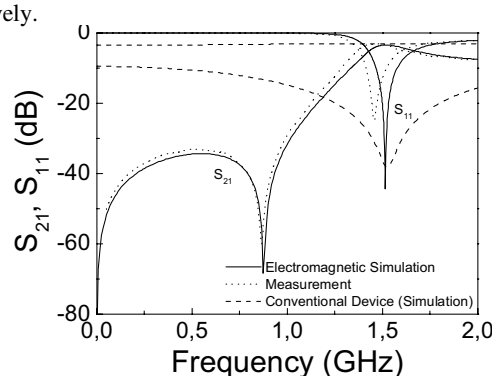


Fig. 4. Simulated and measured frequency responses of the CSRR-based power divider depicted in Fig. 3. It is also included the simulated frequency response of the conventional device.

In order to improve bandwidth, we have implemented another version of the power divider, but this time on a thinner substrate ($h$=0.127μm) with identical dielectric constant. By this means, $C$ can be increased, with the result of an enhanced bandwidth. Device layout of this prototype is shown in Fig. 5, while the frequency response is represented in Fig. 6.

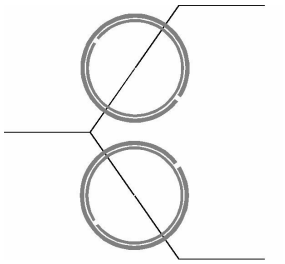

Fig. 5. Layout of the CSRR-based power divider implemented on the *Rogers RO3010* substrate with thickness $h$=0.127mm. Dimensions are: gap separation, $l_g$=0.10mm; width of the host and access lines $w_H$=0.10mm, $w_A$=0.10mm, respectively; internal radius of the CSRRs $r$=4.48mm, distance between concentric rings $d$=0.14mm; and width of the inner and outer rings $c_I$=0.29mm and $c_O$=0.41mm, respectively.

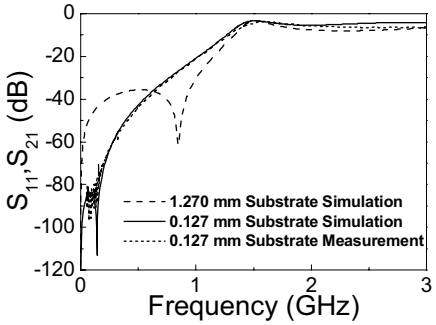


Fig. 6. Simulated and measured frequency response of the prototype shown in Fig. 5, compared to that of the device of Fig. 3.

## VII. Conclusion

In conclusion, it has been shown in this work that left handed microstrip lines implemented by means of CSRRs and series capacitive gaps can be useful for the design of planar microwave devices with small dimensions. Specifically, we have applied the approach to the synthesis of power dividers, where the required impedance inverters have been implemented by means of single cell CSRR-based lines. As compared to conventional implementations, reduction in area by a factor of two has been demonstrated, but further reduction is possible by using advanced fabrication techniques (or technologies) with lower resolution limits. Measured insertion losses between the input and any of the output ports (-3.2dB) have been found to be very close to the ideal values. Bandwidth is smaller than in conventional implementations but it can be enhanced by using narrow substrates. It is believed that these artificial transmission lines can be of interest for the miniaturization of microwave components for moderate or narrow band applications.

Acknowledgement.- This work has been supported by MEC (Spain) by project contract TEC2004-04249-C02-01 METASYSTEMS and by the European Commission (VI Framework Program) through the contract NoE 500252-2 METAMORPHOSE. Thanks also to CIDEM (Generalitat de Catalunya) for funding the Research Center CIMITEC.

## References

[1] J-S. Hong and M.J. Lancaster, *Microstrip filters for RF/microwave applications*, New York (USA), John Wiley & Sons, 2001

[2] A. Görür, C. Karpuz and M. Alkan, "Characteristics of Periodically loaded CPW structures", *IEEE Microwave Guided Wave Lett*., vol. 8, pp. 278-289, August 1998.

[3] F. Martín, F. Falcone, J. Bonache, M.A.G. Laso, T. Lopetegi, M. Sorolla, "New CPW low pass filter based on a slow wave structure", *Microwave and Optical Technology Lett*., vol. 38 pp. 190-193 (2003).

[4] F.R. Yang, K.P. Ma, Y. Qian and T. Itoh, "A uniplanar compact photonic-bandgap structure and its applications for microwave circuits", *IEEE Trans. Microwave Theory Tech*., vol. 47, 1509 (1999).

[5] Y. Yablonovitch, "Photonic bandgap structures", *J. Opt. Soc. Amer. B* vol. 10, pp. 283-295, 1993.

[6] A. K. Iyer and G. V. Eleftheriades. "Negative refractive index metamaterials supporting 2-D waves," in *IEEE-MTT Int'l Symp.,* vol. 2, Seattle, WA, pp. 412– 415, June 2002.

[7] A. A. Oliner. "A periodic-structure negative-refractive-index medium without resonant elements," in *URSI Digest, IEEE-AP-S USNC/URSI National Radio Science Meeting,* San Antonio, TX, pp. 41, June 2002.

[8] C. Caloz and T. Itoh. "Application of the transmission line theory of left-hande (LH) materials to the realization of a microstrip LH transmission line," *in Proc.IEEE-AP-S USNC/URSI National Radio Science Meeting,* vol. 2, San Antonio, TX, pp. 412–415, June 2002.

[9] F. Martín, F. Falcone, J. Bonache, R. Marqués and M. Sorolla, "A new split ring resonator based left handed coplanar waveguide", *Appl. Phys. Lett*., vol. 83, pp. 4652-4654, December 2003.

[10] F. Falcone, T. Lopetegi, M.A.G. Laso, J.D. Baena, J. Bonache, R. Marqués, F. Martín, M. Sorolla, "Babinet principle applied to the design of metasurfaces and metamaterials", *Phys. Rev. Lett*., vol. 93, p 197401, November 2004.

[11] D.R. Smith, W.J. Padilla, D.C. Vier, S.C. Nemat-Nasser and S. Schultz, "Composite medium with simultaneously negative permeability and permittivity", *Phys. Rev. Lett*., vol. 84, pp. 4184-4187, May 2000.

[12] J. Bonache, F. Martín, F. Falcone, J. García, I. Gil, T. Lopetegi, M.A.G. Laso, R. Marqués, F. Medina, M. Sorolla, "Super compact split ring resonators CPW band pass filtres", *IEEE-MTT International Microwave Symposium Digest*, Fort Worth (TX), USA, pp. 1483-1486, June 2004.

[13] J.D. Baena, J. Bonache, F. Martín, R. Marqués, F. Falcone, T. Lopetegi, M.A.G. Laso, J. García, I Gil and M. Sorolla, "Equivalent circuit models for split ring resonators and complementary split rings resonators coupled to planar transmission lines", *IEEE Trans. Microwave Theory and Tech.*, vol. 53, pp. 1451-1461, April 2005.

[14] D.M. Pozar, Microwave Engineering, Addison Wesley, 1990.

# Broadband Resonant-Type Metamaterial Transmission Lines

Marta Gil, Jordi Bonache, *Member, IEEE*, Jordi Selga, Joan García-García, *Member, IEEE*, and Ferran Martín, *Member, IEEE*

***Abstract*—In this letter, it is shown that, contrary to previous assumptions, the broadband characteristics of metamaterial transmission lines are not exclusive of the so called $CL$ loaded composite right/left handed (CRLH) structures. In the balance condition, the typical frequency gap between the left handed (LH) and right handed (RH) transmission bands of these CRLH lines collapses, the characteristic impedance varies smoothly in the vicinity of the transition frequency, and broadband response results. However, through an appropriate design, similar behavior can be obtained in resonant type metamaterial transmission lines, namely transmission lines loaded with complementary split rings resonators. A detailed analysis of the structures, based on the equivalent circuit model is provided, and implications of balancing are pointed out. In this letter, it is clearly demonstrated that broadband balanced CRLH lines can also be implemented by means of the resonant type approach.**

***Index Terms*—Complementary split rings resonators (CSRRs), metamaterials, transmission lines.**

## I. Introduction

TWO different approaches for the synthesis of left handed (LH) transmission lines are known: the dual transmission line concept [1]–[3], and the resonant type approach [4], [5]. The former consists on periodic loading a host transmission line by means of series capacitances and shunt inductances. In that region where these elements are dominant, left handed wave propagation arises. However, at higher frequencies, line parasitics make the structure to exhibit forward (or right handed-RH) wave propagation. This justifies the terminology used to design such structures, i.e., composite right/left handed (CRLH) lines [6]. It has been demonstrated that CRLH lines can be tailored to exhibit a continuous transition between the backward and forward transmission bands. In this case (balanced CRLH line), the allowed band can be very broad, and the characteristic impedance smoothly varies with frequency in the vicinity of the transition frequency.

With regard to resonant type metamaterial transmission lines, these have been alternatively implemented by loading a host transmission line with split rings resonators (SRRs) [4], or with complementary split rings resonators (CSRRs) [5]. In the former case, SRRs provide the negative effective permeability to the line, whereas the required negative permittivity is achieved by the presence of shunt wires [4] or vias [7]. In the latter case, it has been demonstrated from duality that the CSRRs are responsible for the negative effective permittivity, whereas the negative effective permeability can be obtained by etching series gaps in the conductor strip. Until now, only the left handed band of these resonant type metamaterial structures has been exploited [8]. However, forward wave propagation is also present at higher frequencies due to line parasitics. The main aim of this letter is to demonstrate that resonant type metamaterial transmission lines also exhibit a composite behavior, and that they can also be designed to be balanced, with the result of broadband characteristics. Hence, we can designate such lines as CRLH resonant lines. Specifically, we will consider CSRR based lines in this study. From their lumped element equivalent circuit model, the dispersion relation and the characteristic impedance will be derived. A balanced broadband prototype CSRR line will also be provided to illustrate what is claimed in this work.

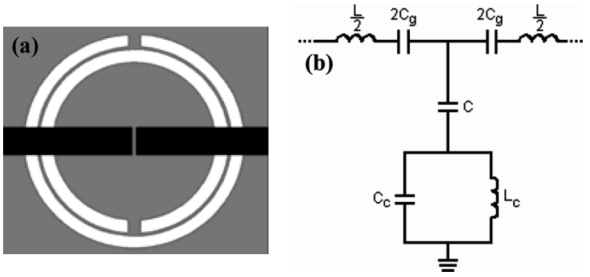


Fig. 1. Topology of the basic cell of the (a) CSRR-based CRLH transmission line and (b) equivalent circuit model. Ground plane metal is depicted in gray whereas upper metal level is depicted in black.

## II. Topology, Circuit Model and Analysis of CRLH CSRR-Based Transmission Lines

The layout corresponding to the basic cell of the CRLH resonant line, as well as its lumped element equivalent circuit model are depicted in Fig. 1 (losses have been excluded). The structure consists on a microstrip line with a series gap etched in the conductor strip and a CSRR printed in the ground plane. The structure is described by means of the circuit model shown in Fig. 1(b), where the CSRRs are modeled by the resonant tank formed by the capacitance $C_c$ and the inductance $L_c$, whereas the gaps are described through the capacitance $C_g$. $L$ is the inductance of the line, whereas $C$ accounts for the line capacitance and the fringing capacitance of the gaps, and it models the electric coupling between the line and the CSRRs. In previous analysis, where we were only interested in the LH band, which was

Manuscript received July 6, 2006; revised October 18, 2006. This work was supported by Spain-MEC under Contract TEC2004-04249-C02-01, by the European Union for funding the Network of Excellence NoE METAMORPHOSE,, by the Catalan Government (CIDEM) for funding CIMITEC, and by MEC under FPU Grant AP2005-4523.

The authors are with the Departament d'Enginyeria Electrónica, Universitat Autónoma de Barcelona, Barcelona 08193, Spain (e-mail: ferran.martin@uab.es).

Color versions of one or more of the figures in this paper are available online at http://ieeexplore.ieee.org.

Digital Object Identifier 10.1109/LMWC.2006.890327

in turn substantially separated from the RH band, the inductance $L$ was ignored [8]. However, this is relevant to explain the RH band, and it is necessary to account for it to properly describe device behavior at high frequencies, or to accurately predict the frequency response in balance or near-balance conditions.

The analysis of the structure can be driven through Bloch theory. The phase shift per cell, $\phi$, and the characteristic impedance, $Z_B$, which are the key parameters for microwave circuit design, are given by [9]

$$\cos\phi = 1 + \frac{Z_s(j\omega)}{Z_p(j\omega)} \tag{1}$$

$$Z_B = \sqrt{Z_s(j\omega)[Z_s(j\omega) + 2Z_p(j\omega)]} \tag{2}$$

where $Z_s$ and $Z_p$ are the series and shunt impedances, respectively, for the circuit of Fig. 1(b). Propagation is allowed in that regions where both $\phi$ and $Z_B$ are real numbers.

Let us now analyze in detail the dispersion diagram and the dependence on frequency of the characteristic impedance. Two different conditions will be considered: 1) the unbalanced case, where the series impedance and shunt admittance are null at different frequencies and 2) the balanced case, where the series and shunt resonance frequencies are identical. In the former case, the frequency gap between the LH and RH bands is delimited by the following frequencies:

$$\omega_{G1} = \min(\omega_s, \omega_p) \tag{3}$$

$$\omega_{G2} = \max(\omega_s, \omega_p) \tag{4}$$

where $\omega_s$ and $\omega_p$ are the series and shunt resonance frequencies, respectively, and the structure is left/right handed below/above that gap (as for the structures reported in [6]). For the balanced case, these frequencies are identical, namely $\omega_s = \omega_p = \omega_o$, and the transition between the left and right handed bands is continuous (i.e., it takes place at the transition frequency, $\omega_o$). The general expression providing the phase shift per cell and the characteristic impedance are given by

$$\cos\phi = \frac{2\omega\left(\omega^2-\omega_p^2\right)+2\omega^3\omega_p^2L_cC+\left(\omega^2-\omega_s^2\right)\left(\omega_p^2-\omega^2\right)LC}{2\left(\omega^2-\omega_p^2\right)+2\omega^2\omega_p^2L_cC} \tag{5}$$

$$Z_B = \sqrt{\frac{L}{C_c}\frac{\left(1-\frac{\omega_s^2}{\omega^2}\right)}{\left(1-\frac{\omega_p^2}{\omega^2}\right)} - \frac{L\omega^2}{4}\left(1-\frac{\omega_s^2}{\omega^2}\right)^2 + \frac{L}{C}\left(1-\frac{\omega_s^2}{\omega^2}\right)} \tag{6}$$

and these expressions are simplified to

$$\cos\phi = \frac{2\omega\left(\omega^2-\omega_o^2\right)+2\omega^3\omega_o^2L_cC-\left(\omega^2-\omega_o^2\right)^2LC}{2\left(\omega^2-\omega_o^2\right)+2\omega^2\omega_o^2L_cC} \tag{7}$$

$$Z_B = \sqrt{\frac{L}{C_c} - \frac{L\omega^2}{4}\left(1-\frac{\omega_o^2}{\omega^2}\right)^2 + \frac{L}{C}\left(1-\frac{\omega_o^2}{\omega^2}\right)} \tag{8}$$

for the balanced case. Contrary to the nonresonant CRLH lines, where for the balanced case the characteristic impedance is a maximum at $f_o$ [10], for those structures described by the circuit of Fig 1(b) the impedance is maximum above the transition frequency. In Fig. 2, the variation of $Z_p, Z_s$, and $Z_B$ with frequency for a transmission line model [Fig. 1(b)] in the balanced case is depicted. Model parameters are indicated in the caption. At $f_o$, both the series and shunt impedances change sign and the LH behavior switches to RH wave propagation.

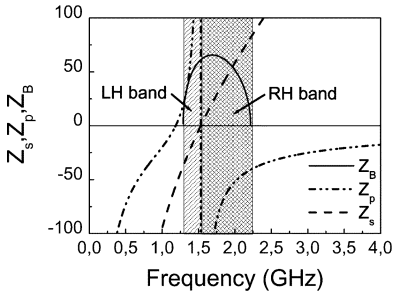


Fig. 2. Representation of the series, $Z_s$, shunt, $Z_p$ and characteristic impedance, $Z_B$, for a CRLH transmission line corresponding to the model of a balanced CSRR-based structure. Electrical parameters are: $L = 45$ nH, $C_g = 0.48$ pF, $C = 10$ pF, $C_c = 3$ pF, $L_c = 3$ pF. The depicted values of $Z_s$ and $Z_p$ are actually the reactances. The transmission frequency has been set to $f_o = 1.5$ GHz.

## III. Discussion

Inspection of Fig. 1(b) reveals that the equivalent circuit model of the CSRR-based CRLH transmission line is identical to that circuit describing the $CL$-based CRLH [9], except for the presence of the coupling capacitance $C$. Indeed, for large values of such capacitance both circuits become indistinguishable. Thus, the narrow band that has been previously attributed to CSRR-based left handed lines is not something intrinsic, but rather due to the difficulty of tailoring the geometry of the lines (CSRR and gap dimensions) to the required values to achieve wide left handed bands. This occurs also in the dual transmission line approach. To obtain wide left handed bands, lumped elements may be used, but to actually synthesize huge bands, the balance condition is forced. However, the balance condition can also be imposed in CSRR-based CRLH transmission lines, as has been demonstrated in Section II. Hence, it is potentially possible to achieve broadband characteristics by using CSRR loaded lines.

## IV. Illustrative Results

In order to demonstrate the achievable broadband characteristics of CSRR-loaded CRLH transmission lines, a one-cell balanced structure has been designed and fabricated. The transition frequency has been set to $f_o = 1$ GHz. To determine CSRR dimensions, the formulas given in [11] have been used. Gap and line dimensions have been estimated from standard formulas [12]. Optimization has been required since the expressions given in [11] are valid under restrictive conditions, not strictly of application in the structures under study. Thus, CSRR dimensions have been scaled until the impedance seen from the ports has been found to be located in the unit resistance circle of the Smith Chart at $f_o$. This is indicative of a null admittance for the parallel branch at $f_o$, as required. On the other hand, to set the series resonant frequency to $f_o$, line length and gap dimensions have been tailored until the reflection coefficient has been found to be $S_{11} = 0$ (center of the Smith Chart). The fabricated device is

Fig. 3. Layout and photograph (top face) of the fabricated device. Dimensions are: line width $W = 0.8$ mm, external radius of the outer ring $r = 7.3$ mm, rings width $c = 0.4$ mm and rings separation $d = 0.2$ mm; the interdigital capacitor, formed by 28 fingers separated 0.16 mm, has been used to achieve the required capacitance value.

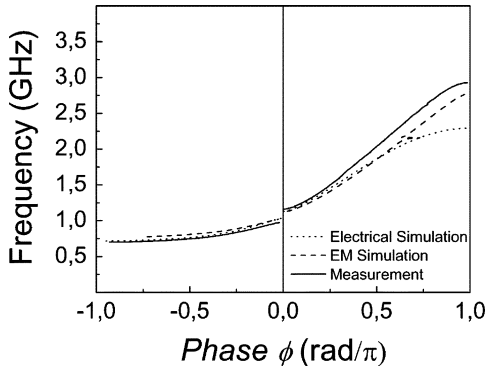


Fig. 4. Dispersion diagram of the fabricated structure.

depicted in Fig. 3 (geometrical parameters are indicated in the caption). The commercial *Rogers RO3010* substrate with dielectric constant $\varepsilon_r = 10.2$ and thickness $h = 1.27$ mm has been used. The dispersion relation has been obtained from measurement and electromagnetic simulation (Fig. 4). To this end, we have obtained the phase of the transmission coefficient, $\phi_{21}$, and from it we have obtained $\phi$ by means of

$$\cos\phi = \frac{\cos\phi_{21}}{|S_{21}|}. \tag{9}$$

The CRLH structure is roughly balanced. The phase shift has been compared to the phase response obtained from the electrical circuit model with extracted parameters (Fig. 4). These parameters have been inferred following a procedure similar to that described in [13]. However, instead of using the impedance of the series branch to univocally determine the five parameters as described in [13], we have used the series resonance frequency, which can be identified from the intercept of $S_{11}$ with the unit conductance circle in the Smith chart. In addition, we have forced the Bloch impedance inferred from electrical and electromagnetic simulation to be 50 $\Omega$ at the same frequency in the RH band. The simulated and measured insertion and return losses are depicted in Fig. 5. As in Fig. 4, good agreement between all the curves has been obtained up to 2 GHz. Above this frequency, the lumped element circuit model depicted in Fig. 1(b) is no longer valid since the basic cell is not electrically small. This explains the disagreement at high frequencies. Nevertheless a broadband frequency response clearly results in the fabricated device. The application to high pass filters by cascading several cells to control rejection in the stop band is foreseen.

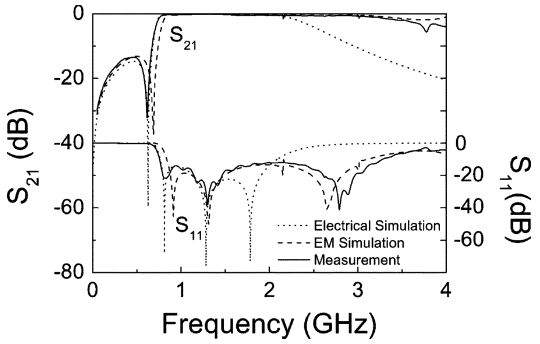


Fig. 5. Measurement (solid line), electromagnetic simulation (dashed line), and electrical simulation (dotted line) of the frequency response corresponding to the fabricated prototype device.

## V. Conclusion

In conclusion, it has been demonstrated that resonant type metamaterial transmission lines based on CSRRs exhibit a CRLH behavior. By designing the structures under the balance condition a broad transmission band results. This has been corroborated experimentally and supported by theory.

## References

[1] A. K. Iyer and G. V. Eleftheriades, "Negative refractive index metamaterials supporting 2-D waves," in *IEEE MTT-S Int. Dig.*., Seattle, WA, Jun. 2002, vol. 2, pp. 412–415.

[2] A. A. Oliner, "A periodic-structure negative-refractive-index medium without resonant elements," in *Proc. IEEE-AP-S USNC/URSI Nat. Rad. Sci. Meeting*, San Antonio, TX, Jun. 2002, pp. 41.

[3] C. Caloz and T. Itoh, "Application of the transmission line theory of left-handed (LH) materials to the realization of a microstrip LH transmission line," in *Proc. IEEE-AP-S USNC/URSI Nat. Rad. Sci. Meeting*, San Antonio, TX, Jun. 2002, vol. 2, pp. 412–415.

[4] F. Martín, F. Falcone, J. Bonache, R. Marqués, and M. Sorolla, "A new split ring resonator based left handed coplanar waveguide," *Appl. Phys. Lett.*, vol. 83, pp. 4652–4654, Dec. 2003.

[5] F. Falcone, T. Lopetegi, M. A. G. Laso, J. D. Baena, J. Bonache, R. Marqués, F. Martín, and M. Sorolla, "Babinet principle applied to the design of metasurfaces and metamaterials," *Phys. Rev. Lett.*, vol. 93, pp. 197401–4, Nov. 2004.

[6] A. Sanada, C. Caloz, and T. Itoh, "Characteristics of the composite rigth/left handed transmisión lines," *IEEE Microw. Wireless Compon. Lett.*, vol. 14, no. 2, pp. 68–70, Feb. 2004.

[7] I. Gil, F. Martín, J. Bonache, and J. García-García, "Tunable metamaterial transmission lines based on varactor loaded split rings resonators," *IEEE Trans. Microw. Theory Tech.*, vol. 54, no. 6, pp. 2665–2674, Jun. 2007.

[8] M. Gil, J. Bonache, I. Gil, J. García-García, and F. Martín, "On the transmission properties of left handed microstrip lines implemented by complementary split rings resonators," *Int. J. Numer. Model.: Electron. Networks, Devices Fields*, vol. 19, pp. 87–103, 2006.

[9] D. M. Pozar, *Microwave Engineering*. Reading, MA: Addison Wesley, 1990.

[10] C. Caloz and T. Itoh, *Electromagnetic Metamaterials: Transmission Line Theory and Microwave Applications*. New York: Wiley, 2005.

[11] J. D. Baena, J. Bonache, F. Martín, R. Marqués, F. Falcone, T. Lopetegi, M. A. G. Laso, J. García, I. Gil, and M. Sorolla, "Equivalent circuit models for split ring resonators and complementary split rings resonators coupled to planar transmission lines," *IEEE Trans. Microw. Theory Tech.*, vol. 53, no. 4, pp. 1451–1461, Apr. 2005.

[12] I. Bahl and P. Bhartia, *Microwave Solid State Circuit Design*. New York: Wiley, 1988.

[13] J. Bonache, M. Gil, I. Gil, J. García-García, and F. Martín, "On the electrical characteristics of complementary metamaterial resonators," *IEEE Microw. Wireless Compon. Lett.*, vol. 16, no. 10, pp. 543–545, Oct. 2007.

# Composite Right/Left-Handed Metamaterial Transmission Lines Based on Complementary Split-Rings Resonators and Their Applications to Very Wideband and Compact Filter Design

Marta Gil, *Student Member, IEEE*, Jordi Bonache, *Member, IEEE*, Joan García-García, *Member, IEEE*, Jesús Martel, *Member, IEEE*, and Ferran Martín, *Member, IEEE*

***Abstract*—In this paper, we discuss in detail the transmission characteristics of composite right/left-handed transmission lines based on complementary split-rings resonators. Specifically, the necessary conditions to obtain a continuous transition between the left- and right-handed bands (balanced case) are pointed out. It is found that very wide bands can be obtained by balancing the line. The application of this technique to the design of very wideband and compact filters is illustrated by means of two examples. One of them is based on the hybrid approach, where a microstrip line is loaded with complementary split-rings resonators, series gaps, and grounded stubs; the other one is a bandpass filter, also based on a balanced line, but in this case, by using only complementary split-rings resonators and series gaps (purely resonant-type approach). As will be seen, very small dimensions and good performance are obtained. The proposed filters are useful for ultra-wideband systems.**

***Index Terms*—Complementary split-rings resonators, metamaterials, microwave filters, transmission lines.**

## I. Introduction

COMPLEMENTARY split-rings resonators were introduced by Falcone *et al.* in 2004 as new resonant particles for the synthesis of metamaterials with negative effective permittivity [1]. It was first demonstrated that by etching these elements in the ground plane of a microstrip line, the structure was able to inhibit signal propagation in the vicinity of their resonance frequency. Later, the first left-handed line based on complementary split-rings resonators was implemented by etching series capacitive gaps in the conductor strip, above the positions occupied by the complementary split-rings resonators [2]. The series gaps were then responsible for the negative effective permeability of the structure. Thus, by combining these elements (gaps and complementary split-rings resonators), a narrow band with simultaneously negative permittivity and permeability appeared in the vicinity of the resonance frequency of the resonators and, hence, a left-handed behavior in that band. In the design of such structures, the main attention was directed to achieve a left-handed behavior in the desired band. However, these structures also exhibit a forward wave (right-handed) behavior at higher frequencies due to the parasitic elements of the host line. Similar behavior was previously demonstrated by Sanada *et al.* [3] by simply loading a host transmission line with series gaps and shunt inductors. This nonresonant structure was called a composite right/left-handed line to clearly point out its composite (left- and right-handed) nature.

The main goal of this paper is to study the left- and right-handed transmission in complementary split-rings resonators loaded metamaterial transmission lines, and to obtain practical implications for the design of wideband and ultra-wideband (UWB) pass filters based on them. Two types of metamaterial transmission lines will be considered, which are: 1) those lines where complementary split-rings resonators are simply combined with series gaps (purely a resonant-type approach [2]) and 2) lines including complementary split-rings resonators, series gaps, and grounded stubs in the unit cell (hybrid approach [4]). As will be shown in Section II, the purely resonant metamaterial transmission line can be modeled by means of a lumped element circuit model, which is very similar to that circuit that describes the composite right/left-handed transmission line implemented by series capacitors and shunt inductors [3]. With regard to the hybrid approach, it provides a further degree of flexibility due to the presence of additional elements (i.e., grounded stubs acting as shunt connected inductors). It will be shown that by balancing the lines, a continuous transition between the left- and right-handed band results, and wide or ultrawide passbands appear. For the hybrid approach, it will be shown that these wide bands can be allocated either below or above the typical transmission zero, intrinsic to the presence of complementary split-rings resonators.

In section III, two prototype device examples are given. One is a three-stage purely resonant balanced structure, which ex-

Manuscript received September 29, 2006; revised February 20, 2007. This work was supported by Spain–Ministerio de Educación y Ciencia under Project Contract TEC2004-04249-C02-01, by the Seiko Epson Corporation, by the European Union under the Network of Excellence METAMORPHOSE, and by the Catalan Government under the Centre d'Investigació en Metamaterials per a la Innovació en Tecnologia Electrònica i de Comunicacions. The work of M. Gil was supported by the Ministerio de Educación y Ciencia under Formación de Profesorado Universitario Grant AP2005-4523.

M. Gil, J. Bonache, J. García-García, and F. Martín are with the Grup d'Enginyeria de Microones i Milimètriques Aplicat/Centre d'Investigació en Metamaterials per a la Innovació en Tecnologia Electrònica i de Comunicacions, Departament d'Enginyeria Electrònica, Escola Tècnica Superior d'Enginyeria, Universitat Autònoma de Barcelona, 08193 Bellaterra (Barcelona), Spain (e-mail: Marta.gil.barba@uab.es; jordi.bonache@uab.es; joan.garcia@uab.es; Ferran.martin@uab.es).

J. Martel is with the Grupo de Microondas, Departamento de Física Aplicada 2, Escuela Técnica Superior de Arquitectura. Universidad de Sevilla, 41012 Seville, Spain (e-mail: martel@us.es).

Digital Object Identifier 10.1109/TMTT.2007.897755

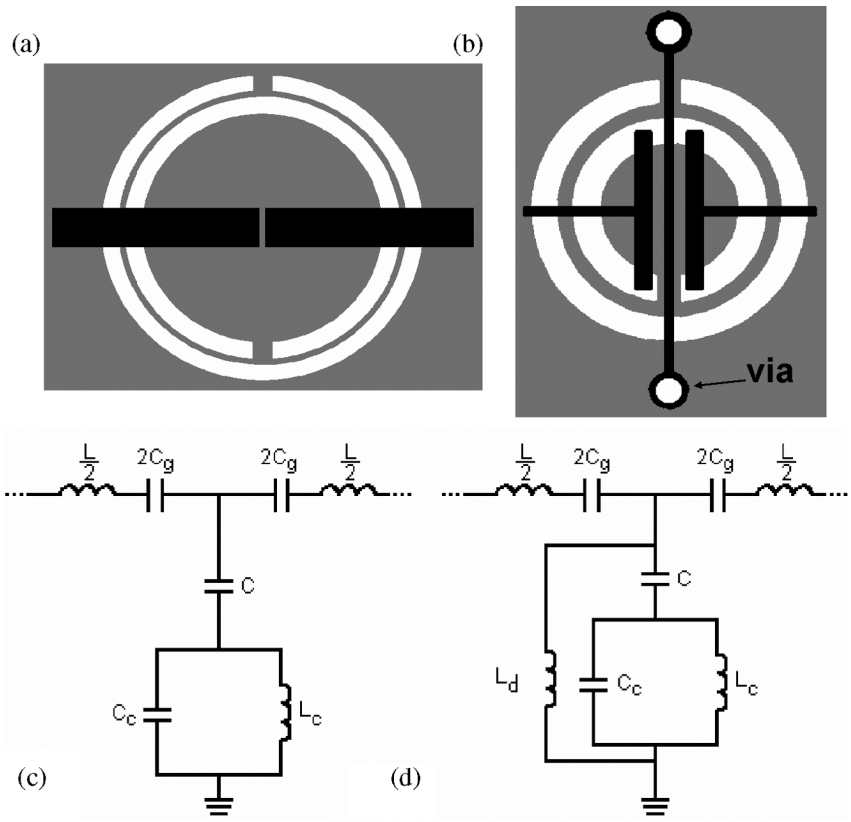


Fig. 1. Topologies of the: (a) resonant-type and (b) hybrid left-handed cells and equivalent circuits (c) and (d). Ground plane metal is depicted in gray, whereas the upper metal level is depicted in black. In the topology of (b), two series gaps are included and shunt stubs are grounded through metallic vias.

hibits a wide transmission band. This structure is very useful as a high-pass structure (though transmission is limited at high frequencies). The second one is a bandpass filter, which was presented in [5], and is based on the hybrid approach. Details on the design procedures are given here for the first time. As will be seen, to describe the behavior of such a structure, it is necessary to include in the lumped element circuit model the necessary elements to account for the second resonance of complementary split-rings resonators. It is the first time that the first and second resonance of a complementary split-rings resonator are used in a circuit.

The main conclusions of this study are highlighted in Section IV. It is clear that composite right/left-handed transmission lines based on complementary split-rings resonators are of actual interest for the synthesis of microwave filters with wide bands or UWBs. The small dimensions of the unit cells make this approach very attractive for the fabrication of low-cost and miniature modules where such filters are necessary.

## II. Topology, Circuit Model, and Analysis of Composite Right/Left-Handed Complementary Split-Rings Resonator-Based Transmission Lines

The layouts of the purely resonant and hybrid left-handed cells, as well as their corresponding lumped-element equivalent-circuit models are depicted in Fig. 1. The purely resonant unit cell consists of a microstrip line with a series gap etched in the strip and a complementary split-rings resonator printed in the ground plane. The structure is described by the circuit model shown in Fig. 1(c), where the complementary split-rings resonators are modeled by means of the resonant tank formed by the capacitance $C_c$ and the inductance $L_c$, whereas the gaps are described by means of the capacitance $C_g$. $L$ is the inductance of the line, whereas $C$ models the electric coupling between the line and complementary split-rings resonators. The topology corresponding to the hybrid line [see Fig. 1(b)] is analogous to that of Fig. 1(a), but with the addition of two shunt stubs. These elements are described through a shunt connected inductance $L_d$, as can be appreciated in the model of Fig. 1(d). These circuit models are indeed simplified versions of the more general circuit model reported in [6]. In the model reported in [6], inter-resonator's coupling and the effects of the line capacitance corresponding to that portion of the host line outside the influence of the rings are also considered. However, as was discussed in [6], coupling between neighboring complementary split-rings resonators can be neglected if circular geometries are used (as is the case in this study), and the effects of the line capacitance can also be neglected, unless the complementary split-rings resonators are substantially separated. According to these comments, the circuit models depicted in Fig. 1 are justified (these models and the layouts have been previously reported [4], but they are reproduced here for completeness of this paper).

An inspection of these circuit models reveals that there are regions where the series reactance and shunt susceptance are

both negative (left-handed regions), zones where they are both positive (right-handed bands), and intervals where they have opposite signs (forbidden bands). These topologies and the corresponding circuit models have been previously used by the authors [2], [4], [7], but not for the synthesis of bandpass filters with wide bands based on the composite behavior of the lines and balanced designs.

Let us now analyze in detail the transmission characteristics of these composite right/left-handed transmission lines on the basis of their equivalent-circuit models. This analysis can be carried out through the Bloch theory. The phase shift per cell $\phi = \beta l$ and the characteristic impedance $Z_B$, which are the key parameters for microwave circuit design, are given by [8]

$$\cos \beta l = 1 + \frac{Z_s(j\omega)}{Z_p(j\omega)} \tag{1}$$

$$Z_B = \sqrt{Z_s(j\omega)\left[Z_s(j\omega) + 2Z_p(j\omega)\right]} \tag{2}$$

where $Z_s$ and $Z_p$ are the series and shunt impedances, respectively, for the circuits of Fig. 1. Propagation is allowed in that regions where both $\phi$ and $Z_B$ are real numbers. The cells can be designed to be either unbalanced or balanced [9]. In the first case, the series impedance and shunt admittance are null at different frequencies. Conversely, the series and shunt resonance frequencies are identical for balanced designs. Thus, for unbalanced structures, a frequency gap appears between the following frequencies:

$$\omega_{G1} = \min(\omega_s, \omega_p) \tag{3}$$

$$\omega_{G2} = \max(\omega_s, \omega_p) \tag{4}$$

where $\omega_s$ and $\omega_p$ are the series and shunt resonance frequencies, respectively, and the structure is left/right-handed below/above that gap. For the balanced case, these frequencies are identical, namely, $\omega_s = \omega_p = \omega_o$, and the transition between the left- and right-handed band is continuous (i.e., it takes place at the transition frequency $\omega_o$).

For the purely resonant complementary split-rings resonator-loaded line, the general expression providing the phase shift per cell and the characteristic impedance are given by

$$\cos\phi = \frac{2\left(\omega^2-\omega_p^2\right)+2\omega^2\omega_p^2L_cC+\left(\omega^2-\omega_s^2\right)\left(\omega_p^2-\omega^2\right)LC}{2\left(\omega^2-\omega_p^2\right)+2\omega^2\omega_p^2L_cC} \tag{5}$$

$$Z_B = \sqrt{\frac{L}{C_c}\frac{\left(1-\dfrac{\omega_s^2}{\omega^2}\right)}{\left(1-\dfrac{\omega_p^2}{\omega^2}\right)} - \frac{L^2\omega^2}{4}\left(1-\frac{\omega_s^2}{\omega^2}\right)^2 + \frac{L}{C}\left(1-\frac{\omega_s^2}{\omega^2}\right)} \tag{6}$$

and these expressions are simplified to

$$\cos\phi = \frac{2\left(\omega^2-\omega_o^2\right)+2\omega^2\omega_o^2L_cC-\left(\omega^2-\omega_o^2\right)^2LC}{2\left(\omega^2-\omega_o^2\right)+2\omega^2\omega_o^2L_cC} \tag{7}$$

$$Z_B = \sqrt{\frac{L}{C_c} - \frac{L^2\omega^2}{4}\left(1-\frac{\omega_o^2}{\omega^2}\right)^2 + \frac{L}{C}\left(1-\frac{\omega_o^2}{\omega^2}\right)} \tag{8}$$

for the balanced case, where $\omega_o = (LC_g)^{-1/2}$. Thus, for the balanced design, signal transmission changes from left- to right-handed at $\omega_o$, whereas the lower limit of the left-handed region and the upper limit of the right-handed band are obtained by forcing (8) to be zero (the calculation is tedious and, hence, it is not reproduced here).

As occurs in balanced lines implemented through nonresonant elements, the group velocity is finite at $\omega_o$ (although the phase constant $\beta$ is null at that frequency). The characteristic impedance is null at the extremes of the propagation band and it varies smoothly in the vicinity of the transition frequency. However, for the cells described by the circuit of Fig. 1(c), $Z_B$ is maximized above $\omega_o$. This does not represent any limitation of these complementary split-rings resonator based lines, as compared to those implemented through nonresonant elements. Diagrams corresponding to the dispersion relation and Bloch impedance for the balanced case in purely resonant composite right/left-handed transmission lines are thus similar to those of composite right/left-handed lines based on nonresonant elements [9]. However, a transmission zero located near the lower edge of the transmission band and given by

$$f_z = \frac{1}{2\pi\sqrt{(C+C_c)L_c}} \tag{9}$$

is present in purely resonant metamaterial transmission lines (this transmission zero is at the origin for nonresonant composite right/left-handed lines).

Let us now consider the hybrid cell, described by the circuit model of Fig 1(d). In this case, the analysis is more complicated due to the presence of the inductance $L_d$. Specifically, there are three relevant frequencies relative to the shunt impedance: namely, two frequencies that null the corresponding admittance, and a transmission zero frequency in between [also given by (9)]. Let us now consider the balanced case, which is of particular interest to achieve broadband structures. Since there are two shunt resonances, there are actually two alternatives to achieve the balanced condition: that where the series resonance is identical to the lower resonance frequency $(\omega_{pL})$ of the shunt impedance, and that case where the higher resonance of the shunt impedance $(\omega_{pH})$ coincides with the series resonance. Rather than obtaining the analytical expressions for the dispersion relation and characteristic impedance, it is more useful to illustrate the two balance solutions mentioned by means of a representation of the characteristic impedance and dispersion diagram (see Fig. 2). For both alternatives, the characteristic impedance and phase constant in the vicinity of the transition frequency exhibit similar behavior to that of the purely resonant-type approach. However, there is an additional allowed band. In the former case $(\omega_s = \omega_{pL})$, it appears above the transition frequency, and this band exhibits forward wave propagation. Conversely, for $\omega_s = \omega_{pH}$, this additional allowed band is left-handed and it is located below the transition frequency. Nevertheless, these bands are typically very narrow and they are not useful in practical applications. The transmission zeros are more valuable since they can be used to suppress undesired harmonics that may appear as consequence of parasitic resonances [7], or to enhance frequency selectivity at the lower edge of the transmission band.

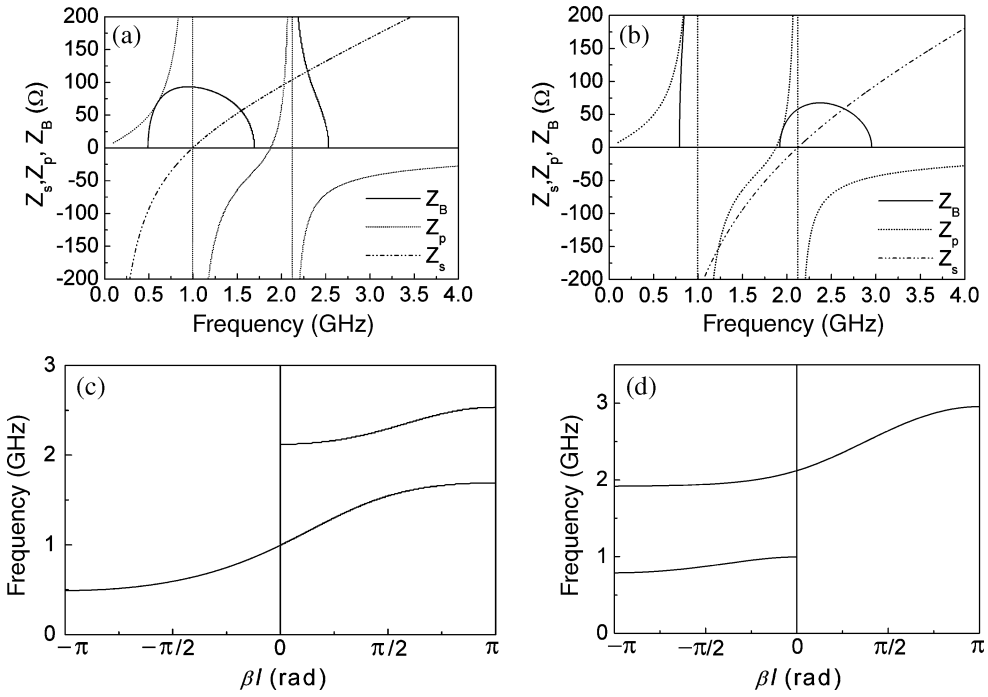


Fig. 2. Representation of the series, shunt, and characteristic impedance for the hybrid composite right/left-handed line model for the two situations described in the text. (a) Balanced case with the series resonance identical to the lower resonance frequency of the shunt impedance; electrical parameters are: $L = 20$ nH, $C_g = 1.28$ pF, $C = 2$ pF, $C_c = 10$ pF, $L_c = 0.6$ nH, and $L_d = 12$ nH. (b) Balanced case with the series resonance identical to the higher resonance frequency of the shunt impedance electrical parameters are: $L = 20$ nH, $C_g = 0.28$ pF, $C = 2$ pF, $C_c = 10$ pF, $L_c = 0.6$ nH, and $L_d = 12$ nH. (c) and (d) depict the dispersion diagrams corresponding to the cases considered in (a) and (b), respectively. In (a) and (b), only the real part of $Z_B$ is depicted. For $Z_s$ and $Z_p$, only the absolute value has been represented (these impedances are purely reactive).

In Section III, these structures are applied to the design of wideband microwave filters. Actually, the presented models [see Figs. 1(c) and (d)] are able to explain device behavior up to a limited frequency. At the upper limit of the composite right/left-handed transmission band, either the lumped-element approximation fails, or it is necessary to include additional elements to the models in order to account for the second resonance frequency of the complementary split-rings resonators. This latter aspect will be discussed in Section III since it is fundamental to explain the characteristics of one of the presented filters.

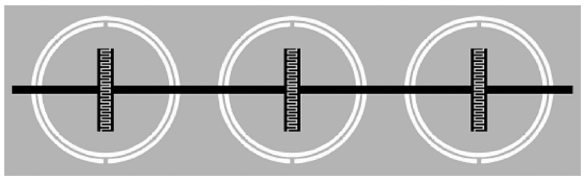

Fig. 3. Layout of the filter formed by three balanced purely resonant cells. The metallic parts are depicted in black in the top layer, and in gray in the bottom layer. The rings are etched on the bottom layer. Dimensions are: total length $l = 55$ mm, linewidth $W = 0.8$ mm, external radius of the outer rings $r = 7.3$ mm, ring width $c = 0.4$ mm and ring separation $d = 0.2$ mm; the interdigital capacitors are formed by 28 fingers separated 0.16 mm.

## III. Design Examples

To illustrate the potentiality of balanced composite right/left-handed lines loaded with complementary split-rings resonators to the design of wideband filters, two prototype device examples are provided. The first one is a three-stage bandpass filter based on the purely resonant-type approach. The layout of the filter is depicted in Fig. 3. The structure is roughly balanced (contrary to previous bandpass filters based on similar topologies [4]), as revealed by the dispersion diagram depicted in Fig. 4, which has been inferred from the simulated (through Agilent Momentum) and measured $S$-parameters of a single cell. This figure points out a wide band for signal transmission. To achieve the quasi-balance condition, optimization has been required; namely, the interdigital capacitors are tuned until the series resonance (given by $L$ and $C_g$) coincides with the shunt resonance ($L_c - C_c$ tank) to a good approximation. Under perfect balance, the input port is matched and, hence, $S_{11}$ is located in the center of the Smith chart. In practice, perfect balance (or perfect matching) is not actually achieved and we adopt that solution where $S_{11}$ reaches the closest position to the center of the Smith chart at $\omega_o$ (possible reasons for this imperfect balance will be discussed later in reference to the next example).

The design of the filter to satisfy any given specifications can be done with the help of the electrical circuit model of the unit cell and the parameter-extraction method published in [10]. Nevertheless, this has not been the case and we simply have designed a balanced line to demonstrate the possibilities of the approach. We have simulated the frequency response of two-, three-, and four-stage structures, and we have fabricated the device with three complementary split-rings resonators (the Rogers RO3010 substrate has been used with thickness $h = 1.27$ mm and dielectric constant $\varepsilon_r = 10.2$) in order to obtain measured data for one case. These results are depicted in Fig. 5. The structure exhibits high-frequency selectivity at the

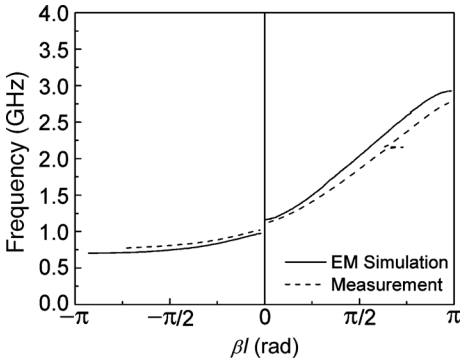


Fig. 4. Dispersion diagram for the structure of Fig. 3.

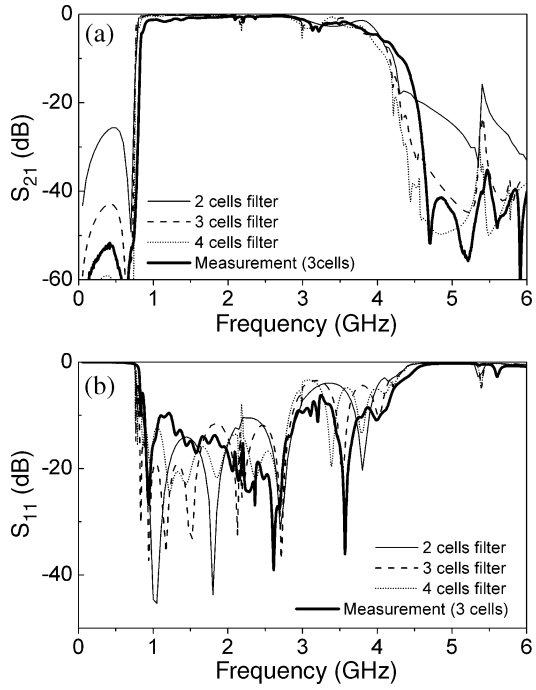


Fig. 5. Simulated: (a) insertion and (b) return losses of the three filters composed of two-, three-, and four-stages identical to those of Fig. 3. The measured frequency response of the fabricated prototype (Fig. 3) is also depicted.

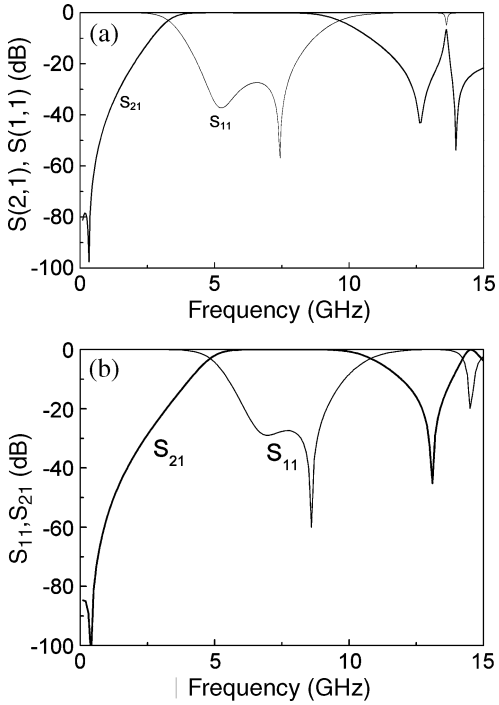


Fig. 6. (a) Simulated reflection and transmission coefficient of a single balanced cell corresponding to the filter shown in Fig. 10. (b) Phase of $S_{21}$. Backward wave propagation corresponds to positive values of phase in (b). Hence, the left-handed band is extended from 3.3 up to 5.5 GHz.

lower band edge and controllable rejection below the cutoff frequency. The lower limit of the passband can be accurately controlled since the electrical model perfectly describes the frequency response up to regions well beyond the transition frequency. However, in general, the model does not properly fit the measured or simulated (full-wave electromagnetic) device responses in the vicinity of the upper band edge, as has been previously discussed relative to unbalanced structures [11] (the limitation is related to the fact that the lumped-element model is valid only in a limited frequency interval). Thus, though the device is by nature a bandpass structure, it must be actually considered as a high-pass filter, useful to eliminate interfering signals present below the lower limit of the band (conventional microwave high-pass filters do also exhibit rejection at high frequencies).

The second example is a bandpass filter, which was presented in [5], and subjected to the following specifications: active area below 1 $cm^2$, bandwidth covering the 4–6-GHz range or wider, at least 80-dB rejection at 2 GHz, in-band ripple lower than 1 dB, and group-delay variation smaller than 1 ns. This device has been designed by means of the hybrid approach [see Fig. 1(b)], which has been demonstrated to offer small size solutions in moderate or narrow bandpass filters [4], [7]. In this case, the substrate is the Rogers RO3010 ($\varepsilon_r = 10.2$) with thickness $h = 0.127$ mm to achieve the required rejection at 2 GHz (as is explained in [5]). For the design of the unit cell, we have chosen the hybrid complementary split-rings resonator loaded line with the series resonance frequency as close as possible to the higher resonance of the shunt impedance $(\omega_s = \omega_{pH})$. This gives a transmission zero below the passband of interest, which is useful to obtain high rejection, as required, in the vicinity of 2 GHz. Although below that transmission zero there is a left-handed passband present (see Fig. 2), it is very narrow for the designed structures and its effects are irrelevant (as will be seen).

To achieve the required specifications, the purpose is to design a balanced unit cell exhibiting a flat response covering the required bandwidth. From simulation, the required number of stages to achieve 80-dB rejection level at 2 GHz can be determined. With the help of the equivalent-circuit model of Fig. 1(d), we have designed a balanced unit cell satisfying the previous requirement. The simulated frequency response of this unit cell is depicted in Fig. 6. From the phase response, it is clearly seen that backward wave transmission is switched to forward wave transmission within the band. Above the passband of interest, which extends approximately from 3 to 10 GHz, there is an additional transmission zero (between 12 GHz–13 Hz), which is not explained by means of the equivalent-circuit model [see Fig. 1(d)] for the situation that we

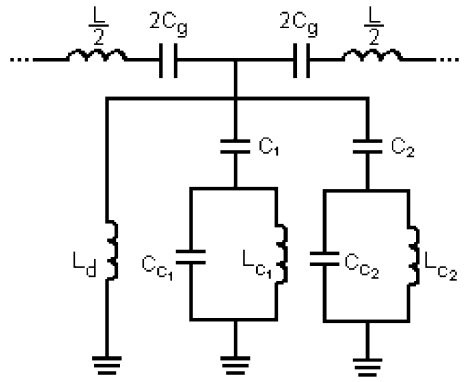


Fig. 7. Equivalent-circuit model of the unit cell of the considered filter (Fig. 10) that includes the effects of the second resonance frequency of the complementary split-rings resonators. For coherence, we have added a sub-index that indicates the resonance order that each shunt branch models.

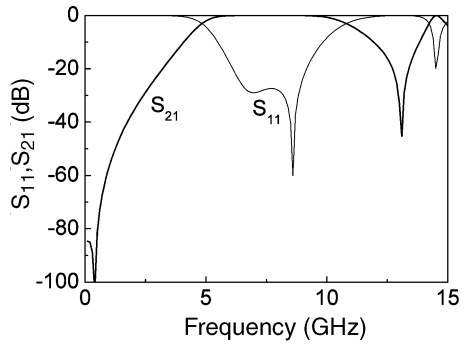


Fig. 8. Electrical simulation of the circuit of Fig. 7. Parameters are: $L = 2.6$ nH, $C_g = 0.2$ pF, $L_d = 5.4$ nH, $C_1 = 305$ pF, $C_{C1} = 0.65$ pF, $L_{C1} = 0.55$ nH, $C_2 = 0.21$ pF, $C_{C2} = 0.32$ pF, and $L_{C2} = 0.27$ nH.

are considering ($\omega_s = \omega_{pH}$). In addition, a transmission peak is also present at 13.7 GHz. This behavior can be explained by considering the effects of the second resonance frequency of the complementary split-rings resonators. Namely, these particles exhibit several resonance frequencies [12], [13]. The first one, the quasi-static resonance, is the resonance of interest for most of the applications of complementary split-rings-resonator-based circuits. However, at higher frequencies, there are additional resonance frequencies (dynamic), which may play a role under certain circumstances. This is the case in the current design. Namely, if we add to the circuit of Fig. 1(d), an additional parallel branch to account for the second resonance of the complementary split-rings resonator, the transmission zero, as well as the transmission peak above it, are perfectly explained. The equivalent circuit that includes the effects of the second resonance is depicted in Fig. 7. The parameters of the new parallel branch have been adjusted to obtain the behavior observed in Fig. 6. From the electrical simulation of this circuit model (obtained by means of Agilent ADS), we obtain a frequency response (see Fig. 8), which is qualitatively very similar to that depicted in Fig. 6. It is interesting to mention that the coupling capacitance of this new branch, i.e., $C_{c2}$, is very small. This is consistent with the fact that electric coupling is very weak at the second resonance of complementary split-rings resonators [12], [13]. We would like to clarify that optimization of the filter unit cell has been done directly from layout due to the difficulty of handling with such a large number of parameters. Rather than obtaining an accurate description of the frequency response of the filter unit cell through the circuit model, our intention has been to justify the presence of the second resonance of the complementary split-rings resonators, which plays a fundamental role in order to obtain a sharp cutoff above the passband of interest, and this is clear from the qualitative comparison of Figs. 6 and 8. The position of the two transmission zeros can be controlled with the dimensions of the complementary split-rings resonators and gaps. From the circuit model of Fig. 7, both transmission zeros are given by (9) by replacing $C$, $L_c$, and $C_c$ by the corresponding reactive elements ($C_1$, $Lc_1$, and $C_{c1}$ for the lower transmission zero and $C_2$, $L_{c2}$, and $C_{c2}$ for the upper transmission zero). Obviously, the small frequency value of the first transmission zero can be only explained by a large coupling capacitance $C_1$, which has been estimated to be in the vicinity of 300 pF (see caption of Fig. 7). This capacitance is much larger than the coupling capacitance corresponding to the second resonance, as expected since the electric excitation of the second resonance is very weak. However, the large value of $C_1$ is not intuitive and we have verified it from the analysis of the gap pair alone (i.e., by excluding the complementary split-rings resonator and removing the vias). From the simulated $S$-parameters of this structure, we have inferred the capacitance values of the well-known $\pi$-model of the gap, and through $\pi$-T transformation, the capacitances of the T-model have been inferred. These capacitances are in qualitative agreement with the capacitor values of $C_g$ and $C_1$, given in the caption of Fig. 8 (perfect agreement is not expected due to the effects of the complementary split-rings resonators and vias). Hence, the element values of the circuit model given in the caption of Fig. 8 are reasonable, including the large value of the capacitance $C_1$.

The return loss of the structure (Fig. 6) exhibits two reflection zeros. To explain the origin of such reflection zeros, the characteristic impedance of the structure (inferred from the simulated $S$-parameters according to standard formulas [8]) has been obtained (Fig. 9). According to this illustration, the reflection zero located at 7.5 GHz is due to impedance matching (the characteristic impedance is 50 $\Omega$ at that frequency). Two additional reflection zeros would be expected: one of them at that frequency where the impedance again takes the value of 50 $\Omega$; the other one at the transition frequency (phase matching). Since these frequencies do almost coincide, the two reflection zeros merge. Actually this second reflection zero is obscured by the fact that the device is not exactly balanced, as Fig. 9 reveals. Nevertheless, the effect of this imperfect balance is not appreciable in the frequency response of the structure, which is flat in the region of interest. We would like to clarify that the imperfect balance is not related to an improper design. The balance condition is achieved when the series resonance coincides with the shunt resonance identified as $\omega_{pH}$. This resonance roughly coincides with the first (quasi-static) resonance of the complementary split-rings resonator (given by the tank $L_{c1} - C_{c1}$). However, this quasi-static resonance can also be excited magnetically, as was discussed in [12], through the component of the magnetic field contained in the plane of the particle. This magnetic coupling is weak, but it may suffice to prevent "perfect"

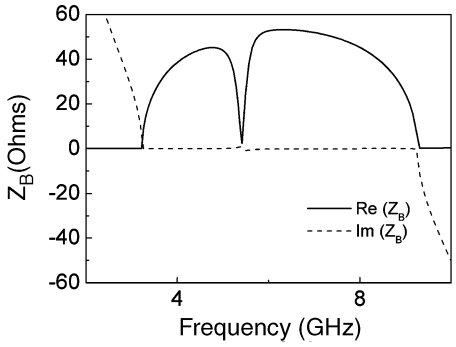


Fig. 9. Characteristic impedance inferred from electromagnetic simulation of the unit cell of the filter depicted in Fig. 10.

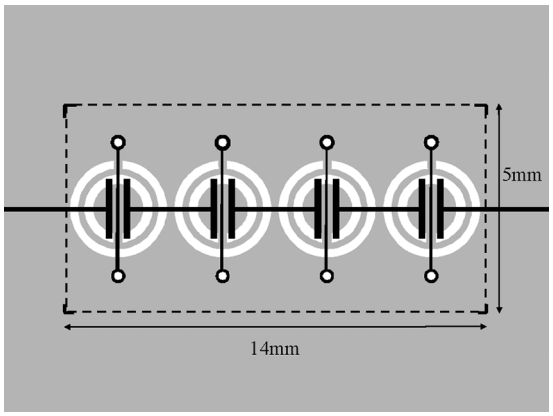


Fig. 10. Layout of the fabricated filter, formed by cascading four balanced hybrid cells. The metallic parts are depicted in black in the top layer, and in gray in the bottom layer. The rings are etched on the bottom layer. The dashed rectangle has an area of 1 cm$^2$. Dimensions are: linewidth $W = 0.126$ mm, external radius of the outer rings $r = 1.68$ mm, rings width $c = 0.32$ mm and rings separation $d = 0.19$ mm; inductor width is 0.10 mm and the distance between the metals forming the gap is 0.4 mm. From [5].

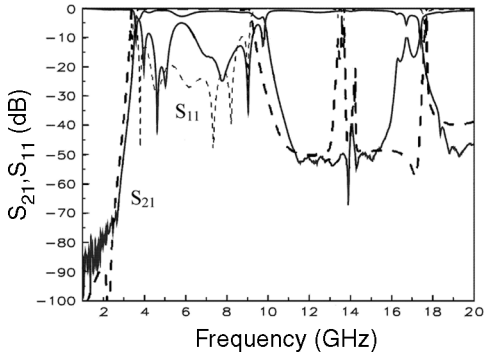


Fig. 11. Simulated (dashed line) and measured (solid line) frequency response of the fabricated filter depicted in Fig. 10. Measured in-band losses are better than 3 dB in the transmission band. From [5].

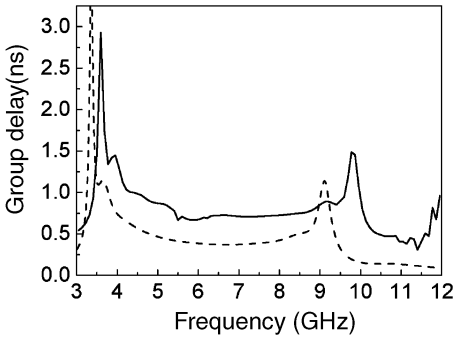


Fig. 12. Simulated (dashed line) and measured (solid line) group delay of the filter of Fig. 10.

balance since its effect is to open the series branch just at the transition frequency [14]. This may explain the behavior of the characteristic impedance in the vicinity of 5.5 GHz. The fact that perfect balance has not been achieved in spite of the fine tuning of the series elements support this argument. Nevertheless, this aspect requires further study, which is out of the scope of this paper.

The fabricated filter is depicted in Fig. 10. Four stages have been enough to achieve the required rejection at 2 GHz. Fig. 11 illustrates the simulated (through Agilent Momentum) and measured (by means of the Agilent 8720ET Vector network analyzer) frequency response of the filter. Finally, Fig. 12 depicts the simulated and measured group delay. Reasonable agreement between simulation and experiment has been achieved. The size ($A = 0.7$ cm$^2$), as well as the measured results indicate that specifications are satisfied, with the exception of ripple, which is slightly higher than 1 dB. This excess of ripple is attributed to fabrication related tolerances. Nevertheless, the combination of size and performance for this periodic filter is a relevant aspect to highlight. A very wide measured bandwidth (3.5–10 GHz) has been achieved with high selectivity at both band edges, and the first spurious located at 17 GHz (measurement). This has been achieved by means of a planar implementation with an area clearly below 1 cm$^2$. Group-delay variation is also very small in the allowed band (<1 ns). A similar filter has been reported in [15] by loading a composite right/left-handed line with capacitively coupled resonators. The equivalent circuit of the unit cell is similar to the circuit of Fig. 7. The main difference is the presence of the inductive element $L_d$, which is absent in the structure of [15] and the two coupling capacitances, $C_1$ and $C_2$, responsible for the presence of two transmission zeros (only one coupling capacitance is present in the structure reported in [15]). The performance of the filters is similar, though dimensions are clearly smaller in our design.

The effect of the complementary split-rings resonator in the filter of Fig. 10 can be easily evaluated by means of full wave electromagnetic simulations (not shown in this paper). If the complimentary split-rings resonators are removed from the structure, the frequency response dramatically changes (both the passband and transmission zeroes disappear). This fact demonstrates that the shunt susceptance of the unit cells is strongly affected by the presence of the complimentary split-rings resonators. In other words, though the series gaps and shunt stubs do produce a composite right/left-handed behavior by themselves, complimentary split-rings resonators are clearly needed to achieve the required performance.

In the opinion of the authors, these UWB metamaterial filters based on balanced cells, including both the purely resonant and hybrid models, are of interest in practical applications since

they seem to be competitive in terms of dimensions and performance. Other UWB pass filters based on other approaches, recently proposed, can be found in [16]–[19].

## IV. Conclusion

In conclusion, it has been demonstrated that resonant type metamaterial transmission lines based on complementary split-rings resonators exhibit a composite right/left-handed behavior that is useful for the synthesis of compact size and high-performance planar filters in terms of bandwidth. Two models have been analyzed, which are 1) the purely resonant approach, where complementary split-rings resonators are simply combined with series gaps and 2) the hybrid model, where grounded stubs are added to the previous model. The key point to achieve wideband or UWB is the design of balanced cells, where the transition between the left- and the right-handed band is continuous.

Two prototype device examples have been reported in order to illustrate the design procedure and the achievable results by means of the two mentioned models. It has been found that rejection and cutoff at the lower edge of the band are perfectly controllable for the purely resonant metamaterial filters, whereas at high frequencies, the cutoff is not easily controllable due to the limitations of the electric model to properly describe device behavior at high frequencies. Nevertheless, a fractional bandwidth higher than 100% has been measured in the fabricated prototype. These filters are useful to eliminate interfering signals present below the frequency region of interest. For the metamaterial filter based on the hybrid approach, we have roughly obtained the required specifications and size. In this case, device behavior has been explained also including the frequency response above the passband of interest. To this end, it has been necessary to include in the electric model of the unit cell the effects of the second resonance frequency of the complementary split-rings resonators. This is the first time that the second resonance of complementary split-rings resonators is used in the design of a filter (a symmetric frequency response for the final filter has been obtained). To our knowledge, the combination of dimensions and performance for the filter based on the hybrid cell is unique. These results demonstrate the potentiality of metamaterial based filters in applications requiring wide band and UWBs.

## References


[1] F. Falcone, T. Lopetegi, J. D. Baena, R. Marqués, F. Martín, and M. Sorolla, "Effective negative- $\varepsilon$ stop-band microstrip lines based on complementary split ring resonators," *IEEE Microw. Wireless Compon. Lett.*, vol. 14, no. 6, pp. 280–282, Jun. 2004.

[2] F. Falcone, T. Lopetegi, M. A. G. Laso, J. D. Baena, J. Bonache, R. Marqués, F. Martín, and M. Sorolla, "Babinet principle applied to the design of metasurfaces and metamaterials," *Phys. Rev. Lett.*, vol. 93, Nov. 2004, 197401.

[3] A. Sanada, C. Caloz, and T. Itoh, "Characteristics of the composite right/left handed transmission lines," *IEEE Microw. Wireless Compon. Lett.*, vol. 14, no. 2, pp. 68–70, Feb. 2004.

[4] J. Bonache, M. Gil, I. Gil, J. García-García, and F. Martín, "Limitations and solutions of resonant-type metamaterial transmission lines for filter applications: The hybrid approach," in *IEEE MTT-S Int. Microw. Symp. Dig.*, San Francisco, CA, Jun. 2006, pp. 939–942.

[5] J. Bonache, J. Martel, I. Gil, M. Gil, J. García-García, F. Martín, I. Cairó, and M. Ikeda, "Super compact ($< 1$ cm$^2$) bandpass filters with wide bandwidth and high selectivity at *C*-band," in *Proc. Eur. Microw. Conf.*, Manchester, U.K., Sep. 2006, pp. 599–602.

[6] I. Gil, J. Bonache, M. Gil, J. García-García, F. Martín, and R. Marqués, "Accurate circuit analysis of resonant type left handed transmission lines with inter-resonator's coupling," *J. Appl. Phys.*, vol. 100, Oct. 2006, Paper 074908-1-10.

[7] J. Bonache, I. Gil, J. García-García, and F. Martín, "Novel microstrip bandpass filters based on complementary split rings resonators," *IEEE Trans. Microw. Theory Tech.*, vol. 54, no. 1, pp. 265–271, Jan. 2006.

[8] D. M. Pozar, *Microwave Engineering*. Reading, MA: Addison-Wesley, 1990.

[9] C. Caloz and T. Itoh, *Electromagnetic Metamaterials: Transmission Line Theory and Microwave Applications*. New York: Wiley, 2005.

[10] J. Bonache, M. Gil, I. Gil, J. Garcia-García, and F. Martín, "On the electrical characteristics of complementary metamaterial resonators," *IEEE Microw. Wireless Compon. Lett.*, vol. 16, no. 10, pp. 543–545, Oct. 2006.

[11] I. Gil, J. Bonache, M. Gil, J. García-García, and F. Martín, "Left handed and right handed transmission properties of microstrip lines loaded with complementary split rings resonators," *Microw. Opt. Technol. Lett.*, vol. 48, no. 12, pp. 2508–2511, Dec. 2006.

[12] J. D. Baena, J. Bonache, F. Martín, R. Marqués, F. Falcone, T. Lopetegi, M. A. G. Laso, J. García, I. Gil, and M. Sorolla, "Equivalent circuit models for split ring resonators and complementary split rings resonators coupled to planar transmission lines," *IEEE Trans. Microw. Theory Tech.*, vol. 53, no. 4, pp. 1451–1461, Apr. 2005.

[13] J. García-García, F. Martín, J. D. Baena, and R. Marqués, "On the resonances and polarizabilities of split rings resonators," *J. Appl. Phys.*, vol. 98, pp. 033103-1–033103-9, Sep. 2005.

[14] F. Martín, F. Falcone, J. Bonache, R. Marqués, and M. Sorolla, "A new split ring resonator based left handed coplanar waveguide," *Appl. Phys. Lett.*, vol. 83, pp. 4652–4654, Dec. 2003.

[15] H. V. Nguyen and C. Caloz, "Broadband highly selective bandpass filter based on a tapered coupler resonator (TCR) CRLH structure," in *Proc. Eur. Microw. Assoc.*, Mar. 2006, vol. 2, pp. 44–51.

[16] L. Zhu, S. Sun, and W. Menzel, "Ultra wide band (UWB) bandpass filters using multiple mode resonator," *IEEE Microw. Wireless Compon. Lett.*, vol. 15, no. 11, pp. 796–708, Nov. 2005.

[17] H. N. Shaman and J.-S. Hong, "A compact ultra-wideband (UWB) bandpass filter with transmission zero," in *Proc. 36th Eur. Microw. Conf.*, Manchester, U.K., Sep. 2006, pp. 603–605.

[18] D. Packiaraj, M. Ramesh, and A. T. Kalghatgi, "Broad band filter for UWB communications," in *Proc. 36th Eur. Microw. Conf.*, Manchester, U.K., Sep. 2006, pp. 606–608.

[19] J. García-García, J. Bonache, and F. Martín, "Application of electromagnetic bandgaps (EBGs) to the design of ultra wide bandpass filters (UWBPFs) with good out-of-band performance," *IEEE Trans. Microw. Theory Tech.*, vol. 54, no. 12, pp. 4136–4140, Dec. 2006.



**Marta Gil** (S'07) was born in Valdepeñas (Ciudad Real), Spain, in 1981. She received the Physics degree from the Universidad de Granada, Granada, Spain, in 2005, and is currently working toward the Ph.D. degree in subjects related to metamaterials and microwave circuits at the Universitat Autònoma de Barcelona, Bellaterra (Barcelona), Spain.

She studied for one year at the Friedrich Schiller Universität Jena, Jena, Germany. She is currently with the Universitat Autònoma de Barcelona under the framework of METAMORPHOSE.


Ms. Gil was the recipient of a Formación de Profesorado Universitario Research Fellowship (Reference AP2005-4523) presented by the Spanish Government (MEC).

**Jordi Bonache** (S'05–M'06) was born in Cardona (Barcelona), Spain, in 1976. He received the Physics and Electronics Engineering degrees and Ph.D. degree in electronics engineering from the Universitat Autònoma de Barcelona, Bellaterra (Barcelona), Spain, in 1999, 2001, and 2007, respectively.

In 2000, he joined the High Energy Physics Institute of Barcelona (IFAE), where he was involved in the design and implementation of the control and monitoring system of the MAGIC telescope. In 2001, he joined the Department d'Enginyeria Electrònica, Universitat Autònoma de Barcelona, where he is currently an Assistant Professor. His research interests include active and passive microwave devices and metamaterials.

**Joan García-García** (M'05) was born in Barcelona, Spain, in 1971. He received the Physics degree and Ph.D. degree in electrical engineering from the Universitat Autònoma de Barcelona, Bellaterra (Barcelona), Spain, in 1994 and 2001, respectively.

He then became a Post-Doctoral Research Fellow with the Institute of Microwaves and Photonics, The University of Leeds, Leeds, U.K., under the INTERACT European Project. In 2002, he was a Post-Doctoral Research Fellow with the Universitat Autònoma de Barcelona, under the Ramon y Cajal Project of the Spanish Government. In November 2003, he become an Associate Professor of electronics with the Departament d'Enginyeria Electrònica, Universitat Autònoma de Barcelona.

**Jesús Martel** (M'07) was born in Seville, Spain, in 1966. He received the Licenciado and Doctor degrees in physics from the University of Seville, Seville, Spain, in 1989 and 1996, respectively.

Since 1992, he has been with the Department of Applied Physics II, University of Seville, where, in 2000, he became an Associate Professor. His current research interest is focused on the numerical analysis of planar transmission lines, modeling of planar microstrip discontinuities, design of passive microwave circuits, microwave measurements, and artificial media.

**Ferran Martín** (M'05) was born in Barakaldo (Vizcaya), Spain, in 1965. He received the B.S. degree in physics and Ph.D. degree from the Universitat Autònoma de Barcelona (UAB), Bellaterra (Barcelona), Spain, in 1988 and 1992, respectively.

From 1994 to 2006, he was an Associate Professor of electronics with the Departament d'Enginyeria Electrònica, Universitat Autònoma de Barcelona, and since January 2007, he has been a Full Professor of electronics. He is the Head of the Microwave and Millimeter Wave Engineering Group, UAB. He is a partner of the Network of Excellence (NoE), European Union METAMORPHOSE. Since January 2006, he has been the Head of Centre d'Investigació en Metamaterials per a la Innovació en Tecnologia Electrònica i de Comunicacions (CIMITEC), a Research Center on metamaterials funded by the Catalan Government, which has been created for technology transfer on the basis of metamaterial concepts. He has authored or coauthored over 200 technical conference, letter and journal papers. He is currently coauthoring the monograph on metamaterials *Metamaterials with Negative Parameters: Theory, Design and Microwave Applications*. He has been Guest Editor for two Special Issues on metamaterials in two international journals. He is member of the Editorial Board of the *IET Proceedings on Microwaves Antennas and Propagation*. He has filed several patents on metamaterials and has headed several development contracts. In recent years, he has been involved in different research activities including modeling and simulation of electron devices for high-frequency applications, millimeter-wave and terahertz generation systems, and the application of electromagnetic bandgaps to microwave and millimeter-wave circuits. He is currently also very active in the field of metamaterials and their application to the miniaturization and optimization of microwave circuits and antennas.

Dr. Martín has organized several international events related to metamaterials, including two workshops of the 2005 and 2007 IEEE Microwave Theory and Techniques Society (IEEE MTT-S) International Microwave Symposium (IMS). He is a member of the Technical Program Committee of the International Congress on Advanced Electromagnetic Materials in Microwave and Optics (Metamaterials). He and the members of CIMITEC were the recipients of the 2006 Duran Farell Prize for technological research.

ation in the NDR region of the RTD we have chosen transmission lines with a (I-V) characteristic stabilized by the voltage source. The agreement between the numerical simulations and measurements is reasonably good. Harmonics are also presented, which are generated additionally to the fundamental mode. Figure 3 demonstrates, as an example, the measured spectra of a distributed RTD-NLTL oscillator consisting of 10 elements. The dominant frequencies are 9.65 and 19.3 GHz, the frequencies 38.7 and 46.7 GHz are additionally excited higher harmonics. The FWHM of the fundamental wave is 5 MHz and the output power is −10 dBm.

## 5. CONCLUSION

In this letter RTD–NLTL oscillators, capable to generate millimetre wave power are presented. The NLTLs are compact, easily fabricated using standard InP technology, suitable for monolithic integration and provide high output power compare to the output power −35 dBm of the single RTD [9]. We therefore conclude that the travelling wave concept can provide a solution for efficient power mm-wave signal sources. Simulations show (Fig. 4) that oscillations up to a frequency of 200 GHz could be achieved in the AlGaAs/AlAs system and indicate the potential for fundamental oscillations up to about 600 GHz.

## REFERENCES


1. R.Y. Yu, Y. Konishi, S.T. Allen, M. Reddy, and M.J.M. Rodwell, A travelling-wave resonant tunnel diode pulse generator, IEEE Microwave Guid Wave Lett 4 (1994), 220–222.
2. I. Mehdi, J.R. East, and G.I. Haddat, Characterisation of resonant tunnelling diodes for microwave.
3. E.R. Brown, C.D. Parker, A.R. Calawa, M.J. Manfra, C.L. Chen, L.J. Mahoney, W.D. Goodhue, J.R. Söderströöm, and T.C. McGill, High-frequency resonant-tunneling oscillators Microwave Opt Technol Lett 4 (2007), 19–23.
4. D. Jäger, Characteristics of travelling waves along nonlinear transmission lines for monolithic integrated circuits: A review, Int J Electron 58 (1985), 649–669 (invited paper).
5. H. Mitzuta and T. Tanone, Physics and applications of the resonant tunneling diodes,Cambridge University press, Cambridge, UK, 1995.
6. F. Capasso, K. Mohammedand, and A.L. Cho, Resonant tunneling through double barriers, perpendicular quantum transport phenomena in superlattices, and their device applications, IEEE J Quantum Electron, 22 (1986), 1853–1869.
7. M. Reddy, S.C. Martin, A.C. Molner, R.E. Muller, R.P. Smith, P.H. Siegel, M.J. Mondry, M.J. Rodwell, H. Kremer, and S.J. Allen, Jr., Monolithic Schottky-collector resonant tunnel diode oscillator arrays to 650 GHz, IEEE J Quantum Electron, 2 (1997), 188–195.
8. I. Ryjenkova, V. Mezentsev, S. Musher, S. Turitsyn, R. Hülsewede, and D. Jäger, Millimeter wave generation on nonlinear transmission lines, Ann des Telecomm 52 (1997), 134–139 (Special Issue, invited paper).
9. U. Auer, W. Prost, G. Jansen, M. Agethen, R. Teuter, and F.J. Tegude, A novel 3D integrated HFET/RTD frequency multiplier, IEEE J Sel Top Quantum Electron 2 (1996), 650–654.






# METAMATERIAL FILTERS WITH ATTENUATION POLES IN THE PASS BAND FOR ULTRA WIDE BAND APPLICATIONS

**Marta Gil, Jordi Bonache, and Ferran Martín**
CIMITEC, Departament d'Enginyeria Electrònica. Universitat Autònoma de Barcelona. 08193 Bellaterra (Barcelona), Spain;
Corresponding author: Ferran.Martin@uab.es

*Received 11 May 2007*

**ABSTRACT:** *In this work, a composite right/left handed (CRLH) transmission line implemented by means of complementary split rings resonators (CSRRS) and interdigital capacitors is designed to provide a transmission band useful for ultra wide band (UWB) applications, i.e., in the interval 3.1–10.6 GHz. This huge bandwidth is obtained by balancing the line, namely by merging the left handed (LH) and right handed (RH) bands typical of these structures. The result is a single and broad transmission band, which exhibits a sharp cut-off at the lower edge due to the presence of a transmission zero. In these UWB band pass filters, an attenuation pole within the band may be of interest for the elimination of possible interfering signals. It is demonstrated that such attenuation poles can be introduced by adding properly designed spiral resonators (SRs) at both sides of the host line on the top layer of the design. The fabricated device is small (area A = 0.66 cm$^2$) and exhibits reasonable performance. This work contributes to demonstrate the potentiality of transmission line metamaterials for the design of microwave components in planar technology.* © 2007 Wiley Periodicals, Inc. Microwave Opt Technol Lett 49: 2909–2913, 2007; Published online in Wiley InterScience (www.interscience.wiley.com). DOI 10.1002/mop.22901

**Key words:** *metamaterials; complementary split rings resonators (CSRRs); composite right/left handed (CRLH) lines; microwave filters; ultra wide band (UWB)*

## 1. INTRODUCTION

Complementary split rings resonators (CSRRs, see Fig. 1) were introduced by Falcone et al. [1] as new particles for the synthesis of effective media with negative permittivity. It was also demonstrated that by loading a microstrip line with CSRRs (etched in the ground plane) and series capacitive gaps, the structure exhibits a transmission band with backward (or left handed -LH) wave propagation [2]. These artificial lines belong to the so-called resonant type approach of metamaterial transmission lines, which was first proposed by Martín et al. in 2003 [3], on the basis of the former resonant particles that were used for the implementation of LH or negative permeability metamaterials, namely the SRRs [4] (see also Fig. 1). CSRR-based LH lines have been successfully applied to the design of compact band pass filters [5, 6], diplexers [7], and other microwave devices [8]. However, chronologically there was an earlier approach for the synthesis of metamaterial transmission lines, i.e., the dual transmission line approach [9–11]. It consists on periodic loading a transmission line with series capacitors and shunt inductors. These reactive elements are responsible for the LH band, which appears in a certain frequency interval. However, due to line parasitics (inductance and capacitance of the line), these structures do also exhibit a forward (or right handed -RH) transmission band at higher frequencies, typically separated from the LH band by a stop band (frequency gap). Because of the composite (right and left handed) behavior of L-C loaded lines, these structures were called composite right/left handed (CRLH) transmission lines [12]. The lumped element equivalent circuit model of the unit cell of CRLH lines is depicted

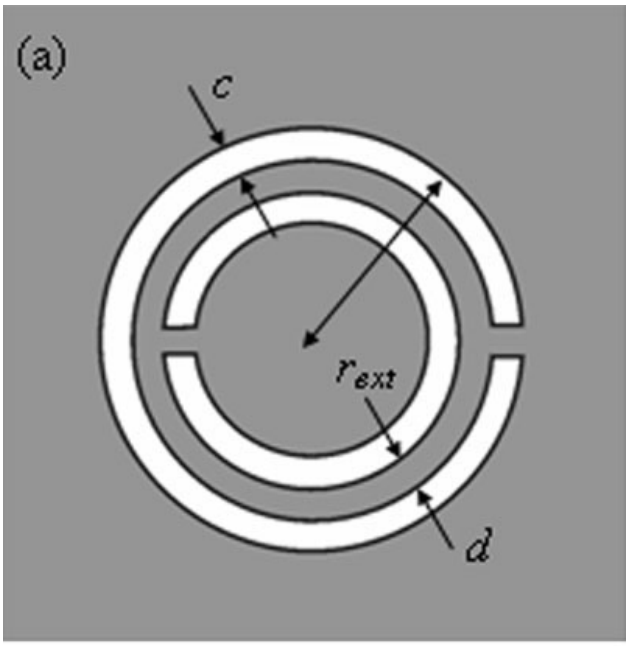


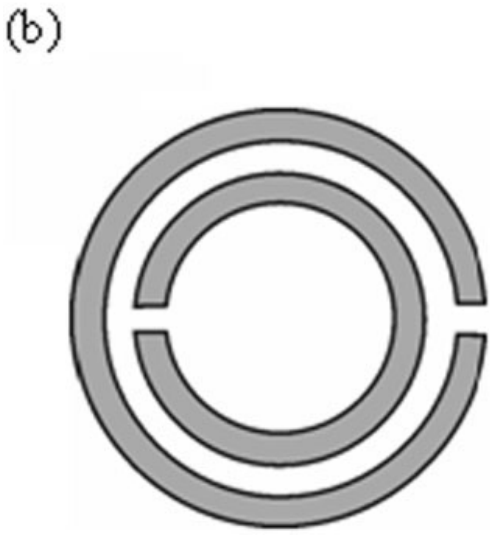


**Figure 1** Topology of the CSRR (a) and SRR (b) and their relevant dimensions. Metallic parts are depicted in grey

in Figure 2 [13]. Analysis of this model [13] reveals that the frequency gap between the LH and RH band collapses if the series resonance, $f_s$, is identical to the resonance frequency of the parallel resonant tank, $f_p$ (balance condition, or $f_s = f_p = f_o$). Moreover, the characteristic impedance of the structure varies smoothly in the vicinity of the transition frequency, $f_o$, and the group velocity is finite at $f_o$ (where the phase constant is null). These characteristics are also potentially achievable through the resonant type approach, on account of the equivalent circuit model of the unit cell of CSRR/gap loaded lines (also depicted in Fig. 2) [14]. It has been recently demonstrated that balanced CRLH lines can be implemented by means of CSRR-loaded microstrip lines [15]. Since broad bandwidths are achievable in CRLH balanced lines by properly designing the device, the application of CSRR-loaded lines to ultra wide band (UWB) pass filter design can be envisaged. In this work, these balanced structures have been applied to the synthesis of a planar filter covering a transmission band that roughly coincides with the UWB mask supplied by the Federal Communication Commission (FCC) in February 2002 (this mask extends from 3.1 GHz up to 10.6 GHz). Since UWB systems cover a very wide spectrum, interference with existing regulated communication services may occur. To eliminate such critical frequencies, the introduction of attenuation poles within the UWB filter band is of interest [16, 17]. For this reason, several UWB band pass filters have been designed in this work as illustrative examples, exhibiting attenuation poles at different frequencies, which have been located within the CRLH pass band at 5.5 and 4.5 GHz. This has been achieved by simply adding spiral resonators (SRs) on the top layer, at both sides of the host line.

## 2. TOPOLOGY OF THE BALANCED CSRR-BASED CRLH TRANSMISSION LINE AND DESIGN

As has been indicated, very wide bands can be obtained by balancing CRLH metamaterial transmission lines. In CSRR-based lines, this is achieved by designing the structure to have identical resonance frequencies for the series branch and the tank formed by $L_c$ and $C_c$, namely [15]:

$$f_o = \frac{1}{2\pi\sqrt{LC_g}} = \frac{1}{2\pi\sqrt{L_cC_c}} \tag{1}$$

The filter will consist on cascading several unit cells of the type given in Fig. 2(d). Relevant parameters for filter design are the upper and lower limits of the transmission band, frequency selectivity (usually specified by a certain rejection level at given frequencies), and in-band behavior (insertion and return losses and group delay). In UWB communications, bandwidth requirements for filters depend on the particular application. In this work we will consider the design of band pass filters roughly covering the whole allowed UWB band (3.1–10.6 GHz). This represents a huge fractional bandwidth of FBW $\approx$110%.

The design of the filter can be carried out from the equivalent circuit model of the unit cell [Fig. 2(b)] and the following expres-

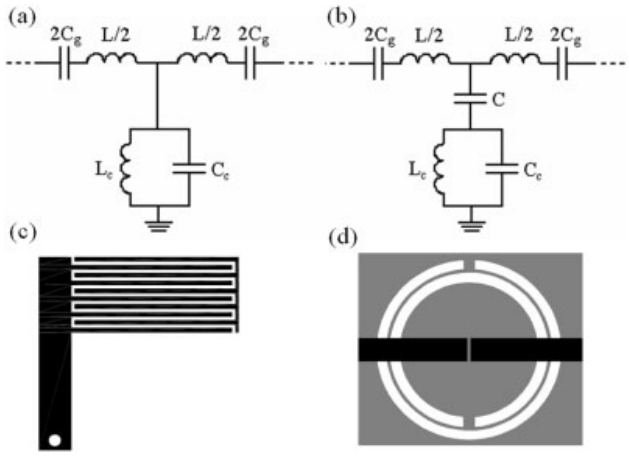


**Figure 2** Lumped element equivalent circuit of the unit cell of a CRLH line based on the dual transmission line (a) and resonant-type CSRR-based model (b). In (c) and (d) are depicted the unit cells for each model. In (b), $C_c$ and $L_c$ model de CSRR, and its electric coupling to the host line is described by the capacitance $C$. $L$ and $C_g$ correspond to the line inductance and series capacitance, respectively. Losses have been excluded in these models. On (d) the bottom side, metal (ground plane) is depicted in grey

**Figure 3** Unit cell of the balanced CSRR-based CRLH transmission line used for the design of the UWB band pass filter. The considered substrate is the *Rogers RO3010* with thickness $h = 635$ $\mu$m and dielectric constant $\varepsilon_r = 10.2$. Dimensions are as follows (in reference to Fig. 1): $r_{ext} = 2.10$ mm, $d = 0.11$ mm, $c = 0.22$ mm, and $c = 0.16$ mm for the external and internal ring, respectively; the width of the host line is $W = 0.80$ mm and the capacitor is formed by five face-to-face fingers separated a distance of 0.16 mm (finger length and width are 0.84 and 0.14 mm, respectively)

sions providing the dispersion diagram and characteristic impedance of the structure, respectively:

$$\cos\phi = 1 + \frac{Z_s(j\omega)}{Z_p(j\omega)} \tag{2}$$

$$Z_B = \sqrt{Z_s(j\omega)[Z_s(j\omega) + 2Z_p(j\omega)}} \tag{3}$$

where $Z_s$ and $Z_p$ are the series and shunt impedance of the equivalent circuit model [see Fig. 2(b)], respectively, and $\phi = \beta l$ is the phase shift per cell ($\beta$ and $l$ being the phase constant and period of the structure, respectively). According to expressions (2) and (3), signal transmission is possible in those regions where both the phase shift, $\phi$, and characteristic impedance, $Z_B$, are real numbers. In balanced lines this occurs in a frequency interval delimited by the two frequencies ($f_L$ and $f_H$) that satisfy the following equation:

$$Z_s(j\omega) = -2Z_p(j\omega) \tag{4}$$

In general, this frequency interval does not necessarily coincide with the 3-dB filter bandwidth. However, if the characteristic impedance of the structure varies smoothly in the vicinity of 50Ω, impedance matching is roughly preserved in the whole transmission band, and filter bandwidth can be considered to be delimited by those frequencies satisfying (4). Below the lower frequency limit, $f_L$, there is a transmission zero given by:

$$f_z = \frac{1}{2\pi\sqrt{L_c(C + C_c)}} \tag{5}$$

This transmission zero is typically very close to $f_L$ in balanced structures [15], and it provides a very sharp cut-off at the lower edge of the band. Thus, for filters having the fractional bandwidth necessary for UWB applications, it is reasonable to consider that the onset of signal transmission is roughly given by $f_z$. With regard to the upper band limit, it has been previously found that it is underestimated by the model. In other words, the transmission band actually extends above $f_H$. This discrepancy is due to the inability of the model to describe device behavior at high frequencies [18]. Namely, the lumped element model is valid in a limited frequency interval that does not cover the transmission band that typical balanced structures exhibit. Indeed, the periodic filters implemented by means of the unit cells depicted in Figure 2 do not have a controllable upper cut-off frequency. Thus, they actually exhibit high pass characteristics, and it is necessary to add a low pass or a stop band section to effectively achieve a band pass behavior.

The balanced CRLH unit cell of the filter designed in this work is depicted in Figure 3. Interdigital capacitors have been used since relatively large values of the gap capacitance, $C_g$, are required to balance the line. The structure has been designed to exhibit a transmission zero at $f_z = 2.4$ GHz and a characteristic impedance varying in the vicinity of 50Ω (the formulas given in [15] have been used). This provides a very wide band that extends from 3 GHz up to more than 10 GHz, as is revealed by the simulated frequency response (obtained through *Agilent Momentum*) depicted in Figure 4.

### 3. UWB BAND PASS FILTER WITH ATTENUATION POLES

To design the UWB filter based on the unit cell depicted in Figure 3, we need to determine its order, and we have to add additional elements to obtain the notch as well as to control the upper cut-off frequency. The order is determined by the required rejection level at the lower stop band. We have carried out electromagnetic simulations of the structure shown in Figure 3, by considering different number of stages. In the order-three structure, significant stop band rejection has been obtained. Thus, this structure has been used as the basis for the fabrication of the final prototype device.

To obtain the upper stop band, we have introduced additional rectangular shaped SRRs tuned at the required cut-off frequency. These SRRs have been located next to the host line at the beginning and the end of the filter on the top layer of the substrate. In this manner there is no area increase. Four of these SRRs have been added, as Figure 5 illustrates.

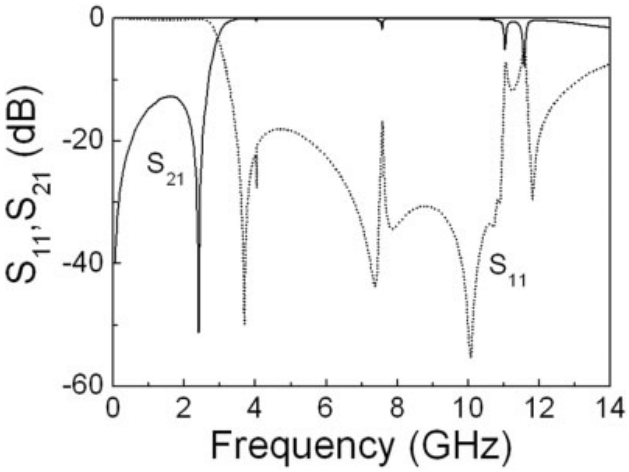


**Figure 4** Simulated insertion and return losses of the unit cell depicted in Figure 3

Finally, in order to obtain the desired notch inside the pass band of the filter, two SRs have been located on the top layer in a similar way than in the case of the SRRs, but this time they lay on the central part of the filter. Such topologies (SRs) have been chosen to minimize filter area, since the electrical size of SRs is roughly half the electrical size of CSRRs with identical dimensions [19]. The attenuation pole is due to the presence of the SRs, which have been tuned to provide a transmission zero at a particular frequency. Two filters with different notch frequencies (4.5 and 5.5 GHz) have been designed to illustrate the possibilities of locating this transmission zero at any specific frequency in order to eliminate undesired interfering signals. The topology (layout) of one of the designed filters is depicted in Figure 5. The simulated (through *Agilent Momentum*) and measured (by means of the *Agilent 8720ES* vector network analyzer) frequency responses of the structures (only the one with the notch at 5.5 GHz has been fabricated) are depicted in Figure 6. Measured 3-dB filter bandwidth extends from 3.08 GHz up to 11.09 GHz, namely it is very close to the UWB mask. Insertion losses are better than −2.5 to −1.3 dB above/below the notch and the rejection level at the lower stop band is higher than 45 dB. As desired, a notch is visible in the vicinity of 5.5 GHz, due to the presence of the SRs. The frequency shift between simulation and measurement at the upper transition band is attributed to the fabrication process, since certain dimensions are very close to the limits of resolution.

As compared with previous implementations of UWB band pass filters with attenuation poles in the pass band, the proposed structure exhibits a very sharp cut-off at the lower band edge (due to the presence of a transmission zero), and rejection below that frequency can be easily controlled. This can be of interest in certain applications, since there are many allocated radio frequency bands in that region, which may cause interference. Finally we would like to highlight the compact dimensions of the filter (Area = 0.66 $cm^2$), consequence of the small electrical size of the constitutive elements (CSRRs, SRRs, and SRs). This is the first time that a UWB band pass filter is designed using a CRLH resonant type structure where SRs and SRRs are added to set the upper limit of the band and an attenuation pole at specific frequencies of interest.

## 4. CONCLUSIONS

In conclusion, it has been demonstrated that CSRR-based CRLH metamaterial transmission lines are useful for the design of UWB band pass filters. The fabricated device, which includes an attenuation pole within the pass band for the rejection of specific interfering signals, is small and it exhibits reasonable performance in terms of in-band behavior and stop band rejection. In opinion of the authors, the proposed structure can be of interest in UWB systems subjected to interfering environments.

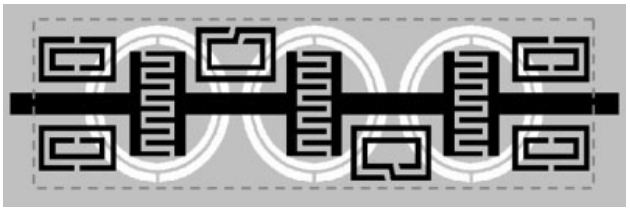

**Figure 5** Layout of the fabricated UWB band pass filter. Dimensions of the SRRs are $c$ = 0.14 mm, $d$ = 0.165 mm $l_{ext}$ = 2.1 mm and $h_{ext}$ = 1.2 mm ($l_{ext}$ and $h_{ext}$ are the length and the width of the SRRs). SRs provide a transmission zero at 5.5 GHz ($c$ = 0.14 mm, $d$ = 0.166 mm $l_{ext}$ = 2.03 mm, and $h_{ext}$ = 1.46 mm). The area of the device (dashed rectangle) is $A$ = 1.57 cm × 0.42 cm = 0.66 $cm^2$. CSRRs are etched on the ground plane (in grey)

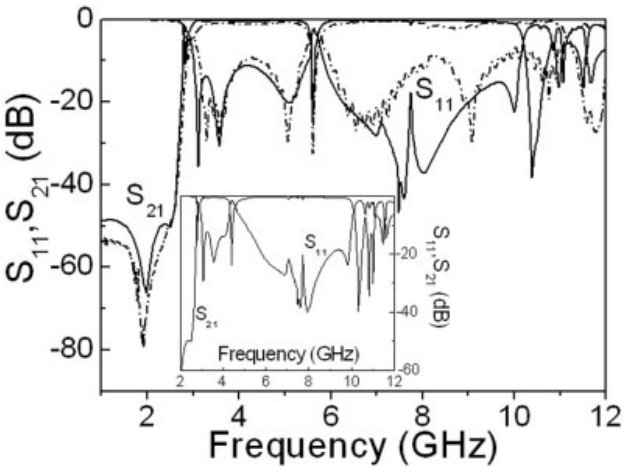


**Figure 6** Simulated (solid line) and measured (dashed line) insertion and return losses for the designed filters. The small graph shows the simulated response of the filter with the notch at 4.5 GHz


## ACKNOWLEDGMENT

This work has been supported by the European Commission (VI Framework Program) through the contract NoE. 500252–2 METAMORPHOSE and by MEC (Spanish Goverment) by project contract TEC 2004–04249-C02–01 METASYSTEMS and by a FPU grant awarded to Marta Gil (Ref. AP2005–4523).


## REFERENCES


1. F. Falcone, T. Lopetegi, J.D. Baena, R. Marqués, F. Martín, and M. Sorolla, Effective negative-ε stop-band microstrip lines based on complementary split ring resonators, IEEE Microwave Wireless Compon Lett 14 (2004), 280–282.
2. F. Falcone, T. Lopetegi, M.A.G. Laso, J.D. Baena, J. Bonache, R. Marqués, F. Martín, and M. Sorolla, Babinet principle applied to the design of metasurfaces and metamaterials, Phys Rev Lett 93 (2004), 197401.
3. F. Martín, F. Falcone, J. Bonache, R. Marqués, and M. Sorolla, A new split ring resonator based left handed coplanar waveguide, Appl Phys Lett 83 (2003), 4652–4654.
4. J.B. Pendry, A.J. Holden, D.J. Robbins, and W.J. Stewart, Magnetism from conductors and enhanced nonlinear phenomena, IEEE Trans Microwave Theory Tech 47 (1999), 2075–2084.
5. J. Bonache, I. Gil, J. García-García, and F. Martín, Novel microstrip band pass filters based on complementary split rings resonators, IEEE Trans Microwave Theory Tech 54 (2006), 265–271.
6. J. Bonache, M. Gil, I. Gil, J. García-García, and F. Martín, Limitations and solutions of resonant type metamaterial transmisión lines for filter applications: The hybrid approach, IEEE-MTT-S Intl Microwave Symp Dig, San Francisco (CA), USA, June 2006, pp. 939–942.
7. J. Bonache, I. Gil, J. García-García, and F. Martín, Complementary split rings resonator for microstrip diplexer design, Electron Lett 41 (2005), 810–811.
8. M. Gil, J. Bonache, I. Gil, J. García-García, and F. Martín, Artificial left-handed transmission lines for small size microwave components: application to power dividers, Proc. of the 36th European Microwave Conf. (EuMC 2006), Manchester (UK), September 2006, pp. 1135–1138.
9. A.K. Iyer and G.V. Eleftheriades, Negative refractive index metamaterials supporting 2-D waves, in IEEE-MTT Intl Symp, Seattle, WA, June 2002, Vol. 2, pp. 412–415.
10. A.A. Oliner, A periodic-structure negative-refractive-index medium

without resonant elements, in URSI Digest, IEEE-AP-S USNC/URSI National Radio Science Meeting, San Antonio, TX, June 2002, pp. 41.
11. C. Caloz and T. Itoh, Application of the transmission line theory of left-hande (LH) materials to the realization of a microstrip LH transmission line, in Proc.IEEE-AP-S USNC/URSI National Radio Science Meeting, San Antonio, TX, June 2002, Vol. 2, pp. 412–415.
12. C. Caloz and T. Itoh, Novel microwave devices and structures based on the transmission line approach of metamaterials, IEEE-MTT Intl Microwave Symposium Digest, Philadelphia, PA, June 2003, Vol. 1, pp. 195–198.
13. C. Caloz and T. Itoh, Electromagnetic metamaterials: Transmission line theory and microwave applications, Wiley, New Jersey, 2006.
14. J.D. Baena, J. Bonache, F. Martín, R. Marqués, F. Falcone, T. Lopetegi, M.A.G. Laso, J. García, I Gil, and M. Sorolla, Equivalent circuit models for split ring resonators and complementary split rings resonators coupled to planar transmission lines, IEEE Trans Microwave Theory Tech 53 (2005), 1451–1461.
15. M. Gil, J. Bonache, J. Selga, J. García-García, and F. Martín, Broadband resonant type metamaterial transmission lines, IEEE Microwave Wireless Compon Lett 17 (2007), 97–99.
16. W. Menzel and P. Feil, Ultra-wide band (UWB) filter with WLAN notch, Proc. of the 36th European Microwave Conference, Manchester (UK), September 2006, pp. 595–598.
17. K. Li, D. Kurita, and T. Matsui, UWB band pass filters with multi notched bands, Proc. of the 36th European Microwave Conference, Manchester (UK), September 2006, pp. 591–594.
18. I. Gil, J. Bonache, M. Gil, J. García-García, and F. Martín, On the left handed and right handed transmission properties of microstrip lines loaded with complementary split rings resonators, Microwave Opt Technol Lett 48 (2006), 2508–2511.
19. F. Falcone, F. Martín, J. Bonache, M.A.G. Laso, J. García-García, J.D. Baena, R. Marqués, and M. Sorolla, Stop band and band pass characteristics in coplanar waveguides coupled to spiral resonators, Microwave Opt Technol Lett 42 (2004) 386–388.



# COMPACT WIDEBAND INVERTED PLANAR MONOPOLE ANTENNA

**J. W. Baik,[1] Y. J. Sung,[2] and Y.-S. Kim[1]**
[1] Department of Radio Sciences and Engineering, Korea University, Seoul 136–713, Korea; Corresponding author: baik-jw@korea.ac.kr
[2] Mobile Communication Division, Telecommunication Network Business, Samsung Electronics Co., LTD., Suwon 443–742, Korea

*Received 12 May 2007*

**ABSTRACT:** *In this article, an inverted planar monopole antenna with two shorting plates is proposed. This inverted planar monopole antenna provides a 3.55:1 impedance bandwidth (for VSWR < 2). Owing to its compact size and wide impedance bandwidth, this antenna is suitable for CDMA, GSM, DCS, PCS, and wireless LAN (IEEE 802.11b) applications.* © 2007 Wiley Periodicals, Inc. Microwave Opt Technol Lett 49: 2913–2914, 2007; Published online in Wiley InterScience (www.interscience.wiley.com). DOI 10.1002/mop.22900

**Key words:** *wideband antenna; inverted monopole; planar monopole*

## 1. INTRODUCTION

For future wireless communication systems, antennas must be either multiband or wideband to cover desired bands such as CDMA (824–894 MHz), GSM (880–960 MHz), DCS (1710–1880 MHz), PCS (1850–1990 MHz), Wireless LAN (IEEE 802.11b), and so on. But it is not easy to achieve either the above all or some frequency bandwidths using multiband antennas and may cause higher manufacturing cost per terminal. Planar monopole antennas with wide impedance bandwidth and omnidirectional radiation have been investigated [1], but the height of the existing planar monopole antennas included CDMA, GSM, DCS, PCS, and Wireless LAN bands is so high to implement in a portable handset. Several techniques have been proposed for reducing the size of a planar monopole antenna, such as the use of an inverted structure [2] and a shorting pin [3, 4]. In this article, a compact wideband double-fed inverted planar monopole antenna with double shorting plates is proposed to achieve size reduction with keeping good radiation at the desired frequency range.

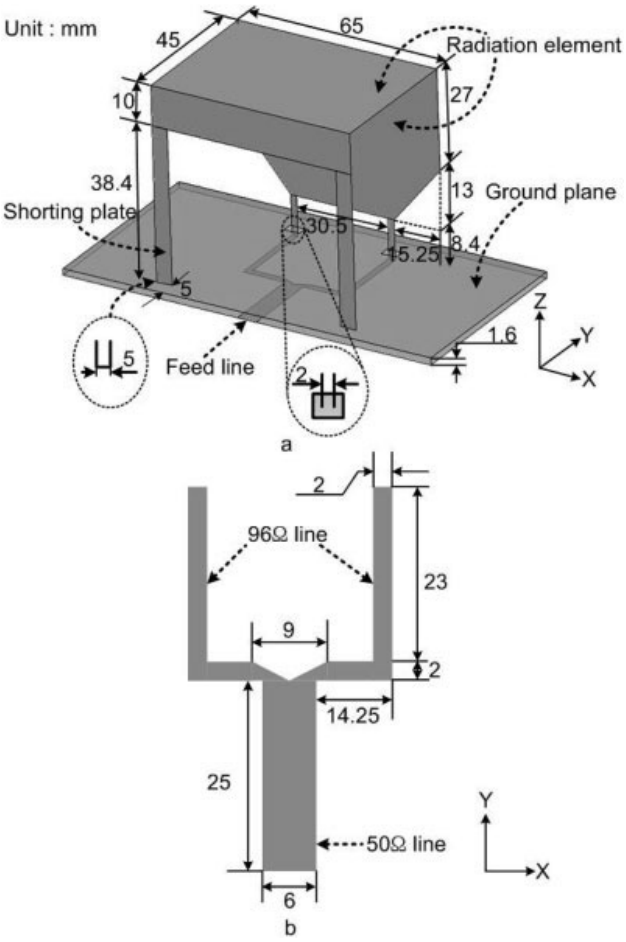


**Figure 1** Geometry of inverted planar monopole antenna and feed network (a) radiation element and (b) feed network

## 2. ANTENNA DESIGN

In this design, inverted structure, double shorting plates, beveling angle, and T-divider are used for the size reduction and achieving desired impedance bandwidth (0.8–2.5 GHz). Beveling technique [5] is utilized to increase the bandwidth with good control of the upper edge frequency. The geometry and dimensions of the inverted double shorted planar monopole are shown in Figure 1. The proposed antenna consists of an inverted planar monopole with double shorting plates located at the end of the radiation element and a feed network based on T-divider under a ground plane for avoiding mutual coupling between the feed line and the radiation element. Since the input impedance of the radiation element is about 120 Ω, the feed line with high

# New Left Handed Microstrip Lines with Complementary Split Rings Resonators (CSRRs) Etched in the Signal Strip

Marta Gil, Jordi Bonache, Joan García-García and Ferran Martín

GEMMA/CIMITEC, Departament d'Enginyeria Electrònica. Universitat Autònoma de Barcelona. 08193 BELLATERRA (Barcelona), Spain. E-mail: Ferran.Martin@uab.es

*Abstract* — **In this work, left handed (LH) microstrip lines with complementary split rings resonators (CSRRs) and series capacitive gaps, both etched in the upper metal level (signal strip), are presented for the first time. Contrarily to previous implementations of CSRR-based LH or negative permittivity microstrip lines, where the CSRRs were etched in the ground plane, the bottom metal is not printed in the proposed structures. This is of interest in many practical applications, where the substrate lies in a metallic holder. Moreover, no vias are required in these implementations since the shunt positive reactance needed to generate the LH band is provided by the CSRRs. It will be shown in the paper that to accurately describe the proposed structures in the region of interest, additional elements in the lumped element circuit (as compared to previous models) must be introduced. Advantages and drawbacks of this new implementation of the resonant-type approach of metamaterial transmission lines (as compared to previous ones) are pointed out, and an illustrative example is given.**

*Index Terms* — **Metamaterials, complementary split rings resonators (CSRRs), left handed (LH) lines, microstrip technology.**

## I. Introduction

There are two main approaches for the synthesis of metamaterial transmission lines: (i) that based on the dual transmission line concept, and (ii) the resonant-type approach. The former approach, that was almost simultaneously proposed by Iyer [1], Oliner [2] and Caloz [3], simply consists on periodic loading a host transmission line with series capacitors and shunt connected inductors. As long as these reactive elements dominate over the per-section capacitance and inductance of the line in a certain frequency band, the effective permeability and permittivity of the medium (in that interval) are both negative, and left handed (LH) wave propagation (i.e. with contra directional phase and group velocities) arises.

Concerning the resonant-type approach, this was initially proposed by Martín *et al.* [4] by etching split rings resonators (SRRs –see Fig. 1) [5] in the back substrate side of a coplanar waveguide (CPW) transmission line periodic loaded with shunt connected metallic wires. SRRs, which are electrically small resonators, provided the negative value of the effective permeability, whereas the required negative permittivity was achieved thanks to the presence of the inductive wires. Alternatively, left handedness in planar transmission media can be obtained by using the dual counterparts of SRRs, namely the complementary SRRs (CSRRs –see Fig. 1) [6]. By etching these resonators in the ground plane of a microstrip transmission line, it has been demonstrated that signal propagation is inhibited in a narrow band in the vicinity of resonance, and this has been interpreted as consequence of the negative effective permittivity of the medium, due to the presence of the CSRRs [6]. By adding series capacitive gaps to the structure (which provide the required negative permeability), the previous stop band behavior switches to a band pass with LH wave propagation, as was shown in [7]. It has also been demonstrated that by properly designing the structure, the typical frequency gap present between the LH band and the forward wave transmission band can be eliminated [8], with the result of a balanced composite right/left handed (CRLH) line (a concept previously introduced by others [9]) implemented by means of CSRRs.

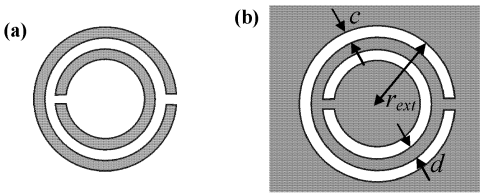


Fig. 1. Topology of the SRR (a) and CSRR (b), and relevant dimensions. Metal is depicted in grey.

CSRR-based LH lines have been applied to the design of filters [10], diplexers [11] and other microwave components [12], where miniaturization and/or the possibility to obtain device characteristics not easily achievable through conventional implementations [13] has been demonstrated. However, in these microstrip implementations, CSRRs are printed in the ground plane, and this may constitute a severe limitation in certain applications, where the substrate must be placed on top of a metallic holder. The main reason to etch the CSRRs in the ground plane was the relatively narrow strip widths of the host microstrip lines required to obtain the typical 50Ω characteristic impedance. However, there is not a reason that justifies such impedance value for the host line. Namely, the characteristic impedance of the structure (host line loaded with CSRRs and series gaps) in the region of interest (LH band) depends not only on the dimensions of the host line, but also on the gaps and CSRRs geometry [14].

1-4244-0688-9/07/$20.00 ©2007 IEEE

Thus, the characteristic impedance can be set to the required value without the need to implement CSRR-based structures with narrow widths for the signal strip. This is fundamental since by widening the strip of the host line, CSRR can be etched on it (as is demonstrated in this work), and the ground plane is thus absent of any defect. By doing this, the structure can no longer be described by the lumped element equivalent circuit model of CSRR-based LH lines that was proposed before [15]. Additional elements must be introduced. The accuracy of the new model, as well as the advantages and limitations of these new LH structures, as compared to previous ones, are discussed in the paper.

## II. The New CSRR-based LH Microstrip Lines

The basic cell of the new CSRR-based LH microstrip line and its lumped element equivalent circuit model are depicted in Fig. 2 (losses have been excluded in this model). As in the model reported in [15,16], the CSRRs and their coupling to the host line are described by the $C_c$-$L_c$ resonant tank and by the capacitance $C$, respectively. $L$ models the inductance of the line and $C_g$ accounts for the capacitance of the series gap. Actually, these series gaps do also introduce a fringing capacitance, $C_f$, which must be taken into account to accurately describe the structures (i.e., the series gaps are modelled by a $\pi$-circuit formed by $C_g$ and $C_f$). In the model reported in [15,16], the fringing capacitance, $C_f$, was indeed included in $C$. In other words, the fringing capacitance contributed to the coupling capacitance between the CSRRs and the host line, and this contribution was found to be significant [16]. The reason is that in the LH structures described by the model reported in [15,16], the series gaps are etched above the positions of the CSRRs. However, this is not the case in the structure of Fig. 2, and hence $C_f$ must be explicitly included in the model.

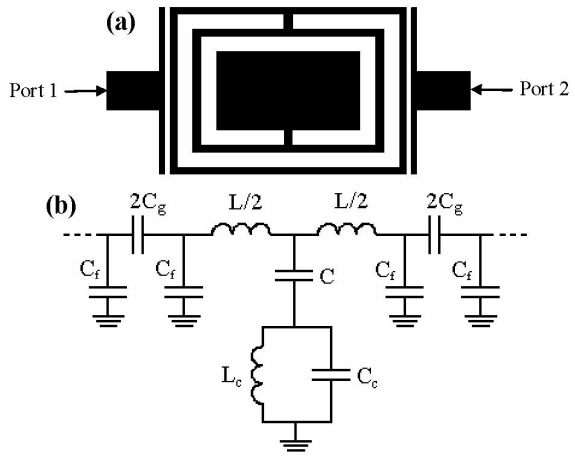


Fig. 2. Basic cell of the new CSRR-based LH microstrip lines with CSRRs etched in the signal strip (a) and equivalent circuit model (b).

## III. Simulations and Parameter Extraction

The structure shown in Fig. 2 has been simulated by means of the commercial electromagnetic software *Agilent Momentum*. The parameters of the *Rogers RO3010* substrate have been used, namely thickness $h$=1.27mm, dielectric constant $\varepsilon_r$=10.2. The dimensions of the structure are indicated in the caption of Fig. 3, where the insertion and return losses are depicted. The structure exhibits a LH pass band centered at 2.35GHz. This is corroborated from the phase response, shown in Fig. 3(b). The LH pass band is relatively narrow since the coupling capacitance, $C$, is small, but transmission characteristics similar to those that ground plane etched CSRR-based structures exhibit, are obtained. Specifically, a transmission zero is visible to the left of the LH band. This provides a sharp transition band at the lower band edge, with significant stop band rejection. Typical of these structures, attenuation above the LH band is softer.

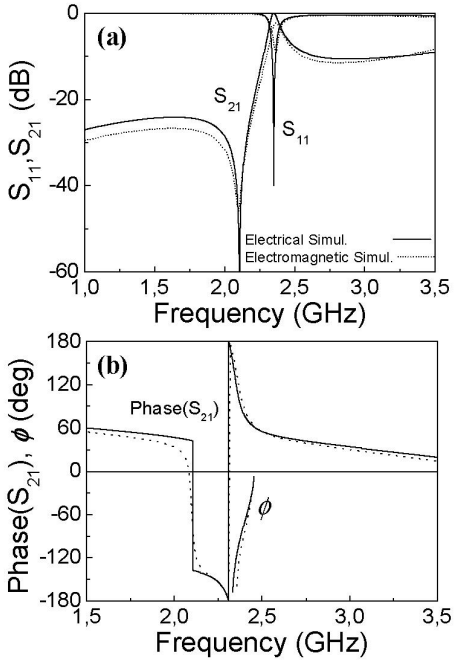


Fig. 3. Insertion and return losses (a) and phase response (b) for the microstrip LH unit cell depicted in Fig. 2(a). Dispersion characteristics ($\phi$-$\omega$) in the region of interest are also included in (b) and indicate LH wave propagation. The width of the host line is $W$=5.0mm and gap separation is $s$=0.17mm. CSRR dimensions are: $c$=0.46mm, $d$=0.26mm and the area occupied by the CSRRs is 6.62mm×4.58mm. The distance between gap centers is 7.19mm.

The electrical parameters of the equivalent circuit model have been extracted from electromagnetic simulations by following a procedure similar to that reported in [16]. However, due to the presence of the fringing capacitances. $C_f$, the method given in [16] can not be directly applied. Specifically, at the intrinsic resonance frequency of the CSRRs the shunt branch formed by $C$ and the $C_c$-$L_c$ resonator

opens, but there is still a shunt connection to ground through $C_f$. Hence, neither the intrinsic resonance frequency of the CSRRs can be obtained from the intersect of $S_{11}$ with the normalized unity resistance circle (as was done in [16]), nor the reactance of the series branch can be inferred. To determine the electrical parameters we have considered the structure without the series gaps (negative permittivity transmission line) and we have applied the method given in [16]. From this, $L$, $C$, $C_c$ and $L_c$ have been obtained. Since the gap and the CSRRs are not coupled in the present structures, gap parameters ($C_g$ and $C_f$) can be independently embedded from the electromagnetic simulation of the isolated gap structure. The following equations link the normalised admittances, related to $C_f$ and $C_g$ respectively, with the S-Parameters:

$$\bar{Y}_f = \frac{S_{11}+S_{21}-1}{1+S_{11}+S_{21}} \qquad \bar{Y}_g = \frac{S_{21}(\bar{Y}_f+1)}{1+S_{11}-S_{21}} \qquad (1)$$

The electrical simulation of the circuit model with the extracted parameters (given in table I) is also represented in Fig. 3. The good agreement between the electrical and electromagnetic simulations (both in magnitude and phase) validates the proposed model and points out the need to account for the fringing capacitances of the gap.

TABLE I
EXTRACTED ELEMENT PARAMETERS FOR THE STRUCTURE SHOWN IN FIG.2.

| $C_g$ (pF) | L (nH) | C(pF) | $C_c$ (pF) | $L_c$ (nH) | $C_f$ (pF) |
|---|---|---|---|---|---|
| 0.47 | 3.23 | 1.93 | 3.97 | 0.97 | 0.12 |

The main advantage of the proposed LH lines over previous implementations based on CSRRs is the fact that the ground plane is left unaltered. This simplifies fabrication and opens the application of these structures to those systems where the ground plane is in contact to a metallic holder. The main drawback is the limited electric coupling between the line and the CSRRs, which restricts the application of these structures to narrow band systems. Nevertheless, miniaturization as well as the potentiality of these LH lines for the design of microwave devices based on new functionalities can also be exploited.

## IV. Fabricated Structure and Characterization

A three-stage LH line based on the unit cell depicted in Fig. 2 has been fabricated (Fig. 4). A drilling machine *LPKF HF100* has been used for this purpose. 50Ω access lines have been cascaded to the input and output ports of the device for connectors soldering. The frequency response of the device has been measured by means of the *Agilent 8720ES* vector network analyzer. The results are depicted in Fig. 5, together with the simulated data that has been inferred from full wave electromagnetic simulation of the structure of Fig. 4. As compared to electromagnetic simulation, measured in-band insertion losses are slightly degraded and the overall frequency response is shifted 0.27GHz. This is attributed to some differences between final device geometry and nominal values. Frequency selectivity is good with attenuation better than 55dB/40dB at the lower/upper stop bands, respectively.

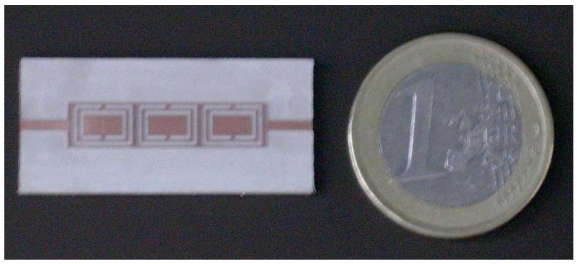

Fig. 4. Photograph of the fabricated 3-stage CSRR-based LH line with unaltered ground plane.

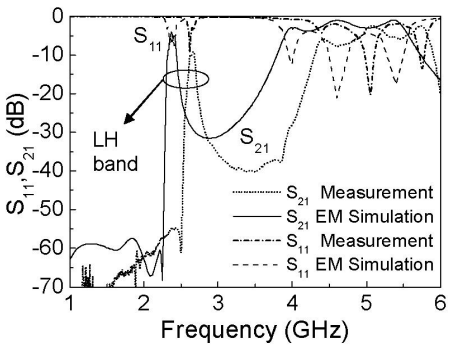


Fig. 5. Simulated and measured insertion and return losses for the structure of Fig. 4.

To further corroborate the LH nature of signal propagation in the allowed band, we have simulated a 10-stage structure with unit cells identical to that depicted in Fig. 2, and utilized for the fabricated device (Fig. 4). As frequency increases within the LH band, guided wavelength, $\lambda_g$, also increases, as revealed by the current diagrams of Fig. 6. Thus, the phase constant decreases with frequency, a necessary and sufficient condition for LH wave propagation.

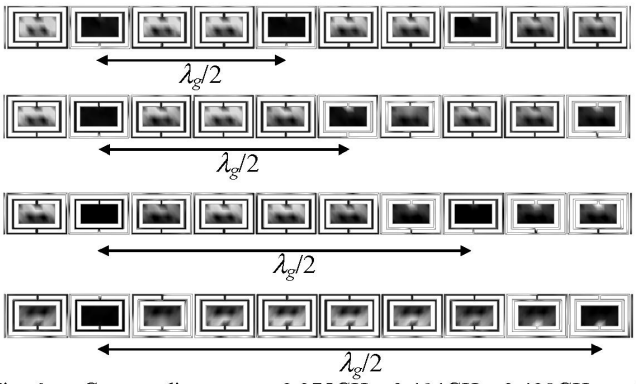


Fig. 6. Current diagrams at 2.375GHz, 2.404GHz, 2.428GHz and 2.439GHz (from top to bottom) provided by the *Agilent Momentum* simulator for a structure identical to that depicted in Fig. 4 (or Fig. 2) with 10 stages.

## V. Conclusions

In conclusion, left handed microstrip lines based on CSRRs and implemented by etching the CSRRs in the signal strip, have been presented for the first time. As compared to previous CSRR-based left handed lines, the ground planed is absent of any defect in these new structures. Thus, one of the drawbacks of CSRR-based metamaterial transmission lines (ground plane etching) has been solved, and this may expand the applicability of CSRR-based structures. It has been demonstrated that the presented structures can be no longer described by the equivalent circuit model of existing CSRR-based left handed lines. The fringing capacitance related to the presence of the gaps must be included in the model due to the decoupling between the series gaps and the CSRRs. It has been found that by including such capacitors, the structures are adequately described by the lumped element model. A three-stage left handed line based on this new approach has been fabricated and characterized. As expected, the device exhibits a LH pass band. Though the topology imposes more severe limitations to bandwidth control and in-band losses (as compared to previous CSRR-based implementations), extension of the ideas presented in this work to the hybrid approach (where CSRRs are combined with series gaps and grounded stubs for bandwidth improvement and flexibility enhancement) is in progress.

## Acknowledgement

This work has been supported by MEC (Spain) by project contract TEC2004-04249-C02-01 METASYSTEMS and by the European Commission (VI Framework Program) through the contract NoE. 500252-2 METAMORPHOSE. Thanks are also given to CIDEM (*Generalitat de Catalunya*) for funding CIMITEC (*Centro de Investigación en Metamateriales para la Innovación en Tecnologías Electrónica y de Comunicaciones*). MEC has given an FPU Grant to Marta Gil (Reference AP2005-4523).

## References

[1] A. K. Iyer and G. V. Eleftheriades. "Negative refractive index metamaterials supporting 2-D waves," in *IEEE-MTT Int'l Symp.*, vol. 2, Seattle, WA, pp. 412– 415, June 2002.

[2] A. A. Oliner. "A periodic-structure negative-refractive-index medium without resonant elements," in *URSI Digest, IEEE-AP-S USNC/URSI National Radio Science Meeting,* San Antonio, TX, pp. 41, June 2002.

[3] C. Caloz and T. Itoh. "Application of the transmission line theory of left-handed (LH) materials to the realization of a microstrip LH transmission line," *in Proc. IEEE-AP-S USNC/URSI National Radio Science Meeting,* vol. 2, San Antonio, TX, pp. 412–415, June 2002.

[4] F. Martín, F. Falcone, J. Bonache, R. Marqués and M. Sorolla, "A new split ring resonator based left handed coplanar waveguide", *Appl. Phys. Lett.*, vol. 83, pp. 4652-4654, December 2003.

[5] J.B. Pendry, A.J. Holden, D.J. Robbins and W.J. Stewart, "Magnetism from conductors and enhanced nonlinear phenomena", *IEEE Transactions Microwave Theory Tech.,* vol. 47, pp. 2075-2084 (1999).

[6] F. Falcone, T. Lopetegi, J.D. Baena, R. Marqués, F. Martín, M. Sorolla, "Effective negative-ε stop-band microstrip lines based on complementary split ring resonators", *IEEE Microwave and Wireless Comp. Lett.,* vol.14, pp.280-282 (2004).

[7] F. Falcone, T. Lopetegi, M.A.G. Laso, J.D. Baena, J. Bonache, R. Marqués, F. Martín, M. Sorolla, "Babinet principle applied to the design of metasurfaces and metamaterials", *Phys. Rev. Lett.*, vol. 93, p 197401, November 2004.

[8] M. Gil, J. Bonache, J. Selga, J. García-García and F. Martín, "Broadband resonant type metamaterial transmission lines", *IEEE Microwave and Wireless Comp. Lett.*, to be published in February 2007.

[9] C. Caloz and T. Itoh, "Novel microwave devices and structures based on the transmission line approach of metamaterials", *IEEE-MTT Int'l Microwave Symposium Digest*, vol. 1 Philadelphia, PA, pp. 195-198, June 2003.

[10] J. Bonache, I. Gil, J. García-García and F. Martín, "Novel Microstrip Band Pass Filters Based on Complementary Split Rings Resonators", *IEEE Transactions on Microwave Theory and Techniques*, vol. 54, pp. 265-271 January 2006.

[11] J. Bonache, I. Gil, J. García-García and F. Martín, "Complementary split rings resonator for microstrip diplexer design", *Electronics Letters*, vol. 41, pp. 810-811, July 2005.

[12] M. Gil, J. Bonache, I. Gil, J. García-García and F. Martín, "Artificial Left-handed Transmission Lines for Small Size Microwave Components: Application to Power Dividers", *Proc. of the 36th European Microwave Conf. (EuMC 2006)*, pp. 1135-1138, Manchester (UK), September 2006.

[13] J. Bonache, J. Martel, I. Gil, M. Gil, J. García-García, F. Martín, I. Cairó and M. Ikeda, "Super compact (<1cm$^2$) band pass filters with wide bandwidth and high selectivity at C-band", *Proc. of the 36th European Microwave Conf. (EuMC 2006)*, pp. 599-602, Manchester (UK), September 2006.

[14] M. Gil, I. Gil, J. Bonache, J. García-García and F. Martín, "Metamaterial transmission lines with extreme impedance values", *Microwave and Optical Technology Letters*, vol. 48, pp. 2499-2505, December 2006.

[15] J.D. Baena, J. Bonache, F. Martín, R. Marqués, F. Falcone, T. Lopetegi, M.A.G. Laso, J. García, I Gil and M. Sorolla, "Equivalent circuit models for split ring resonators and complementary split rings resonators coupled to planar transmission lines", *IEEE Trans. Microwave Theory and Tech.*, vol. 53, pp. 1451-1461, April 2005.

[16] J. Bonache, M. Gil, I. Gil, J. Garcia-García and F. Martín, "On the electrical characteristics of complementary metamaterial resonators", *IEEE Microwave and Wireless Components Letters*, vol. 16, pp. 543-545, October 2006.

Published in IET Microwaves, Antennas & Propagation
Received on 27th September 2007
Revised on 21st January 2008
doi: 10.1049/iet-map:20070225

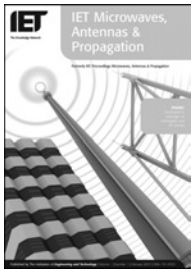


ISSN 1751-8725

# Synthesis and applications of new left handed microstrip lines with complementary split-ring resonators etched on the signal strip

*M. Gil J. Bonache F. Martín*

*GEMMA/CIMITEC, Departament D'Enginyeria Electrònica, Universitat Autònoma de Barcelona, Bellaterra (Barcelona)08193, Spain*
*E-mail: marta.gil.barba@uab.es*

**Abstract:** A new type of left handed microstrip lines implemented by means of complementary split-ring resonators (CSRRs) is proposed. The CSRRs are etched on the signal strip alternating with series gaps. Additionally, shunt connected stubs are introduced for the first time to the previous structure. The combination of these three elements, that is, the series gaps, the CSRR and the shunt inductance, enhances design flexibility. By this means, the ground plane is left unaltered and narrow band artificial transmission lines with good performance and compact dimensions can be synthesised. The lumped element equivalent circuit model of the structure is proposed and validated. To demonstrate the applicability of these new left handed transmission lines, two compact microwave components have been designed and fabricated: (i) a narrow band power divider and (ii) a band pass filter. The resulting power divider is 75% smaller than the conventional implementation and 50% smaller than previous power dividers implemented by means of CSRRs. The band pass filter performance is comparable to that of previous CSRR-based filters with ground plane etching, whereas its size is smaller. This work represents a significant progress on the design of microwave components based on CSRRs, that is, the approach is opened to those systems where the ground plane cannot be etched.

## 1 Introduction

Since the synthesis of the first left handed medium by Smith *et al.* [1] in 2000, different approaches have been developed to design artificial propagating structures supporting backward waves. In particular, in planar technology, Iyer and Eleftheriades [2], Oliner [3] and Caloz and Itoh [4] proposed almost simultaneously in 2002 the dual transmission line-based approach, where a host transmission line is periodically loaded with series capacitances and shunt inductances. Soon after the emersion of the previous approach, Martin *et al.* [5] succeeded in trying to apply Pendry's split-ring resonators to synthesise a one-dimensional left handed medium by loading a coplanar waveguide (CPW) transmission line with split-ring resonators and shunt metallic strips. In a similar way, lefthanded propagation is also achievable using complementary split-ring resonators (CSRRs) [6]. These particles are the dual counterparts of the split-ring resonators and can be combined with capacitive gaps to periodically load a microstrip line and, thus, create a left-handed transmission line [7]. To guarantee CSRR excitation through an axial electric field (as is required), these elements have been previously etched on the ground plane, beneath the conductor strip of the host line [6, 7].

A new approach based on CSRRs has been recently proposed: the hybrid approach [8]. In these new structures, these resonators are combined with series capacitive gaps and shunt connected inductances to implement left-handed lines. The particularity of this approach is the presence of a transmission zero above the main left-handed transmission band [9]. The presence of this additional element (shunt inductance) and the transmission zero has led us to the implementation of compact filters with a good out-of-band



doi: 10.1049/iet-map:20070225

performance. Indeed, the hybrid approach can be considered an extension of the resonant-type approach, in which the design flexibility is enhanced because of the presence of the additional element.

During the last years, the resonant-type approach (as well as the hybrid approach) has revealed to be a good strategy to synthesise left handed transmission lines and microwave components with competitive performance and small dimensions [10, 11]. The study of the possibilities offered by this kind of left handed lines shows that, as in the case of the dual transmission line approach, resonant- type metamaterial transmission lines do also exhibit a composite right–left handed behaviour. Thus, broadband responses can be obtained when the balance condition is satisfied [12]. Using these artificial left handed transmission lines, it is also possible to control both the phase and the line impedance at any specific frequency and, thus, synthesise artificial lines with small dimensions, as well as extreme impedance values (sometimes not achievable through conventional lines [13]).

Although these structures have proved to be a good solution in many microwave applications, they can become unsuitable for those applications in which the bottom side of the substrate lies on the top of a metallic surface (holder), as in this case the resonators etched or printed on the bottom layer are disabled. As a solution to this problem, we have recently proposed a new type of left-handed lines based on CSRRs and implemented in microstrip technology [14]. In such artificial lines, all the constituent elements are etched on the top metal layer, so that the ground plane is left unaltered. The layout of a typical structure, which has been published in [14], is reproduced here for completeness (Fig. 1). The CSRRs are etched on the signal strip, alternating with the series gaps. The left-handed nature of the first transmission band has been demonstrated in [14]. However, line performance and bandwidth are limited mainly because of the moderate/

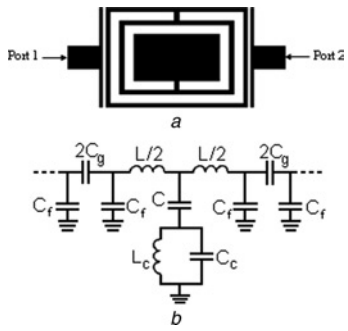


**Figure 1** *Basic cell of the complementary split-ring resonator-based left handed microstrip lines proposed in [14] (a), and its lumped element equivalent circuit model (b)*

$L_c$ and $C_c$ model the complementary split-ring resonator and $C$ its electrical coupling to the line. $L$ represents the line inductance. The fringing capacitances $C_f$ must be included to model the capacitive gaps together with $C_g$

small resonator to line coupling (which is in turn because of the decoupling between the series gaps and the CSRRs). To solve these limitations and gain flexibility, new left handed microstrip structures that combine CSRRs, series gaps and shunt stubs, all of them etched on the top metal level, are proposed in this work. The combination of all these elements facilitates the achievement of the required values of the different elements to obtain the desired response characteristics. To illustrate the possibilities of this new approach, two prototype devices have been designed and fabricated: a compact power divider and a band pass filter. In both designs, the ground plane is not etched. With these new left handed lines, many other applications can be envisaged. This new approach may open the door to new applications in which the limitative aspects of previous left handed microstrip lines based on CSRRs precluded their use.

## 2 New proposed left handed structures

As a first step to develop left handed CSRR-based structures with the absence of ground plane etching, the authors recently proposed a purely resonant left handed structure where CSRRs, etched on the signal strip, were combined with capacitive gaps (Fig. 1*a*) [14]. The frequency response of this structure is similar to those obtained in purely resonant left-handed structures with CSRRs etched on the ground plane [15]. However, the equivalent circuit model of the structure of Fig. 1*b* must include new elements to properly describe its behaviour. Specifically, since the series gaps and the CSRRs are decoupled, the fringing capacitances of the gaps, $C_f$, must be added to the model, as Fig. 1*b* illustrates [14]. In the model reported in [15] to describe microstrip lines with CSRRs etched on the ground plane, this fringing capacitance contributes to the coupling capacitance between the line and the resonator, and hence it is included in $C$. The most fundamental limitation of the left-handed lines based on the unit cell of Fig. 1 is bandwidth and, hence, losses. The presence of the series gaps alternating with the CSRRs decreases the electric coupling between the line and rings, and bandwidth is severely degraded.

In this work, losses and bandwidth are improved, modifying the previous structure. The new unit cell is based on the previous one, but includes a shunt inductive stub (Fig. 2) in order to enhance design flexibility and, thus, achieve the required characteristics (line impedance and phase) with broader bandwidths. The resulting structure is a hybrid cell, equivalent to that described in previous works [9], but with the advantage of presenting all its constituent elements on the top metallic layer of the substrate and, thus, avoiding ground plane etching. As expected for a hybrid structure, a transmission zero, because of the presence of the CSRRs, is located above the main left handed transmission band (Fig. 3), whereas such a

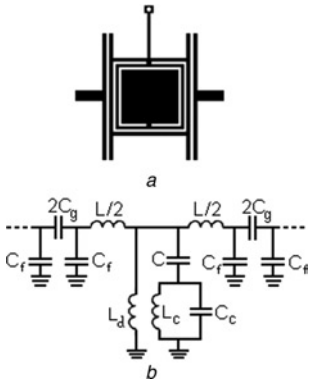


**Figure 2** *Layout of the new left handed basic hybrid cell, including a shunt inductance (a), and its lumped element equivalent circuit model (b)*

transmission zero is situated below the left-handed band in the case of the purely resonant structure. To properly describe the structure of Fig. 2, we must also include the fringing capacitances in the equivalent circuit model. Thus, the circuit describing the hybrid left handed cell with CSRRs etched on the signal strip is identical to that of Fig. 1*b*, but including the inductance $L_d$, which accounts for the presence of the grounded stub. In comparison with the structure of Fig. 1, the hybrid cell can be designed to exhibit a frequency response with a wider left handed transmission band (Fig. 3) and lower in-band losses.

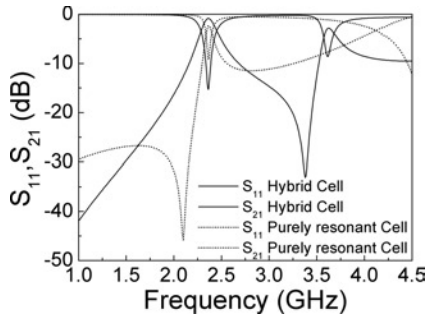


**Figure 3** *Comparison between the responses of a hybrid and a purely resonant cell*

In both cases all the elements have been etched on the top metallic layer of the substrate. The addition of the shunt inductance provides a wider and more symmetric response, as well as lower losses. For the purely resonant cell, the width of the host line is $W = 5.0$ mm and gap separation is $s = 0.17$ mm. Complementary split-ring resonator dimensions are: width of the rings $c = 0.46$ mm, distance between inner and outer rings $d = 0.26$ mm and the area occupied by the complementary split-ring resonator is 6.62 mm × 4.58 mm. The distance between gap centers is 7.19 mm. For the hybrid cell, $W = 3.80$ mm and $s = 0.23$ mm, whereas gaps total length, that is, the length in the orthogonal direction to the line is $l = 4.97$ mm. The complementary split-ring resonators have $c = 0.16$ mm, $d = 0.15$ mm, and a total area $A = 3.36$ mm × 3.41 mm. Shunt stub length is $l_s = 1.45$ mm, and the via hole diameter is $v = 0.3$ mm. The distance between gap centers is 4.00 mm. The considered substrate in these simulations is the Rogers R03010 with thickness $h = 1.27$ mm and dielectric constant $\varepsilon_r = 10.2$

Moreover, the presence of a transmission zero above the left handed band makes possible the synthesis of a symmetric response. Although this is irrelevant, if these structures are intended to be used as artificial transmission lines, this aspect can be important for filter design, as will be seen in Section 4.

## 3 Parameter extraction

From the electromagnetic simulation (using the commercial electromagnetic software Agilent Momentum) of the hybrid unit cell, the parameters of the equivalent circuit model can be extracted. Through the later comparison of the electromagnetic and electrical responses, the circuit model of Fig. 2*b* can be validated. Because of the high number of involved parameters, we cannot infer them simultaneously from the simulation of the whole structure. However, since the series gaps and the CSRRs/stubs alternate, we will assume that they are decoupled and, hence, we will consider the gaps and the rest of the structure separately. Thus, from the simulation of the isolated gaps, the values of $C_g$ and $C_f$ will be obtained. From the simulation of the structure formed by the rings and the shunt stub, we can obtain the rest of the parameters, in a similar way as it was done in [14]. The following expressions provide the normalised admittances corresponding to $C_g$ and $C_f$ from the simulated S-parameters of the series gap

$$\overline{Y}_f = -\frac{S_{11} + S_{21} - 1}{1 + S_{11} + S_{21}} \quad \overline{Y}_g = \frac{S_{21}(\overline{Y}_f + 1)}{1 + S_{11} - S_{21}} \tag{1}$$

The five remaining parameters of the model can be extracted from the electromagnetic simulation of the structure without gaps. To do that, some relevant frequencies must be identified from the electromagnetic simulation, following a method analogous to the one fully described in [16]. One of these frequencies is the transmission-zero frequency, $f_z$, which can be easily identified from the representation of $S_{21}$, and is related to the electrical parameters of the circuit model through the expression

$$\omega_Z = 2\pi f_z = \frac{1}{\sqrt{L_c(C + C_c)}} \tag{2}$$

On the other hand, the series and shunt impedances of this structure are

$$Z_s = j\omega\frac{L}{2} \tag{3}$$

$$Z_p = j\omega L_d \frac{1 - \omega^2 L_c(C + C_c)}{1 - \omega^2(L_c C + L_c C_c + L_d C) + \omega^4 L_c C_c L_d C} \tag{4}$$

Regarding previous structures, the parameter extraction method of this cell had to include some variations that its transmission characteristics require. In fact, the shunt branch formed by $L_d$, $C$, $C_c$ and $L_c$ exhibits not one, but two resonance frequencies, which can be inferred from the representation of the $S_{11}$ parameter in the Smith Chart.




doi: 10.1049/iet-map:20070225

Analytically, these two frequencies can be obtained by forcing the denominator of $Z_p$ in (4) to be zero. The solutions are given by

$$\omega_{0\pm} = \sqrt{\frac{\omega_r^2(1 + L_d C\omega_Z^2) \pm \sqrt{\omega_r^4(1 + L_d C\omega_Z^2(2 + L_d C\omega_Z^2)) - 4L_d C\omega_Z^4\omega_r^2}}{2L_d C\omega_Z^2}} \quad (5)$$

In (5), $\omega_z$ represents the transmission-zero angular frequency and $\omega_r$ is the resonance frequency of the CSRR, which is given by

$$\omega_r = 2\pi f_r = \frac{1}{\sqrt{L_c C_c}} \quad (6)$$

When the shunt path to ground is opened, that is at $\omega_{0+}$ and $\omega_{0-}$, the reactive part of the input impedance seen from the ports is only because of the line inductance $L$, whereas the resistive part has the value of the opposite port impedance, 50 Ω. This results in an intersection between the curve of the $S_{11}$ and the unit normalised resistance circle in the Smith Chart. This allows us to calculate the value of the inductance $L$ from the reactive part of the input impedance at $f_0$, which can be obtained from the simulation. On the other hand, if we represent the phase shift $\beta l$, we can find the frequency at which $\beta l = 90^\circ$ where, according to

$$\cos \beta l = 1 + \frac{Z_s(j\omega)}{Z_p(j\omega)} \quad (7)$$

the following condition is satisfied

$$Z_s(j\omega_{90}) = -Z_p(j\omega_{90}) \quad (8)$$

Thus, we have five conditions (given by expressions 2, 3, 5 and 8) and five parameters, so that circuit parameters are univocally determined. With this aim, the previous expressions have been inverted by using the commercial Maple 10 software. As a result of the application of this parameter extraction method to the structure of Fig. 2*a*, the values reported in Table 1 have been obtained

The seven extracted parameters provide the electrical response represented in Fig. 4, which also includes the electromagnetic simulation of the whole structure. Only $C$ has been slightly tuned to adjust the electrical and electromagnetic responses. This can be understood taking into account that this capacitance can be faintly influenced by the presence of series gaps. As can be seen in Fig. 4, there is very good agreement between the electrical and the electromagnetic simulations and, thus, the model properly describes this hybrid left handed structure and is validated with these results.

**Table 1** Extracted element parameters for the structure shown in Fig. 2a

| $C_g$, pF | $C_f$, pF | $C$, pF | $C_c$, pF | $L_c$, nH | $L_d$, nH | $L$, nH |
|---|---|---|---|---|---|---|
| 0.31 | 0.23 | 2.47 | 13.45 | 0.24 | 2.86 | 1.28 |

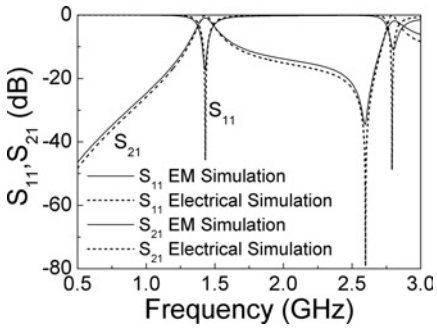


**Figure 4** *Electromagnetic simulation of the structure depicted in Fig. 2 compared with the electrical response of the circuit model using the parameter values obtained through the extraction method described above (see TABLE I)*

For this structure, the dimensions are $W = 4.41$ mm and $s = 0.16$ mm, whereas the length in the perpendicular direction to the line is $l = 7.02$ mm. The complementary split-ring resonators have $c = 0.16$ mm, $d = 0.15$ mm, and a total area $A = 4.01$ mm × 4.16 mm. Shunt stub length is $l_s = 2.99$ mm, and the via hole diameter is $v = 0.22$ mm. The distance between gap centers is 4.75 mm. The Rogers R03010 substrate, with thickness $h = 1.27$ mm and dielectric constant $\varepsilon_r = 10.2$, has been considered

## 4 Design and applications of the new artificial left handed transmission lines

To demonstrate the possibility of applying this new kind of artificial transmission lines to the design of microwave devices, a band pass filter and a power divider have been designed and fabricated. The power divider has been implemented by means of two identical left handed transmission lines with characteristic impedance $Z_0 = 70.71\ \Omega$ and electrical length $\beta l = -90^\circ$ (impedance inverters) at the desired operating frequency. The inverters have been designed to exhibit such electrical characteristics at 1.5 GHz. Fig. 5*a* shows the simulated insertion and return losses of the designed inverter that have been obtained through Agilent Momentum by using 70.71 Ω ports. It can be seen that impedance matching is obtained at 1.5 GHz, showing that the line exhibits the desired characteristic impedance at the operating frequency. The dispersion characteristics, depicted in Fig. 5*b*, indicate that the required phase is achieved at the design frequency (actually, the magnitude of the $\beta l$ has been depicted in this figure).

This artificial line has been used for the design of a narrow band 1:2 power divider at 1.5 GHz. The device consists of two left-handed lines exhibiting the indicated characteristics and three 50 Ω access lines. A high miniaturisation level is achieved by implementing the 70.71 Ω impedance inverters with left-handed lines. This can be appreciated in Fig. 6*a*,

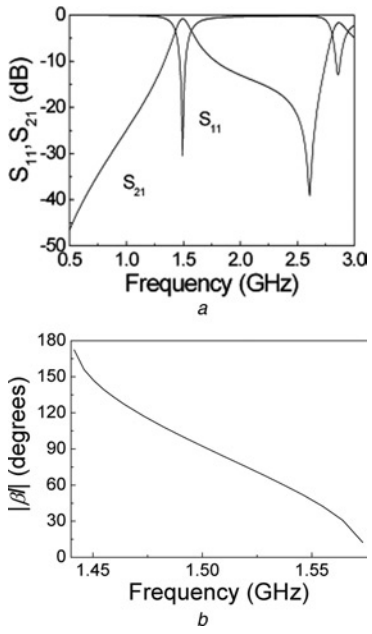


**Figure 5** *Electromagnetic simulation of the frequency response (a) and phase shift (b) of the transmission line designed to be applied in a two-output power divider*

At 1.5 GHz it exhibits a phase of 90° (b) and an impedance value of $Z_o = 70.71\ \Omega$ as can be seen in (a), where the $S_{21}$ and $S_{11}$, parameters have been simulated using 70.71 Ω ports

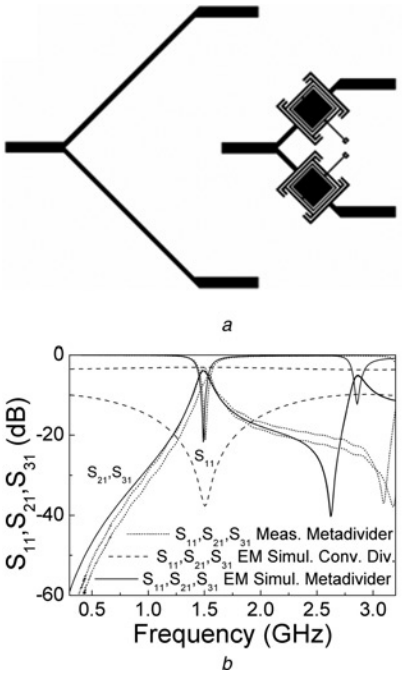


**Figure 6** *Layouts of the designed metadivider and a conventional power divider (a) and their electromagnetic simulation (b)*

In (b), the experimental response of the fabricated prototype is also shown. The dimensions of the unit cell used as inverter are the ones specified in Fig. 4, but the extremes of the gaps have been bent to increase size reduction. The total length of the inverters is 9.3 mm. The area of the metadivider, excluding access lines is $A = 8.0\ \text{mm} \times 13.6\ \text{mm}$

where the layouts of the 'metadivider' and conventional divider are compared. The 'metadivider' exhibits an area, which is approximately four times smaller than the area of the conventional device. This size reduction is significantly higher than that achieved by implementing the power divider through left handed lines with CSRRs etched on the ground plane [10], where 50% size reduction was obtained (when compared with the conventional device).

The 'metadivider' of Fig. 6 has been fabricated on the Rogers RO3010 substrate with thickness $h = 1.27$ mm and dielectric constant $\varepsilon_r = 10.2$. The measured (by means of the Agilent 8720ET vector network analyser) frequency response of this device is depicted in Fig. 6*b* together with the electromagnetic simulations of the conventional and designed left-handed power divider. A very good agreement between the experimental and simulated curves for the 'metadivider' can be observed, except around the transmission zero, where the deviation is attributed to the fabrication process. This is because of the small dimensions of some of the geometrical parameters, which are close to the resolution limits. The designed device exhibits good performance around its operating frequency (1.5 GHz). Measured power splitting is in the vicinity of −3 dB (the slight degradation in $S_{21}$ is also attributed to fabrication related tolerances) and return losses are better than −20 dB. This power divider is, thus, suitable for narrow band applications. The main advantage of the device when compared with conventional implementations is the size demonstrated to be better than in other proposals based on left handed lines with CSRRs etched on the ground plane. Moreover, the ground plane has not been altered with the proposed implementation. Obviously, the bandwidth is limited, and hence this type of power dividers are of interest for narrow band applications where size reduction is the main concern. There are quite recent works on the field based on composite right–left handed transmission lines based on series capacitances and shunt inductances [18, 19] which have achieved an important miniaturisation level and wide bandwidths. The results in this work are not presented as an improvement with respect to the previously mentioned works, but as a demonstration of the application possibilities of these structures based on CSRR where the ground plane is left unaltered and there is no need of using lumped elements.

To further demonstrate the application possibilities of these hybrid left handed structures, a narrow band pass filter has also been designed and fabricated. In this case, the presence of the transmission zero above the transmission band becomes important to improve (when compared with the purely resonant approach) the upper out-of-band filter performance and to obtain a symmetric response. The fabricated device is a periodic structure formed by three identical left handed cells constituted by two series gaps, a shunt connected stub and a complementary spiral resonator (instead of a CSRR, see Fig. 7). In this design, the spiral resonator has been used in order to move the transmission zero further away from the



*IET Microw. Antennas Propag.*, 2008, Vol. 2, No. 4, pp. 324–330
doi: 10.1049/iet-map:20070225

pass band of interest and to reduce unit cell dimensions [17]. This improves the out-of-band filter performance. The design methodology of this filter is that reported in [9], where a periodic band pass filter with CSRRs etched on the ground plane was designed and fabricated. As was done in [9], the part of the metallic film lying within the spirals has been removed to control the electric coupling (modelled by $C$). For the ease of comparison, the present band pass filter has been designed to exhibit an identical central frequency to that of the filter reported in [9], namely $f_o = 1$ GHz, although the fractional bandwidth is smaller (4.5%). Following [9], each filter section has been designed to exhibit a phase shift of $\beta l = -90^\circ$ and a characteristic impedance of $Z_o = 50\ \Omega$ at the central filter frequency, and the topology of each cell has been optimised to achieve the required 3 dB bandwidth (i.e. that providing the nominal fractional bandwidth 4.5%). Fig. 7*a* shows the layout of the designed filter, whose dimensions are $12 \times 54\ \text{mm}^2$ (dashed rectangle). These dimensions are significantly smaller than those of the periodic filter reported in [9] ($22 \times 45\ \text{mm}^2$). The simulated (by excluding losses) and measured frequency responses of the filter are depicted in Fig. 7*b*. The slight discrepancies between full wave electromagnetic simulation and the experiment are because of fabrication related tolerances (i.e. several filter dimensions are too close to the limits of tolerance of the available drilling machine LPKF HF100) and to the fact that losses have been ignored in the simulation to verify that the filter has been properly designed. The measured fractional bandwidth of the fabricated filter is 5%. This narrow band explains the measured level of in-band losses, which is in the vicinity of 5 dB. The unloaded $Q$-factor of the resonators has been estimated to be $Q_u = 77$ from the standard expression given below [20]

$$\text{IL(dB)} = \frac{4.343 \cdot f_0}{\text{BW} \cdot Q_u} \sum_{i=1}^{N} g_i \tag{9}$$

In (9) IL represents the insertion losses, $g_i$ are the prototype element values and $\text{BW}/f_0$ is the equal ripple frequency bandwidth. Return losses are better than $-15$ dB in the interval 0.997–1.020 GHz and the measured out-of-band rejection is better than 60 dB up to 1.71 GHz. Finally, the filter exhibits a very symmetric frequency response. We would like to emphasise that the losses of the designed filter are because of the considered narrow band and the number of unit cells, rather than being related to an improper filter design.

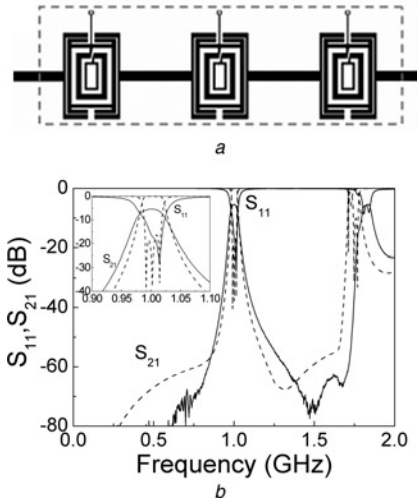


**Figure 7** *Layout of the designed band pass filter (a) and its simulated (dashed line) and measured (solid line) broadband response (b)*

The electromagnetic simulation of the device has been carried out without taking losses into account. The filter has been fabricated on identical substrate as the power divider. For the unit cell, $W = 7.43$ mm and $s = 0.16$ mm. The length of the lateral stubs forming the gaps is $l = 13.6$ mm, including the bent extremes. The complementary spiral resonators have $c_{inner} = 050$ mm, $c_{outer}0.62$ mm, $d = 0.5$ mm, and a total area $A = 4.77$ mm $\times$ 6.7 mm. Shunt stub length is $l_s = 3.97$ mm, and the via hole diameter is $v = 0.22$ mm. The distance between gap centers is 5.93 mm. The dimensions of the rectangle etched in the centre of the CSRs are $S = 1.1$ mm $\times$ 2.9 mm. The considered substrate in these simulations is the Rogers R03010 with thickness $h = 1.27$ mm and dielectric constant $\varepsilon_r = 10.2$. The dimensions of the dashed rectangle in (a) are $12 \times 54$ mm

## 5 Conclusion

In this work, a new type of one-dimensional left-handed structures based on CSRRs has been presented. All the elements of the structure lie on the top metal layer of the substrate, thus avoiding ground plane etching. In addition, shunt stubs have been introduced, in combination with the rest of the elements in the structure, to enhance design flexibility. This represents a clear advantage over previous CSRR-based left handed structures since small dimensions, good performance at the design frequency and device versatility (because of the fact that the structures can rest on a metallic holder) are simultaneously achieved. We would like to emphasise the fact that the structures presented in this work solve the problem of the left handed structures presented in [14], that is, the limited performance in terms of in-band losses. This limitation was attributed to the limited coupling between the line and the CSRRs. Introducing the shunt connected stubs, such a coupling is not relevant anymore and bandwidth and losses are improved.

An equivalent circuit model for these new left handed structures has been proposed and validated through a parameter extraction method. The new transmission lines are suitable for the design of compact narrow band microwave devices, as has been demonstrated through the design and fabrication of a power divider and a narrow band pass filter.

## 6 Acknowledgments

This work has been supported by MEC (Spain) under project contract TEC2004-04249-C02-01. Thanks are also given to the European Union for funding the Network of Excellence NoE METAMORPHOSE and to CIDEM

(Generalitat de Catalunya) for funding CIMITEC. Marta Gil was awarded with a FPU Grant by MEC (Spain) (Reference AP2005-4523)

## 7 References

[1] SMITH D.R., PADILLA W.J., VIER D.C., NEMAT-NASSER S.C., SCHULTZ S.: 'Composite medium with simultaneously negative permeability and permittivity', *Phys. Rev. Lett.*, 2000, **84**, pp. 4184–4187

[2] IYER A.K., ELEFTHERIADES G.V.: 'Negative refractive index metamaterials suppporting 2-D waves'. IEEE-MTT Int. Symp, Seattle, WA, June 2002, vol. 2, pp. 412–415

[3] OLINER A.A.: 'A periodic-structure negative-refractive-index medium without resonant elements'. URSI Digest, IEEE-AP-S USNC/URSI National Radio Science Meeting, San Antonio, TX, June 2002, p. 41

[4] CALOZ C., ITOH T.: 'Application of the transmission line theory of left-handed (LH) materials to the realization of a microstrip LH transmission line'. Proc. IEEE-AP-S USNC/URSI National Radio Science Meeting, San Antonio, TX, June 2002, vol. 2, pp. 412–415

[5] MARTÍN F., FALCONE F., BONACHE J., MARQUÉS R., SOROLLA M.: 'A new split ring resonator based left handed coplanar waveguide', *Appl. Phys. Lett.*, 2003, **83**, pp. 4652–4654

[6] FALCONE F., LOPETEGI T., LASO M.A.G., BAENA J.D., BONACHE J., MARQUÉS R., *ET AL.*: 'Babinet principle applied to the design of metasurfaces and metamaterials', *Phys. Rev. Lett.*, 2004, **93**, p. 197401

[7] BONACHE J., FALCONE F., BAENA J.D., LOPETEGI T., GARCÍA-GARCÍA J., LASO M.A.G., *ET AL.*: 'Application of complementary split-ring resonators to the design of compact narrow band pass structure in microstrip technology', *Microw. Opt. Technol. Lett.*, 2005, **46**, pp. 508–512

[8] BONACHE J., GIL M., GIL I., GARCÍA-GARCÍA J., MARTÍN F.: 'Limitations and solutions of resonant-type metamaterial transmission lines for filter applications: the hybrid appproach'. 2006 IEEE MTT-S Int. Microwave Symp. Digest, San Francisco, CA, USA, June 2006, pp. 939–942

[9] BONACHE J., GIL I., GARCÍA-GARCÍA J., MARTÍN F.: 'Novel microstrip band pass filters based on complementary split-ring resonators', *IEEE Trans. Microw. Theory Tech.*, 2006, **54**, pp. 265–271

[10] GIL M., BONACHE J., GIL I., GARCÍA-GARCÍA J., MARTÍN F.: 'Artificial left-handed transmission lines for small size microwave components: application to power dividers'. Proc. 36th European Microwave Conf. (EuMC 2006), Manchester, UK, September 2006, pp. 1135–1138

[11] BONACHE J., MARTEL J., GIL I., GIL M., GARCÍA-GARCÍA J., MARTÍN F., *ET AL.*: 'Super compact ($<1$ cm$^2$) band pass filters with wide bandwidth and high selectivity at C-band'. Proc. 36th European Microwave Conf. (EuMC 2006), Manchester, UK, September 2006, pp. 599–602

[12] GIL M., BONACHE J., SELGA J., GARCÍA-GARCÍA J., MARTÍN F.: 'Broadband resonant type metamaterial transmission lines', *IEEE Microw. Wirel. Compon. Lett.*, 2007, **17**, pp. 97–99

[13] GIL M., GIL I., BONACHE J., GARCÍA-GARCÍA J., MARTÍN F.: 'Metamaterial transmission lines with extreme impedance values', *Microw. Opt. Technol. Lett.*, 2006, **48**, pp. 2499–2505

[14] GIL M., BONACHE J., GARCÍA-GARCÍA J., MARTÍN F.: 'New left-handed microstrip lines with complementary split-ring resonators (CSRRs) etched in the signal strip'. 2007 IEEE MTT-S Int. Microwave Symp. Digest, Honolulu, (Hawaii), USA, June 2007, pp. 1419–1422

[15] GIL M., BONACHE J., GIL I., GARCÍA-GARCÍA J., MARTÍN F.: 'On the transmission properties of left handed microstrip lines implemented by complementary split-ring resonators', *Int. J. Numer. Model., Electron. Netw. Devices Fields*, 2006, **19**, pp. 87–103, Special Issue on Metamaterials

[16] BONACHE J., GIL M., GIL I., GARCIA-GARCÍA J., MARTÍN F.: 'On the electrical characteristics of complementary metamaterial resonators', *IEEE Microw. Wirel. Compon. Lett.*, 2006, **16**, pp. 543–545

[17] BAENA J.D., MARQUÉS R., MEDINA F., MARTEL J.: 'Artificial magnetic metamaterial design by using spiral resonators', *Phys. Rev. B*, 2004, **69**, (1), p. 014402

[18] ANTONIADES M.A., ELEFTHERIADES G.V.: 'A broadband series power divider using zero-degree metamaterial phase-shifting lines', *IEEE Microw. Wirel. Compon. Lett.*, 2005, **15**, pp. 808–810

[19] OKABE H., CALOZ C., ITOH T.: 'A compact enhanced-bandwidth hybrid ring using an artificial lumped-element left-handed transmission-line section', *IEEE Trans. Microw. Theory Tech.*, 2004, **52**, pp. 798–804

[20] BAHL I., BHARTIA P.: 'Microwave solid state circuit design' (John Wiley & Sons, 1998)



doi: 10.1049/iet-map:20070225

based interconnects, Electrical Performance of Electronic Packaging, 2005. IEEE 14th Topical Meeting, Oct 2005, pp. 147–150.
6. F. Capolino, D.R. Jackson, and D.R. Wilton, Mode excitation from sources in two-dimensional EBG waveguides using the array scanning method, Microwave Wireless Compon Lett IEEE 15 (2005), 49–51.
7. G. Goussetis, A.P. Feresidis, and P. Kosmas, Efficient analysis, design, and filter applications of EBG waveguide with periodic resonant loads, Microwave Theory Tech IEEE Trans 54 (2006), 3885–3892.



# PARAMETRIC ANALYSIS OF MICROSTRIP LINES LOADED WITH COMPLEMENTARY SPLIT RING RESONATORS

**Jordi Bonache, Marta Gil, Oscar García-Abad, and Ferran Martín**
GEMMA/CIMITEC, Departament d'Enginyeria Electrònica, Universitat Autònoma de Barcelona, 08193 Bellaterra (Barcelona), Spain; Corresponding author: Ferran.Martin@uab.es

*Received 5 December 2007*

**ABSTRACT:** *In this article, the effects of varying the geometry of complementary split ring resonators (CSRRs) in microstrip lines loaded with such resonant elements is analyzed. Specifically, from a parameter extraction technique previously proposed by some of the authors, the electrical parameters of CSRR-loaded lines (namely, the line inductance, the inductance and capacitance of the CSRR, and the coupling capacitance between the line and the CSRRs), are inferred. This analysis is of interest because, in spite of the existence of analytical models that predict the electrical parameters of these CSRR-loaded lines, the validity of these models is limited, and the parameter extraction method is necessary to accurately determine the electrical parameters from geometry. From the analysis carried out in this work, interesting conclusions for the design of CSRR-loaded lines are obtained.* © 2008 Wiley Periodicals, Inc. Microwave Opt Technol Lett 50: 2093–2096, 2008; Published online in Wiley InterScience (www.interscience.wiley.com). DOI 10.1002/mop.23571

**Key words:** *complementary split ring resonators (CSRRs); metamaterials; microstrip technology*

## 1. INTRODUCTION

Complementary split ring resonators (CSRRs), first proposed by Falcone et al. [1], are useful particles for the synthesis of resonant-type metamaterial transmission lines. By periodically loading a host (microstrip) line with CSRRs (etched in the ground plane), a one-dimensional effective medium with negative permittivity in a narrow band below the resonance frequency of CSRRs is created [1]. By adding series capacitive gaps above the positions of the CSRRs, a negative effective permittivity and permeability simultaneously arise, and the structure exhibits left handed wave propagation [2]. The small size of the unit cell of such artificial lines and the possibility to tailor their dispersion diagram and characteristic impedance has lead to many microwave applications of CSRR-loaded lines, where device miniaturization [3] and/or performance improvement [4] have been key aspects. The field of filters deserves special attention, since it has been found that CSRRs are also appropriate resonators either for the synthesis of novel compact planar filters [5–8] or to improve the performance (through spurious pass band suppression) of existing ones [9].

A typical unit cell of a microstrip line loaded with CSRRs and its lumped element equivalent T-circuit model are both depicted in Figure 1. In this model, which has been reported before [10], $L$ is the line inductance, $C$ is the coupling capacitance between the line and the CSRRs, and $C_c$ and $L_c$ model the reactive elements of the CSRRs, which are described by parallel resonant tanks. It has been demonstrated that this circuit model accurately describes the behavior of the unit cell structure and also the behavior of multiple cell structures, where the coupling between adjacent CSRRs is negligible [11, 12]. This has been confirmed from a parameter extraction method reported in Ref. 11. In this work, this method is applied to extract the parameters of a single-cell CSRR loaded line where the geometrical parameters of the CSRRs are varied. This includes the CSRR radius, as well as the width and separation of the slots (see Fig. 1 for details). From this parametric analysis, design guidelines for the CSRR-loaded lines will be obtained. This is useful since, in spite of the fact that there are analytical models

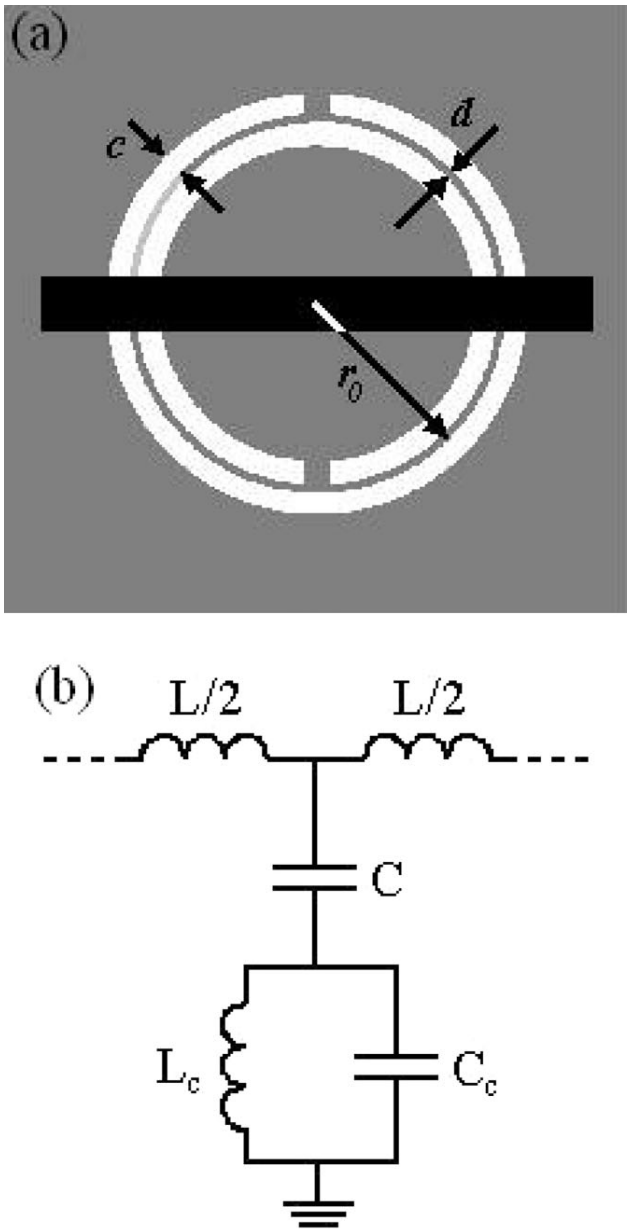


**Figure 1** Typical unit cell of a microstrip line loaded with CSRRs (a) and lumped element equivalent circuit model (b). The ground plane, where the CSRR is etched, is depicted in gray

that link the geometrical and electrical parameters of CSRRs [10], these models are valid under restrictive conditions, and they can only be used to provide an initial seed for the CSRR geometry, which needs optimization.

## 2. PARAMETRIC ANALYSIS

For the study, the parameters of the *Rogers RO3010* substrate with dielectric thickness $h = 1.27$ mm are considered (the dielectric constant is $\varepsilon_r = 10.2$). Losses are excluded in the simulations, hence metal thickness and tan $\delta$ are irrelevant for us. This "lossless" substrate is considered since the presence of losses may cause certain "noise" in the determination of the electrical parameters of the CSRRs. Nevertheless, the parameter extraction method perfectly works under lossy conditions since it has been applied to determine the electrical parameters of fabricated structures and these parameters have been inferred from the measured reflection and transmission coefficients (see Ref. 11 for details). With regard to the host line, it has a characteristic impedance of $Z_0 = 50\ \Omega$, which corresponds to a line width of $W = 1.16$ mm in such substrate.

In the first analysis, we set $c = d = 0.2$ mm and we obtain the electrical parameters of the unit cell model as a function of the average radius $r_0$ of the CSRR. The capacitance of the CSRR, $C_c$, is the edge capacitance of a metallic disk of radius $r_0 - c/2$, surrounded by a metal (ground plane) at a distance $c$ of its edge. The CSRR inductance, $L_c$, is given by the parallel connection of the two inductances connecting the inner disk to the ground. Each inductance is given by $L_0/2$, where $L_0 = 2\pi r_0 L_{opul}$ and $L_{opul}$ is the per unit length inductance of the CPWs connecting the inner disk to the ground [10]. According to this, one expects a linear dependence of $C_c$ and $L_c$ with $r_0$, or, in other words, we expect no dependence of these parameters with $r_0$ when they are divided by the average perimeter of the CSRR, namely, $2\pi r_0$. Such per unit length parameters, $C_{cpul}$ and $L_{cpul}$, have been inferred from the parameter extraction method for different values of the average radius, ranging in the interval 0.7 mm $< r_0 <$ 8 mm. The results are depicted in Figure 2. The parameters that result when dividing $L$ and $C$ by the average CSRR perimeter ($L_{pul}$ and $C_{pul}$), even though they do not have a physical meaning, have also been depicted in Figure 2. $L_{pul}$ and $C_{pul}$ are constant (except for small values of $r_0$, where this values become unrealistic), this being an expected result. However, $C_{cpul}$ and $L_{cpul}$ exhibit a certain variation with $r_0$ for small $r_0$ values, and then they saturate. This variation of $C_{cpul}$ and $L_{cpul}$ not accounted for by the analytical model [10], is attributed to the presence of the strip line at the other side of the substrate, the influence being more significant in small CSRRs.

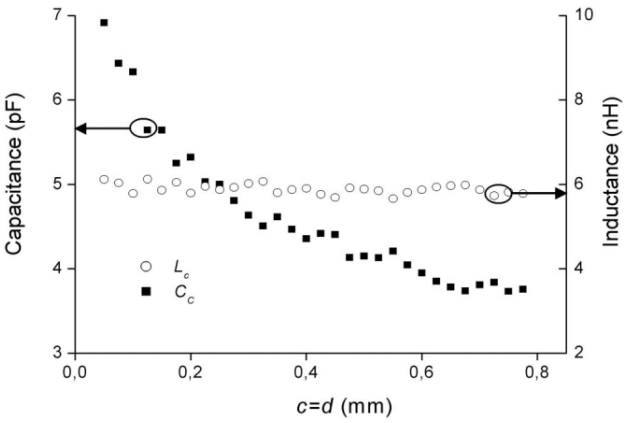


**Figure 3** Variation of $L_c$ and $C_c$ with $c = d$

The second analysis that has been carried out is the effect of varying $c$ and $d$, for a fixed value of the average radius. This has been set to $r_0 = 8$ mm, that is, in the region of saturation of the precedent analysis. Specifically, we have considered $c = d$ in this analysis. Obviously, this is not necessary, but by making this assumption, we reduce the number of variables. The effects of varying $c$ and $d$ on $L_c$ and $C_c$ are depicted in Figure 3. $L_c$ is weakly dependent on $c$ and $d$, whereas $C_c$ varies significantly. The ratio between these parameters is depicted in Figure 4. In the considered range (0.05 mm $< c = d <$ 0.75 mm), the ratio $L_c/C_c$ changes roughly between 900H/F and 1600H/F. Thus, this result can be obtained for design purposes. Namely, from the required values of $L_c$ and $C_c$ (determined from circuit specifications), the ratio $L_c/C_c$ can be obtained and from the curve of Figure 4, $c$ and $d$ can be determined. Once determined $c$ and $d$, the average radius can be modified to obtain the required value of either element. Obviously, the achievable values are limited since the CSRR can be neither large nor small.

It is worth mentioning that this study reveals that by using CSRRs, the ratio between the reactive elements ($L_c/C_c$) is limited to the resulting interval (see Fig. 4). If different values are necessary, other resonators such as the complementary spiral resonator

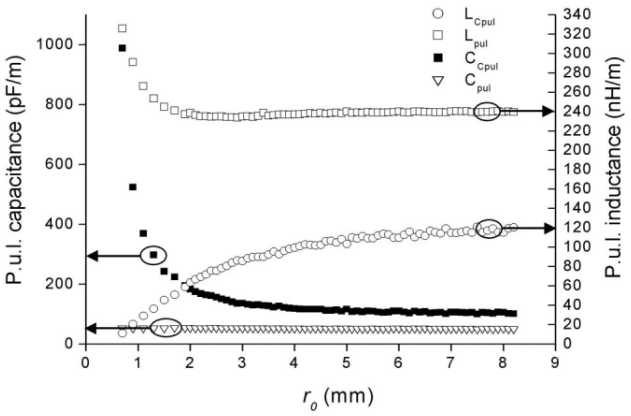


**Figure 2** Variation of *C*cpul, *L*cpul, *L*pul, and *C*pul with the average radius, $r_0$, of the CSRRs

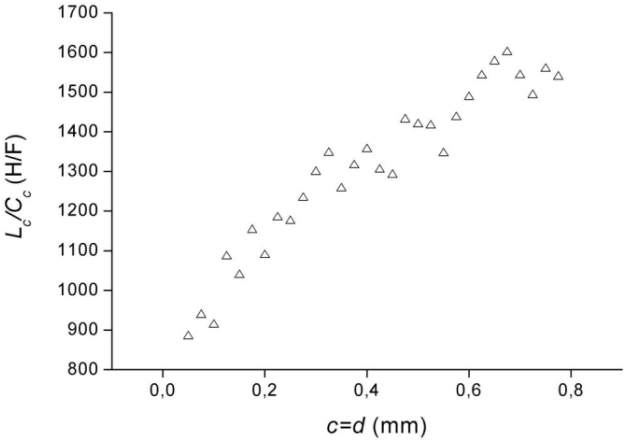


**Figure 4** Dependence of the ratio $L_c/C_c$ with $c = d$

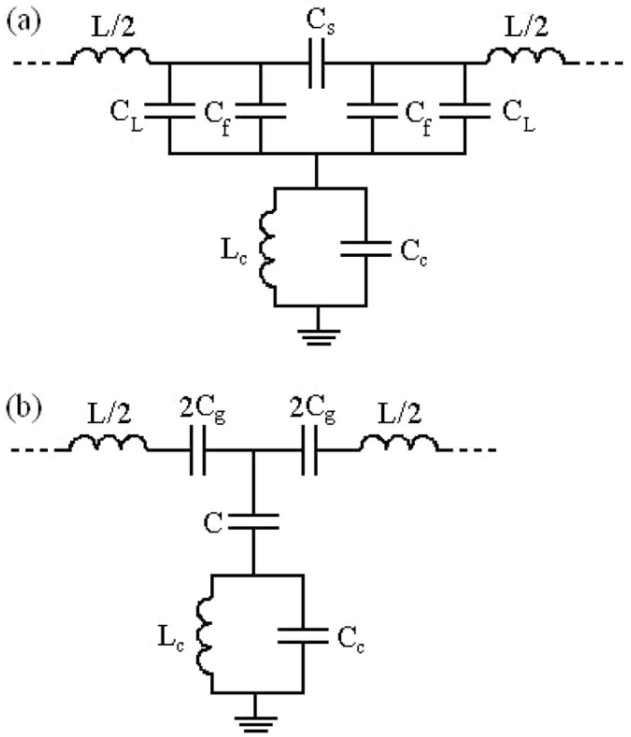


**Figure 5** Improved model (a) and previous model (b) of the unit cell of a microstrip line loaded with CSRRs and series gaps on top of it

(CSR) can be used (the circuit model of CSRs and its relationship with the circuit model of CSRRs has been reported before [10]).

## 3. THE PRESENCE OF A SERIES GAP IN THE STRUCTURE: DISCUSSION

In the preceding analysis, the presence of a series gap in the structure has been ignored. Indeed, the parameter extraction technique has also been applied to microstrip lines loaded with both CSRRs and series capacitive gaps etched above the position of the CSRRs [11]. With the presence of the series gaps, the structure exhibits a pass band behavior with left handed wave propagation in the first allowed band, as has been exhaustively reported [2, 10]. It has been previously found that the extracted parameters of CSRRs ($L_c$ and $C_c$) do not vary with and without the presence of the series capacitive gaps [11]. However, it has been found that the coupling capacitance $C$ is significantly enhanced when the series gap is present. The series capacitive gap introduces an extra capacitance to ground (fringing capacitance), but this can not actually explain such enhancement.

Actually, the series gap must be modeled by means of a $\pi$-circuit composed of three capacitors in either branch ($C_s$ for the series branch and $C_f$ for the fringing/parallel capacitance). According to this, the circuit model of the unit cell structure with the presence of the series gaps, should be modeled as Figure 5(a) illustrates, where $C_L$ is the contribution of the line capacitance. Obviously, from $\pi$–T transformation, the circuit model of Figure 5(b), which is the reported model of microstrip lines loaded with CSRRs and series gaps, is obtained, but the values of $C_g$ and $C$ do not actually have a physical interpretation. Indeed, $C_g$ and $C$ can be expressed in terms of $C_s$ and $C_{par} = C_f + C_L$ according to:

$$C_g = 2C_s + C_{par} \tag{1}$$

$$C = \frac{C_{par}(2C_s + C_{par})}{C_s} \tag{2}$$

Thus, if $C_s$ is small, the coupling capacitance can be very large, and this may occur in many practical situations. The main conclusion of this section is that the model of CSRR and gap-loaded lines reported previously is correct. It provides a good description of the structures, but it actually results from a transformation of another circuit model [Fig. 5(a)] where all the parameters have a physical interpretation.

## 4. CONCLUSIONS

In conclusion, from a previously reported parameter extraction method, we have extracted the parameters of the circuit model of a CSRR-loaded line with different CSRR geometries. The results obtained can be of interest to aid the design of planar microwave components based on CSRRs, since the analytical models of CSRR are valid under restrictive conditions. We have also discussed the effects of a gap capacitance etched in the line, and we have modified the equivalent circuit model to account for the enhanced coupling between the line and the CSRRs when the gap is present. Actually, the model can be transformed to the previous reported model with modified parameters. From this, the enhancement of the coupling capacitance when the gap is present can be perfectly explained.

## ACKNOWLEDGMENT

This work has been supported by MEC by project contract TEC2007-68013-C02-02. Marta Gil holds a FPU Grant, awarded by MEC (Reference AP2005-4523). Thanks are also given to the European Union for funding the Network of Excellence NoE METAMORPHOSE, and to the Catalan Government (CIDEM) for funding CIMITEC and for giving support through the action SGR-2005-00624.

## REFERENCES

1. F. Falcone, T. Lopetegi, J.D. Baena, R. Marqués, F. Martín, and M. Sorolla, Effective negative-$\varepsilon$ stop-band microstrip lines based on complementary split ring resonators, IEEE Microwave Wireless Compon Lett 14 (2004), 280–282.
2. F. Falcone, T. Lopetegi, M.A.G. Laso, J.D. Baena, J. Bonache, R. Marqués, F. Martín, and M. Sorolla, Babinet principle applied to the design of metasurfaces and metamaterials, Phys Rev Lett 93 (2004), 197401.
3. M. Gil, J. Bonache, I. Gil, J. García-García, and F. Martín, Miniaturization of planar microwave circuits by using resonant-type left handed transmission lines, IET Microwaves Antennas Propagat 1 (2007), 73–79.
4. G. Sisó, J. Bonache, M. Gil, J. García-García, and F. Martín, Compact rat-race hybrid coupler implemented through artificial left handed and right handed lines, Proceedings of the 2007 IEEE MTT-S International Microwave Symposium Digest, Honolulu, Hawaii, pp. 25–28.
5. J. Bonache, I. Gil, J. García-García, and F. Martín, Complementary split rings resonator for microstrip diplexer design, Electron Lett 41 (2005), 810–811.
6. J. Bonache, I. Gil, J. García-García, and F. Martín, Novel microstrip band pass filters based on complementary split rings resonators, IEEE Trans Microwave Theory Tech 54 (2006), 265–271.
7. M. Gil, J. Bonache, J. García-García, and F. Martín, Composite right/left handed (CRLH) metamaterial transmission lines based on complementary split rings resonators (CSRRs) and their applications to very wide band and compact filter design, IEEE Trans Microwave Theory Tech 55 (2007), 1296–1304.
8. P. Mondal, M.K. Mandal, A. Chaktabarty, and S.Sanyal, Compact

bandpass filters with wide controllable fractional bandwidth, IEEE Microwave Wireless Compon Lett 16 (2006), 540–542.
9. J. García-García, F. Martín, E. Amat, F. Falcone, J. Bonache, I. Gil, T. Lopetegi, M.A.G. Laso, A. Marcotegui, M. Sorolla, and R. Marqués, Microwave filters with improved stop band based on sub-wavelength resonators, IEEE Trans Microwave Theory Tech 53 (2005), 1997–2006.
10. J.D. Baena, J. Bonache, F. Martín, R. Marqués, F. Falcone, T. Lopetegi, M.A.G. Laso, J. García, I. Gil, and M. Sorolla, Equivalent circuit models for split ring resonators and complementary split rings resonators coupled to planar transmission lines, IEEE Trans Microwave Theory Tech 53 (2005), 1451–1461.
11. J. Bonache, M. Gil, I. Gil, J. Garcia-García, and F. Martín, On the electrical characteristics of complementary metamaterial resonators, IEEE Microwave Wireless Compon Lett 16 (2006), 543–545.
12. I. Gil, J. Bonache, M. Gil, J. García-García, and F. Martín, Left handed and right handed transmission properties of microstrip lines loaded with complementary split rings resonators, Microwave Opt Technol Lett 48 (2006), 2508–2511.



# MEMS-RECONFIGURABLE BANDPASS FILTER

**Laura Corchia, Giuseppina Monti, and Luciano Tarricone**
Department of Innovation Engineering, University of Salento, Via Monteroni, 73100, Lecce, Italy; Corresponding author: luciano.tarricone@unile.it

*Received 5 December 2007*

**ABSTRACT:** *This article presents a MEMS-based bandpass filter with a reconfigurable frequency response. The proposed device consists of a stub-loaded Branch-Line Coupler in artificial transmission line technology, resulting in a very compact structure. Furthermore, by using a micro electro mechanical system resistive switch, a reconfigurable frequency response has been obtained.* © 2008 Wiley Periodicals, Inc. Microwave Opt Technol Lett 50: 2096–2099, 2008; Published online in Wiley InterScience (www.interscience.wiley.com). DOI 10.1002/mop.23570

**Key words:** *micro electro mechanical system; artificial transmission lines; reconfigurability; branch-line coupler; bandpass filter*

## 1. INTRODUCTION

High performance bandpass filters are essential components in communication systems, and in the last years several design techniques have been developed to achieve both low insertion loss and high selectivity filtering responses [1–4]. Among these, particularly attractive is the solution proposed in [4], where a branch-line directional coupler (BLC) has been employed to achieve a high-selectivity filter based on signal-interference.

Furthermore, in many modern wireless communication systems there has been considerable interest in developing miniaturized devices with a reconfigurable frequency response [5–9]. Radio frequency (RF) microelectromechanical systems (MEMS) are one of the most promising technologies to meet these requirements providing low insertion loss, low-power consumption, and excellent linearity [7–10].

The bandpass filter proposed in this letter is based on the approach suggested in [4]; specifically, the stub-loaded BLC has been designed in artificial transmission lines (ATLs) technology leading to a very compact device; furthermore, to obtain a variable length loading stub, a micro electro mechanical system (MEMS) series resistive switch has been employed. This way, the filter selectivity and its stopband rejection can be customized acting on the switch state (ON/OFF).

The article is structured as follows: in Section 2 the fundamentals of the ATLs technology are given, later on, Section 3 illustrates the proposed reconfigurable bandpass filter. Finally results are given in Section 4 and some conclusions drawn in Section 5.

## 2. ARTIFICIAL TRANSMISSION LINES

The artificial transmission line concept is based on the possibility to model any dielectric with a distributed *L–C* network in low/high-pass topology. Relating the per-unit-length capacitance ($C_0$) and inductance ($L_0$) to the electric permittivity ($\varepsilon$) and magnetic permeability ($\mu$) of the medium as follows:

$$|\bar{\mu}| = \frac{Z}{j\omega} = \frac{j\omega L_0}{j\omega} = L_0, |\bar{\varepsilon}| = \frac{Y}{j\omega} = \frac{j\omega C_0}{j\omega} = C_0 \tag{1}$$

The transmission line (TL) propagation constant and its characteristic impedance become:

$$\beta_0 = \sqrt{-ZY} = \omega\sqrt{|\bar{\varepsilon}||\bar{\mu}|}, Z_0 = \sqrt{\frac{Z}{Y}} = \sqrt{\frac{L_0}{C_0}} = \sqrt{\frac{|\mu|}{|\varepsilon|}} \tag{2}$$

Consequently, the TL phase velocity is given by:

$$v_{p,TL} = \frac{1}{\sqrt{L_0 C_0}} \tag{3}$$

Now, let us consider the periodic structure reported in Figure 1 with a unit cell made of a TL loaded with a shunt capacitance; from the effective medium theory, one can derive that at frequencies corresponding to wavelengths much larger than the TL-length ($d$), this artificial transmission line (ATL) behaves as an "effectively homogeneous " TL, whose effective characteristic impedance and phase velocity are:

$$Z_{0ATL} = \sqrt{\frac{L_0}{(C_0 + C_p/d)}}, v_{pATL} = \frac{1}{\sqrt{L\left(C_0 + \frac{C_p}{d}\right)}} \phi_{ATL} = \frac{Nd\omega_0}{v_{pATL}} = Nd\omega_0\left[L_0\left(C_0 + \frac{C}{d}\right)\right]^{1/2} \tag{4}$$

Being $C_p$ the loading element, whilst $N$ is the number of unit cells.

From (3) and (4), it is evident that the ATL is characterized by a lower effective characteristic impedance and phase velocity. Consequently, the same electrical length can be achieved with a

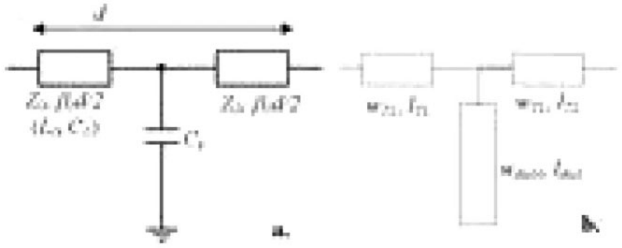

**Figure 1** Unit cell of an artificial TL obtained by periodically loading a conventional TL with a shunt capacitance and corresponding realization in microstrip technology

# Ultra Compact Band Pass Filters Implemented Through Complementary Spiral Resonators (CSRs)

Marta Gil, Jordi Bonache and Ferran Martín

GEMMA/CIMITEC, Departament d'Enginyeria Electrònica. Universitat Autònoma de Barcelona.
08193 BELLATERRA (Barcelona), Spain. E-mail: Ferran.Martin@uab.es

***Abstract* — In this work, it is shown that complementary spiral resonators (CSRs) etched in the ground plane of a microstrip line are useful for the implementation of band pass filters with very small dimensions and wide stop bands. By combining the CSRs with two series capacitive gaps and inductive vias, two transmission zeros arise. By properly allocating such transmission zeros at both sides of the pass band of interest, the out-of band rejection and frequency selectivity of the filters can be controlled. A prototype device example is reported to illustrate the performance and size of these CSR-based filters. This is an order-three Chebyshev band pass filter centered at $f_o$=1.1GHz with 10% fractional bandwidth. Measured in-band losses (optimum value) are *IL*=-4.42dB, in-band return losses are better than 9dB, and stop band rejection is better than 55dB up to 2.57GHz. Filter area is as small as 23.2 mm × 8.9 mm, that is $0.22\lambda \times 0.08\lambda$, where $\lambda$ is the wavelength (at the central filter frequency) of a 50Ω microstrip line in the considered substrate. The key novel and advantageous aspect of the reported filters is their small size, which is related to the small electrical size of CSRs. Another advantage is frequency selectivity, which is due to the presence of a transmission zero at both edges of the pass band. The limitative aspect is their relatively small un-loaded quality factor ($Q_u$), this being attributed to the small dimensions of the considered resonators. These CSR-based devices can be of interest in those applications where size and frequency selectivity are the most severe requirements.**

***Index Terms* — Microwave filters, complementary spiral resonators (CSRs), complementary split-ring resonators (CSRRs) split-ring resonators (SRRs).**

## I. INTRODUCTION

High performance and ultra compact planar filters are required in many microwave applications. To achieve small dimensions in planar technology, the semi-lumped approach is necessary. Within this approach, the reactive elements of the filters, that is, inductors, capacitors and/or resonators, are implemented by means of small size patterns printed in the substrate. A good description of semi-lumped element filters and related references is given in [1] and [2]. Among the different strategies to obtain filter miniaturization, split ring resonators (SRRs) have appeared in the scene (see their topology in Fig. 1). Originally proposed by Pendry [3], and subsequently employed for the synthesis of one- and two-dimensional left handed metamaterials by the group of D.R. Smith [4,5], SRRs have also been used as small resonant particles in the design of planar filters in coplanar waveguide (CPW) [6-9] and microstrip technologies [9,10]. In microstrip technology, compact band pass filters [11,13] and diplexers [14] have also been designed and fabricated by etching the complementary particles of the SRRs, namely the complementary split ring resonators (CSRRs) [15], in the ground plane.

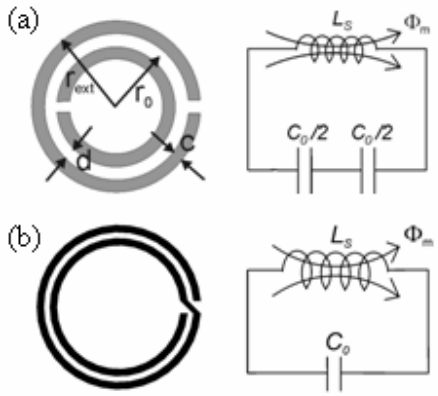


Fig. 1. Topologies of the SRR (a) and 2-SR (b), and their equivalent circuit models. $C_o$ is the edge capacitance between the concentric rings and $L_s$ is the inductance of a single closed ring with radius $r_o$ and width $c$ (see [17] for more details).

The electric coupling between the individual open rings forming the SRR is the cause of the small electrical size achievable with this particle [16] (from duality arguments, the electrical size of CSRRs and SRRs of identical dimensions is roughly the same [17]). However, due to technological constraints, it is difficult in practice to obtain diameters significantly smaller than $\lambda/10$ ($\lambda$ being the signal wavelength at resonance) in SRRs and CSRRs. To further reduce dimensions, SRRs have been implemented by using two metal levels separated by narrow substrates [18]. This enhances coupling (due to the broadside capacitance), but this strategy cannot be applied to CSRRs. Another possibility is a change in the topology of the particle, that is, to use two-turn or multi-turn spirals [19,20]. As compared to the SRR, the two-turn spiral resonator (2-SR, see Fig. 1) exhibits its first resonance at half the resonance frequency of the SRR (provided dimensions are identical) [17]. Thus, spiral resonators are a good solution to enhance miniaturization in microstrip filters based on complementary resonant particles etched in the ground plane.

978-1-4244-1780-3/08/$25.00 © 2008 IEEE

The purpose of this work is to demonstrate the miniaturization capability of complementary spiral resonators (CSRs) for the design of microstrip band pass filters with two transmission zeros and dual plane configuration. Such transmission zeros are useful to attenuate the stop band level and to sharpen the pass band response. The reported device example, an order-three band pass filter centered at $f_o$=1.1GHz, is very small ($0.22\lambda \times 0.084\lambda$), it exhibits reasonable in-band behavior, and the first spurious band appears close to $3f_o$.

## II. Filter Unit Cell and Analysis

The topology of the unit cell of the new filters is depicted in Fig. 2. It consists on a microstrip line configuration with a CSR etched in the ground plane, two series gaps and a metallic via (eventually, such via can be located at the extreme of a shunt stub to gain further design flexibility).

Fig. 2. Typical topology of the unit cell of the CSR-based structures applied in the design of the new filters. Metallic parts on the top layer are depicted in black. The CSR, which has been etched on the ground plane, has been depicted in gray for a proper view.

This kind of structure exhibits a left handed pass band response with two transmission zeros (one at each edge of the pass band), regardless of whether the structure is loaded with CSRs or CSRRs. The lower transmission zero frequency, $f_{z1}$, is mainly controlled by partially removing the metal inside the resonator, whereas the upper transmission zero frequency, $f_{z2}$, has been found to be very dependent on the diameter of the metallic via and/or stub length. Specifically, increasing the etched area inside the resonators, uppers $f_{z1}$, whereas increasing the length of the stub or reducing the diameter of the via, lowers $f_{z2}$. This behavior is illustrated in Fig. 3, where the simulated frequency response (obtained through the *Agilent Momentum* commercial software) of three different topologies is depicted (the parameters of the *Rogers RO3010* substrate with dielectric constant $\varepsilon_r$=10.2 and thickness $h$=1.27mm have been used).

In this paper, it is the first time that the two transmission zeros present in the structure are used to shape the frequency response. In previous works [11], where a similar topology to that of Fig. 2 was considered (but using only CSRRs), the first transmission zero was ignored. Actually, such transmission zero was found to be present at very small frequencies from electromagnetic simulation, but it was obscured by the floor noise in measurement. This is, therefore, the first time that this additional transmission zero located below the main transmission band is exploited.

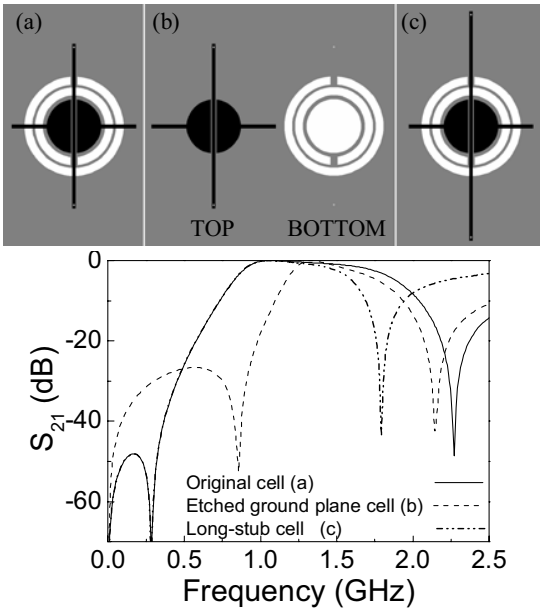


Fig. 3. Layouts and simulated insertion losses ($S_{21}$) corresponding to the indicated unit cells to appreciate the effects of varying the stub length and removing part of the metal inside the CSRRs.

Fig. 4(a) depicts the simulated and measured (through the *Agilent 8720ET* vector network analyzer) frequency response of the unit cell of Fig. 4(b). As can be appreciated, the transmission zeros are very close to the pass band of interest, thus providing high frequency selectivity to the resonator. This resonator, centered at 1.2GHz, has been designed to exhibit a 5% 3dB bandwidth.

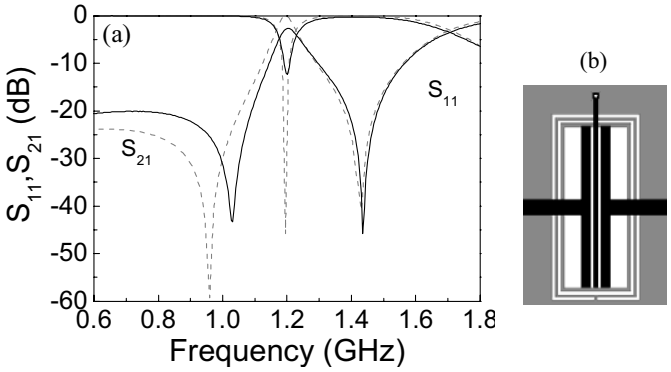


Fig. 4. (a) Measured (solid line) and simulated (dashed line) insertion and return losses for the fabricated resonator. The area of the rings is $a$=14.23 mm × 6.71 mm, their width is $c$=0.27 mm, separation between them $d$=0.17 mm, central etched area $a_p$= 12.24 mm × 4.82 mm. Regarding the top layer: line width and length $w_f$= 1.15 mm and, $l_f$= 2.5 mm, width and length of the central stub $w_s$=0.28 mm and $l_s$=14.8 mm, via radius $r_v$=0.1 mm, separation of the gap $g$=0.26 mm, total length of the gap, $l_g$= 12.28 mm, width of the lateral stubs forming the gap $w_g$=0.7 mm. (b) Layout of the structure.

978-1-4244-1780-3/08/$25.00 © 2008 IEEE

## III. FILTER DESIGN AND RESULTS

Based on one of the previous unit cells we have designed a band pass filter subjected to a standard Chebyshev response. In this case, CSRs have been used in order to obtain a more compact device. The initial specifications of the filter were: *FBW*= 10%, central frequency, $f_0$ =1.1GHz, 0.3 dB ripple, and 30dB rejection at 1.3GHz. The resulting filter is a 3-stage filter whose design coefficients are $g_1$=$g_3$=1.371, $g_2$=1.138, $g_4$=$g_0$=1. The methodology followed to obtain the different stages forming the filter was similar to that described in [11]. The different unit cells can be designed to set the position of the transmission zeros at the desired frequencies. In this case, the rejection band above the main transmission band has been widened by means of locating the upper transmission zero of each of the unit cells at different frequencies.

Fig. 5. Layout of the 3rd-order CSR-based Chebyshev filter. The black parts represent the metallic sections on the top layer whereas the CSRs etched on the ground plane are depicted in gray. The substrate employed is *Rogers RO3010* with $h$=0.635 mm and $\varepsilon_r$=10.2

The resulting device (Fig. 5) has very compact dimensions (0.22λ x 0.08λ) and it exhibits reasonable performance (see Figs. 6, 7). Its frequency response has been compared with that of a 3-stage standard parallel coupled line band pass filter with similar performance, but with a larger ripple (0.5 dB). As can be seen in Fig. 7(a), the responses of the two filters are very similar in the vicinity of the pass band. The CSR-based filter, in addition to its compact dimensions (nearly 5 times shorter than the coupled line filter, as Fig. 6 illustrates), presents its first spurious band at a higher frequency than the conventional does. We have also compared the dimensions of the new filter with those of a filter reported in [11], both exhibiting similar characteristics and implemented in substrates with identical dielectric constant. The area occupied by the new filter is significantly smaller, although in-band losses are also higher.

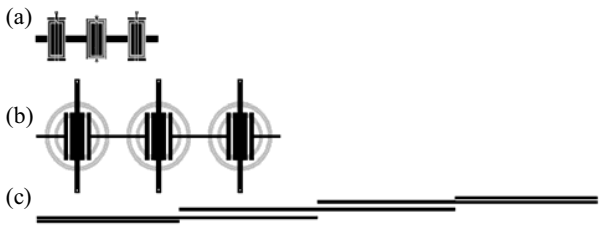


Fig. 6. Layout of the new CSR-based filter (a) compared with two similar filters: (b) The CSRR-based filter reported in [11] and (c) an order-3 filter based on parallel coupled lines.

The designed filter was fabricated and measured in order to corroborate the simulation results. The experimental results are shown in Fig. 7(b). As can be seen, the measured insertion and return losses are in good agreement with the simulation (which has been obtained by excluding ohmic and dielectric losses). Measured insertion losses are *IL*=-4.42 dB, and return losses are better than 9dB within the pass band of interest. The moderate values of the un-loaded quality factor ($Q_u$ ~ 47) associated to the compact resonators used in the design of the filter is the main cause of in-band losses. Out-band rejection is better than 55dB up to 0.87 GHz and between 1.9 GHz and 2.6GHz.

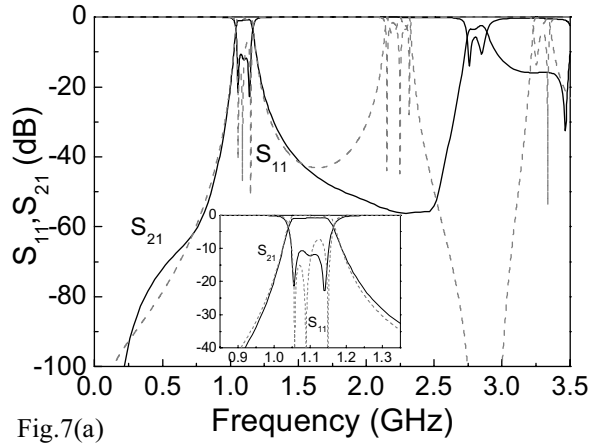


Fig.7(a)

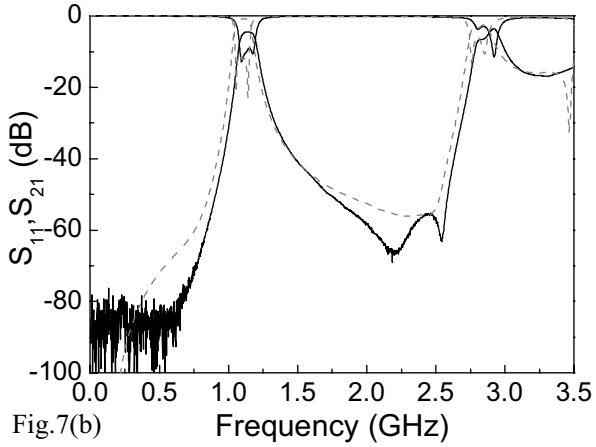


Fig.7(b)

Fig.7. (a) Simulated insertion and return losses for the designed CSR-based filter (solid line) and the coupled line filter (dashed line) designed for comparison. (b) Measured (solid line) and simulated (dashed line) insertion and return losses for the designed CSR-based filter.

## IV. CONCLUSIONS

In conclusion, a new and compact type of filters based on CSRs has been presented in this paper. The presence of two transmission zeros has been exploited for the first time in CSR/CSRR-based cells loaded with capacitive gaps and shunt inductances. The possibility of controlling the position of these two transmission zeros allows to obtain sharp pass

978-1-4244-1780-3/08/$25.00 © 2008 IEEE

bands. These cells can be applied to design standard filters that combine a very compact size and a reasonable performance. It has been demonstrated that the proposed filters can be designed to be five times shorter than conventional parallel coupled line band pass filters and two times shorter (but with a reduction of 500% in area) than other band pass filters previously designed by the authors and based on CSRRs. The stop band behavior is good, with the first spurious being allocated close to $3f_o$. The small size limits the quality factor and hence in-band losses. Obviously this aspect could be improved by using high temperature superconductors (HTS).

## ACKNOWLEDGEMENT

This work has been supported by MEC (Spain) by project contract TEC2004-04249-C02-01 METASYSTEMS and by the European Commission (VI Framework Program) through the contract NoE. 500252-2 METAMORPHOSE. Special thanks are also given to CIDEM (*Generalitat de Catalunya*) for funding CIMITEC. MEC has given an FPU Grant to Marta Gil (Reference AP2005-4523).

## REFERENCES

[1] J-S. Hong and M.J. Lancaster, *Microstrip filters for RF/microwave applications*, John Wiley, New York (USA), 2001.

[2] G.L. Mathaei, L. Young and E.M.T. Jones, *Microwave filters impedance-matching networks, and coupling structures*, Artech House, Norwood (MA), 1980.

[3] J.B. Pendry, A.J. Holden, D.J. Robbins and W.J. Stewart, "Magnetism from conductors and enhanced nonlinear phenomena", *IEEE Transactions Microwave Theory Tech.,* vol. 47, pp. 2075-2084, 1999.

[4] D.R. Smith, W.J. Padilla, D.C. Vier, S.C. Nemat-Nasser and S. Schultz, "Composite medium with simultaneously negative permeability and permittivity", *Phys. Rev. Lett*., vol. 84, pp. 4184-4187, 2000.

[5] R.A. Shelby, D.R. Smith and S. Schultz, "Experimental verification of a negative index of refraction", *Science*, vol. 292, pp. 77-79 (2001).

[6] F. Martín, F. Falcone, J. Bonache, T. Lopetegi, R. Marqués and M. Sorolla, "Miniaturized CPW stop band filters based on multiple tuned split ring resonators" *IEEE Microwave and Wireless Components Letters*, vol. 13, pp. 511-513, December 2003.

[7] F. Falcone, F. Martín, J. Bonache, R. Marqués, T. Lopetegi and M. Sorolla, "Left handed coplanar waveguide band pass filters based on bi-layer split ring resonators", *IEEE Microwave and Wireless Components Letters*, vol. 14, pp. 10-12, January 2004.

[8] J. Bonache, F. Martín, F. Falcone, J. García, I. Gil, T. Lopetegi, M.A.G. Laso, R. Marqués, F. Medina, M. Sorolla, "Super compact split ring resonators CPW band pass filters", *IEEE-MTT-S International Microwave Symposium Digest*, Fort Worth (TX), USA, pp. 1483-1486, June 2004.

[9] J. García-García, J. Bonache, I. Gil, F. Martín, M.C. Velazquez-Ahumada and J. Martel, "Miniaturized microstrip and CPW filters using coupled metamaterial resonators", *IEEE Transactions on Microwave Theory and Techniques*, vol. 54, pp. 2628-2635, June 2006.

[10] García-Lamperez, A., Salazar-Palma, M.. "Dual band filter with split-ring resonators". I*EEE MTT-S International Microwave Symposium Digest*, San Francisco, CA, USA, June 11-16, 2006**.**

[11] J. Bonache, I. Gil, J. García-García, F. Martín, "Novel Microstrip Band Pass Filters Based on Complementary Split Rings Resonators", *IEEE Transactions on Microwave Theory and Techniques*, vol. 54, pp. 265-271, January 2006.

[12] P. Mondal, M. K. Mandal, A. Chaktabarty*, Senior Member, IEEE*, and S. Sanyal. "Compact Bandpass Filters With Wide Controllable Fractional Bandwidth". *IEEE Microwave and Wireless Components Letters*, Vol. 16, No. 10, October 2006.

[13] M. Gil, J. Bonache, J. García-García and F. Martín, "Composite Right/Left Handed (CRLH) Metamaterial Transmission Lines Based on Complementary Split Rings Resonators (CSRRs) and Their Applications to Very Wide Band and Compact Filter Design", IEEE Transactions on Microwave Theory and Techniques, *IEEE Transactions on Microwave Theory and Techniques*, vol. 55, pp. 1296-1304, June 2007.

[14] J. Bonache, I. Gil, J. García-García and F. Martín, "Complementary split rings resonator for microstrip diplexer design", *Electronics Letters*, vol. 41, pp. 810-811, July 2005.

[15] F. Falcone, T. Lopetegi, J.D. Baena, R. Marqués, F. Martín and M. Sorolla, "Effective negative-ε stop-band microstrip lines based on complementary split ring resonators", *IEEE Microwave and Wireless Components Letters*, vol. 14, pp. 280-282, June 2004.

[16] J. García-García, F. Martín, J.D. Baena, R.Maqués, J. Jelinek. "On the resonances and polarizabilities of split rings resonators", *J. Applied Physics*, vol. 98, pp. 033103-1-9, September, 2005.

[17] J.D. Baena, J. Bonache, F. Martín, R. Marqués, F. Falcone, T. Lopetegi, M.A.G. Laso, J. García, I Gil and M. Sorolla, "Equivalent circuit models for split ring resonators and complementary split rings resonators coupled to planar transmission lines", *IEEE Transactions on Microwave Theory and Techniques*, vol. 53, pp. 1451-1461, April 2005.

[18] R. Marqués, F. Mesa, J. Martel and F. Medina in "Comparative analysis of edge and broadside coupled split ring resonators for metamaterial design. Theory and Experiment", *IEEE Trans. Ant. Propag*., vol. 51, pp..2572-2581, 2003.

[19] J.D.Baena, R. Marqués and F. Medina. "Artificial magnetic metamaterial design by using spiral resonators". *Physical Review B*. vol 69, 0.14402, 2004.

[20] K. Boratay, F. Bilotti, E. Ozbay. ''Miniaturized negative permeability materials''. *Applied Physics Letters* vol. **91**, 071121, 2007.

ARTICLE L

Available online at www.sciencedirect.com
ScienceDirect
Metamaterials 2 (2008) 186–197
Metamaterials
www.elsevier.com/locate/metmat

Invited Paper

# Metamaterial filters: A review

M. Gil*, J. Bonache, F. Martín

*GEMMA/CIMITEC, Departament d'Enginyeria Electrònica, Universitat Autònoma de Barcelona, 08193 Bellaterra, Barcelona, Spain*

Received 5 June 2008; received in revised form 17 July 2008; accepted 21 July 2008
Available online 15 August 2008

**Abstract**

In this paper, a review on metamaterial filters is presented. Several filters based on resonant-type composite right/left-handed metamaterial transmission lines are revised. The different results presented show the application possibilities of such structures in the design of filters with different bandwidths and performances. Some results based on other approaches are also shown.


*PACS:* 84.30.Vn; 84.32.-y; 84.40.Az

*Keywords:* Metamaterials; Filter; Split-ring resonator; Complementary split-ring resonator

## 1. Introduction

The main aim of this work is to review the work developed in this research group during the last years in the implementation of metamaterial filters based on resonant-type metamaterial transmission lines, which combine sub-wavelength resonators to, together with other elements like series capacitances or shunt inductances, load a host transmission line and obtain a propagating medium with controllable characteristics. These lines offer the possibility of tailoring their phase and impedance, what makes them suitable for, not only filter, but, in general, microwave device design. Power dividers, rat-race hybrid couplers, phase shifters, are some examples of the application possibilities of these resonant-type metamaterial transmission lines [1–3], which even offer the possibility of bandwidth enhancement [4] or dual-band operation [5].

One of the first issues to be discussed may be, perhaps, the use of the term "metamaterial" to name these devices based on such kind of lines. The authors do not apply the label metamaterial intending to main that such structures compose periodic, homogeneous and isotropic media with negative effective $\varepsilon$ and $\mu$ parameters. Actually, most of our devices are based on only one unit cell and talking about effective parameters has no sense. What the authors try to point out calling these devices as "metadevices" is the fact that they are based on sub-wavelength resonators, like the SRRs [6], whose sub-wavelength characteristics opened the door to the synthesis of the first left-handed medium [7], and the fact that, indeed, most of these transmission lines exhibit backward propagation. In fact, the nature of the propagation is irrelevant in most of the devices based on resonant-type transmission lines. It is, on the contrary, the controllability of their electrical characteristics (beyond what is achievable in conventional lines) and the possibility that they offer to design compact devices what is exploited

* Corresponding author. Tel.: +34 93 581 3524; fax: +34 93 581 2600.
*E-mail addresses:* Marta.Gil.Barba@uab.es (M. Gil), Ferran.Martin@uab.es (F. Martín).

1873-1988/$ – see front matter © 2008 Elsevier B.V. All rights reserved.
doi:10.1016/j.metmat.2008.07.006

from these metamaterial resonator-based transmission lines.

As was mentioned above, in this article we will make a review on the different kinds of metamaterial filters based on resonant-type metamaterial transmission lines since their appearance in 2003 [8]. Their frequency response immediately suggested their application possibilities as filtering structures and, since that moment, an important amount of works has been devoted to the implementation and improvement of this kind of filters. One of the first strategies applying such metamaterial resonators consisted in their inclusion as additional elements in conventional filters for out-of-band rejection improvement [9,10]. Without entailing a considerable area increment, SRRs can be printed close to the coupled-line sections in a conventional coupled-line bandpass filter and, when properly tuned, they can eliminate spurious bands and thus improve out-of-band rejection. In such filters, however, SRRs are merely added to a conventional distributed filter as signal rejecting elements, but they do not contribute as basic elements to generate a controllable transmission band. In the following sections, we will focus on filters in which metamaterial resonators are essential elements in the transmission lines forming the different stages of the filter. Diverse strategies and kinds of unit cells applied to design a big variety of filters with different performances are shown. Finally, several filters based on other approaches are also shown as examples of the application possibilities that metamaterial transmission lines offer in filter design.

## 2. Resonant-type metamaterial transmission lines

As has been previously mentioned, the resonant-type metamaterial transmission lines use different kinds of sub-wavelength resonators like, for example, split-ring resonators (SRRs) [6] or complementary split-ring resonators (CSRRs) [11] to load a host transmission line and, in combination with other elements, obtain a propagating media with controllable characteristics. These properties are mainly the phase shift and the characteristic impedance of the line [12,13]. Due to the small dimensions of these resonators, the resulting transmission lines can be very compact and, once the line has been designed to exhibit certain characteristics to be applied in the design of a specific device, its size can be reduced in an important factor [3,1].

The resonant-type approach is not the only one dedicated to the synthesis of composite right/left-handed transmission lines (CRLH TLs). The first transmission lines with composite characteristics appeared in 2002 [14,15] and consisted on a conventional transmission line loaded with shunt inductances and series capacitances (which can be implemented, for instance, as capacitive gaps). These loading elements provide a series capacitive impedance and a shunt inductive impedance in a certain frequency range, what is necessary to exhibit left-handed propagation [14]. Furthermore, the effect of the parasitic elements of the host line provides right-handed propagation at higher frequencies, where the series impedance is inductive and the shunt impedance is capacitive, giving rise to a composite right/left-handed behaviour. These CL-loaded CRLH TLs can also be applied in the design of microwave devices giving rise to very competitive components applying different design strategies [16,17].

The first resonant-type composite right/left-handed metamaterial transmission line was implemented in 2003 [8]. It consisted on a coplanar waveguide loaded with SRRs etched on the bottom layer of the substrate and signal-to-ground strips. The combination of the resonators, which were excited by the magnetic field generated by the line, and the metallic wires, provided the shunt and series impedance values required to exhibit the left-handed propagation (see Fig. 1), whereas right-handed wave propagation appeared at higher frequencies (not shown in Fig. 1).

The equivalent circuit model for this structure can be seen in Fig. 1(c). In the model, $C$ represents the line capacitance, $L_p$, the metallic connections between line and ground, $L$ corresponds to the line inductance, and the resonators are modelled by the resonant tanks formed by $C_s$ and $L_s$, which are magnetically coupled to the line through the mutual inductance $M$. This circuit can be transformed into the one depicted in Fig. 1(d) by means of the following transformations [18]:

$$L'_s = 2M^2 C_s \omega_0^2 \frac{(1 + L/4L_p)^2}{1 + M^2/2L_pL_s} \tag{1}$$

$$C'_s = \frac{L_s}{2M^2\omega_0^2}\left(\frac{1 + M^2/2L_pL_s}{1 + L/4L_p}\right)^2 \tag{2}$$

$$L' = \left(2 + \frac{L}{2L_p}\right)\frac{L}{2} - L'_s \tag{3}$$

$$L'_p = \left(2L_p + \frac{L}{2}\right) \tag{4}$$

The model shown in Fig. 1(c) is a recently improved version of the previous one and has been proved to be physically more accurate than the existing one. As can be seen in Fig. 1(d), the loading elements, that is, the SRRs and the shunt inductances contribute to obtain a capaci-

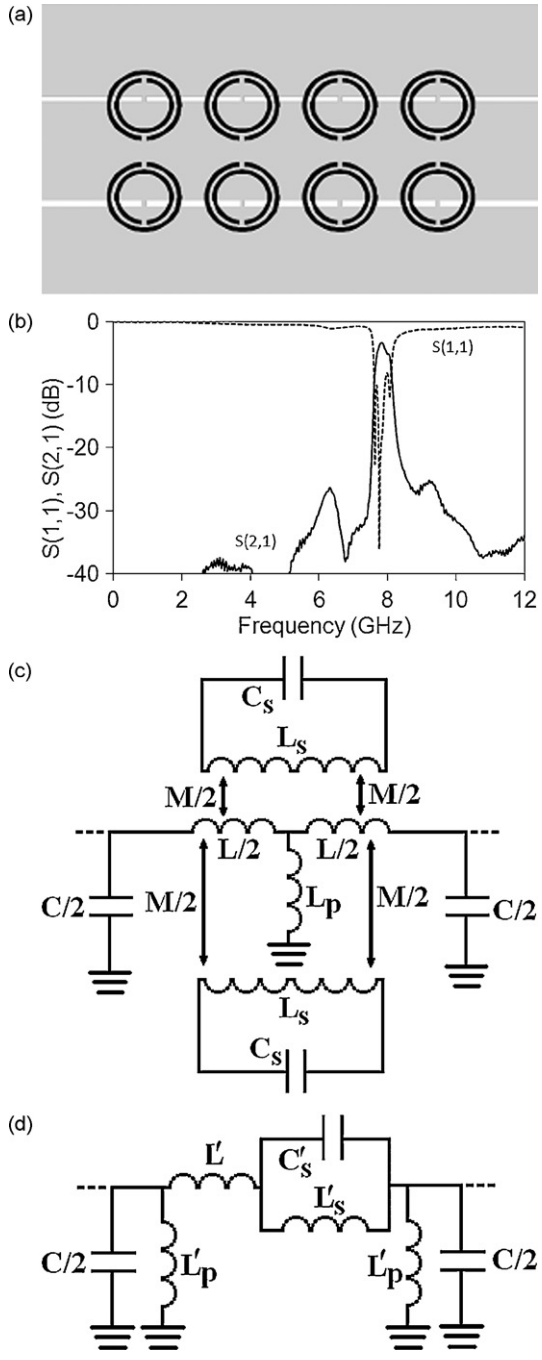


Fig. 1. (a) Layout of a SRR-based CPW left-handed transmission line. The CPW line is loaded with shunt inductances and SRRs lying on the opposite side of the substrate. Metallic parts are depicted in grey for the top layer and in black for the bottom layer. The length of the unit cell is $l = 5$ mm while the centre conductor and slot widths are $W = 4$ mm and $G = 0.3$ mm, respectively. The rings have an internal radius of $r = 1.3$ mm, widths of $c = 0.2$ mm and a separation of $d = 0.2$ mm. Arlon 250-LX-0193-43-11 substrate with dielectric constant $\varepsilon_r = 2.43$ and thickness $h = 0.49$ mm was used. (b) Measured frequency response of the device shown in (a). (c) Equivalent circuit model for the structure shown in (a). (d) Modified circuit (equivalent to that in c).

tive series impedance and an inductive shunt impedance in a certain frequency range, where left-handed propagation will be allowed.

SRR-based transmission lines were the first to appear and to be applied in the design of filters. However, since the appearance of the CSRR as the complementary counterpart of the SRR, several unit cells have been developed based on these particles [19,11,20] and CSRRs have become the most frequently applied resonators. The simplest and most commonly used unit cell combines CSRRs with capacitive gaps etched on a microstrip line. The resonators are etched on the ground plane, below the capacitive gaps (see Fig. 2(a)), and they are excited by the electric field going from the line towards the ground plane. The equivalent circuit model of these structures, as in the case of the SRR-based lines, has been recently improved and a physically more accurate model has been obtained [21]. In the new circuit model (Fig. 2(c)) the inductance of the line is represented by $L$ and the resonant tank formed by $L_c$ and $C_c$ takes into account the presence of the CSRR. Additionally, the model includes three different capacitances to model the capacitive gap ($C_s$, $C_f$) and the electrical coupling between the line and the CSRR ($C_L$). By this means, the gap is modelled by a $\Pi$-circuit in which $C_s$ represents the series capacitance and $C_f$ is the fringing capacitance. The effect of the gap and the coupling between the line and the resonator are taken into account separately. This improved model can be transformed into the former one (Fig. 2(d)) by means of the following transformations:

$$C = \frac{C_{par}(2C_s + C_{par})}{C_s} \tag{5}$$

$$C_g = 2C_s + C_{par} \tag{6}$$

with:

$$C_{par} = C_f + C_L \tag{7}$$

This transformed T-circuit model differs from the LC-loaded transmission line one on the presence of the capacitance $C$, which is responsible for the existence of a transmission zero below the left-handed transmission band.

If a shunt inductance is added to the previous structure, a new unit cell with a different behaviour is obtained: the hybrid cell (see Fig. 2(b)). The additional element contributes to obtain backward propagation at lower frequencies and represents an extra degree of freedom when designing the line. Furthermore, it modifies the characteristics of the line. In this case, at the frequency in which the shunt impedance (see Fig. 2(e)) nulls, the response presents a transmission zero which,

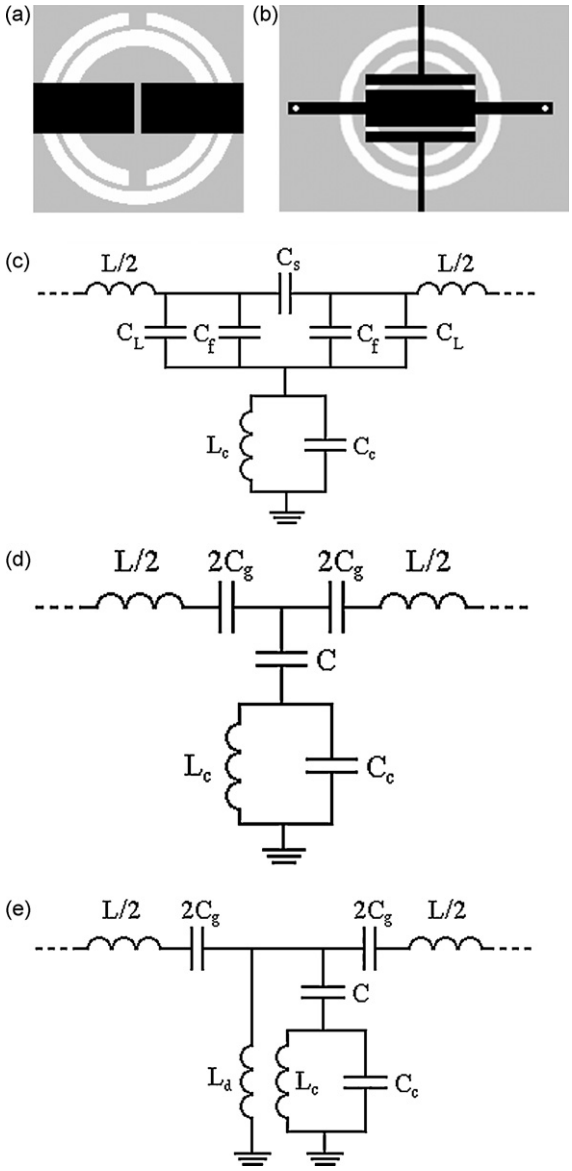


Fig. 2. (a) Layout of a purely resonant CSRR-based unit cell. Metallic parts are depicted in grey for the bottom layer and in black for the top layer. (b) Layout of a hybrid cell based on CSRRs. Metallic parts are depicted in grey for the bottom layer and in black for the top layer. Via have been depicted in white. (c) Improved equivalent circuit model for the purely resonant cell. (d) Modified equivalent circuit model for the purely resonant cell. (e) Equivalent circuit model for the hybrid cell.

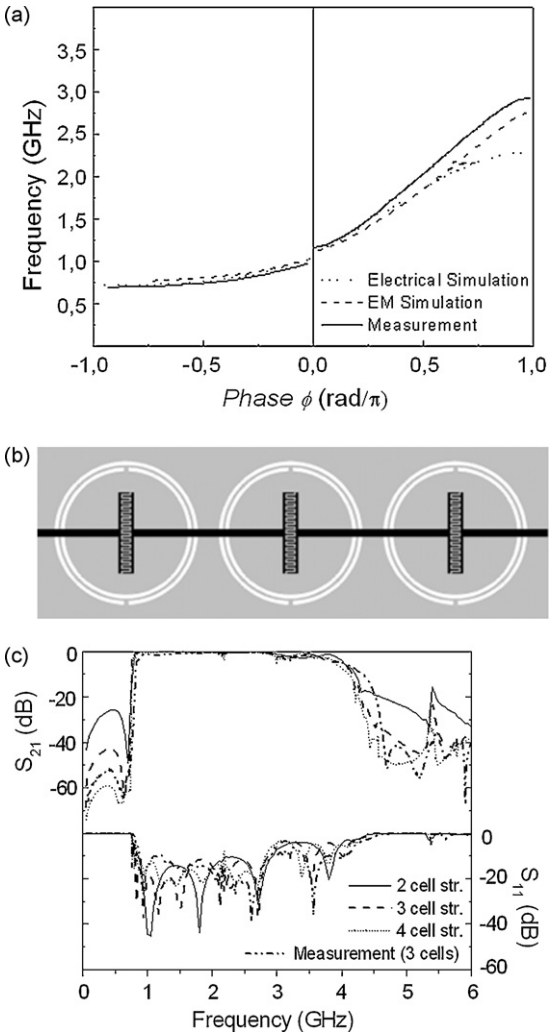


Fig. 3. (a) Dispersion diagram for a purely resonant CSRR-based balanced transmission line. The frequency gap that usually separates the left-handed and the right-handed bands, has been forced to disappear in order to obtain a broad transmission band with composite characteristics. (b) Layout of a high-pass filtering structure formed by three balanced unit cells. Metallic parts are depicted in grey for the bottom layer and in black for the top layer. *Rogers RO3010* substrate has been used, with thickness $h = 1.27$ mm and dielectric constant $\varepsilon_r = 10.2$. Dimensions are: total length $l = 55$ mm, line width $W = 0.8$ mm, external radius of the outer rings $r = 7.3$ mm, ring width $c = 0.4$ mm and ring separation $d = 0.2$ mm; the interdigital capacitors are formed by 28 fingers separated 0.16 mm. (c) Responses of several structures formed by different number of stages. Frequency selectivity is enhanced as the number of stages increases. Figure (a) reprinted with permission from [22]; © 2007 IEEE.

contrary to the purely resonant case, is located above the left-handed band. This transmission zero can be very useful to obtain a good rejection level above the pass band in filter applications.

Provided that both, the purely resonant and the hybrid transmission line, just like the LC-loaded transmission line, have a composite behaviour [22], they can be designed to be balanced and exhibit broad-band responses. The balance condition is satisfied when the upper limit of the left-handed band coincides with the lower limit of the right-handed band. If that is the case, there is a continuous transition between both bands; the

frequency gap that normally separates the bands disappears and, as a result, a broad transmission band with right-handed and left-handed characteristics is obtained (see Fig. 3).

## 3. Metamaterial filters

The frequency selectivity of resonant-type metamaterial transmission lines suggests their application in filter design. Furthermore, the possibility of obtaining such broad responses by means of balanced lines opens the door to the application of these structures in the design of broad-band filters. As has been previously mentioned, the characteristics of the lines can be tailored to some extent in order to obtain the desired response. Additionally, the position of the transmission zeros can be set to eliminate spurious bands and to control the out-of-band rejection, which can also be improved increasing the number of stages. These properties have been exploited and applied to the design of several kinds of filters since the first resonant metamaterial transmission lines arose.

### *3.1. Filters based on alternate right/left-handed cells*

One of the first strategies applied in the design of filters based on these transmission lines was the combination of different cells with right-handed and left-handed behaviour to obtain a bandpass response [23–25]. These two kinds of lines present a transmission zero above and below the first transmission band, what allows to obtain a bandpass behaviour with a sharp cutoff at both sides of the band (see Fig. 4). The use of only one kind of cell provides a poor rejection level

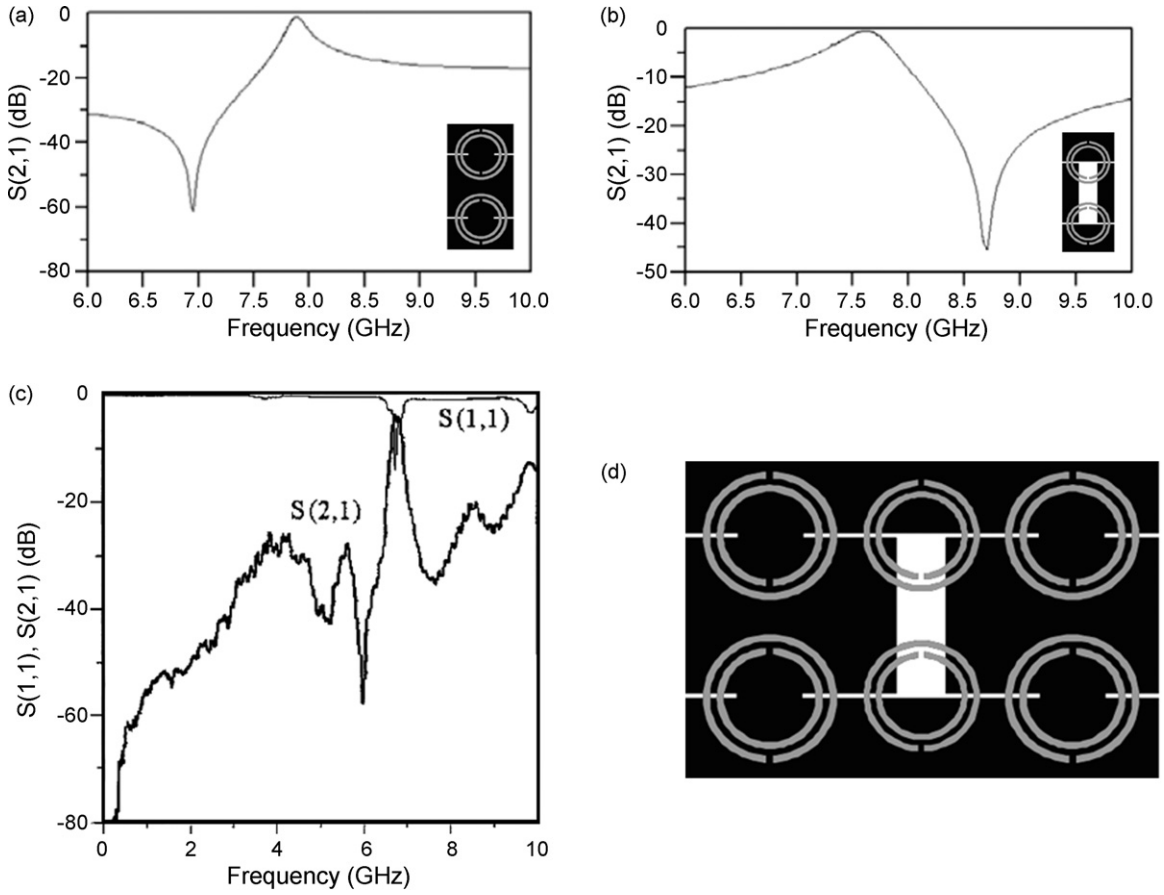


Fig. 4. (a) Frequency response of a SRR-based CPW left-handed line. (b) Frequency response of a SRR-based CPW right-handed line. (c) Measured frequency response of the filter combining one right-handed and two left-handed unit cells. (d) Layout of the filter combining one right-handed and two left-handed unit cells. Metallic parts are depicted in black for the top layer and in grey for the bottom layer of the substrate. Substrate *Arlon 250-LX-0193-43-11* with $\varepsilon_r = 2.43$ and thickness $h = 0.49$ mm was used. The smaller SRR radius is $r = 1.39$ mm, width and distance between the rings $c = d = 0.2$ mm are the same in all SRRs. The radius of the bigger SRRs is $r = 1.52$ mm. Wire width is $w_w = 2.16$ mm, gap length is $l_g = 1.6$ mm and the total length of the filter is 1.5 cm [23]. Figures (c) and (d) reprinted with permission from [23]; © 2004 IEEE.

at one of the edges of the band. This limitation can be solved alternating the two types of cells as explained. This strategy can be applied to design filters with different bandwidths using either SRR-based coplanar transmission lines [23,26], or CSRR-based microstrip structures [24,25,27].

In coplanar technology, the right-handed lines consist on the combination of SRRs etched on the bottom side of the line and capacitive gaps etched on the coplanar waveguide (see Fig. 4(b)). On the contrary, CSRR-based microstrip right-handed structures combine shunt inductances with CSRRs etched on the ground plane to obtain the desired response. As can be seen in Fig. 4(c), the designed filter, as well as being very compact (the length of the active part is 1.5 cm), exhibits a very selective and symmetric narrow-band response obtained thanks to the combination of the two types of coplanar metamaterial unit cells. If the device is compared with a conventional coupled-line filter with similar characteristics (an order-3 Chebyshev filter), the total length of the metamaterial filter is roughly three times shorter than the conventional one.

### 3.2. Ultra-wide bandpass filters based on balanced cells

As was mentioned in the previous section, the composite right/left-handed behaviour that CSRR-based transmission lines exhibit, allows to design balanced lines with a wide transmission band, which can be applied in the design of broad-band filters. Both, the purely resonant and the hybrid cells can be designed to be balanced. Some examples including both kinds of transmission lines are given below. Fig. 3(c) shows the response of several devices implemented in microstrip technology based on the purely resonant model and formed by 2–4 balanced unit cells. The graph shows the variation of the rejection level with the number of stages. As far as no control is exerted on the upper limit of the band, purely resonant balanced lines exhibit high-pass behaviour. However, we have the possibility of controlling the upper edge of the band adding some elements to our design. The signal can be rejected around a certain frequency range if additional resonators tuned at the frequency of interest are included in the device. Fig. 5 shows an ultra-wide bandpass filter (UWBPF) designed following the described strategy.

The filter was designed to cover the standard mask for UWB communications going from 3.1 GHz to 10.6 GHz, as shown in Fig. 5(b). The filter is formed by three balanced unit cells whose high-pass response starts around

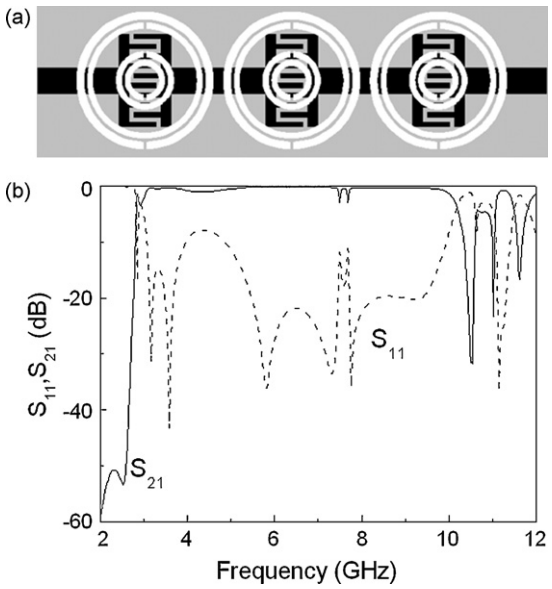


Fig. 5. (a) Layout of a UWBPF filter based on balanced cells containing additional CSRRs to control the upper limit of the band. The considered substrate is the *Rogers RO3010* with thickness $h = 635\ \mu m$ and dielectric constant $\varepsilon_r = 10.2$. Dimensions are as follows—for the big SRRs: external ring radius $r_{ext} = 2.10$ mm, distance between rings $d = 0.11$ mm, $c_{outer} = 0.22$ mm and $c_{inner} = 0.16$ mm for the external and internal ring, respectively. For the small SRRs: external ring radius $r_{ext} = 0.89$ mm, distance between rings $d = 0.11$ mm, $c_{outer} = 0.17$ mm and $c_{inner} = 0.17$ mm for the external and internal ring, respectively. The width of the host line is $W = 0.80$ mm and the capacitor is formed by five face-to-face fingers separated a distance of 0.16 mm (finger length and width are 0.8 4 mm and 0.14 mm, respectively). (b) Simulated frequency response of the filter shown in (a).

3.1 GHz. Three additional CSRRs have been added and located in the centre of the big resonators forming the unit cell. Their task is the rejection of the signal around 10.6 GHz. As a result, the filter exhibits a pass band behaviour covering the desired frequency range and, in addition to this, its dimensions are very small. The inclusion of the small CSRRs does not entail any increment in the total device area, which is around 1.5 cm × 0.4 cm.

These additional resonators are useful, not only to control the upper limit of the transmission band, but also to include attenuation poles, suitable for the rejection of interfering signals which may appear within the transmission band, as can be seen in the examples given below [28]. The resonators used to create the attenuation poles, as well as the ones controlling the upper limit of the band, can be either metallic, being added close to the line on the top layer of the substrate, or complementary, being etched on the ground plane under the transmission lines or inside the bigger resonators like in the previ-

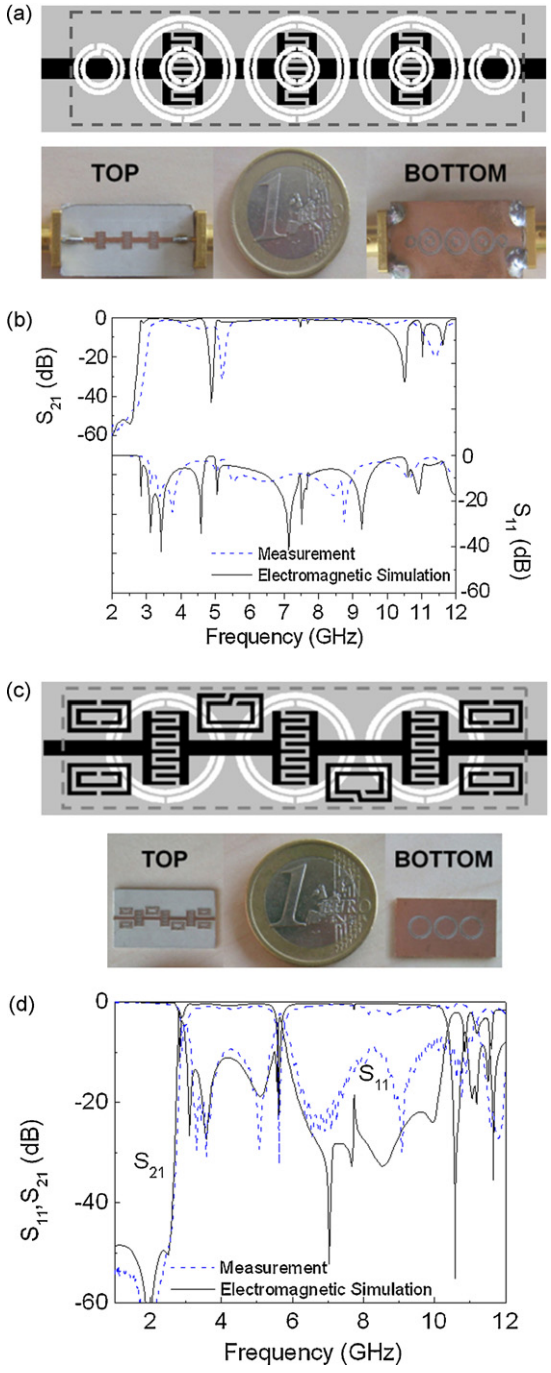


Fig. 6. (a) Layout and photograph of a UWB filter including additional complementary split-ring resonators (CSRRs) and complementary spiral resonators (CSRs) to control the upper limit of the transmission band and to add an attenuation pole at 4.8 GHz, respectively [28]. Dimensions are those indicated in Fig. 5. CSR dimensions are: $c = 0.17$ mm, $d = 0.11$ mm and $r_{ext} = 1.01$ mm. The area of the dashed rectangle is $A = 1.77\ \text{cm} \times 0.41\ \text{cm} = 0.73\ \text{cm}^2$. (b) Frequency response of the filter shown in (a). (c) Layout and photograph of a UWB filter including additional split-ring resonators (SRRs) and spiral resonators (SRs) to control the upper limit of the transmission band and to add an attenuation pole at 5.6 GHz, respectively. CSR dimensions are: $c = 0.14$ mm, $d = 0.166$ mm, $l_{ext} = 2.03$ mm and $h_{ext} = 1.46$ mm. The area of the dashed rectangle is $A = 1.57\ \text{cm} \times 0.42\ \text{cm} = 0.66\ \text{cm}^2$. (d) Frequency response of the filter shown in (c). Figures reprinted with permission of John Wiley & Sons Inc. from the article: [35] © 2004 John Wiley & Sons Inc.

ous example. This can be observed in the two following examples of UWBPF filters with attenuation poles created using spiral resonators (SRs) and complementary spiral resonators (CSRs).

The first of the examples is based on complementary resonators, as can be seen in Fig. 6(a). All the additional resonators are complementary and have been etched on the ground plane. The small CSRRs have been added to reject the signal above 10.6 GHz like in the previous example. The attenuation pole is due to the effect of the CSRs located under the access lines. They can be tuned in order to place the notch at the desired frequency and, thus, eliminate undesired signals. In this case, the CSRs were designed to reject any signal around 4.8 GHz.

In the second filter (Fig. 6(c)) all the additional resonators are metallic and lay on the top layer of the substrate. As can be seen, this filter contains several square-shaped metallic resonators close to the host line. Four SRRs can be found near the extremes of the filter and they are, like the CSRRs in the previous example, responsible for the control of the upper limit of the band. The attenuation pole located at 5.6 GHz is in this case due to the presence of the two SRs situated in the central part of the filter. As can be seen, the addition of the extra resonators does not increase the size of the device. Indeed, the total area of both devices is significantly smaller than 1 $\text{cm}^2$.

UWBPFs can be implemented not only with purely resonant metamaterial transmission lines, but also using balanced hybrid cells [29]. Fig. 7 shows an example of this kind of UWB filters. The filter was designed to satisfy a set of strong specifications: device area $A < 1\ \text{cm}^2$, insertion losses IL $< -80$ dB at 2 GHz, bandwidth from 3.5 GHz to 9 GHz.

The final device was formed by four hybrid unit cells designed to be balanced and cover the desired frequency range. All the mentioned specifications were satisfied by both the designed and the fabricated prototype. The frequency response shown in Fig. 7(b) shows the strong out-of-band rejection achieved below the transmission band; the condition IL $< -80$ dB is satisfied at 2 GHz. In-band insertion losses are low and return losses are better than $-10$ dB in the most part of the band. In addition to this, no spurious bands are present up to 16 GHz. All these characteristics are combined with very small

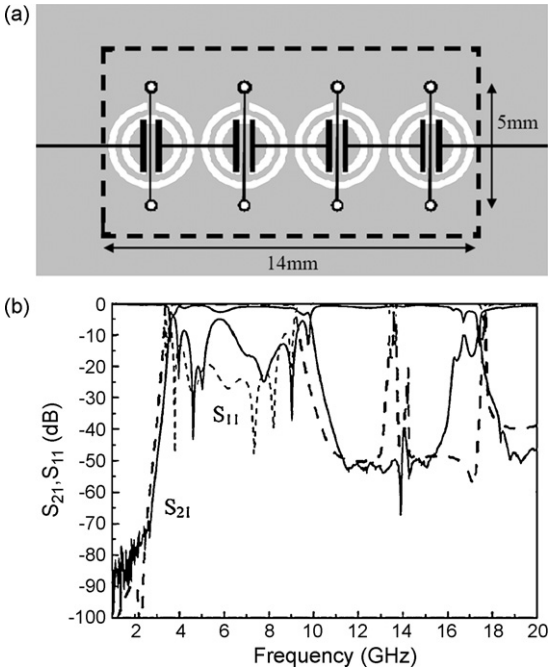


Fig. 7. (a) Layout of the hybrid cell-based UWB filter. The total area of the device is <0.7 cm$^2$. Substrate is *Rogers RO3010* with thickness $h = 127$ μm and dielectric constant $\varepsilon_r = 10.2$. Dimensions are: line width $W = 0.126$ mm, external radius of the outer rings $r = 1.68$ mm, rings width $c = 0.32$ mm and rings separation $d = 0.19$ mm; inductor width is 0.10 mm and the distance between the metals forming the gap is 0.4 mm. (b) Frequency response of the filter. The dashed line is the simulated response, whereas the solid line represents the measured response. Figures (a) and (b) reprinted with permission from [29]; © 2007 IEEE.

dimensions. In fact, the area of the dashed rectangle in Fig. 7(a) is $A = 1$ cm$^2$.

### 3.3. Design methodology for bandpass filters

The design flexibility that hybrid cells provide permits, not only the implementation of UWBPF filters based on balanced lines, but also the design of standard filters based on un-balanced lines. In 2006, a complete methodology for the design of planar bandpass filters based on CSRRs was presented for the first time [19]. Such filters can be modelled as is shown in Fig. 8(a), which represents a cascade of admittance inverters with normalized admittance $\bar{J} = 1$, alternating with shunt resonators tuned at the central frequency of the filter. These resonators can be parallel LC resonant tanks, giving rise to the model shown in Fig. 8(b). As long as the admittances of the resonant elements applied in the design of the filters agree with those of the LC tanks of the model, at least around the resonance, the targeted approximation (Chebyshev and Butterworth) can be applied in the design of filters with limited bandwidth. The admittance inverters can be implemented by means of 90° transmission lines, but we will proceed in a different way, that is, by cascading the hybrid cells of Fig. 2(d). This will reduce dimensions. The target is, as in the circuit in Fig. 8, to achieve total transmission and $\phi = 90°$ per unit cell at the central filter frequency, $f_0$.

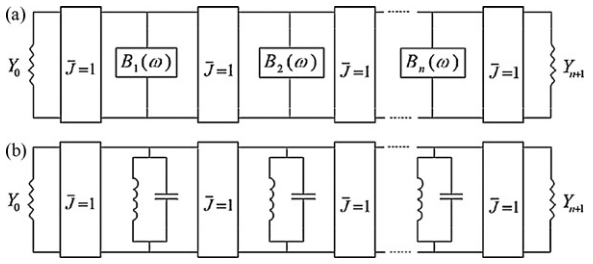


Fig. 8. (a) Bandpass filter model consisting on impedance inverters and shunt resonators. (b) Bandpass filter model with LC resonant tanks as shunt resonators.

The possibility that metamaterial transmission lines offer, to control the phase shift and the characteristic impedance of the lines simultaneously, allows the design of the unit cells needed in the implementation of the filter. As is explained in detail in [19], and mentioned above, the unit cells forming the filter must fulfil two requirements at the central frequency of the filter, $f_0$: the phase shift must be $\phi = 90°$ and $|S_{21}| = 1$, that is, at $f_0$, the characteristic impedance must be the reference impedance of the ports (usually 50 Ω). In the case of Chebyshev filters, the required rejection level and the ripple in the pass band determine the element values of the low-pass filter prototype, $g_i$. Furthermore, the fractional bandwidth settles on the 3-dB bandwidth of each resonator ($\Delta_i$). In addition to this, the central frequency $f_0$, the fractional bandwidth (FBW) of the filter and the position of the transmission zero can be used to determine all the values for the circuit elements of the model. To determine the element values for the circuit of Fig. 2(d), the series and shunt impedances have to be set to $Z_s = -jZ_0$ and $Z_p = jZ_0$, respectively, at $f_0$. This does not univocally determine the element values for the shunt impedance (the series inductance is neglected). These values are also determined by the 3 dB bandwidth of the cells:

$$\Delta = \frac{\omega_2 - \omega_1}{\omega_0} \tag{8}$$

where $\omega_0$, $\omega_1$ and $\omega_2$ are the central frequency and 3 dB frequencies, respectively, and by the transmission zero, which occurs at that frequency where the shunt

impedance reduces to zero, namely

$$f_z = \frac{1}{2\pi\sqrt{L_c(C_c + C)}} \tag{9}$$

For a LC parallel resonant tank, with inductance and capacitance $L_{eq}$ and $C_{eq}$, respectively, we have

$$\Delta = \frac{2}{Z_0}\sqrt{\frac{L_{eq}}{C_{eq}}} \tag{10}$$

If we consider the filter structure of Fig. 8(b), where the $L$ and $C$ values come from the low-pass filter prototype by frequency and element transformation according to

$$C_{eq} = \left[\frac{1}{\mathrm{FBW}\omega_0 Z_0}\right] g_i,\ L_{eq} = \frac{1}{\omega_0^2 C_{eq}} \tag{11}$$

we get the following expression for resonator bandwidths:

$$\Delta_i = \frac{2\mathrm{FBW}}{g_i} \tag{12}$$

The transmission zero frequency, $f_z$, can be tailored to some extent and be used to eliminate spurious bands which may appear close to the main band. The two 3 dB frequencies can be chosen to be equidistant from the central frequency, $f_0$. These two frequencies are, under the approximation that the series impedance is roughly constant along the pass band, the frequencies at which the shunt impedance is $Z_0/2$ and infinity, while, as has been previously indicated, $Z_p = jZ_0$ at $\omega_0$. These conditions can be expressed as:

$$\frac{L_d L_c \omega_1^3 (C + C_c) - L_d \omega_1}{L_c \omega_1^2 (C + C_c) - C\omega_1^2 L_d (L_c C_c \omega_1^2 - 1) - 1} = \frac{Z_0}{2} \tag{13}$$

$$L_c \omega_2^2 (C + C_c) - C\omega_2^2 L_d (L_c C_c \omega_2^2 - 1) - 1 = 0 \tag{14}$$

$$\frac{L_d L_c \omega_0^3 (C + C_c) - L_d \omega_0}{L_c \omega_0^2 (C + C_c) - C\omega_0^2 L_d (L_c C_c \omega_0^2 - 1) - 1} = Z_0 \tag{15}$$

The previous approximation (which is valid for narrow and moderate bandwidths) leads us to simple analytical expressions (Eqs. (13) and (14)). If this approximation is not applied, then the conditions arising from the 3 dB frequencies are not mathematically simple. Solution of Eqs. (13)–(15) and (9) leads us to the parameters of the shunt reactance, while the series capacitance is given by (assuming that $L$ is negligible):

$$C_g = \frac{1}{2Z_0\omega_0} \tag{16}$$

All these specifications and impositions can be used to univocally know all the elements of the circuit model of the structure (see Fig. 2(e)), except for the line inductance, which can be neglected in the frequency range of interest. The application of this methodology has given rise to very competitive filters satisfying different specifications. Fig. 9a and b shows the layout and the frequency response of one filter with 0.3 dB ripple, $f_0 = 2.5$ GHz and FBW = 9%. Relevant dimensions of the layout are indicated in Fig. 9(a), showing that the total length of the filter, excluding access lines is around $0.4\lambda$, being $\lambda$ the signal wavelength at $f_0$. The designed filter presents a good performance, combined with very compact dimensions. Size can still be reduced if CSRs are used instead of CSRRs. Transmission lines based on these resonators are equivalent to the ones based on CSRRs, but the fact that the resonance frequency of a CSR is approximately half the resonance frequency of a CSRR with the same dimensions, makes that CSR-based transmission lines are considerably smaller. One example of these CSR-based filters is shown in Fig. 9c and d. It is a 0.3-dB ripple filter with $f_0 = 1.1$ GHz and FBW = 10%. The device occupies an area $A = 0.22\lambda \times 0.08\lambda$, which is five times smaller than the area that a CSRR-based filter with a similar performance takes up [30]. Size can be reduced thanks to the small electrical size of CSRs, although their worse quality factor causes higher insertion losses.

As the results corroborate, this design methodology makes possible the synthesis of filters with small dimensions, low-losses, high-frequency selectivity and good out-of-band performance, which can be of interest in such applications in which small size and planar technology compatibility are essential aspects.

As was mentioned above, filters modelled by the scheme shown in Fig. 8(b) can be synthesized using different topologies. In the previous example, we did not use 90° transmission lines as admittance inverters. In [31], a variation of the previous methodology is reported, in which the same kind of resonators combining CSRRs and shunt stubs are coupled by means of $\lambda/4$ lines. The same conditions and specifications as in the previous filters can be imposed, giving rise to the necessary design equations. Although some of these equations differ from the former ones, as a consequence of the modification of the unit cell, the methodology is basically the same. The advantage that these new unit cells offer is their bandwidth, which can be much broader than in the case of the hybrid cells. Fig. 10 shows the equivalent circuit, together with the layout and the frequency response of a periodic UWBPF fil-

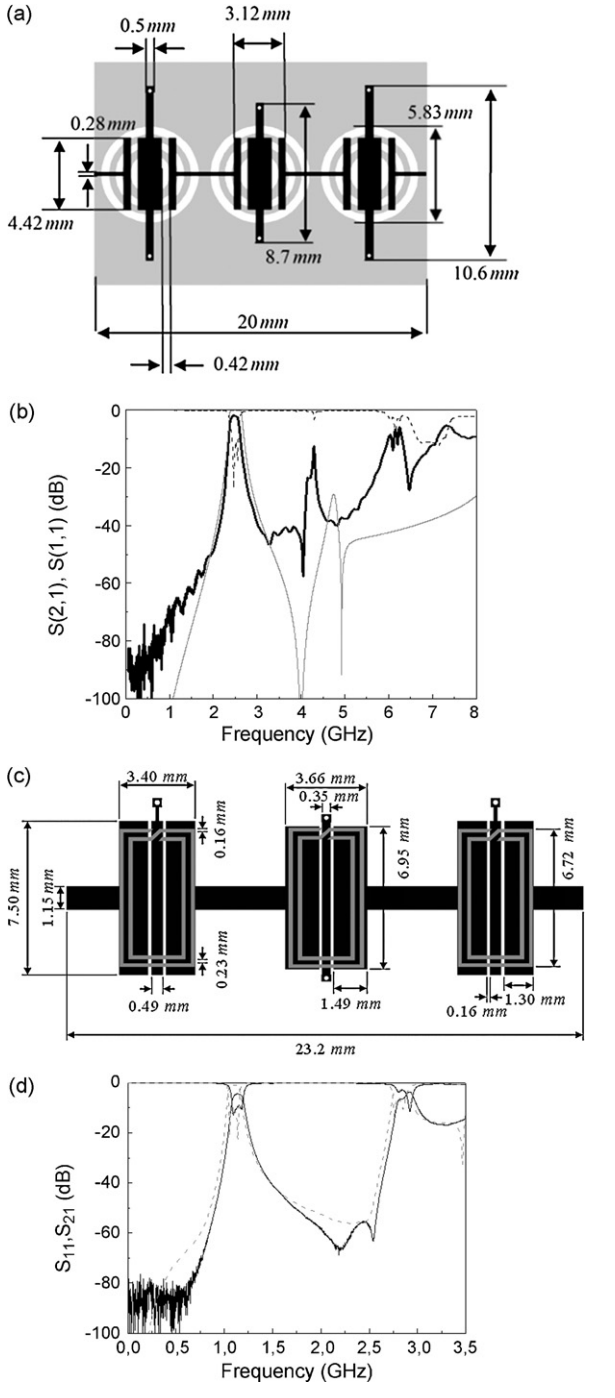


Fig. 9. (a) Layout of the CSRR-based Chebyshev filter. (b) Frequency response of the filter shown in (a). The dashed line is the simulated response, whereas the solid line represents the measured response. (c) Layout of the CSR-based Chebyshev filter. (d) Frequency response of the filter shown in (c). The dashed line is the simulated response, whereas the solid line represents the measured response. Substrate is *Rogers RO3010* with thickness $h = 0.635$ mm and dielectric constant $\varepsilon_r = 10.2$ was used in both filters. Figures (c) and (d) reprinted with permission from [30]; © 2008 IEEE.

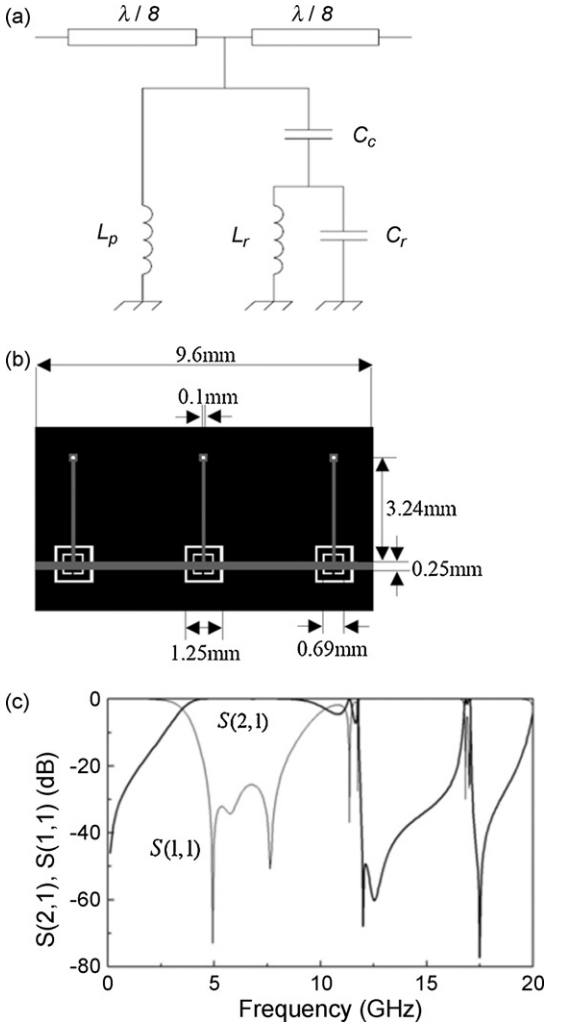


Fig. 10. (a) Equivalent circuit model of the unit cell. (b) Layout of the CSRR-based bandpass filter. Metallic parts are depicted in grey for the top layer and in black for the bottom layer. (c) Simulated frequency response of the filter shown in (b). Substrate is *Rogers RO3010* with thickness $h = 0.635$ mm and dielectric constant $\varepsilon_r = 10.2$ was used. Figures reprinted with permission of John Wiley & Sons Inc. from [31] © 2004 John Wiley & Sons Inc.

ter implemented following the mentioned procedure. The fractional bandwidth is FBW = 90% and the central frequency is $f_0 = 6.8$ GHz, whereas the order of the filter is $N = 3$. The out-of-band rejection can be improved adding at the filter output two CSRRs properly tuned to eliminate the spurious band appearing around 17 GHz.

As can be seen, the use of these unit cells offers the possibility of designing broad-band filters following a complete design methodology and giving rise to compact filters with an interesting performance.

### 3.4. Other approaches

Different approaches, not based on SRR-type resonators, but applying different kinds of artificial transmission lines have also given rise to very competitive filters. Composite right/left-handed metamaterial transmission lines based on LC-loaded transmission lines have also been applied in filter design. As an improved structure, tapered coupled-resonators-based CRLH TLs can be used to design broad-band filters presenting high frequency selectivity. In [32], such a filter implemented in MIM configuration is presented, showing a fractional bandwidth of 115% and a reasonable performance. Such tapered coupled-resonator structures are applied to exhibit transmission zeros at different frequencies and provide a sharp cutoff at the upper edge of the band, improving frequency selectivity.

Thanks to non-linearity and controllability of the dispersion diagram of CRLH transmission lines, it is possible to design dual-band components operating at arbitrary frequencies. In [33], for example, bandpass and bandstop filters based on quarter wave resonators have been implemented by replacing the lines with LC-loaded CRLH TLs. By doing this, the second operating frequency, $f_2$, where the phase is $3\pi/2$ does not have to be an odd multiple of the first one, $f_1$, but it can be chosen freely. The results in [33] prove that this strategy can be applied to the design of dual-band bandpass and bandstop filters with different bandwidths and good performances.

Metamaterial transmission lines can also be used to implement stepped-impedance resonator bandpass filters [34]. In such devices, right- and left-handed transmission line sections with different characteristic impedances alternate. If the length of the right-handed line sections and values of the characteristic impedances are properly chosen, dimensions can be drastically reduced and, at the same time, the first spurious band can be shifted to higher frequencies. As a result, compact bandpass filters with an improved out-of-band rejection can be implemented.

These are some of the examples showing the application possibilities of metamaterial transmission lines in filter design. Work is in progress in our Group and different Groups worldwide to further miniaturize and optimize microwave filters on the basis of metamaterial technology.

## 4. Conclusions

A review on the work developed during the last years in the field of filters using resonant-type metamaterial transmission lines has been carried out. Part of the work carried out by this research group has been exposed, showing different kinds of filters applying diverse structures and design strategies. The presented work shows the possibilities that this kind of metamaterial transmission lines offer in compact filter design. As the results show, different bandwidths, performances and functionalities can be obtained using resonant-type metamaterial transmission lines and, at the same time, dimensions can be considerably reduced without the need of including lumped elements. Such metamaterial filters are, therefore, a good alternative when size and fully planar implementation are key issues.

Other approaches have also been applied to the implementation of filters with excellent results, showing again the possibilities that metamaterial transmission lines offer in filter design.

## Acknowledgements

This work has been supported by MEC (Spain) by project contract TEC2007-68013-C02-02 METAINNOVA and a FPU Grant (Ref. AP2005-4523) awarded to Marta Gil and by the European Commission (VI Framework Program) contract no. 500252-2 METAMORPHOSE. Special thanks are also given to CIDEM (*Generalitat de Catalunya*) for funding CIMITEC.

## References

[1] M. Gil, J. Bonache, I. Gil, J. García-García, F. Martín, Miniaturization of planar microwave circuits by using resonant-type left handed transmission lines, IET Microwave Antennas and Propagation 1 (2007) 73–79.

[2] G. Sisó, M. Gil, J. Bonache, F. Martín, Application of metamaterial transmission lines to design of quadrature phase shifters, Electronics Letters 43 (2007).

[3] G. Sisó, J. Bonache, M. Gil, J. García-García, F. Martín, Compact rat-race hybrid coupler implemented through artificial left handed and right handed lines, in: Proceedings of the IEEE MTT-S Int'l Microwave Symposium Digest, Honolulu, Hawaii, USA, June 2007, pp. 25–28.

[4] G. Sisó, M. Gil, J. Bonache, F. Martín, Applications of resonant-type metamaterial transmission lines to the design of enhanced bandwidth components with compact dimensions, Microwave and Optical Technology Letters 50 (2008) 127–134.

[5] G. Sisó, J. Bonache, F. Martín, Dual-band Y-junction power dividers implemented through artificial lines based on complementary resonators, in: Proceedings of the IEEE MTT-S Int'l Microwave Symposium Digest, Atlanta, USA, June 2008, pp. 663–666.

[6] J.B. Pendry, A.J. Holden, D.J. Robbins, W.J. Stewart, Magnetism from conductors and enhanced nonlinear phenomena, IEEE Transactions on Microwave Theory and Techniques 47 (11) (1999) 2075–2084.

[7] D.R. Smith, W.J. Padilla, D.C. Vier, S.C. Nemat-Nasser, S. Schultz, Composite medium with simultaneously negative permeability and permittivity, Physical Review Letters 84 (2000) 4184–4187.
[8] F. Martín, F. Falcone, J. Bonache, R. Marqués, M. Sorolla, Split ring resonator based left handed coplanar waveguide, Applied Physics Letters 83 (2003) 4652–4654.
[9] J. García-García, J. Bonache, F. Falcone, J.D. Baena, F. Martín, I. Gil, T. Lopetegi, M.A.G. Laso, A. Marcotegui, R. Marqués, M. Sorolla, Stepped-impedance low pass filters with spurious passband suppression, Electronics Letters 40 (2004) 881–883.
[10] A. Ali, M.A. Khan, Z. Hu, High selectivity lowpass filter using negative-e metamaterial resonators, Electronics Letters 43 (2007) 528–530.
[11] F. Falcone, T. Lopetegi, M.A.G. Laso, J.D. Baena, J. Bonache, R. Marqués, F. Martín, M. Sorolla, Babinet principle applied to the design of metasurfaces and metamaterials, Physical Review Letters 93 (2004) 197401–197404.
[12] M. Gil, J. Bonache, I. Gil, J. García-García, F. Martín, On the transmission properties of left handed microstrip lines implemented by complementary split rings resonators, International Journal of Numerical Modeling: Electronic Networks, Devices and Fields 19 (2006) 87–103.
[13] M. Gil, I. Gil, J. Bonache, J. García-García, F. Martín, Metamaterial transmission lines with extreme impedance values, Microwave and Optical Technology Letters 48 (2006) 2499–2505.
[14] G.V. Eleftheriades, A.K. Iyer, P.C. Kremer, Planar negative refractive index media using periodically L–C loaded transmission lines, IEEE Transactions on Microwave Theory and Techniques 50 (2002) 2702–2712.
[15] C. Caloz, T. Itoh, Application of the transmission line theory of left-handed (LH) materials to the realization of a microstrip 'LH line', in: Proceedings of the IEEE Antennas and Propagation Society International Symposium, vol. 2, San Antonio, TX, June 2002, pp. 12–415.
[16] C.-J. Lee, K.M.K.H. Leong, T. Itoh, Metamaterial transmission line based bandstop and bandpass filter designs using broadband phase cancellation, in: Proceedings of the IEEE-MTT International Microwave Symposium Digest, San Francisco, CA, USA, June 2006, pp. 935–938.
[17] M.A. Antoniades, G.V. Eleftheriades, A broadband series power divider using zero-degree metamaterial phase-shifting lines, IEEE Microwave and Wireless Components Letters 15 (2005) 808–810.
[18] F. Aznar, J. Bonache, F. Martín, Improved circuit model for left-handed lines loaded with split ring resonators, Applied Physics Letters 92 (2008) 043512.
[19] J. Bonache, I. Gil, J. García-García, F. Martín, Novel microstrip band pass filters based on complementary split rings resonators, IEEE Transactions on Microwave Theory and Techniques 54 (2006) 265–271.
[20] M. Gil, J. Bonache, F. Martín, Synthesis and applications of new left handed microstrip lines with complementary split-ring resonators etched on the signal strip, IET Microwaves Antennas and Propagation 2 (4) (2008) 324–330.
[21] F. Aznar, M. Gil, J. Bonache, F. Martín, Revising the equivalent circuit models of resonant-type metamaterial transmission lines, in: Proceedings of the IEEE-MTT International Microwave Symposium Digest, Atlanta, USA, June 2008, pp. 323–326.
[22] M. Gil, J. Bonache, J. Selga, J. García-García, F. Martín, Broadband resonant type metamaterial transmission lines, IEEE Microwave and Wireless Components Letters 17 (2007) 97–99.
[23] J. Bonache, F. Martín, F. Falcone, J. García, I. Gil, T. Lopetegi, M.A.G. Laso, R. Marqués, F. Medina, M. Sorolla, Super compact split ring resonators CPW band pass filtres, in: Proceedings of the IEEE-MTT International Microwave Symposium Digest, Fort Worth, TX, USA, June 2004, pp. 1483–1486.
[24] J. Bonache, F. Martín, F. Falcone, J.D. Baena, T. Lopetegi, J. García-García, M.A.G. Laso, I. Gil, A. Marcotegui, R. Marqués, M. Sorolla, Application of complementary split rings resonators to the design of compact narrow band pass structures in microstrip technology, Microwave and Optical Technology Letters 46 (2005) 508–512.
[25] P. Mondal, M.K. Mandal, A. Chaktabarty, S. Sanyal, Compact bandpass filters with wide controllable fractional bandwidth, IEEE Microwave and Wireless Components Letters 16 (2006) 540–542.
[26] J. Bonache, F. Martín, F. Falcone, J. García-García, I. Gil, T. Lopetegi, M.A.G. Laso, R. Marqués, F. Medina, M. Sorolla, Compact coplanar waveguide band pass filter at S-band, Microwave and Optical Technology Letters 46 (2005) 33–35.
[27] J. Bonache, I. Gil, J. García-García, F. Martín, Complementary split rings resonator for microstrip diplexer design, Electronics Letters 41 (2005) 810–811.
[28] F. Martín, M. Gil, J. Bonache, J. García-García, Composite right/left handed (CRLH) transmission lines based on complementary split rings resonators (CSRRs) and applications, in: Proceedings of the International Congress on Advanced Electromagnetic Materials in Microwaves and Optics (Metamaterials 2007), Rome, Italy, October 2007, pp. 872–875.
[29] M. Gil, J. Bonache, J. García, J. Martel, F. Martín, Composite right/left-handed metamaterial transmission lines based on complementary split-rings resonators and their applications to very wideband and compact filter design, IEEE Transactions on Microwave Theory and Techniques 55 (2007) 1296–1304.
[30] M. Gil, J. Bonache, F. Martín, Ultra compact band pass filters implemented through complementary spiral resonators (CSRs), in: Proceedings of the IEEE-MTT International Microwave Symposium Digest, Atlanta, USA, June 2008, pp. 1119–1122.
[31] J. Bonache, F. Martín, J. García-García, I. Gil, R. Marqués, M. Sorolla, Ultra wide band pass filters (UWBPF) based on complementary split rings resonators, Microwave and Optical Technology Letters 46 (2005) 283–286.
[32] H.V. Nguyen, C. Caloz, Broadband highly selective bandpass filter based on a tapered coupled-resonator (TCR) CRLH structure, in: Proceedings of the European Microwave Association, vol. 2, March 2006, pp. 44–51.
[33] C. Tseng, T. Itoh, Dual-band bandpass and bandstop filters using composite right/left-handed metamaterial transmission lines, in: Proceedings of the IEEE-MTT International Microwave Symposium Digest, San Francisco, CA, USA, June 2006, pp. 931–934.
[34] I.B. Vendik, D.V. Kholodnyak, I.V. Kolmakova, E.V. Serbryakova, P.V. Kapitanova, F. Martin, J. Bonache, J. Garcia, I. Gil, M. Gil, Applications of right/left handed and resonant left handed transmission lines for microwave circuit design, in: Proceedings of the 36th European Microwave Conference, Manchester, UK, September 2006, pp. 955–958.
[35] M. Gil, J. Bonache, F. Martín, Metamaterial filters with attenuation poles in the pass band for ultra wide band applications, Microwave and Optical Technology Letters 49 (2007) 2909–2913.

# Electrically tunable split-ring resonators at microwave frequencies based on Barium-Strontium-Titanate thick-films

M. Gil[1,2*], C. Damm[2], A. Giere[2], M. Sazegar[2], J. Bonache[1], R. Jakoby[2], F. Martín[1].

[1]GEMMA/CIMITEC, Departament d'Enginyeria Electrònica, Universitat Autònoma de Barcelona. 08193 Bellaterra (Barcelona). Spain.
[2] MWT, Microwave Engineering, Technische Universität Darmstadt, 64283 Darmstadt, Germany.

* As temporary guest researcher in Technische Universität Darmstadt.

*Abstract*: It is the first time that split-ring resonators (SRRs) are implemented using ferroelectric materials to modify their resonance frequency by means of a tuning voltage. SRRs have been used to load a microstrip transmission line on a multi-layered substrate including a thick film of Barium-Strontium-Titanate (BST) to obtain a tunable stop-band response. The characteristics of the BST layer allow the application of 140V as tuning voltage to obtain frequency tunability values around 12.5%. The applied technology is suitable for the fabrication of cost-effective and reliable planar microwave devices.

*Introduction*: Split-ring resonators (SRRs) have been used in very diverse applications, since their appearance in 1999 [1]. Specifically, they have been widely used, together with other similar resonators, for the implementation of resonant-type metamaterial transmission lines [2,3], this representing an alternative to the CL-loaded approach, formerly proposed by Caloz *et al* [4], and Iyer *et al.* [5]. Different strategies have been followed in order to achieve tunability in such resonators at microwave frequencies, including the use of different kinds of capacitors [6,7,8,9], MEMS [10], or liquid crystals [11]. On the other hand, Barium-Strontium-Titanate (BST) has been used for the implementation of different kinds of ferroelectric varactors [12,13] as well as in the design of tunable SRRs [9]. In this case, however, the resonance frequency was modified by varying the temperature. In the present work, we take advantage of the dependence of the dielectric permittivity of ferroelectric materials with an

external electric field [14], in order to modify the resonance frequency of SRRs by means of an electric voltage. The resonators have been used to load a microstrip transmission line in order to obtain a notch around the resonance frequency of the SRRs. This strategy allows a cheap and easy fabrication process for the implementation of artificial tunable lines based on SRRs, and better reliability than other approaches. In addition, the measurements show very low insertion losses in the pass band, which are lower than 0.4dB up to 4GHz.

*Design and fabrication*: The resonance frequency of the SRR can be varied if the capacitance between the two rings forming the resonator is modified, in a similar way as it is done in BST interdigital varactors [12]. Thanks to the use of BST and with a proper design of the SRRs, this capacitance can be tailored and the desired tunability is achievable. The used BST thick-film with a thickness of 3.5µm is made by screen-printing a Fe-F co-doped BST paste on an alumina substrate and sintering at 1200°C [15]. Based on this ceramic, the structured metallization for the strip of the transmission line and the SRR are realized by a single lithography step and plating 2.5µm thick Au electrode on a Cr/Au seed layer which is afterwards removed by wet etching. A cross section scheme of the substrate is depicted in Fig. 1(a).

The biasing requires the connection of DC feeding lines and pads to the rings forming the SRR as shown in Fig. 1(b), where the relevant dimensions of the structure are also included.. *Rogers RO3003* substrate is used as carrier substrate for the whole device including the biasing network. The carrier substrate is placed on a copper plate which acts as microstrip ground and ensures mechanical stability. Due to the topology of the SRRs, no dc-blocking elements are needed, whereas the RF signal is blocked by means of 100KΩ SMD-resistors. The fabricated device, a microstrip line loaded with a pair of tunable SRRs, is depicted in Fig.2.

*Results*: The measured and simulated responses for the tuned ($V$=140V) and untuned ($V$=0V) states are shown in Fig.3. Simulations have been carried out with the commercial software *Agilent Momentum*, using different values of the effective relative permittivity of the BST layer for the tuned ($\varepsilon_{r,tuned}$=255)

and untuned ($\varepsilon_{r,untuned}$=340) states, which are typical values for the considered inter-ring distance ($d$) and tuning voltages for such BST thick-films. Due to the limitations of the simulation software, a homogeneous permittivity must be assumed for the entire BST layer as an approximation. In general, the permittivity of BST is dependent on the applied electric field strength, which is itself a function of the structure geometry. Hence, permittivity is actually inhomogeneous. Nevertheless, the validity of the homogeneity assumption for the simulation of the proposed structure has been in general verified by simulations using a specialized software for the tuning of BST components [16]. There is a good agreement between simulation and measurements concerning the tuning range, insertion and return losses, although a small frequency shift can be observed. Mismatch can be attributed to some discrepancies between the actual geometrical and physical parameters of the structure and those used in the simulations (dimensions, dielectric permittivity, etc.), in addition to known problems with the appropriate mesh generation for structures with high dielectric constants.

The measured resonance frequencies are $f_{0untuned}$=2.49GHz and $f_{0tuned}$=2.80GHz; that is, the achieved frequency tunability is 12.45%. The measurement shows very low insertion losses in the pass band (better than 0.4dB at least up to 4GHz) and the rejection in the notch is close to –5dB. The rejection level can be easily increased by cascading additional unit cells ($n$). This has been verified through simulations, which indicate a rejection level of –15dB for $n$=3, and –30dB for $n$=6. Work is in progress for experimental demonstration.

*Conclusions*: Electrically tunable SRRs using a BST thick-film layer suitable for planar microwave device applications have been developed for the first time. One fabricated microstrip line loaded with a pair of tunable SRRs has been characterized and it has been found to exhibit a notch with 12.5% tunability and very low insertion losses in the pass-band. Work is in progress in order to design new tunable structures based on BST thick-film technology.

*Acknowledgements*:

This work has been supported by MEC (Spain) (TEC2007-68013-C02-02 METAINNOVA and FPU Grant (ref. AP2005-4523) awarded to M. Gil), MCI (Spain) (EMET project ref. CDS2008-00066 within CONSOLIDER INGENIO 2010 Program), CIDEM (Catalan Government) (SGR-2005-00624) and German Research Foundation (GRK 1037). Thanks are also given to J. R. Binder und X. Zhou from FZ Karlsruhe for substrate preparation and production.

*References*

[1] J. B. Pendry, A. J. Holden, D. J. Robbins, and W. J. Stewart, "Magnetism from conductors and enhanced nonlinear phenomena", IEEE Trans. Microwave Theory Tech, vol. 47, pp. 2075–2081, 1999.
[2] F. Martín, F. Falcone, J. Bonache, R. Marqués and M. Sorolla, "Split ring resonator based left handed coplanar waveguide ", Appl. Phys. Lett., vol. 83, pp. 4652-4654, Dec. 2003.
[3] F. Falcone, T. Lopetegi, M. A. G. Laso, J. D. Baena, J. Bonache, M. Beruete, R. Marqués, F. Martín, and M. Sorolla, "Babinet Principle Applied to the Design of Metasurfaces and Metamaterials" Phys. Rev. Lett. 93, 197401 (2004).
[4] C. Caloz and T. Itoh, "Application of the transmission line theory of left-handed (LH) materials to the realization of a microstrip LH line," in IEEE AP-S/URSI Int. Symp. Dig., San Antonio, TX, Jun. 2002, pp. 412–415.
[5] A. K. Iyer and G. V. Eleftheriades, "Negative refractive index media supporting 2-D waves," in IEEE MTT-S Int. Microw. Symp. Dig., Seattle, WA, 2002, pp. 1067–1070.
[6] I. Gil, J. Bonache, J. García, F. Martín "Tunable Metamaterial Transmission Lines Based on Varactor Loaded Split Rings Resonators", IEEE Trans. Microw. Theory Tech., vol. 54, pp. 2665-2674, June 2006.
[7] Hand, T. H. and S. A. Cummer. "Frequency tunable electromagnetic metamaterial using ferroelectric loaded split rings", Journal of Appl.Phys., v. 103, 066105, 2008.
[8] A. Velez, J. Bonache, F. Martín, "Varactor-loaded Complementary Split Ring Resonators (VLCSRR) and Their Application to Tunable Metamaterial Transmission Lines ", IEEE Microw. and Wirel. Compon.Lett, Vol. 18, No. 1, pp. 28-30, Jan. 2008.
[9] E. Ozbay, K. Aydin, S. Butun, K. Kolodziejak, and D. Pawlak, "Ferroelectric based tuneable SRR based metamaterial for microwave applications," in Proc. of the 37th European Microwave Conf., Munich (Germany), Oct. 2007, pp. 497-499.
[10] I. Gil, F. Martín, X. Rottenberg and W. De Raedt, "Tunable stop-band filter at Q-band based on RF-MEMS metamaterials", Electron. Lett., Vol. 43, Issue 21. Oct. 2007.
[11] Q. Zhao, L. Kang, B. Du, B. Li, J. Zhou, H. Tang, X. Liang, and B. Zhang Electrically tunable negative permeability metamaterials based on nematic liquid crystals. Appl. Phys. Lett. 90, 011112 (2007).
[12] A. Giere, Y. Zheng, H. Gieser, K. Marquardt, H. Wolf, P. Scheele and R. Jakoby, "Coating of Planar Barium-Strontium-Titanate Thick-Film Varactors to Increase Tunability", Proc. 37th European Microwave Conf., 114-117 (2007).
[13] Kuylenstierna, D. Vorobiev, A. Linner, P. Gevorgian, S. "Ultrawide-band tunable true-time delay lines using ferroelectric varactors" IEEE Trans. Microw. Theory Tech.,, Volume: 53, Issue: 6, pp. 2164- 2170, June 2007.
[14] A. K. Tagantsev, V.O. Sherman, K.F. Astafiev, J. Venkatesh, and N. Setter, "Ferroelectric materials for microwave tunable applications". Journal of Electroceramics, 11:5–66, (2003).
[15] F. Paul, A. Giere, W. Menesklou, J. R. Binder, P. Scheele, R. Jakoby and J. Haußelt, "Influence of Fe-F-co-doping on the dielectric properties of $Ba_{0.6}Sr_{0.4}TiO_3$ thick-films", International Journal of Materials Research, 99, 1119-1128 (2008).
[16] A. Giere, P. Scheele, Y. Zheng and R. Jakoby, "Characterization of the Field-Dependent Permittivity of Nonlinear Ferroelectric Films Using Tunable Coplanar Lines". IEEE Microw. and Wirel. Compon.Lett., 17, 442-444 (2007).

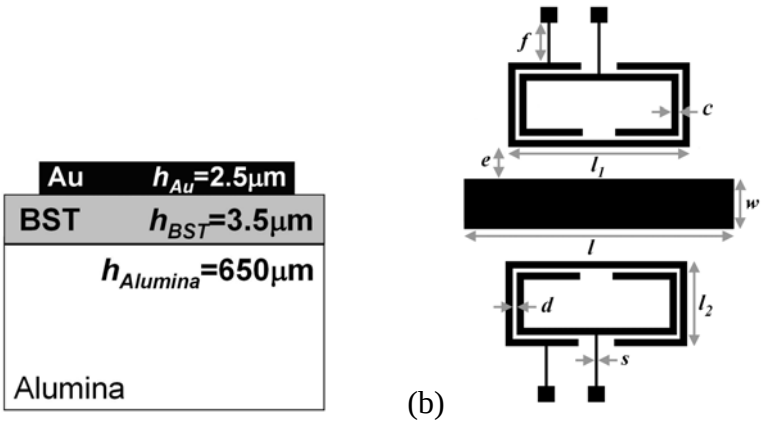


Fig.1. (a) Cross-section scheme of the substrate indicating layer thicknesses. (b) Layout of fabricated microstrip line and SRRs. Dimensions are: $c$=100 μm, $d$=10 μm, $f$=590μm, $s$=30μm, $w$=520μm, $l$=6.1mm, $l_1$=3.1mm, $l_2$=0.8mm, area $a=l_1\times l_2$=2.42mm$^2$ =3.1mm×0.8mm=0.07λ×0.02λ ($\lambda$ is the guided wavelength at the resonance of the SRRs).

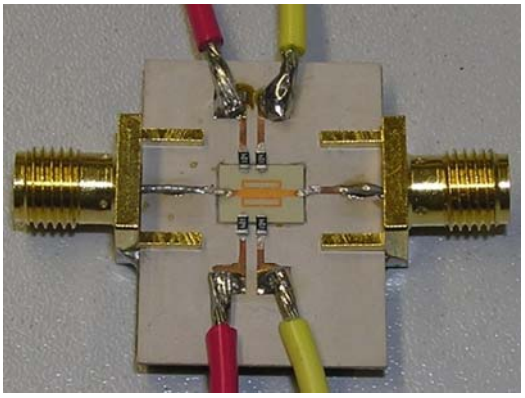

Fig.2. Photograph of the fabricated device.

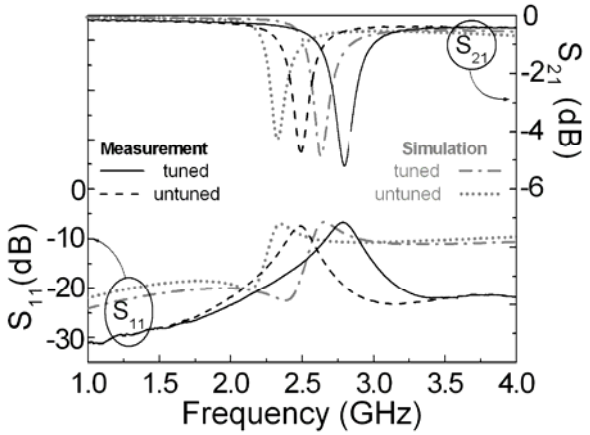


Fig.3 Simulated (gray) and measured (black) frequency responses for the fabricated device for the tuned and untuned states.

## List of Publications of the Author

### International Journals


1. J. Bonache, M. Gil, I. Gil, J. García-García and F. Martín, "On the electrical characteristics of complementary metamaterial resonators", *IEEE Microwave and Wireless Components Letters*, vol. 16, pp. 543-545, 2006.
2. I. Gil, J. Bonache, M. Gil, J. García-García and F. Martín, "Left-handed and right-handed transmission properties of microstrip lines loaded with complementary split rings resonators", *Microwave and Optical Technology Letters*, vol. 48, pp. 2508-2511, 2006.
3. I. Gil, J. Bonache, M. Gil, J. García-García, F. Martín and R. Marqués, "Accurate circuit analysis of resonant-type left handed transmission lines with inter-resonator coupling", *Journal of Applied Physics*, vol. 100, pp. 074908-10, 2006.
4. M. Gil, J. Bonache, I. Gil, J. García-García and F. Martín, "On the transmission properties of left-handed microstrip lines implemented by complementary split rings resonators", *International Journal of Numerical Modelling-Electronic Networks Devices and Fields*, vol. 19, pp. 87-103, 2006.
5. M. Gil, I. Gil, J. Bonache, J. García-García and F. Martín, "Metamaterial transmission lines with extreme impedance values", *Microwave and Optical Technology Letters*, vol. 48, pp. 2499-2505, 2006.
6. M. Gil, J. Bonache, I. Gil, J. García-García and F. Martín, "Miniaturisation of planar microwave circuits by using resonant-type left-handed transmission lines", *IET Microwaves Antennas & Propagation*, vol. 1, pp. 73-79, 2007.
7. F. Aznar, M. Gil, J. Bonache, J. García-García and F. Martín, "Metamaterial transmission lines based on broad-side coupled spiral resonators", *Electronics Letters*, vol. 43, pp. 530-532, 2007.
8. M. Gil, J. Bonache, J. García-García, J. Martel and F. Martín, "Composite right/left-handed metamaterial transmission lines based on complementary split-rings resonators and their applications to very wideband and compact filter design", *IEEE Transactions on Microwave Theory and Techniques*, vol. 55, pp. 1296-1304, 2007.
9. M. Gil, J. Bonache and F. Martín, "Metamaterial filters with attenuation poles in the pass band for ultra wide band applications", *Microwave and Optical Technology Letters*, vol. 49, pp. 2909-2913, 2007.
10. M. Gil, J. Bonache, J. Selga, J. García-García and F. Martín, "Broadband resonant-type metamaterial transmission lines", *IEEE Microwave and Wireless Components Letters*, vol. 17, pp. 97-99, 2007.
11. G. Sisó, M. Gil, J. Bonache and F. Martín, "Application of metamaterial transmission lines to design of quadrature phase shifters", *Electronics Letters*, vol. 43, pp. 1098-1100, 2007.
12. G. Sisó, M. Gil, J. Bonache and F. Martín, "On the dispersion characteristics of metamaterial transmission lines", *Journal of Applied Physics*, vol. 102, pp. 074911-7, 2007.
13. F. Aznar, J. García-García, M. Gil, J. Bonache and F. Martín, "Strategies for the miniaturization of metamaterial resonators", *Microwave and Optical Technology Letters*, vol. 50, pp. 1263-1270, 2008.
14. F. Aznar, M. Gil, J. Bonache, L. Jelinek, J. D. Baena, R. Marqués and F. Martín, "Characterization of miniaturized metamaterial resonators coupled to planar transmission lines through parameter extraction", *Journal of Applied Physics*, vol. 104, pp. 114501-8, 2008.
15. F. Aznar, M. Gil, J. Bonache and F. Martín, "Modelling metamaterial transmission lines: a review and recent developments", *Opto-Electronics Review*, vol. 16, pp. 226-236, 2008.
16. J. Bonache, M. Gil, O. García-Abad and F. Martín, "Parametric analysis of microstrip lines loaded with complementary split ring resonators", *Microwave and Optical Technology Letters*, vol. 50, pp. 2093-2096, 2008.
17. J. Bonache, G. Sisó, M. Gil, A. Iniesta, J. García-Rincón and F. Martín, "Application of composite right/left handed (CRLH) transmission lines based on complementary split ring resonators (CSRRs) to the design of dual-band microwave components", *IEEE Microwave and Wireless Components Letters*, vol. 18, pp. 524-526, 2008.

**18.** M. Gil, J. Bonache and F. Martín, "Synthesis and applications of new left handed microstrip lines with complementary split-ring resonators etched on the signal strip", *IET Microwaves Antennas & Propagation*, vol. 2, pp. 324-330, 2008.
**19.** M. Gil, J. Bonache and F. Martín, "Metamaterial filters: A review", *Metamaterials*, vol. 2, pp. 186-197, 2008.
**20.** G. Sisó, J. Bonache, M. Gil and F. Martín, "Enhanced bandwidth and dual-band microwave components based on resonant-type metamaterial transmission lines", *International Journal of Microwave and Optical Technology*, vol. 3, pp. 345-352, 2008.
**21.** G. Sisó, M. Gil, F. Aznar, J. Bonache and F. Martín, "Dispersion engineering with resonant-type metamaterial transmission lines", *Laser & Photonics Reviews*, DOI: 10.1002/lpor.200810026, 2008.
**22.** G. Sisó, M. Gil, J. Bonache and F. Martín, "Generalized Model for Multiband Metamaterial Transmission Lines", *IEEE Microwave and Wireless Components Letters*, vol. 18, pp. 728-730, 2008.
**23.** G. Sisó, M. Gil, J. Bonache and F. Martín, "Applications of resonant-type metamaterial transmission lines to the design of enhanced bandwidth components with compact dimensions", *Microwave and Optical Technology Letters*, vol. 50, pp. 127-134, 2008.

**National and International Conferences**

**1.** J. García-García, J. Bonache, I. Gil, M. Gil and F. Martín, "Diseño de filtros de microondas mediante metamateriales", *XX Symposium Nacional de la Unión Científica Internacional de Radio*, Gandía, September Spain, 2005.
**2.** J. Bonache, M. Gil, I. Gil, J. García-García and F. Martín, "Limitations and solutions of resonant-type metamaterial transmission lines for filter applications: the hybrid approach", *IEEE MTT-S International Microwave Symposium Digest*, San Francisco (CA), USA, vol. 1-5, pp. 939-942, June 2006.
**3.** J. Bonache, M. Gil, I. Gil, J. García-García and F. Martín, "Recent advances in resonant-type metamaterial transmission lines for planar filter design", *International Workshop on Microwave Filters*, Toulousse, France, October 2006.
**4.** J. Bonache, J. Martel, I. Gil, M. Gil, J. García-García, F. Martín, I. Cairo and M. Ikeda, "Super compact (< 1cm(2)) band pass filters with wide bandwidth and high selectivity at C-band", *European Microwave Conference*, Manchester, United Kingdom, vol. 1-4, pp. 177-180, September 2006.
**5.** J. García-García, F. Aznar, M. Gil, J. Bonache and F. Martín, "New Ultra Compact Resonant Particle based on Split Rings Resonator suitable for Left Handed planar structures", *XXI Symposium Nacional de la Unión Científica Internacional de Radio*, Oviedo, Spain, September 2006.
**6.** I. Gil, J. Bonache, M. Gil, J. García-García and F. Martín, "On the left handed and rigth handed transmission properties of microstrip lines loaded with complementary split rings resonators", *Third Workshop on Metamaterials and Special Materials for Electromagnetic and TLC Applications*, Rome, Italy, pp. 33, March 2006.
**7.** I. Gil, J. Bonache, M. Gil, J. García-García, F. Martín and R. Marqués, "Modelling complementary-split-rings-resonator (CSRR) left-handed lines with inter-resonator's coupling", *IEEE Mediterranean Electrochemical Conference*, Torremolinos, Spain, vol. 1 and 2, pp. 225-228, May 2006.
**8.** M. Gil, J. Bonache, J. García-García and F. Martín, "Resonant-Type Metamaterial Transmission Lines: Design and Applications", *Young Scientist meeting on Metamaterials*, Seville, Spain, November 2006.
**9.** M. Gil, J. Bonache, I. Gil, J. García-García and F. Martín, "Artificial left-handed transmission lines for small size microwave components: Application to power dividers", *36th European Microwave Conference*, Manchester, United Kingdom, vol. 1-4, pp. 130-133, September 2006.
**10.** M. Gil, I. Gil, J. Bonache, J. García-García and F. Martín, "Metamaterial transmission lines with extreme impedance values", *Third Workshop on Metamaterials and Special Materials for Electromagnetic and TLC Applications*, Rome, Italy, pp. 34, March 2006.

**11.** G. Sisó, J. Bonache, M. Gil, I. Gil, J. García-García and F. Martín, "Compact metamaterial Rat-Race Hybrid", *Young Scientist meeting on Metamaterials*, Seville, Spain, May 2006.

**12.** I. B. Vendik, D. V. Kholodnyak, I. V. Kolmakova, E. V. Serbryakova, P. V. Kapitanova, F. Martín, J. Bonache, J. García-García, I. Gil and M. Gil, "Applications of Right/Left Handed and Resonant Left Handed Transmission Lines for Microwave Circuit Design", *36th European Microwave Conference*, Manchester, United Kingdom, pp. 955-958, September 2006.

**13.** J. Bonache, M. Gil, I. Gil, J. García-García and F. Martín, "Metamaterial transmission lines based on complementary split rings resonators: design and applications", *Mediterranean Microwave Symposium*, Geneva, Italy, October 2006 (Invited).

**14.** I. Gil, M. Gil, J. García-García and F. Martín, "Metamaterial transmission lines based on complementary split rings resonators: a review", *Progress in Electromagnetic Research Symposium*, Tokyo, Japan, August 2006 (Invited).

**15.** M. Gil, I. Gil, J. Bonache, J. García-García and F. Martín, "Microwave circuit applications of resonant type left handed lines based on complementary split rings resonators", *Progress in Electromagnetic Research Symposium*, Tokyo, Japan, August 2006 (Invited).

**16.** J. García-García, F. Aznar, M. Gil, J. Bonache and F. Martín, "Size reduction of SRRs for metamaterial and left handed media design", *Progress in Electromagnetics Research Symposium*, Beijing, China, pp. 680-683, March 2007.

**17.** J. García-García, F. Aznar, M. Gil, J. Bonache and F. Martín, "Considerations for the miniaturization of electro-magnetic resonators for metamaterial and left handed media design", *International Congress on Advance Electromagnetic Materials in Microwaves and Optics*, Rome, Italy, October 2007.

**18.** M. Gil, J. Bonache, J. García-García and F. Martín, "New left handed microstrip lines with complementary split rings resonators (CSRRs) etched in the signal strip", *IEEE/MTT-S International Microwave Symposium Digest*, Honolulu (HA), USA, vol. 1-6, pp. 1414-1417, June 2007.

**19.** M. Gil, J. Bonache, I. Gil and F. Martín, "Líneas de Transmisión Compuestas Zurdas/Diestras Basadas en el Modelo Resonante y Aplicaciones", *XXII Symposium Nacional de la Unión Científica Internacional de Radio*, Tenerife, Spain, September 2007.

**20.** G. Sisó, J. Bonache, M. Gil, J. García-García and F. Martín, "Compact rat-race hybrid coupler implemented through artificial left handed and right handed lines", *IEEE/MTT-S International Microwave Symposium Digest*, Honolulu (HA), USA, vol. 1-6, pp. 25-28, June 2007.

**21.** G. Sisó, J. Bonache, M. Gil and F. Martín, "Rat-Race Hybrid Based on Left and Right Handed Metamaterial Transmission Lines", *14th International Student Seminar on Microwave and Optical Applications of Novel Physical Phenomena*, Belfast, United Kingdom, August 2007.

**22.** M. Gil, J. Bonache, J. García-García and F. Martín, "Composite right/left handed (CRLH) transmission lines based on complementary split rings resonators (CSRRs) and applications", *International Congress on Advance Electromagnetic Materials in Microwaves and Optics*, Rome, Italy, October 2007 (Invited).

**23.** M. Gil, J. Bonache, J. Selga, J. García-García and F. Martín, "High-pass filters implemented by composite Right/Left handed (CRLH) Transmission lines based on complementary split rings resonators (CSRRs)", *Progress in Electromagnetics Research Symposium*, Beijing, China, pp. 360-362, March 2007 (Invited).

**24.** G. Sisó, J. Bonache, M. Gil, I. Gil, J. García-García and F. Martín, "Compact rat-race hybrid based on complementary split rings resonators", *Progress in Electromagnetics Research Symposium*, Beijing, China, pp. 357-359, March 2007 (Invited).

**25.** G. Sisó, J. Bonache, M. Gil and F. Martín, "Enhancing bandwidth in microwave components by means of metamaterial transmission lines", *11th International Symposium in Microwave and Optical Technology ISMOT07*, Villa Mondragone, Italy, December 2007 (Invited).

**26.** M. Gil, J. Bonache and F. Martín, "Compact Microwave Filters based on Metamaterial Resonators", *II Young Scientist Meeting on Metamaterials*, Barcelona, Spain, February 2008.

**27.** M. Gil, J. Bonache and F. Martín, "Application of Metamaterial Resonators in the design of Ultra Compact Band Pass Filters", *NATO Advanced Research Workshop: Metamaterials for Secure Information and Communication Technologies*, Marrakesh, Morocco, May 2008.

**28.** F. Martín, J. Bonache, M. Gil and G. Sisó, "Engineering the electrical characteristics of resonant type metamaterial transmission lines", *Proceedings of the SPIE Metamaterials III*, Strasbourg, France, April 2008.

**29.** F. Paredes, G. Sisó, M. Gil, J. Bonache and F. Martín, "Dual-band impedance matching networks based on resonant type metamaterial transmission lines", *IEEE International Symposium on Antennas and Propagation and USNC/URSI National Radio Science Meeting*, San Diego (CA), USA, July 2008.

**30.** J. Selga, M. Gil, G. Sisó, J. Bonache and F. Martín, "Application of complementary spiral resonators (CSRs) to microwave circuit miniaturization", *Workshop on Metamaterials and Special Materials for Electromagnetic Applications and TLC*, Naples, Italy, December 2008.

**31.** G. Sisó, M. Gil, M. Aranda, J. Bonache and F. Martín, "Compact quadrature phase shifter based on complementary spiral resonators (CSRs)", *2nd International Congress on Advanced Electromagnetic Materials in Microwaves and Optics*, Pamplona, Spain, September 2008.

**32.** G. Sisó, M. Gil, J. Bonache and F. Martín, "Bandwidth Enhancement in Metamaterial Microwave Devices", *15th International Student Seminar on Microwave and Optical Applications of Novel Physical Phenomena*, Saint Petersburg, May 2008.

**33.** F. Aznar, M. Gil, J. Bonache and F. Martín, "SRR- and CSRR-loaded metamaterial transmission lines: a comparison to the light of duality", *2nd International Congress on Advanced Electromagnetic Materials in Microwaves and Optics*, Pamplona, Spain, September 2008 (Invited).

**34.** M. Gil, J. Bonache and F. Martín, "Ultra Wide Band Pass Filters based on Metamaterial Transmission Lines", *NATO Advanced Research Workshop: Metamaterials for Secure Information and Communication Technologies*, Marrakesh, Morocco, May 2008 (Invited).

**35.** G. Sisó, M. Gil, J. Bonache and F. Martín, "Dispersion Engineering in Resonant Type Metamaterial Transmission Lines and Applications", *NATO Advanced Research Workshop: Metamaterials for Secure Information and Communication Technologies*, Marrakesh, Morocco, May 2008 (Invited)

**36.** G. Sisó, A. Vélez, M. Gil, J. Bonache and F. Martín, "New approach to the design of multi-band microwave components based on metamaterials", *International Symposium on Antennas and Propagation*, Taipei, Taiwan, October 2008 (Invited).

**37.** F. Aznar, M. Gil, G. Sisó, J. Bonache and F. Martín, "SRR- and CSRR-based Metamaterial Transmission Lines: Modeling and Comparison", *IEEE MTT-S International Microwave Workshop Series on Signal Integrity and High Speed Interconnects*, Guadalajara, México, February 2009 (Accepted).

**38.** J. Selga, F. Aznar, A. Vélez, M. Gil, J. Bonache and F. Martín, "Low-Pass and High-Pass Microwave Filters with Transmission Zero Based on Metamaterial Concepts", *IEEE International Workshop on Antenna Technology*, Santa Mónica (CA), USA, March 2009 (Accepted).

**39.** G. Sisó, M. Gil, F. Aznar, J. Bonache and F. Martín, "Size Reduction and Dispersion/Impedance Engineering with Resonant Type Metamaterial Transmission Lines: Current Status and Future Applications", *IEEE MTT-S International Microwave Workshop Series on Signal Integrity and High Speed Interconnects*, Guadalajara, México, February 2009 (Accepted).